Model Predictive Control For Automated Driving and Collision Avoidance

Master of Science Thesis

Nishant Chowdhri

Design of an integrated NMPC with simultaneous lateral and longitudinal control via steering and braking

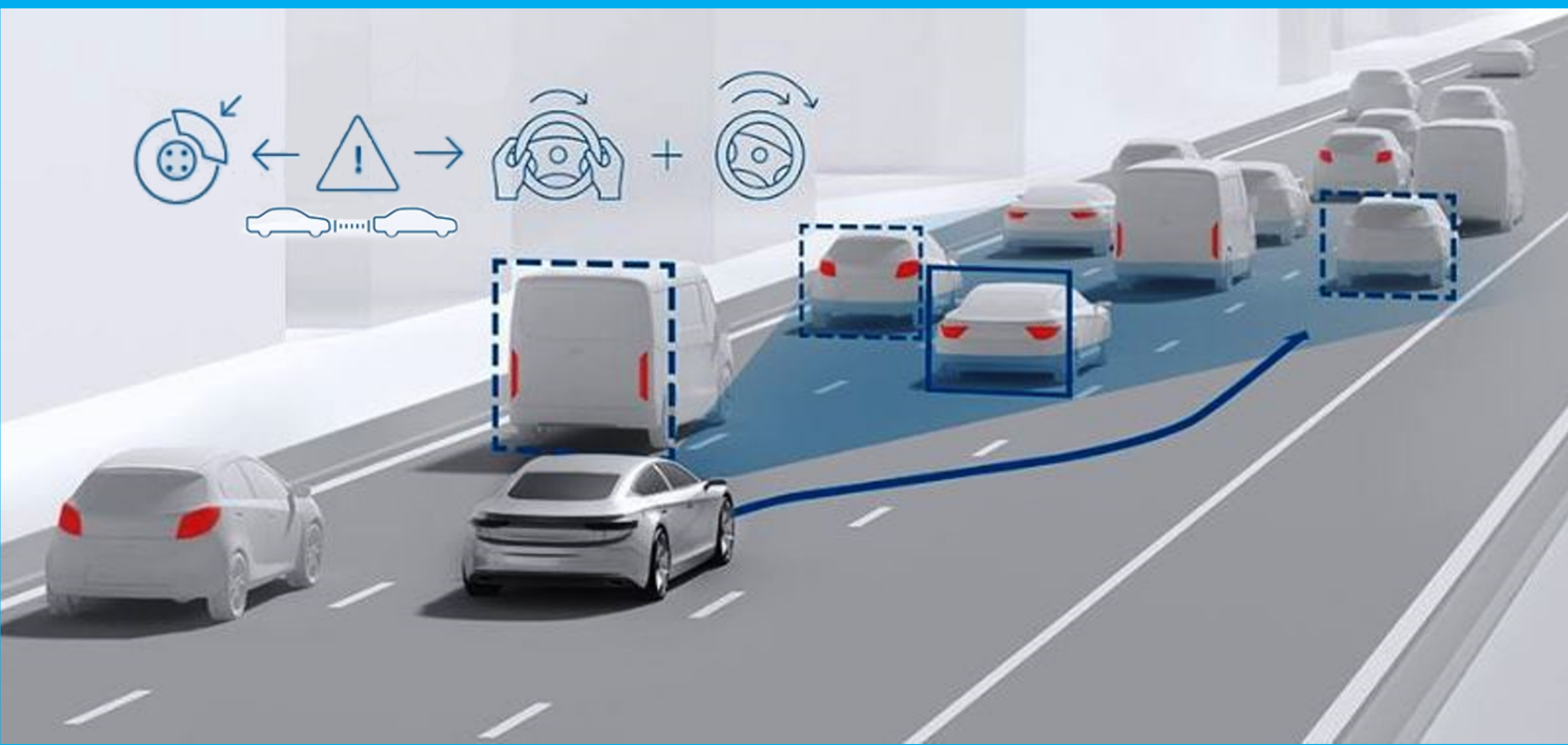

TU Delft

Model Predictive Control For Automated Driving and Collision Avoidance

Master of Science Thesis

by

Nishant Chowdhri

to obtain the degree of Master of Science
at the Delft University of Technology,
to be defended publicly on Wednesday July 03, 2019 at 13:30 PM.

Student number:	4744055	
Thesis committee:	Prof. R. Happee,	TU Delft, Chair
	Prof. B. Shyrokau,	TU Delft, Supervisor
	Dr. L. Ferranti,	TU Delft, Secondary supervisor
	Prof. M. Wang,	TU Delft, Committee member

TU Delft

The work in this thesis was supported by Toyota Motor Europe. Their cooperation is hereby gratefully acknowledged.

Abstract

The automotive sector has seen a rapid transition from sedan to SUVs, SI engine to electric and hybrid cars, normal driving mode to eco and sports mode and continues to evolve with the current research aimed at designing a SAE Level 5 autonomous car that is capable to drive, brake and steer on its own without the intervention of driver. The incessant drive for innovation has resulted in modern passenger cars equipped with plethora of control technologies such as ABS, VSC, AFS via EPS assist etc. all working respectively in various critical and non-critical scenarios to ensure safe and smooth driving at all times. These efforts have reduced the number of road accidents significantly over the past years, yet it was observed that the number of rear-end crashes have not decreased but has rather maintained its proportion which is about $1/3^{rd}$ of all road accidents.

An evasive maneuver, a limit-handling situation, involves quick steering or braking action to avoid colliding with the vehicle in-front (thus avoiding a rear-end crash). But with relatively high reaction times, the ability of driver to avoid the collision is limited. A normal human driver is not trained to drive and control car in such demanding and high stress inducing task. This warrants the need of an autonomous controller design that can itself take over the control of car and perform the maneuver successfully, ensuring collision avoidance and passenger safety at all times.

The aim of this research was to verify this statement by designing a novel control scheme that can steer and brake simultaneously and can avoid the collision autonomously. At the same time, the formulation of the overall control scheme was done in such a manner that the controller is not specific to only evasive maneuver but can also work autonomously in other non-critical driving scenarios, contributing towards the aim of a SAE Level 5 car.

The controller designed uses the state-of-the-art model predictive control scheme with all the nonlinear prediction model and constraint formulations embedded in its architecture such that best possible performance can be extracted even in critical driving scenarios. A three layer formulation involving decision making calculations, reference trajectory formulation and MPC control architecture constitutes the major pillars of the simulation design with specific and in-depth focus on LMPC and NMPC control designs. The controller designed was tested on a Toyota vehicle in simulation environment for performance validation.

The research done here is novel as for the first time, actuator dynamics are included in the prediction model for better future predictions. Nonlinear constraints such as EBD and kamm circle are included in the formulation to ensure optimal straight-line braking and tire force generation within its working envelope. A real-time cost update method is developed to improve tracking performance and lastly the integrated scheme of braking and steering is generic in its formulation and hence works efficiently with varying velocities, road friction coefficient and lateral wind disturbance. It can also perform maneuvers ranging from evasive action to normal lane change and is robust to sensor information delay and other external disturbances.

The simulation results for a single-lane change maneuver along with well-defined set of KPI's were drafted to investigate and accurately quantify the performance of the controllers which further bolstered the claim of using integrated model predictive control scheme for vehicle control design and also to highlight effectively the contributions made by this research.

The thesis report ends with future work and steps needed to be taken to further enhance the controller's performance and successfully implement this powerful control scheme on all road vehicles.

Table of Contents

List of Figures

Page

List of Tables

Page

Acknowledgement

A journey that contained good times and challenging times, success and failures, long hard working days and countless discussions, the idea to sum up this remarkable two year experience in just a few lines is difficult to comprehend. While I write this section, my mind is filled with all the countless memories that I made both at the Delft University of Technology, Netherlands and at Toyota Motor Europe (TME), Belgium. And my heart is brimming with emotions as I fathom the reality that this journey is coming to an end. In these two years I learned a lot about vehicle dynamics and controls, met some wonderful people, shared an amazing time with my friends and colleagues and improved myself as a person. For all this, I want to thank each and every person who made a difference in my life and moulded me in what I am today.

First and foremost, from the bottom of my heart, I want to thank my supervisor Barys Shyrokau who was always by my side and was a constant pillar of help and support to me. He has imparted the knowledge of vehicle dynamics and controls to me and for that I am always grateful. It was his faith in me that I got a chance to do this thesis with TME and for that I will always be thankful. I also want to thank my second supervisor Laura Ferranti who helped me so much with MPC and ACADO. The discussions I had with her were truly enlightening and extremely motivating.

Secondly, I want to thank all my colleagues at TME, who gave me this wonderful opportunity to be a part of their team and helped me each time whenever I got stuck during my research. I want to specifically thank Felipe Santafe, my manager and mentor at TME who, no matter how busy with work, would always give time to me, listen my problems and help me solve them. A wonderful and hardworking person, it was a privilege to share these wonderful five months with him and Toyota.

I want to thank my parents and family who always supported me and gave me the opportunity to come to Netherlands to pursue higher education. I don't even have words to describe how grateful I am to them and how blessed I feel to have them in my life.

Lastly, a big shout out to all my friends and my wonderful roommates who made this journey an enriching experience. They were always there no matter what to motivate and support me and help me get through some difficult times together.

Delft University of Technology — Nishant Chowdhri

June 20, 2019

1
Introduction

1.1. Transportation and Safety

Transportation is one of the basic necessities of life. Be it transportation of goods, transportation of animals, everyday commute or travelling on holidays, the importance of mobility for the modern society cannot be undermined. One of the machines designed to satisfy this incessant demand is a car which has catered to daily needs of transport successfully and still continues to do so. The ACEA 2018 report articulates 257 million passenger cars on road in EU with 511 cars per 1000 inhabitants [18]. The number of registered vehicles owned in U.S. in 2018 was 276 million [19]. But the advent of technology comes with both boon and bane.

The NHTSA reported that the number of fatal motor vehicle crashes in year 2016 increased by 5.6% to 37,461 deaths as compared to year 2015 [20]. The number of pedestrians killed and injured in 2016 by passenger vehicles in U.S.A was 2,307 and 49,000 respectively [21]. The numbers reported in EU were equally staggering with annual number of pedestrian fatalities in 2016 reported at 5,527 (an increase of 1% from year 2015) [2]. It can be seen that the vehicles have caused high percentage of road accidents and requires immediate attention to curb these figures. The automotive society therefore introduced new technologies and control systems in cars to curb the issue of road accidents as highlighted in the timeline shown in Fig 1.1.

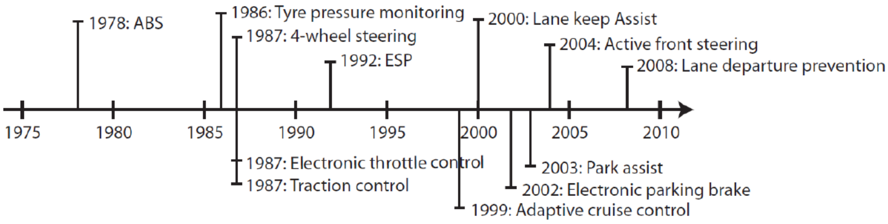

Figure 1.1: Driver Assistance Systems developed over the years by [1]

The advent of these systems has certainly made a difference in reducing the number of road accidents over the years as shown in Fig 1.2.

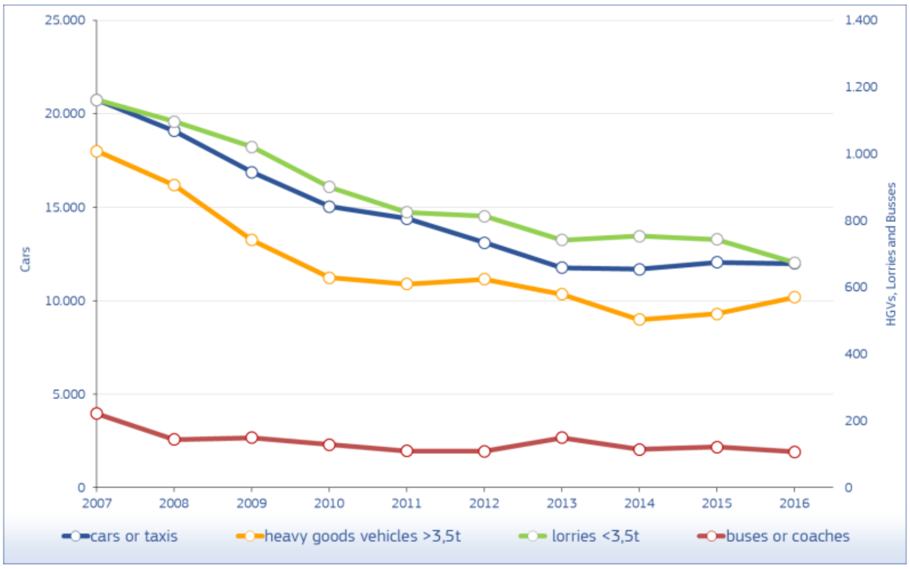

Figure 1.2: Annual number of driver and passenger fatalities by mode of transportation in EU, 2007-2016 [2]

The number of fatalities has reduced from 20,774 in year 2007 to 11,990 in year 2016. Yet we are far away from achieving the aim of zero road accidents. Thus, innovation and more sophisticated control strategies need to be invented for the betterment of road safety and human safety. In this respect, the idea was to perform research on a particular type of road accident which has predominantly been a major cause of fatalities and propose solution to solve that issue.

Of all the different type of road accident scenarios, one very common accident type witnessed in both urban and highway scenarios was that of rear-end crash in which the difference in relative speeds between the subject vehicle (SV) and lead vehicle (LV) in front causes the collision. It was reported that in the year 2005, about 35% of all crashes in Japan [22] were rear-end collisions. In year 2006, 500,000 crashes in U.S.A. (28% of all), 284,000 crashes in Japan (32% of all) and 266,000 crashes in the EU (16% of all) have been rear-end collision in which between 80%-90% rear-end crashes involved cars [23]. NHTSA data highlighted that around 32% of all road accidents in 2014 in the U.S.A. have been rear-end collision [24]. In 2015, the NHTSA crash data showed that a total of 2,101,000 crashes were rear-end in nature accounting for 33.4% of all the crashes, the highest of all crash types [25]. And the trend continued in 2016 with 2,369,000 rear-end crashes leading to 32.6% of all motor vehicle accidents in the US [26].

In conclusion, rear-end collisions are the most frequently occurring crashes [27], with a collision rate of 1 accident per 8 seconds [28]. It is clear that even with ADAS technologies and other driving assistance systems, rear-end collision still continues to take place and accounts for major proportion of all the road accidents. Therefore, it was decided to address this issue and develop a control strategy that helps in reducing this type of accident.

But before designing, it was necessary to understand the root cause behind such high and continuously rising rates of rear-end crashes. The reason why driver is not being able to cope up in this scenario is essential to know to effectively address this issue.

1.2. Driver Behaviour

The numbers written above are a clear motivation to understand what causes such collision from driveability perspective. It has been observed that a human's instinctive reaction to safety on road is associated with braking and reducing vehicle speed. In this context, the severity of brake action depends on the criticality of the maneuver. In case of any hazardous situation, the driver prefers to brake than to steer [29]. In a data set of 635 rear-end crashes encountered in the early 2000's in Germany, 82% of the driver's reaction was 'no steering' [23]. A driver-vehicle interaction analysis conducted by Daimler-Benz AG also reported that braking is a subconscious reaction shown by drivers during an evasive maneuver [30].

An extensive simulator based experiment and analysis was performed by [3] to understand driver behaviour during the event of rear-end collision. With three different levels of LV deceleration (0.3g, 0.5g and 0.75g respectively) and initial headway time (1.5s and 2.5s respectively), the performance of test subjects in the SV was studied under varying critical scenarios. Of the 141 evasive scenarios, it was seen that 85.82% of them were performed by only braking, as shown in Fig 1.3, out of which 30% of the time the driver ended in collision. But with the action of braking and steering both, no collision was observed.

Defining the headway time <1s as 'S', 1-1.5s as 'M' and 1.5-2.5s as 'L', the proportion of collision in high critical scenario, as shown in Fig 1.4, highlights that in these situations even though steering is the preferred option, the driver opts for braking and is unable to avoid the collision. This demonstrates the fact that in majority of cases, driver is not capable to choose the appropriate action required to avoid collision. A pre-dominant bias towards braking is seen in humans and this is the major reason why rear-end collisions are reported at such high rates.

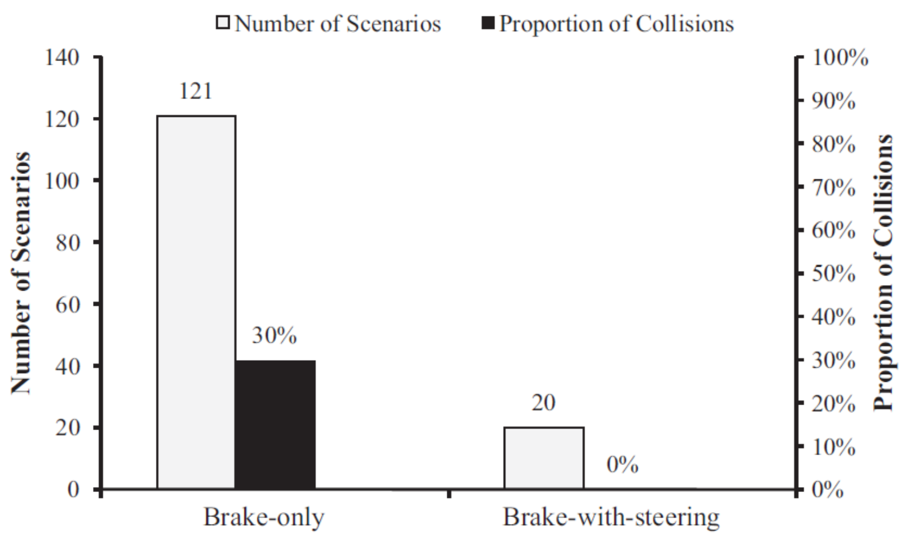

Figure 1.3: Brake and steer proportion for collision avoidance maneuver by [3]

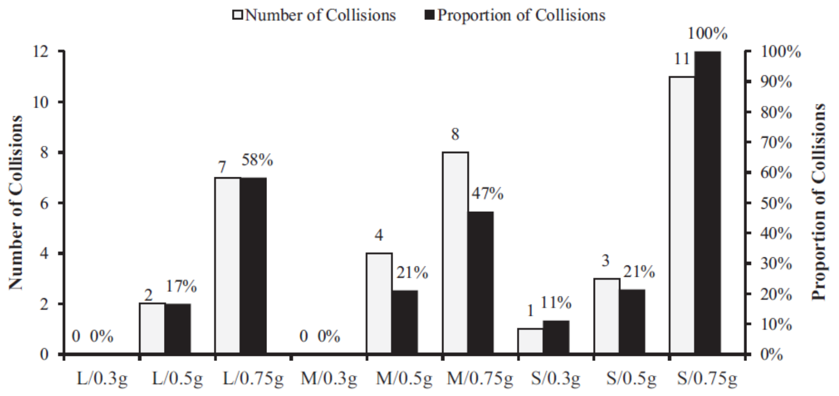

Figure 1.4: Brake-only case break down based on event criticality by [3]

Another reason for these crashes is the relatively high reaction and response time of the drivers. In their simulator study [3], the KPI's defined to analyze driver behaviour are shown in Fig 1.5.

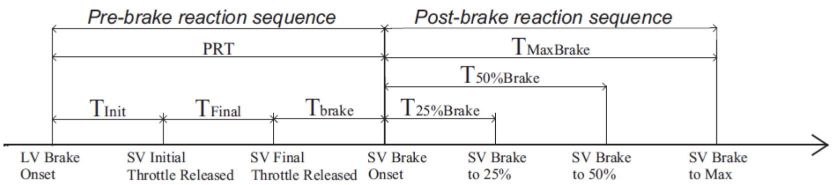

Figure 1.5: KPI's for driver behaviour analysis by [3]

PRT here is the Perception Response Time defined as the time elapsed between LV's deceleration initiation and SV's steer/brake onset. The reader is advised to refer to [3] for better understanding of all the KPI definitions. It was seen that as the criticality of the situation increased, the PRT of the driver reduced as shown in Fig 1.6. This shows that the driver is able to react quickly to the situation to act. But the absolute values of PRT as shown are seen to be very high. The best example is the right-most case in which the headway time is less than 1s and it takes driver 1.35s to take off the foot from gas pedal and apply brakes. If the driver's reaction time is so high, there is a good chance that he/she might not be able to avoid collision which is clearly shown in Fig 1.3. On the other hand, a controller will be able to perceive and act more quickly, giving a better chance to avoid the collision.

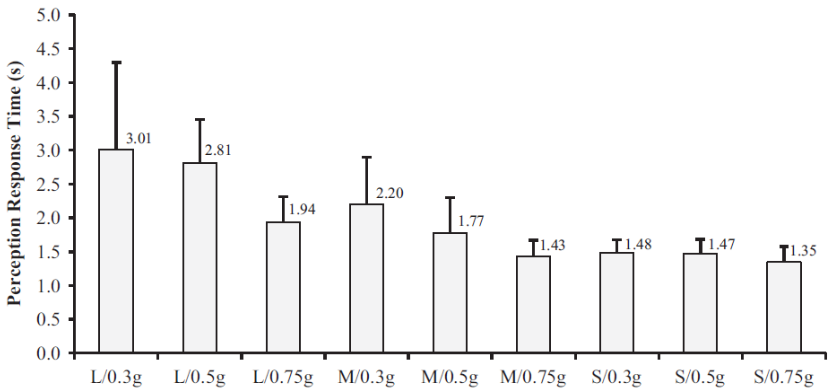

Figure 1.6: PRT by [3]

To further understand the time elapsed in the pre-brake sequence, a complete breakdown of the PRT is shown in Fig 1.7. While the throttle release times did reduce as the maneuver became more severe, the Time to Brake T_{brake} (time between that throttle is released completely and initiation of pressing the brake pedal begins) did not alter significantly with mean value reported around 0.5s. The same value was reported by [31], [32] highlighting that irrelevant of the situation, it takes normal driver 0.5s to shift pedals which again is a significant time lost in case of an evasive maneuver. The controllers on the other hand are fast in their initiation.

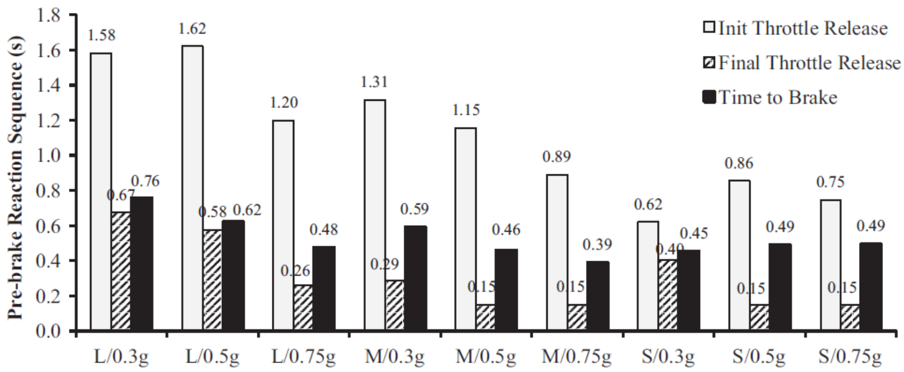

Figure 1.7: PRT breakdown by [3]

Designing therefore a control system which is reactive and assists the driver in performing the maneuver (just like ABS or VSC) will be less effective. The controller rather designed should be active instead of reactive. By designing an autonomous control which does not take the driver into account, it is believed that quick actuation will be achieved which will definitely lead to an improved performance. The controller should take control of the car to perform the maneuver safely and quickly and should not be designed to provide assistance to driver or wait for the driver's action to initiate as it is a high-end critical situation where driver safety is of extreme importance than driver comfort.

The third reason for such high rates of rear-end crashes corresponds to the fact that a normal driver is not trained to handle the vehicle successfully in the critical scenarios in which the vehicle motion is in the nonlinear regime where tire fores are near the saturation region and lateral accelerations are higher than $4m/s^2$. This has been very explained in [33] and has been quoted below.

"If the limits of the tires are exceeded, the vehicle can exhibit undesired behavior. This can happen for a variety of reasons. One is that drivers do not have a sufficiently accurate model of force generation capabilities of tires. When a vehicle is well within the limits of handling, the tires react in a generally linear manner. However, in highly dynamic situations, the limits of friction force between the tire and the road become important. The tires generate the maximum amount of force at some point before they completely lose grip and slide. This nonlinear behaviour of tires can catch untrained drivers off-guard, even causing some to react inappropriately, exacerbating the undesired vehicle dynamics."

It is very clear that in case of an evasive maneuver, the vehicle will be operating in the nonlinear regime of motion and the vehicle dynamics will be very challenging for the driver to handle. The linear regime of motion i.e. linear handling behaviour comes naturally to the driver but as soon as the vehicle is pushed to limits of handling, the situation becomes challenging for the driver [9]. And then to manage both steering and braking together in such fraction of seconds seems beyond the abilities of the driver. In an effort to highlight this, Volvo Technology Corporation in association with Chalmers University reviewed the driver models designed by various researchers to replicate collision avoidance by steering in case of a rapid evasive maneuver [4]. Fig 1.8 shows the performance of these driver models for the designed maneuver - a $20m$ single lane change at $20m/s$ with preview time of $1.3s$.

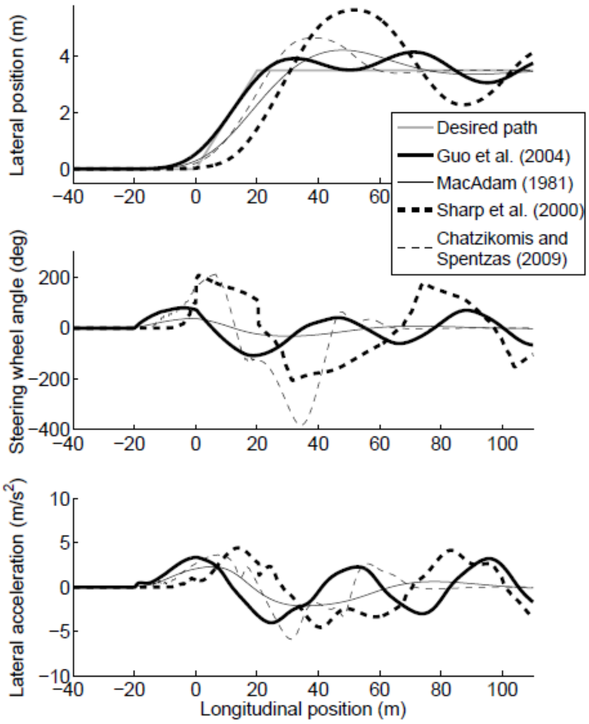

Figure 1.8: Steering behaviour of the driver models by [4]

It is evident that at high lateral accelerations, the driver is finding it hard to maneuver the vehicle successfully. It will be of no use again to design a reactive stability control system which intervenes when the vehicle has already ended up in an undesired condition which cannot be corrected anymore [33]. Thus, it is the authors belief to have an active and autonomous technology for this scenario for superior and safe performance.

The last reason for such poor performance of the driver in safety critical scenario is associated with the panic reactions the driver faces in these situations. The idea of potential crash induces fear reactions in the driving, impairing his or her judgment, leading to only brake action when steering is a better possibility to evade the collision. The domination of instinctive and default action towards braking rather than rational thinking can be induced due to sudden increase in both anxiety and driver workload. These elements of fear and panic will completely be eliminated if the control system takes control of the car, increasing the chances of correct decision making.

Other psychological reasons of the driver's inclination towards braking instead of steering, given by [4] and [34], are mentioned below.

- Tendency to maintain its own lane at all times
- Potential lack of knowledge of performing steering to drive on an alternative route
- Handling capability of vehicle becomes challenging while steering
- Mentality of the driver that braking will reduce the severity of the collision

Therefore, all these arguments give sufficient understanding of the reasons of driver failure leading to such high proportions of rear-end crashes. It also gives a fundamental understanding of how the controller needs to be designed and what level of performance is expected from it. Clearly, during this scenario it is clear that the motive of the driver is to ensure safety and does not give much priority to comfort. From Fig 1.9, it is clear that during post-brake analysis, in all situations the driver applies full brake with a mean deceleration of $8.71 m/s^2$ [3]. The only thing in the driver's mind here is to bring the car to full stop and safely avoid the collision, not caring about vehicle's pitching motion which will induce discomfort during driving. Hence, the designed controller in this research also emphasizes vehicle stability and safe avoidance of collision as its major KPI's and little importance is given to driver comfort.

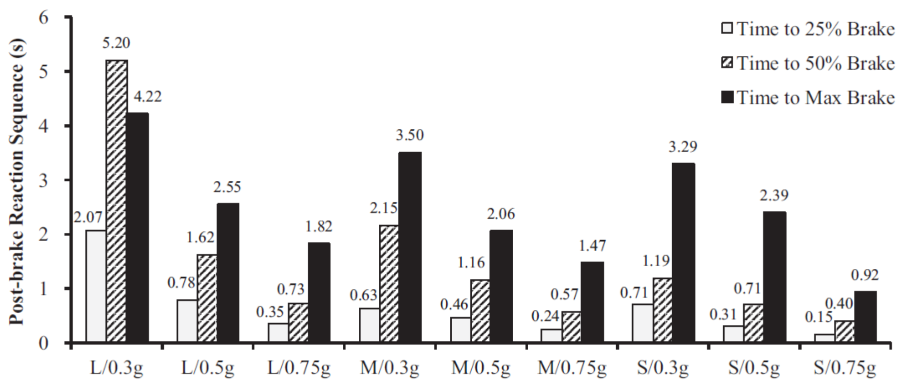

Figure 1.9: Post-brake reaction times by [3]

While the controller takes over the control of car, it is necessary that the driver is informed of this transition and at the same time is warned beforehand multiple times in hope that the driver itself will be able to respond to the situation. Fig 1.10 shows that at TTC of $3s$ and $5s$ respectively, the tactile warning is most effective to help make the driver react quickly [5]. In this case, systems such as ABS and VSC can assist the driver for better maneuver performance. But in case the driver does not respond to ADAS systems Forward Collision Warning and Attention Assist [35] or the TTC is beyond a set threshold value, then the control system should take over and perform the desired maneuver. This according to the author should be the proposed method of warning, activation and transition.

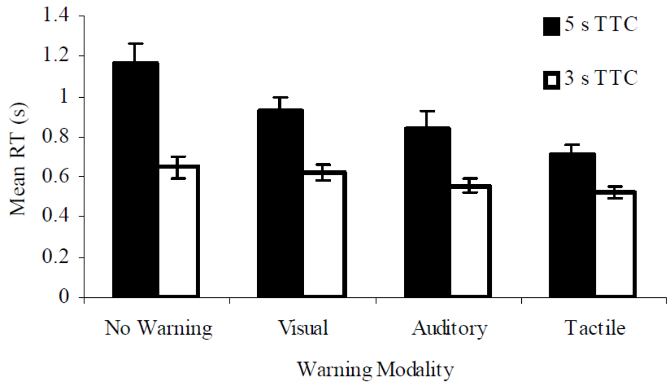

Figure 1.10: Reaction time of driver for various warning methods by [5]

1.3. Literature Review

An extensive review was performed on understanding the control design architecture and the control strategies designed for an evasive maneuver. A layout for designing the Emergency Driving System (EDS) was given by [12] as mentioned below.

- Risk Monitoring
- Driver Monitoring
- Decision Making
- Path Planning
- Control System

With the concentration of this thesis focused towards designing the controller, techniques for Driver Monitoring was not researched further. The Risk Monitoring is done through many parameters, most commonly used being TTC, TTS, TTB which are then used to make the decision whether to brake or steer. Once the decision is made, a path is planned and subsequent trajectory is generated which then the controller is supposed to follow. Hence, the basic design layout for this integrated control architecture is a three layer structure.

- Decision Making Process
- Trajectory Generation Techniques
- Control Schemes

A detailed understanding of all the three layers was reported by the author in [36]. An extensive review of various control strategies was also performed in [36], [37] based on which three important conclusions were reported which, if are followed in control design should provide better performance.

- Design of an integrated control involving both Steering and VSC via Differential Braking (DB) [12], [38]
- Designing an optimal control strategy [39]

- Designing a nonlinear control scheme which can handle tire non-linearities during highly dynamic situation [38]

Hence, an optimal and nonlinear control with integrated control action should in-principle be able to handle an evasive maneuver successfully. Based on these observations, it was concluded that MPC is the most suitable control technique as it covers all the three findings. Not only this, MPC is a predictive control technique which can predict in future and accordingly calculate the optimal control action. This ability of MPC will allow in its design formulation to adapt to changing reference trajectories (based on live surrounding conditions) online and accordingly react for better control. Hence, both LMPC and NMPC formulations have been designed in this research for performing an evasive maneuver.

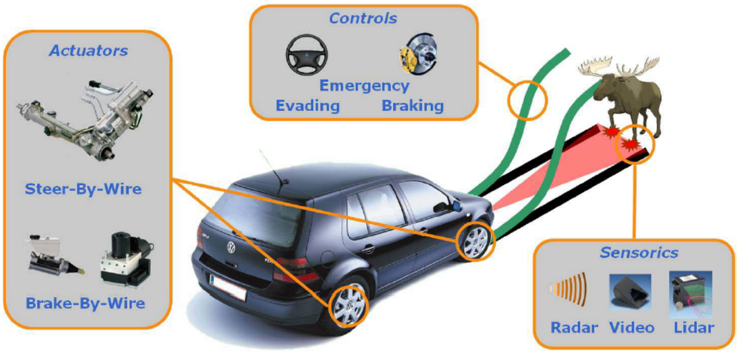

Figure 1.11: Simultaneous action of detection, trajectory planning and vehicle control for evasive action [6]

1.4. Scope of Thesis

While performing the literature review, it was noticed that only a handful work has been reported with integrated controller design using MPC [40], [41], [42]. Given the MPC technology is new and due to lack of publications in the field of integrated MPC control, it was motivating to perform research and contribute in this domain. Designing a MIMO MPC controller which works efficiently even with challenges such as computational demand, parameter tuning, robustness etc. was dealt successfully. And the performance clearly highlighted that there is an immense research scope in the field of integrated control which can completely eliminate the philosophy of high level and low level control which has been the traditional approach since the advent of ADAS systems.

Thus, the scope of this research curtails in designing a new concept of control design with modern control technologies that by the design of their formulation can work under variety of situations ranging from simple brake or lane change to complicated evasive action. The formulation is unique as only a single controller can control individual wheels and steering both, and requires no allocater or low-level controller for control action distribution. Given actuator dynamics can significantly vary the controller's performance, an effort was successfully made in integrating the actuator dynamics within the MPC prediction model which will be further explained in this report.

The three MPC controllers designed were tested on Toyota vehicle in simulation software, subjected to varying road conditions, sensor information delay and lateral wind disturbances to highlight the robustness of MPC in general.

1.4.1. Thesis Goals

With the above brief description of what this research curtails, the two major goals of this thesis are as follows.

To design a NMPC formulation such that one controller is able to control autonomously both the lateral and longitudinal dynamics simultaneously via steering and braking respectively.

To validate the designed controller's performance in various scenarios ranging from a highly dynamic single lane change evasive maneuver (to help curb the accidents caused by rear-end collision) to normal lane change maneuvers, varying vehicle velocities and road friction coefficient to external disturbances.

To achieve these aims, following were the objectives set.

- Develop a sophisticated MPC prediction model that captures the relevant information of the car accurately
- Design the three layer control formulation by integrating the decision making and trajectory formulation along with controller designed to emulate the real-life methodology concept
- Extend Toyota's vehicle model developed in IPG CarMaker and integrate it with the three layer control design successfully
- Co-simulate the developed and well-tuned NMPC planar car based controller with the Toyota vehicle to allow them to communicate among each other in real-time and produce accurate results of the vehicle dynamics affecting performance
- Compare the control strategy with other two MPC controllers (linear bicycle and nonlinear bicycle prediction model based) designed by performing same maneuver under variety of scenarios
- Precisely identify the strengths and weaknesses of the proposed control strategy by means of well-defined KPI

1.4.2. Thesis Contribution

The contributions made by this research helps in achieving the future aim of making a SAE Level 5 autonomous drive. Firstly, the designed controller is novel and one-of-its kind with its formulation containing EBD logic, actuator dynamics and nonlinear friction ellipse constraint apart from highly nonlinear prediction model designed with great accuracy. The ability of the controller to decide, predict and optimally actuate both steering and braking together successfully highlights the power of this control scheme and the potential of working in all kinds of scenarios. It also paves way for future research towards the field of integrated control technology instead of high and low level based control technology.

In a vehicle, both the longitudinal and lateral dynamics are coupled. By designing two separate control structures for each dynamics and then dividing it at vehicle body level and actuation level not only leads to loss of performance due to poor synchronization but also makes the whole control system architecture very complex. Instead, one unified control strategy, developed in this research, which captures both vehicle and actuator dynamics offers ease of implementation, ease in debugging and at the same provides better performance as the coupled effects of both the dynamics is well-captured in one formulation.

Secondly, this research designed involved co-simulating three different software platforms namely ACADO, IPG CarMaker and MATLAB in vehicle dynamics framework. This novelty allowed the use of MPC controller's generated s-function and Inter-Process-Communication (IPC) simultaneously making it realistic and one step closer towards the close-to-production software architecture.

Thirdly, the controller's design was kept simple and generic but efficient such that it is just not limited to evasive action but can handle all range of scenarios. This is shown by varying the velocity, friction coefficient and wind disturbance velocity during the single lane change maneuver. Also maneuver dynamics were changed from evasive action to normal lane change to highlight the controller's capability of working in all the different cases.

A new and completely novel method of real-time cost function update was designed for improved tracking performance. Using the reference trajectory points, the cost function was updated along the maneuver by varying the tuning parameters which practically led MPC to know at each instant, which error needs to be minimized and which not.

Only a mathematical equation was used for reference trajectory generation to show pure controller tracking performance even with a trajectory that does not consider vehicle dynamics in its formulation and thus is not sophisticated. The aim of this research was to design a good controller and not a well-defined reference trajectory generation method. By giving a non-realistic reference trajectory, the idea was to still show the controller's ability to track it successfully providing a further proof of concept.

Lastly, this would be the first time that an in-house model based integrated NMPC was designed and developed at Toyota Motor Europe (TME).

1.4.3. Thesis Outline

This thesis comprises of seven chapters and 6 Appendices. A brief introduction to remaining six chapters is stated below.

- Chapter 2 provides a description of MPC and its key design elements. An introduction to software ACADO in which the MPC controller was designed along with various controller parameter and solver settings is provided. This is followed by an explanation of the optimization technique used to solve the MPC's OCP online.
- Chapter 3 provides an in-depth explanation on designed MPC controller's modelling and various equations used to define the prediction model and the constraints for each controller respectively, along with its cost function equation

- Chapter 4 focuses on the simulation architecture in which decision making parameters and equations for reference trajectory are documented. The maneuver and KPI's defined are then explained. Lastly, analysis done on the vehicle's tire is reported to showcase how the tire nonlinearities were captured in the formulation.
- Chapter 5 introduces the controller's activation logic and explains the designed real-time cost function update method and MPC tuning process for improved trajectory tracking
- Chapter 6 contains all the simulation results, controller performance results and KPI evaluations for the three MPC controllers
- Chapter 7 presents the conclusions as well as the recommendations for the future work in this field

The Appendix section contains the simulation results for each of the three designed controllers, an understanding of vehicle modelling and actuator dynamics, the issue found with the reference point calculation by reference trajectory and lastly a screenshot of the dugoff tire fitting on the Magic formula.

1.5. Summary

This chapter provided an introduction to the problem of rear-end collision and its ever rising statistics even with the advent of ADAS systems. To understand the cause behind this rise, the driver behaviour was analyzed where it was found that the driver is not capable to perform an evasive maneuver successfully due to its preference towards braking than on steering, high reaction time, inability to control the vehicle during highly nonlinear and critical maneuver and due to fear and anxiety developed affecting the driver's performance. This clearly justified the need of an autonomous control system required particularly for this maneuver. An overview of the literature review performed on various control strategies was given and major conclusions made were summarized which were that the controller designed should be optimal and nonlinear with an integrated design. MPC covers all these aspects and was chosen as the control design method. Lastly, the scope of the thesis was elaborated where the goals, major contributions and outline of this research was documented.

2

MPC and ACADO

2.1. Introduction

MPC offers a modular framework and is efficient in handling MIMO systems. All the controllers designed in this research uses MPC as the control technique and therefore it is essential that before going into the controller's formulation, one has a basic understanding of MPC concepts and how it works in general. This chapter provides a summarized introduction to optimal control scheme called MPC along with its key design elements. The MPC controller was designed using a software toolkit ACADO. Thus, an introduction to the toolkit is given to understand how the optimal problem is being solved along with the controller settings fixed for all the three MPC controllers designed. The OCP is solved by ACADO and another embedded software in ACADO called qpOASES by using the methods SQP and ASM which have been explained in the last section of this chapter.

2.2. Model Predictive Control

A driver has the ability to judge its surrounding and look ahead in time to predict the scenario and accordingly drive and control the car. This is in-line with the working principle of MPC, to predict in future and accordingly act at the current time [43].

Model Predictive Control is an optimal control technique that involves the formulation of a prediction model and solving an optimization problem at every sampling instant [44]. Having the advantage of being simple and modular in its architecture along with the ability to handle MIMO systems efficiently and optimally, MPC can be designed both in linear (LMPC) and nonlinear (NMPC) way and therefore is considered to be a powerful closed-loop control technique.

MPC uses a prediction model as the basis for calculating the future predictions over a user-defined time horizon. An Optimal Control Problem (OCP) is defined to minimize the cost function subject to constraints such that the optimal control action calculated satisfies the constraints and is feasible for control. Lastly, by using the concept of Receding Horizon Principle (RHP), only the first control action calculated is applied on the plant so that new information can be utilized immediately.

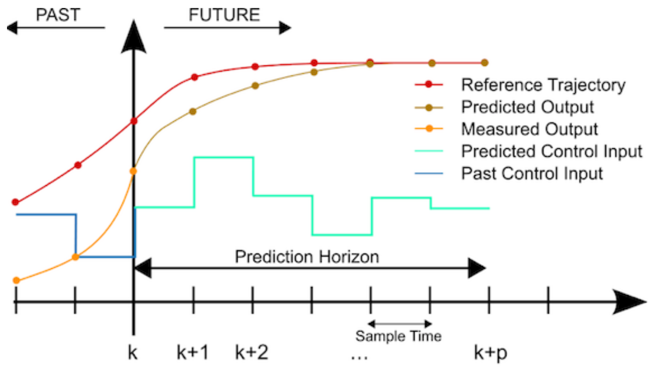

Figure 2.1: MPC working scheme

The ability of MPC to handle constraints in its formulation makes it a unique control algorithm, different from other optimization control techniques such as LQR.

MPC can be broken down into five key elements for efficient understanding. The key elements are mentioned below.

- Prediction Model
- Performance index
- Constraints
- Optimization
- Receding Horizon Principle

Prediction Model
Probably, the most critical part of the MPC design, the prediction model contains the dynamics of the plant to help MPC understand how the plant will behave if a control action is applied. Therefore, the more accurate the prediction model is, the better the MPC will be able to understand the plant dynamics and more accurate will be the future predictions. This prediction model can be linear as well as nonlinear in its formulation and can have either a single state or multiple states.

The modular design of MPC stems from the fact that MPC can work for different plant dynamics ranging from automotive to petrochemical industry, as long as a model with accurate representation of the respective plant's dynamics can be modelled or estimated. A general representation of the prediction model is given in the form shown below.

$$x(k+1) = f(x(k), u(k)) \tag{2.1}$$

Here, $x(k)$ represents the states of the system, $u(k)$ is the control action and f is the linear or nonlinear function describing the prediction model's equations. Assuming f to be linear, the Linear Time Varying (LTV) prediction model's equation for MPC can be defined in two ways.

Direct Input-Output (IO) model: It is of the form:

$$x(k+1) = Ax(k) + Bu(k) \tag{2.2}$$

Incremental IO (IIO) model: It is defined as:

$$x(k+1) = Ax(k) + B\Delta u(k) \tag{2.3}$$

$$u(k) = u(k-1) + \Delta u(k) \tag{2.4}$$

The augmented model for IIO presented by [45] is shown in Eq (2.5).

$$\begin{bmatrix} x(k+1) \\ u(k) \end{bmatrix} = \begin{bmatrix} A & B \\ 0 & I \end{bmatrix} \begin{bmatrix} x(k) \\ u(k-1) \end{bmatrix} + \begin{bmatrix} B \\ I \end{bmatrix} \Delta u(k) \tag{2.5}$$

The IIO model has the advantage of providing integral action to the system which ensures no offset with the reference signal at steady state. The control action $\Delta u(k)$ is calculated until the tracking error becomes zero after which $\Delta u(k)$ becomes zero, thus offset is eliminated [46].

Considering the IO model equation, the j^{th} prediction for system's state is given by Eq (2.6).

$$x(k+j) = A^j x(k) + \sum_{i=0}^{j-1} \left(A^i Bu(k+j-1-i) \right) \tag{2.6}$$

Assuming the output $y(k)$ of the LTV system as shown in Eq (2.7):

$$y(k) = Cx(k) \tag{2.7}$$

Simple substitution of Eq (2.6) in Eq (2.7) gives the prediction equation for the output shown in Eq (2.8).

$$y(k+j) = CA^j x(k) + \sum_{i=0}^{j-1} \left(CA^i Bu(k+j-1-i) \right) \tag{2.8}$$

For a given prediction horizon N_p and using Eq (2.8), the prediction model can be written as:

$$Y_p(k) = A_p x(k) + B_p U(k) \tag{2.9}$$

where,

$$Y_p(k) = \begin{bmatrix} y(k+1) \\ y(k+2) \\ . \\ . \\ . \\ . \\ y(k+N_p) \end{bmatrix}, \qquad A_p = \begin{bmatrix} CA \\ CA^2 \\ . \\ . \\ . \\ . \\ CA^{N_p} \end{bmatrix},$$

$$B_p = \begin{bmatrix} CB & 0 & 0 & . & . & . & 0 \\ CAB & CB & 0 & . & . & . & 0 \\ CA^2B & CAB & CB & . & . & . & 0 \\ . & & & . & & & . \\ . & & & & & . & . \\ CA^{N_p-1}B & . & . & . & . & . & CB \end{bmatrix}, U(k) = \begin{bmatrix} u(k) \\ u(k+1) \\ . \\ . \\ . \\ . \\ u(k+N_p-1) \end{bmatrix} \tag{2.10}$$

Here, $Y_p(k)$ is the predicted output, A_p is the extended observability matrix, B_p is the Toeplitz matrix and $U(k)$ is the predicted control action sequence. This is how using the plant dynamics in its formulation, a prediction model is developed and used to calculate series of control action.

Performance Index

The performance index is the cost function designed to keep the tracking error between process output and given reference as small as possible and at the same time, minimize the control action energy. For a prediction horizon N_p with Q, P, R and S being the symmetric and positive-definite weighing matrices, a general cost function is defined in Eq (2.11).

$$J_k = \sum_{i=1}^{N_p-1} \big[(y(k+i)-r(k+i))^T Q_i (y(k+i)-r(k+i)) + u(k+i-1)^T P_i u(k+i-1) +$$
$$\Delta u(k+i-1)^T R_i \Delta u(k+i-1)\big] + ((y(k+N_p)-r(k+N_p))^T S(y(k+N_p)-r(k+N_p)) \quad (2.11)$$

The cost function tells the controller exactly which states or outputs need to be minimized or tracked accurately based on the weights defined. Higher the weights, more is tracking desired. The addition of control action in the cost allows the flexibility of telling MPC which control action can be used more than the other based on its tuning as well. This is very helpful in case of MIMO systems where selectively, the user can limit usage of one control action over others to save control action energy and cost.

The performance index is very crucial as it is the basis of solving the optimization problem and needs to be designed carefully. Also, terminal cost function is defined to ensure that at the end of prediction horizon, the plant is at or near the desired trajectory. This is done to ensure that the plant remains in the stable region and the predictions made ensure that control action will keep the plant near the stability region. Finally, the evolution of states in time to predict the future state values comes from the prediction model of the MPC as shown in Eq (2.9) for the case of linear systems.

Constraints

MPC can be designed such that the optimal problem to be solved is either constrained or unconstrained. The ability of MPC to handle constraints makes it a very powerful control technique because a plant in general always has certain mechanical or electrical limits in which it can work efficiently. By setting these constraints, one can be ensured that the control action calculated will always be within the limits of the system and will not make the system unstable.

This advantage of formulating constraints is of immense importance for vehicle control. A vehicle has actuators which can only work in the defined range. Also, there are physical limits on vehicle states and tires. By defining constraints such that the vehicle remains within this operating envelope, it can be ensured that the vehicle shall always be in the stable and working region.

Mainly constraints are defined as certain equality or inequality bounds on states, control action or an expression of the form $G(x,u,\Delta u)$ which can be linear or nonlinear in nature.

$$G(x,u,\Delta u) \leq g \tag{2.12}$$

Here, g is the bound value. Sometimes, equality constraint like control horizon constraint is also defined as shown below.

$$\Delta u(k+j) = 0 \;\; for \;\; j \geq N_c \tag{2.13}$$

The idea behind defining a control horizon N_c is that after N_c, the control input is assumed to be constant for remaining predictions to reduce the computational effort of the controller. Generally, $N_c \leq N_p$.

$$u(k+j) = u(k+N_c-1) \;\; for \;\; j \geq N_c \tag{2.14}$$

A set of general constraints usually defined for the MPC formulation are initial conditions, vehicle dynamics, output states, state bounds and actuator constraints on control action as mentioned below respectively.

$$x(t_0) = x_0 \tag{2.15}$$

$$\dot{x}(t) = f(x(t), u(t)) \tag{2.16}$$

$$y(t) = g(x(t), u(t)) \tag{2.17}$$

$$x_{min}(t) \leq x(t) \leq x_{max}(t) \tag{2.18}$$

$$u_{min}(t) \leq u(t) \leq u_{max}(t) \tag{2.19}$$

Optimization

Once the cost function is defined and the constraints for the optimization problems are formed, the next step is to solve this optimization problem in which the aim is to minimize the cost function value subject to constraint satisfaction by calculating the optimal control action. It is therefore indeed important to formulate a cost function that covers essential tracking states and reference values. The optimization problem can be constrained or unconstrained in nature.

Two sets of problems can be defined, linear or nonlinear problems. The linear problems are less computationally expensive and are mostly solved using QP. The nonlinear problems are more time consuming to solve. SQP and IP algorithms are most common to solve these problems. In this research, SQP and ASM are used to solve the nonlinear optimization problem and have been described in Section 2.4.

Receding Horizon Principle

The last key point of MPC is the RHP which states that after calculation of the vector of control actions $(u(k)......u(k+N_p-1))$, only the first control action is applied to the plant for control. At next sample, again the set of control actions is calculated and the same process of applying the first control action $u(k)$ is repeated.

One may find it strange to calculate control actions over the entire prediction horizon but only implement the first value. RHP actually allows new information and the recent measurement to be utilized immediately and not ignore it till the entire prediction horizon [46]. If not for RHP, all the predictions and control action vector will be based on old information, affecting the system dynamics badly because of the unmeasured disturbance.

A sixth key element can be the MPC tuning. Often considered as one of the issues with MPC, the tuning of MPC is often very challenging as there is no golden rule yet to tune the controller and is currently an open topic for research. The number of parameters to be tuned are the sampling time t_s, prediction horizon N_p and control horizon N_c along with the tuning weights for each state defined in the cost function of OCP. Hence while designing, one needs to think which states become a part of the cost function and which not to reduce the amount of tuning and the complexity in general.

2.3. ACADO

2.3.1. Introduction

After getting an introduction to MPC, this section introduces the software used to design the MPC. ACADO Toolkit is a platform with collection of optimization algorithms and other algorithms to solve problems of direct optimal control, parameter estimation and robust optimization, and designing model predictive control problem. Capable of working in MATLAB and Simulink environment, the major highlights of ACADO is to tackle Nonlinear Optimal Control problem and Multi-Objective Optimal Control problem efficiently. It generates the designed controller's script directly in C code and therefore provides an easy implementation to vehicle ECU.

To solve the OCP, ACADO currently implements SQP which consists of successive linearization of the NLP to convert it to QP problem and then solving it to get a convex solution [47]. Using condensing techniques, the state variables / optimization variables are eliminated / reduced and the resulting small-scale QP is solved by ASM using the solver qpOASES [48]. The Real Time Iteration (RTI) involves performing a single SQP iteration per sampling time for quick solution [47].

2.3.2. OCP solving

To solve the OCP successfully, the main idea is to first obtain a finite dimensional optimization problem by parametrizing the original problem. Using the prediction samples N_p to generate a equidistant shooting grid $(t(k), t(k+1), ..., t(k+N_p))$ for the states and control action, the OCP is solved through Direct Sequential Methods either by single shooting or multiple shooting.

In the single shooting method the model simulation and optimization are done sequentially. The numerical integration of the prediction model is performed first to find the sensitivity of the cost function to the control action. Then, the optimization is performed. The main advantage is simple implementation and by following the plant dynamics to integrate throughout the shooting interval, all the iterates by default become feasible during optimization.

The multiple shooting method involves more parameters in its formulation as the optimization parameters are both control action and the states at the beginning of each sub-interval s_i [49]. The prediction model equation's integration is performed on each sub-intervals and the resulting trajectories are optimized separately. To ensure continuity of trajectories between each sub-interval, a set of equality constraints are also modelled in the optimization problem.

$$x(t_{k+i}) = s_{k+i} \tag{2.20}$$

The multiple shooting approach has the ability to handle unstable and nonlinear systems better than the single shooting method. But, the number of variables gets increased. Since the designed MPC formulations have nonlinear and coupled expressions in the formulation, the multiple shooting method was preferred for better optimization performance. The advantage of formulating a discretized OCP cost function over a continuous one is the reduction of computation cost needed for integration of cost function over time. Now only a sum over discrete sampling time instants is required.

There are implicit and explicit integrators with efficient sensitivity propagation embedded in ACADO and are used as solvers for solving the OCP in real-time. Since the nonlinear prediction models designed included implicit terms in which state variables are coupled with each other, as well as the presence of other cross-coupling terms, the integrator used in this research was also implicit in nature. The solving of OCP is a two step process for efficient RTI as shown in Fig 2.2.

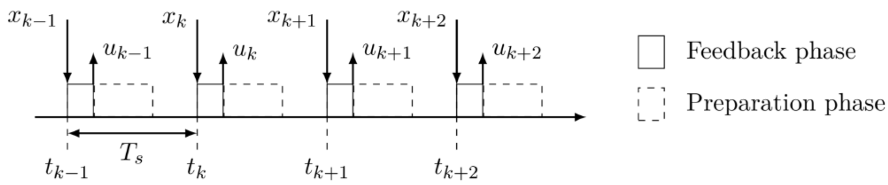

Figure 2.2: Task scheduling of ACADO RTI [7]

These two steps are summarized below.

- Phase 1 of NLP linearization, discretization and condensing to form in Eq (2.10)
- Phase 2 of solving the condensed QP by the set user-defined solver

Since phase 1 discretizes the problem for OCP formulation, one can design the prediction model of MPC in continuous form as well. In this research, all the prediction models are designed in continuous domain. Phase 1 is performed using standard optimization technique SQP. Once the linearized QP is formed, ASM technique using the software qpOASES is used to solve the optimization problem and get the desired optimal control action $u(k)$. qpOASES is an open-source platform designed to solve QP using ASM [50]. The method of successive online linearization of the nonlinear plant along the prediction horizon into a LTV system reduces the computational complexity of solving the optimization problem and is therefore a good strategy for real-time implementation [51].

To design an OCP successfully in ACADO, one needs follow the below mentioned steps.

- Set the sampling time and prediction horizon of the MPC
- Design and formulate the prediction model equations and the constraints for the MPC controller
- Select the shooting method (either single shooting or multiple shooting)
- Select the integrator and other optimization options such as KKT value, maximum number of integration steps, hessian calculation methods, hotstart QP etc.
- Provide the tuning weights of the cost function as well as the state information and other online data required by MPC

In this research, the settings chosen for defining and solving the optimization problem is shown in Fig 2.3.

```
mpc = acado.OCPexport( ocp );
mpc.set( 'HESSIAN_APPROXIMATION',        'GAUSS_NEWTON'      );
mpc.set( 'DISCRETIZATION_TYPE',          'MULTIPLE_SHOOTING' );
mpc.set( 'SPARSE_QP_SOLUTION',           'FULL_CONDENSING_N2');
mpc.set( 'INTEGRATOR_TYPE',              'INT_IRK_GL4'       );
mpc.set( 'NUM_INTEGRATOR_STEPS',        3*N                  );
mpc.set( 'QP_SOLVER',                    'QP_QPOASES'        );
mpc.set( 'GENERATE_SIMULINK_INTERFACE', 'YES'                );
mpc.set( 'LEVENBERG_MARQUARDT',          1e-4                );
mpc.set( 'CG_USE_VARIABLE_WEIGHTING_MATRIX', 'NO'            );
mpc.set( 'HOTSTART_QP', 'YES');
```

Figure 2.3: Solver settings of OCP in ACADO

2.3.3. Handling of Infeasibility

One of the issues related to a NMPC formulation is the inability to find a global optimal solution, even though the solution do exist! Generally, a local optimal solution is formed due to non-convex formulation of the nonlinear OCP. But a bigger issue would be if no solution was found which may lead to plant instability and loss of control. Mainly two reasons can be thought of leading to infeasibility problem.

- The optimization of NLP itself is infeasible. This can be due to poor initial conditions violating the OCP constraints.
- The defined QP becomes infeasible, for example due to linearization of constraints or if QP becomes unbounded

In ACADO, one can get status flags to check if the optimal problem was solved successfully or not. *Status flag 0* indicates optimization was successfully solved and optimal solution was found. *Status flag 1* indicates maximum number of iterations were reached. For the case of maximum iterations, ACADO provides the solution of the last iteration as the final control action as it is feasible and is closest to the optimal solution. In the next sampling time, the warm start method allows to find the solution close to optimal one.

In case the status flag returned is not 0 or 1 and is any other value like -1 or -2, then solution of that sampling time is discarded and the last successful solution is used as control action. This does not guarantee good control of the plant but this implementation is still better than choosing to implement an infeasible solution to the plant.

2.4. SQP and ASM

2.4.1. Introduction

As mentioned in Section 2.3.2, the preparation phase in ACADO of linearization, discretization and condensing is done using SQP and subsequent solving of the QP is done through ASM. This section gives an idea regarding how the optimization problem is solved and the associated math behind optimization methods SQP and ASM.

2.4.2. Sequential Quadratic Programming

One of the state-of-the-art algorithm for solving constrained nonlinear optimization problem, SQP is an iterative solution technique which models the NLP for a given iterate x^k, $k \in \mathbb{N}$ to a QP subproblem and later solves the QP to use the solution to construct new iterate x^{k+1} [52]. The generation of next iterates of x^k is done in such a way so that the sequence of x^k converges to the local optimal solution x^* of the nonlinear OCP. The unique thing of SQP is its ability to handle constraints to solve the OCP problem.

Consider a general NLP problem of the form shown below.

$$\begin{aligned} \text{minimize} \quad & f(x) \\ x \in \mathbb{R} & \\ \text{subject to} \quad & h(x) = 0 \\ & g(x) \leq 0 \end{aligned} \tag{2.21}$$

Where, $f : \mathbb{R}^n \rightarrow \mathbb{R}$ is the objective function to be minimized, the constraint functions $h : \mathbb{R}^n \rightarrow \mathbb{R}^m$ and $g : \mathbb{R}^n \rightarrow \mathbb{R}^p$ represent the equality and inequality constraints respectively. To convert the NLP into a QP problem, the first step is to define a Lagrange function as the objective function of the OCP problem. Using Lagrange multipliers λ and μ, the Lagrange function is defined as shown in Eq 2.22.

$$\mathscr{L}(x, \lambda, \mu) = f(x) + \lambda^T h(x) + \mu^T g(x) \tag{2.22}$$

The function $\mathscr{L} : \mathbb{R}^{nxmxp} \rightarrow \mathbb{R}$ with the help of vectors $\lambda \in \mathbb{R}^m$ and $\mu \in \mathbb{R}^p_+$ couples the constraints and objective function in one formulation. Taking the first derivative of Lagrange function $\mathscr{L}$ gives directly the first KKT condition as shown in Eq (2.24).

$$\nabla_x \mathscr{L}(x, \lambda, \mu) = 0 \tag{2.23}$$

$$\nabla f(x) + \lambda^T \nabla h(x) + \mu^T \nabla g(x) = 0 \tag{2.24}$$

Now, to convert the NLP into a QP problem in which the cost function is quadratic in nature and the constraints are linear functions, Taylor series expansion is used. To get the quadratic cost function, the Taylor series expansion up to 2nd order and for the linear constraints, expansion up to 1st order is performed as shown in Eq (2.25) and Eq (2.26) respectively.

$$\begin{aligned}\mathscr{L}(x,\lambda_k,\mu_k) \approx \mathscr{L}(x_k,\lambda_k,\mu_k) + \nabla_x \mathscr{L}(x_k,\lambda_k,\mu_k)(x-x^k)\\ +\frac{1}{2}(x-x^k)^T H_{\mathscr{L}}(x_k,\lambda_k,\mu_k)(x-x^k)\end{aligned} \tag{2.25}$$

$$\begin{aligned}h(x) &\approx h(x^k) + \nabla_x h(x^k)(x-x^k)\\ g(x) &\approx g(x^k) + \nabla_x g(x^k)(x-x^k)\end{aligned} \tag{2.26}$$

Here, $H_{\mathscr{L}}(x_k,\lambda_k,\mu_k)$ is the hessian matrix of the cost function. Calculating the hessian matrix is computationally expensive and therefore methods such as Levenberg - Marquardt algorithm, Broyden - Fletcher - Goldfarb - Shanno quasi-Newton method or Davidon - Fletcher - Powell quasi-Newton method are used to approximate the hessian matrix and calculate it. In this research, one such method called Gauss-Newton algorithm was chosen to approximate the Hessian matrix as shown in Fig 2.3. Now, assuming,

$$d(x) = x - x^k \tag{2.27}$$

the, standard QP optimization problem is written in the form shown below.

$$\begin{aligned}\text{minimize}\;\; \nabla_x \mathscr{L}(x_k,\lambda_k,\mu_k)d(x) + \frac{1}{2}d(x)^T H_{\mathscr{L}}(x_k,\lambda_k,\mu_k)d(x)\\ \text{over}\;\; d(x) \in \mathbb{R}^n\\ \text{subject to}\;\; h(x^k) + \nabla_x h(x^k)d(x) = 0\\ g(x^k) + \nabla_x g(x^k)d(x) \leq 0\end{aligned} \tag{2.28}$$

To solve this QP problem, Active Set Method via the software qpOASES is invoked to get the next iterate.

2.4.3. Active Set Method

Active Set Method is a time efficient optimal strategy to solve QP by creating a set of active constraints that are considered in the optimization problem's solution. ASM has the ability to determine which constraints will influence the final result of optimization and accordingly changes the set of constraints to find the optimal solution. Once the QP is designed, the ASM solves Eq (2.29) to find the next iterate x^{k+1}.

$$x^{k+1} = x^k + \alpha_k d^k \tag{2.29}$$

Here, ASM determines two key parameters: the search direction d_k and the step length α_k. Referring to the work of [53], the algorithm to determine these two parameters is explained here. To determine the search direction, at current iterate x^k the first step is to determine the set of active inequality constraints.

$$\mathscr{A}^k = \{j \mid g_j(x^k) + \nabla_x g_j^T(x)x^k = 0, j = 1, \ldots.., p\} \tag{2.30}$$

Ignoring α_k at this moment and substituting Eq (2.29) in Eq (2.28) gives the optimization problem of the form shown in Eq (2.31).

$$
\begin{aligned}
\min_{d} \ & \frac{1}{2}(x^k + d)^T H_{\mathscr{L}}(x^k + d) + \nabla_x \mathscr{L}(x^k + d) \\
\text{subject to } \ & h_i(x^k) + \nabla_x h_i(x)(x^k + d) = 0 \ , \ i = 1, ..., m \\
& g_j(x^k) + \nabla_x g_j^T(x)(x^k + d) = 0 \ , \ j \in \mathscr{A}^k
\end{aligned}
\tag{2.31}
$$

On expanding the problem above (Refer to [53] for all the steps), the final form of the optimization problem obtained is shown in Eq (2.32).

$$
\begin{aligned}
\min_{d} \ \frac{1}{2}(d^T H_{\mathscr{L}} d) + \left(H_{\mathscr{L}} x^k + \nabla_x \mathscr{L}\right)^T d \\
\text{subject to } \ \nabla_x h(x) d = 0 \\
\nabla_x \tilde{g}(x) d = 0
\end{aligned}
\tag{2.32}
$$

where,

$$
\tilde{g}(x) = \begin{bmatrix} . \\ . \\ \nabla_x g_j^T(x) \\ . \\ . \end{bmatrix} \ , \ j \in \mathscr{A}^k
\tag{2.33}
$$

Setting,

$$
g^k = \left(H_{\mathscr{L}} x^k + \nabla_x \mathscr{L}\right)
\tag{2.34}
$$

to obtain the search direction d^k, the objective is to solve the equality constrained QP of the form shown in Eq (2.35).

$$
\begin{aligned}
\min_{d} \ \frac{1}{2}(d^T H_{\mathscr{L}} d) + \left(g^k\right)^T d \\
\text{subject to } \ \nabla_x h(x) d = 0 \\
\nabla_x \tilde{g}(x) d = 0
\end{aligned}
\tag{2.35}
$$

By applying the algorithms to solve the equality constrained QP such that the KKT conditions (mentioned in Eq (2.36)) are satisfied, the search direction d^k is obtained.

$$
\begin{aligned}
H_{\mathscr{L}} d + g^k + \nabla_x h^T(x) \lambda^k + \nabla_x \tilde{g}^T(x) \mu^k = 0 \\
\nabla_x h(x) d^k = 0 \\
\nabla_x \tilde{g}(x) d^k = 0
\end{aligned}
\tag{2.36}
$$

Two possible cases can arise on solving this optimization:

- $d^k = 0$

- $d^k \neq 0$

For the case if $d^k = 0$, two scenarios can arise.

Case 1: $d^k = 0$ and $\mu^k \geq 0$

$$x^{k+1} = x^k \text{ is a KKT point} \tag{2.37}$$

Case 2: $d^k = 0$ and $\mu^k < 0$

In this case, the obtained solution is not the optimal one. By making an assumption $\mu_{j_0} = \min\{\mu_j \mid \mu_j < 0,\ j \in \mathscr{A}^k\}$, the corresponding negative μ with index j_0 is removed from the active set $\mathscr{A}^k$ and the QP in Eq (2.32) is again solved with only change in the defined set in Eq (2.33) now to $j \in \mathscr{A}^k \sim \{j_0\}$.

In the case if the descent direction is non-zero i.e. $d^k \neq 0$, one needs to then determine the step length α^k such that the next iterate (Eq (2.29)) is defined. Based on checking and satisfying all the conditions, elaborated in [53], the final formula to calculate α^k is given in Eq (2.38).

$$\alpha_k = \min\left\{1, \frac{\nabla_x g_j(x) - \nabla_x g_j^T(x) d^k}{\nabla_x g_j^T(x) d^k} \mid j \notin \mathscr{A}^k \text{ and } \nabla_x g_j^T(x) d^k > 0\right\} \tag{2.38}$$

In the event if $\alpha^k < 1$, the active set needs to be updated as $\mathscr{A}^{k+1} = \mathscr{A}^k \cup j_0$.

This is the entire process of the ASM method. By defining an active set based on inequality constraints, those inequality constraints are converted to equality constraints and an equality constrained QP is solved to get the search direction d^k. After calculating the optimal step length α^k by either updating or not updating the active set $\mathscr{A}^k$, the next iterate x^{k+1} is defined which is the optimal solution to the NLP optimization problem. This process is repeated for the entire prediction horizon to get a set of optimal solutions of the optimization problem and the subsequent control action.

2.5. Summary

This chapter gave a brief description about MPC and its principal design elements to provide the reader sufficient context in understanding how this control scheme is designed and used for control. This is necessary as the entire research was focused on using LMPC and NMPC for vehicle control. Then, an introduction to software ACADO was reported in which the three controllers designed in this research were formulated. MPC is an optimal control as it solves the OCP. In this research, this OCP is solved online using ACADO to ensure real-time feasibility is nor compromised. The method to solve the OCP involves the use of SQP and ASM which were then explained in depth to provide the reader with some perspective about optimization techniques and their modelling.

3

MPC Controller Design

3.1. Introduction

This chapter contains all the dynamic prediction model formulations and OCP constraint formulations for the three controllers designed in this research. The idea to design three controllers was to show gradual improvements in the design made to achieve superior performance and to highlight successfully the claim made in the literature review by the author with three major conclusions as mentioned in Section 1.3. The chapter is divided in four sections, first section covering the vehicle dynamics coupling followed by each section corresponding to respective controller.

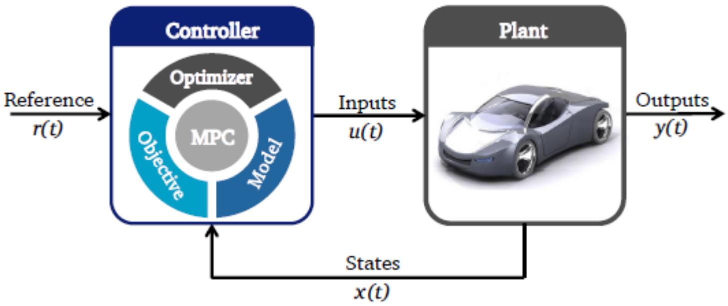

Figure 3.1: Vehicle control with MPC by [8]

3.2. Vehicle Dynamics Coupling

Grasping the knowledge of vehicle dynamics and its associated coupling effect is essential as it helps in understanding the vehicle behaviour during the maneuver. Based on this, the prediction model of the MPC can be effectively designed and intuitively understood regarding its capabilities to handle various dynamic scenarios. It gives an idea how contribution of each term in prediction model can potentially improve the predictions and overall control of vehicle. Designing an integrated control is a non-trivial problem due to the strong couplings in the vehicle dynamics. Listed by [54] and explained in depth by [55], three longitudinal and lateral coupling arises in case of vehicle motion:

- Kinematic and dynamic coupling

- Tire-road coupling
- Load transfer phenomenon

Kinematic and dynamic coupling
This coupling arises due to the yaw motion caused by the wheels steering. Steering angle affects the longitudinal dynamics by changing the direction of application of lateral cornering force on the steered wheels. When the wheels are steered at an angle relative to the vehicle body, the lateral cornering force on the steered wheels has a component in the longitudinal direction. On the other hand, longitudinal controls affects the lateral dynamics in two major ways:

- The lateral centripetal force is a function of the longitudinal velocity and the curvature of travel
- The rate of lateral deviation from the road center is also a function of longitudinal velocity when the vehicle heading is not aligned with the road center-line. This is shown in the prediction model's Eq (3.40)

Tire-road coupling
This is a surface based coupling because of the application of lateral and longitudinal traction forces by the tire. For a given coefficient of friction, the magnitude of the resultant of lateral and longitudinal forces on each tire is limited by the so-called friction ellipse. Making an approximation of the ellipse into a circle, the coupling is well preserved in Eq (3.64) - Eq (3.67) of the Kamm circle. The fact that the tire friction forces are based on a non-linear relationship between tire force and tire slip, tire force coupling has an effect even when the tires are operating well below the saturation limit. The tire force coupling effect becomes increasingly significant as the friction forces on the tire approach saturation. The most extreme coupling occurs at saturation, at which point it becomes necessary to reduce the applied force in one direction in order to increase the applied force in the other.

Load transfer phenomenon
Arising because of the vehicle's longitudinal and lateral accelerations, a third form of coupling is a result of weight shift due to longitudinal acceleration which affects the lateral dynamics by redistributing the tire normal forces. Longitudinal accelerations change the weight distribution between the front and rear tires. Because the magnitude of lateral force produced for a given slip angle increases with increasing normal force, longitudinal weight shift results in a change in the vehicle yaw dynamics. In this manner, longitudinal acceleration has a significant effect on lateral dynamics. Lateral accelerations change the weight distribution between the left and right tires. Analogous to the effect on lateral force, tires with increased normal force will have smaller slip ratios to apply the same longitudinal force as the tires with reduced normal force.

Please note, the above description of all the coupling has been taken from [55] and the reader is advised to refer to the same for further elaborate understanding.

So, this gives an idea why designing an integrated control is challenging. The complex coupling affects the vehicle dynamics at all times and ensuring that the controller is able to understand these couplings is very crucial. In this research, the prediction model of the planar car NMPC controller (Eq (3.35) - Eq (3.49)) is modelled in such a way that the essential parts of the coupling is fairly captured.

In the linear regime of motion, the states of the vehicle varies and so do the tire slip angles and cornering stiffness. It is during the transient part of maneuver performed at limits of handling that the tire slip angles become large. This may lead to instability and phenomenon such as vehicle spinning out. The designed maneuver of single lane change is an excellent example to highlight this phenomenon and captures all the three couplings explained above.

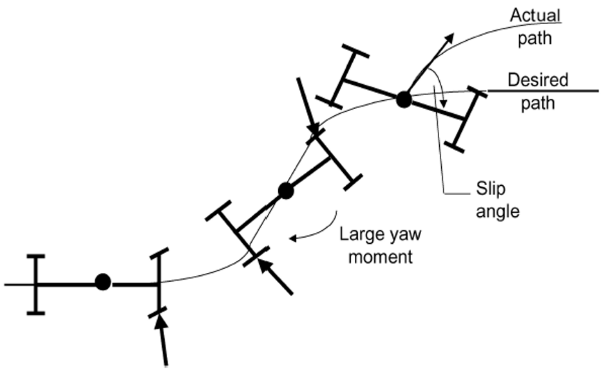

Figure 3.2: Graphical representation of Single lane change maneuver [9]

As shown in Fig 3.2 and explained in the words of [9], an emergency lane change maneuver involves first a left steer, saturating tire forces of both axles. Then the direction of steering wheel is changed rapidly, while vehicle is still yawing to the left (counterclockwise). This causes a change in the direction of lateral force of the front axle, but the lateral force at the rear axle lags that of the front axle. Both lateral forces, which are opposite in sign, generate a large clockwise yaw moment that begins to rotate the vehicle more rapidly. During a large portion of this maneuver, the cornering stiffness of the rear axle C_{α_r} is either negative or small positive, and vehicle is unstable. If this situation lasts long enough, and countersteering is not performed, the vehicle will develop a large slip angle and may spin out of control.

An active brake control, generates a yaw moment directly by developing longitudinal forces on one side of vehicle, but also indirectly by reducing the lateral force on the wheels to which brakes are applied, thus producing an additional change in the yaw moment. To eliminate the effect of laterally uneven weight distribution on longitudinal dynamics and to counter the situation of vehicle spinning out, differential braking via independent brake torques is used to address this situation using the commercial control system named VSC.

Thus, it can be qualitatively concluded that an integrated control has more capability in handling such critical event scenarios and should in principle give the best performance as compared to only steering control. In Chapter 6, this qualitative understanding will be quantitatively proven by performing the evasive single lane change maneuver under variety of scenarios.

3.3. LMPC - Linear Bicycle Model

The first controller was designed using a linear bicycle model to asses the performance of a linear controller for a nonlinear evasive maneuver. This was crucial because the first preference is always given to a linear model as it is less computationally expensive. It can also give an insight as to how formulation needs to improved to ensure the nonlinearity is well captured, in case if the linear model does not give desired performance.

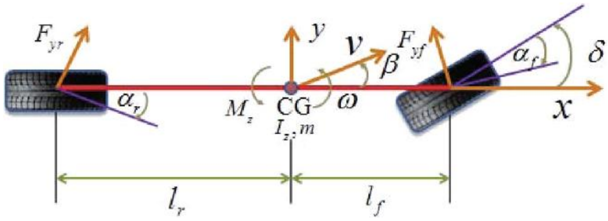

Figure 3.3: Bicycle model [10]

3.3.1. Prediction Model

The prediction model involved 7 states with standard linear bicycle model formulation as shown in Eq (3.1) - Eq (3.3). The assumptions made in this model were:

- Use of small angle approximation i.e. $\sin\theta \approx \theta$ and $\cos\theta \approx 1$
- Constant longitudinal velocity i.e. $a_x = 0$
- Clubbing of the respective front and rear two tires of the axle into one tire
- No longitudinal or lateral load transfer
- Use of linear tire model
- No roll, pitch and vertical motion considered
- No suspension and compliance effects considered
- Front left and front right wheel turn by same amount i.e. Ackermann geometry is not followed
- Effect of wheel slip is not considered

The controller's formulation of the complete linear bicycle prediction model is shown below in Eq (3.1) - Eq (3.7).

$$\dot{v}_x = v_y r \tag{3.1}$$

$$\dot{v}_y = -\left(\frac{C_{\alpha_f} + C_{\alpha_r}}{m v_x}\right) v_y + \left(\frac{l_r C_{\alpha_r} - l_f C_{\alpha_f}}{m v_x} - v_x\right) r + \left(\frac{C_{\alpha_f}}{m}\right)\delta \tag{3.2}$$

$$\dot{r} = \left(\frac{l_r C_{\alpha_r} - l_f C_{\alpha_f}}{I_{zz} v_x}\right) v_y - \left(\frac{l_r^2 C_{\alpha_r} + l_f^2 C_{\alpha_f}}{I_{zz} v_x}\right) r + \left(\frac{l_f C_{\alpha_f}}{I_{zz}}\right)\delta \tag{3.3}$$

$$\dot{\psi} = r \tag{3.4}$$

$$\dot{x}_p = v_x \cos(\psi) - v_y \sin(\psi) \tag{3.5}$$

$$\dot{y}_p = v_x \sin(\psi) + v_y \cos(\psi) \tag{3.6}$$

$$\dot{\delta} = d_\delta \tag{3.7}$$

Here, C_{α_f} and C_{α_r} are the combined cornering stiffness of the front and rear tires respectively, δ is the wheel angle for both the front wheels and d_δ is the control action which is the wheel angle velocity for both the front wheels. Since in a vehicle, one cannot implement full wheel angle δ directly but can increase or decrease it gradually, the control action throughout this research is the rate change. Lastly, as the controller is position tracking, the global position of the vehicle is also added in the prediction model in Eq (3.5) and Eq (3.6).

3.3.2. Constraints

Since vehicle is a mechanical unit with many electrical components, its performance is always bounded to certain working limits. Also, the vehicle stability is important at all times and therefore an envelope needs to be defined in which one can ensure the car remains stable. To do so, six constraints were defined as shown below.

$$0 \le v_x \le \frac{170}{3.6} \qquad \textit{bound on vehicle longitudinal velocity} \tag{3.8}$$

$$\frac{-5\pi}{180^o} \le \frac{v_y}{v_x} \le \frac{5\pi}{180^o} \qquad \textit{bound on vehicle bodyslip angle} \tag{3.9}$$

$$\frac{-25\pi}{180^o} \le \frac{\dot{v}_y}{v_x} \le \frac{25\pi}{180^o} \qquad \textit{bound on vehicle bodyslip rate} \tag{3.10}$$

$$\frac{-2.76\pi 360^o}{s_{\text{st}}180^o} \le \delta \le \frac{2.76\pi 360^o}{s_{\text{st}}180^o} \qquad \textit{bound on wheel angle} \tag{3.11}$$

$$\frac{-800^o\pi}{s_{\text{st}}180^o} \le \dot{\delta} \le \frac{800^o\pi}{s_{\text{st}}180^o} \qquad \textit{bound on wheel angle rate} \tag{3.12}$$

$$-0.85\mu g \le (\dot{v}_y + v_x r) \le 0.85\mu g \qquad \textit{bound on vehicle lateral acceleration } a_y \tag{3.13}$$

The first constraint limits the vehicle's speed to 170 km/hr which is the top speed of the vehicle. Constant value of 3.6 is used to convert the speed to SI units m/s. Now, to ensure vehicle stability, not only the bodyslip angle β but also the bodyslip angle rate $\dot{\beta}$ needs to to be bounded. Based on the concept of stable β - $\dot{\beta}$ reference region by [56] and the evaluations on the same phase plane by [57] and [58], it was seen that a bound of 5^o for β and $25^o/s$ for $\dot{\beta}$ were sufficient values to define a stable region for vehicle motion. The constraints defined ensure that the car remains within this stable region at all times and does not spin away. This is extremely essential. Since the bound of 5^o is small, therefore using the small angle approximation, $\tan\beta \approx \beta$ and then approximating, $\beta \approx v_y/v_x$ gives the 2 constraints as mentioned in Eq (3.9) and Eq (3.10).

Eq (3.11) and Eq (3.12) are the constraints on the SWA and SWV, which using the steering ratio s_{st} have been written in the form of wheel angle so as to directly bound the state. Instead of bounding the SWA to certain value based on an open-loop test which is usually done in the literature review, the idea here was to give the mechanical / electrical limit value as the bound on the states and then the MPC should be capable enough to calculate the optimal control action. One does not want to bound the controller to a certain value. It is more generic design if the maximum limit values are given so that the controller has the complete limit envelope to work and then it calculates the necessary control action required to perform the maneuver successfully. This contributes towards the idea of designing a generic control design.

The SWA can turn a maximum of 2.76 rotations. This has been converted to rad by multiplying it by $\pi/180^o$ as seen in Eq (3.12). Regarding SWV bound, based on multiple evasive maneuver tests performed by Daimler [30], it was seen that an average of $746^o/s$ was the SWV applied by the driver in the designed moose test. This is very high and can be considered as a suitable bound for this research. The steering system on the target Toyota vehicle of this research provided guaranteed performance capabilities up to $800^o/s$ SWV. The EPS motor specifications were checked and based on power rating, this value was within the electrical limits of the system and hence was chosen as the bound for SWV. Again, steering ratio s_{st} was used to write SWV in terms of wheel velocity.

The last constraint is crucial with regards to lateral movement of the vehicle. Since the designed maneuver involves evasive single lane change, bounding lateral acceleration is important to ensure that the vehicle is within the working limits. To bound a_y, equation from [59] was referred as shown below.

$$a_y = v_x r + tan\left(\beta\right)\dot{v}_x + \frac{v_x\dot{\beta}}{\sqrt{1+tan^2\left(\beta\right)}} \tag{3.14}$$

It was reported in [59] that if the vehicle bodyslip angle β is considered small, which in this case is assumed, then the second and third term of Eq (3.14) has a fraction of contribution to the final value of a_y. Considering only a 15% contribution (according to [59]), these last two terms of Eq (3.14) can be ignored and a suitable bound of $0.85\mu g$ on a_y is defined as seen in Eq (3.13).

The reference trajectory used in this research provides reference values for position, yaw angle and yaw rate i.e. y_{ref}, ψ_{ref} and r_{ref} respectively. Hence the cost function defined for this controller involved the states y_p, ψ and $\dot{\psi}$. Along with this, SWA in the form of wheel angle δ was also kept in cost function to control the magnitude of SWA as at higher speeds, high SWA and SWV may lead to vehicle spinning out and instability. Lastly, the control action on SWV in the form of wheel velocity d_δ was also in the cost function to keep a control of amount of control action required. The cost function thus formulated has the following form shown in Eq (3.15).

$$\begin{aligned} J_k = \sum_{i=1}^{N_p-1} \left[(X(k+i))^T Q_i (X(k+i)) + d_\delta(k+i-1)^T P_i d_\delta(k+i-1)\right] \\ +((X(k+N_p))^T S_i (X(k+N_p)) \end{aligned} \tag{3.15}$$

$$X(k+i) = \begin{bmatrix} \dot{\psi}(k+i) - r_{\text{ref}}(k+i) \\ \psi(k+i) - \psi_{\text{ref}}(k+i) \\ y_p(k+i) - y_{\text{ref}}(k+i) \\ \delta(k+i) \end{bmatrix} \tag{3.16}$$

Here, matrices Q, P and S are diagonal matrices containing the tuning parameter. This therefore defines the entire MPC formulation for the case of linear bicycle model.

3.4. NMPC - Nonlinear Bicycle Model

To further improve the formulation and capture the nonlinear dynamics of the maneuver, the next logical step was to design a nonlinear controller. As a result, a nonlinear bicycle model was used to design the next MPC controller. And therefore, to improve the performance, now a nonlinear tire model was used for higher accuracy and better calculation of tire forces. A Dugoff tire model was used in this research to capture the nonlinearity of the tire dynamics as shown in the below equations.

$$\mu = \mu_o \left(1 - e_r V_{x_{\text{ij}}} \sqrt{{\kappa_{\text{ij}}}^2 + \tan^2 \alpha_{\text{ij}}}\right) \tag{3.17}$$

$$\lambda = \frac{\mu F_{z_{t_{\text{ij}}}} \left(1 - \kappa_{\text{ij}}\right)}{2\sqrt{\left(C_{\kappa_{\text{ij}}} \kappa_{\text{ij}}\right)^2 + \left(C_{\alpha_{\text{ij}}} \tan\left(\alpha_{\text{ij}}\right)\right)^2}} \tag{3.18}$$

$$f(\lambda) = \begin{cases} \lambda(2-\lambda), & \lambda < 1 \\ 1, & \lambda \geq 1 \end{cases} \tag{3.19}$$

$$F_{x_{\text{ij}}} = \frac{C_{\kappa_{\text{ij}}} \kappa_{\text{ij}}}{1 - \kappa_{\text{ij}}} f(\lambda) \tag{3.20}$$

$$F_{y_{\text{ij}}} = \frac{C_{\alpha_{\text{ij}}} \tan\left(\alpha_{\text{ij}}\right)}{1 - \kappa_{\text{ij}}} f(\lambda) \tag{3.21}$$

Here, μ_o and e_r are tuning parameters. $V_{x_{\text{ij}}}$ is the each wheel's longitudinal velocity and was calculated using the Eq (3.22) - Eq (3.25).

$$V_{x_{\text{fl}}} = \left(v_y + l_f r\right) \sin(\delta) + \left(v_x - \frac{t_f r}{2}\right) \cos(\delta) \tag{3.22}$$

$$V_{x_{\text{fr}}} = \left(v_y + l_f r\right) \sin(\delta) + \left(v_x + \frac{t_f r}{2}\right) \cos(\delta) \tag{3.23}$$

$$V_{x_{\text{rl}}} = v_x - \frac{t_r r}{2} \tag{3.24}$$

$$V_{x_{\text{rr}}} = v_x + \frac{t_r r}{2} \tag{3.25}$$

Wheel slip angle α_{ij} was calculated using Eq (D.21) - Eq (D.24). And wheel slip κ_{ij} for each wheel was calculated by using the conditional equation shown in Eq (3.26) and Eq (3.27).

$$s_\kappa = sign\left(\omega_{\text{ij}} r_{\text{eff}} - V_{x_{\text{ij}}}\right) \tag{3.26}$$

$$\kappa_{\text{ij}} = \begin{cases} s_\kappa \frac{\left(\omega_{\text{ij}} r_{\text{eff}} - V_{x_{\text{ij}}}\right)}{V_{x_{\text{ij}}}}, & V_{x_{\text{ij}}} > \omega_{\text{ij}} r_{\text{eff}} \\ s_\kappa \frac{\left(\omega_{\text{ij}} r_{\text{eff}} - V_{x_{\text{ij}}}\right)}{\omega_{\text{ij}} r_{\text{eff}}}, & V_{x_{\text{ij}}} \leq \omega_{\text{ij}} r_{\text{eff}} \end{cases} \tag{3.27}$$

3.4.1. Prediction Model

Similar to the linear bicycle model, the prediction model for the nonlinear bicycle model involved 7 states. The assumptions made in this model were:

- Clubbing of the respective front and rear two tires of the axle into one tire
- No longitudinal or lateral load transfer
- No roll, pitch and vertical motion considered
- No suspension and compliance effects considered
- Front left and front right wheel turn by same amount i.e. Ackermann geometry is not followed
- Effect of wheel slip is not considered

The formulation of the complete nonlinear bicycle prediction model is shown in Eq (3.28) - Eq (3.34).

$$\dot{v}_x = \frac{F_{x_f} cos(\delta) - C_{\alpha_f}\left(\delta - \frac{v_y + l_f r}{v_x}\right) sin(\delta) + F_{x_r}}{m} + v_y r \tag{3.28}$$

$$\dot{v}_y = \frac{F_{x_f} sin(\delta) + C_{\alpha_f}\left(\delta - \frac{v_y + l_f r}{v_x}\right) cos(\delta) - C_{\alpha_r}\left(\frac{v_y - l_r r}{v_x}\right)}{m} - v_x r \tag{3.29}$$

$$\dot{r} = \frac{\left(F_{x_f} sin(\delta) + C_{\alpha_f}\left(\delta - \frac{v_y + l_f r}{v_x}\right) cos(\delta)\right) l_f + C_{\alpha_r}\left(\frac{v_y - l_r r}{v_x}\right) l_r}{I_{zz}} \tag{3.30}$$

$$\dot{\psi} = r \tag{3.31}$$

$$\dot{x}_p = v_x \cos(\psi) - v_y \sin(\psi) \tag{3.32}$$

$$\dot{y}_p = v_x \sin(\psi) + v_y \cos(\psi) \tag{3.33}$$

$$\dot{\delta} = d_\delta \tag{3.34}$$

Since the control action is again steering wheel velocity and no brakes are there to vary the longitudinal dynamics, the controller designed again is essentially lateral control. The longitudinal dynamics therefore in principal shall remain constant here as well. Hence the longitudinal tire forces F_{x_f} and F_{x_r} are kept constant throughout the prediction horizon. This is a design trade-off. Due to parameter uncertainty, the predictions might be slightly inaccurate but on the other hand, there is improvement in the formulation as now the dynamics in the longitudinal direction is also captured which was not the case with the linear bicycle model.

Also, the cornering stiffness now in prediction model is the fitted nonlinear cornering stiffness calculated from the Dugoff tire model. Rest of the formulation is similar to that of the linear bicycle model.

3.4.2. Constraints

The constraints again defined for this MPC controller is exactly similar to that of the six constraints defined in linear bicycle model (Eq (3.8) - Eq (3.13)). This is because the controller is again pure lateral control and the constraints defined before very well captures the working envelope region for the case of lateral controller. Finally, the cost function for this scheme is again same as linear bicycle model (Eq (3.15) - Eq (3.16)).

3.5. NMPC - Planar Car Model

The most important and probably the biggest contribution of this research is the design of the integrated control involving the control action of both steering and braking in synchronization for better vehicle control. To do so, it was necessary to give away with the assumption of lumping the front and rear tires on respective axles as one. By considering all the wheels separately, not only one can capture the vehicle dynamics more accurately, but the formulation naturally brings differential braking action into picture which was previously not possible with the bicycle models.

The controller designed here controls both the lateral and longitudinal dynamics simultaneously and therefore it is necessary that the prediction model and the constraints defined capture the relevant dynamics for both the directions well. Hence, a planar car model was used as the prediction model and constraints involving friction circle and Kamm circle were defined.

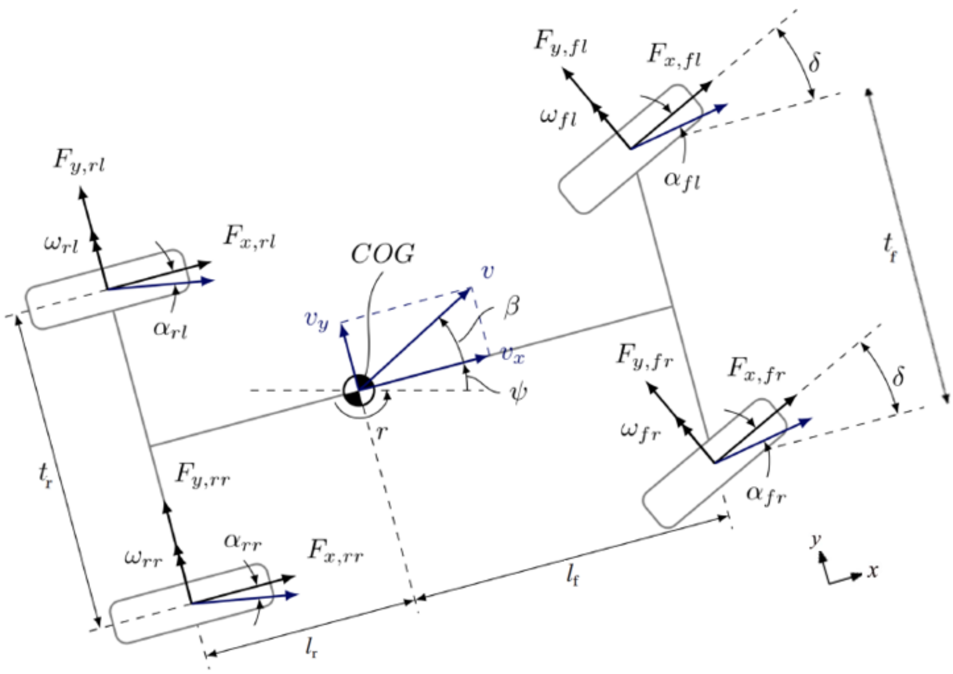

Figure 3.4: Planar car model [7]

3.5.1. Prediction Model

The prediction model used for the planar car NMPC involved 15 states and 5 control actions making it a MIMO system which an MPC controller is very efficient at handling. The prediction model involved no small angle approximation and had the relevant terms to capture the coupled dynamics. The approximations made in the formulation for this prediction model are mentioned below.

- No roll, pitch and vertical motion considered
- No suspension and compliance effects considered
- Front left and front right wheel turn by same amount i.e. Ackermann geometry is not followed
- Effect of wheel slip is not considered

By assuming that the pitch and roll motion in this combined steering and braking maneuver will be small and have no significant contribution to the dynamics, both roll ϕ and pitch θ angle dynamics were neglected from prediction model formulation. The 15 equations representing the planar car NMPC model is documented in Eq (3.35) - Eq (3.49).

$$\dot{v}_x = \frac{(F_{x_{\text{fl}}} + F_{x_{\text{fr}}})\cos(\delta) - (F_{y_{\text{fl}}} + F_{y_{\text{fr}}})\sin(\delta) + (F_{x_{\text{rl}}} + F_{x_{\text{rr}}})}{m} + v_y r \tag{3.35}$$

$$\dot{v}_y = \frac{(F_{x_{\text{fl}}} + F_{x_{\text{fr}}})\sin(\delta) + (F_{y_{\text{fl}}} + F_{y_{\text{fr}}})\cos(\delta) + (F_{y_{\text{rl}}} + F_{y_{\text{rr}}})}{m} - v_x r \tag{3.36}$$

$$\begin{aligned} \dot{r} = \big[&(F_{x_{\text{fl}}} + F_{x_{\text{fr}}})\sin(\delta)\, l_f + (F_{y_{\text{fl}}} + F_{y_{\text{fr}}})\cos(\delta)\, l_f - (F_{y_{\text{rl}}} + F_{y_{\text{rr}}})\, l_r \\ &+ \frac{t_f}{2}(F_{x_{\text{fr}}} - F_{x_{\text{fl}}})\cos(\delta) + \frac{t_f}{2}(F_{y_{\text{fl}}} - F_{y_{\text{fr}}})\sin(\delta) + \frac{t_r}{2}(F_{x_{\text{rr}}} - F_{x_{\text{rl}}})\big] / I_{zz} \end{aligned} \tag{3.37}$$

$$\dot{\psi} = r \tag{3.38}$$

$$\dot{x}_p = v_x \cos(\psi) - v_y \sin(\psi) \tag{3.39}$$

$$\dot{y}_p = v_x \sin(\psi) + v_y \cos(\psi) \tag{3.40}$$

$$\dot{\delta} = d_\delta \tag{3.41}$$

$$\dot{T}_{b_{\text{fl}_{\text{act}}}} = \frac{T_{b_{\text{fl}_{\text{cal}}}} - T_{b_{\text{fl}_{\text{act}}}}}{0.12} \tag{3.42}$$

$$\dot{T}_{b_{\text{fr}_{\text{act}}}} = \frac{T_{b_{\text{fr}_{\text{cal}}}} - T_{b_{\text{fr}_{\text{act}}}}}{0.12} \tag{3.43}$$

$$\dot{T}_{b_{\text{rl}_{\text{act}}}} = \frac{T_{b_{\text{rl}_{\text{cal}}}} - T_{b_{\text{rl}_{\text{act}}}}}{0.05} \tag{3.44}$$

$$\dot{T}_{b_{\text{rr}_{\text{act}}}} = \frac{T_{b_{\text{rr}_{\text{cal}}}} - T_{b_{\text{rr}_{\text{act}}}}}{0.05} \tag{3.45}$$

$$\dot{T}_{b_{\text{fl}_{\text{cal}}}} = d_{T_{b_{\text{fl}}}} \tag{3.46}$$

$$\dot{T}_{b_{\text{fr}_{\text{cal}}}} = d_{T_{b_{\text{fr}}}} \tag{3.47}$$

$$\dot{T}_{b_{\text{rl}_{\text{cal}}}} = d_{T_{b_{\text{rl}}}} \tag{3.48}$$

$$\dot{T}_{b_{\text{rr}_{\text{cal}}}} = d_{T_{b_{\text{rr}}}} \tag{3.49}$$

Here, to make the future predictions more accurate, the lateral and longitudinal forces ($F_{y_{\text{ij}}}$ and $F_{x_{\text{ij}}}$) were not kept constant throughout the prediction horizon, but was formulated in terms of the prediction model's states. This allowed that along the horizon, the forces also do vary, varying and improving the states evolution along the prediction horizon, the cost function, the optimization problem and ultimately the desired control action as well. This accuracy is very important for improved performance.

The equations used for the lateral forces are mention in Eq (3.50) - Eq (3.53).

$$F_{y_{\mathrm{fl}}} = \frac{C_{\alpha_{\mathrm{fl}}}\left(\delta - (v_y + l_f r)\right)}{v_x - \frac{t_f r}{2}} \tag{3.50}$$

$$F_{y_{\mathrm{fr}}} = \frac{C_{\alpha_{\mathrm{fr}}}\left(\delta - (v_y + l_f r)\right)}{v_x + \frac{t_f r}{2}} \tag{3.51}$$

$$F_{y_{\mathrm{rl}}} = \frac{C_{\alpha_{\mathrm{rl}}}\left(-(v_y - l_r r)\right)}{v_x - \frac{t_r r}{2}} \tag{3.52}$$

$$F_{y_{\mathrm{rr}}} = \frac{C_{\alpha_{\mathrm{rr}}}\left(-(v_y - l_r r)\right)}{v_x + \frac{t_r r}{2}} \tag{3.53}$$

And to model the longitudinal forces, the single corner tire model Eq (D.40) was used. The dynamics of a single corner model has been explained in Section D.4 in the Appendix. By making approximation that the wheel angular acceleration $\dot{\omega}$ is a noisy signal and is difficult to estimate in real-life, the term $\left(J_{\mathrm{yy_{ij}}}\dot{\omega}_{\mathrm{ij}}\right)$ from the LHS of Eq (D.40) was dropped. After rearranging the equation in terms of longitudinal force F_x, the final equation used to approximate the tire longitudinal force is mentioned in Eq (3.54).

$$F_{x_{\mathrm{ij}}} = \frac{T_{e_{\mathrm{ij}}} - T_{b_{\mathrm{ij_{act}}}}}{r_{\mathrm{eff_{ij}}}} \quad , \quad \mathrm{ij} = (\mathrm{fl}, \mathrm{fr}, \mathrm{rl}, \mathrm{rr}) \tag{3.54}$$

Substituting Eq (3.54) and Eq (3.50) - Eq (3.53) in the respective tire force terms of Eq (3.35) - Eq (3.37) gives the final formulation for the 15 state prediction model. The prediction model equations Eq (3.42) - Eq (3.45) are the equations capturing the brake actuator's dynamics. The reader is advised to refer Eq (D.45) in Section D.5.2 of Appendix for in-depth understanding of brake actuator modelling equations. Now, since the actuator delay is small for both the front and rear calipers, it has been ignored in the prediction model formulation. The idea is here to improve the estimates to get a better performance. While designing, one needs to carefully think which information is necessary for the prediction and which can be approximated.

By giving the actuator dynamics to the prediction model, the controller now understands how and at what rate will the brake pressure build up in each wheel's caliper, allowing accordingly to calculate the control action i.e. four brake torque rates $d_{T_{b_{\mathrm{ij}}}}$. The performance improvements due to this inclusion is shown in Chapter 6 through performing the maneuver with and without the brake actuator equations in the prediction model.

The second reason to include actuator dynamics in prediction model was to highlight the idea of 'one for all' control strategy which instead of only calculating the upper-level control action can now directly calculate the control action that needs to be applied to the wheels. Instead of separately designing control allocators, the idea here is to model those dynamics directly in one controller and design one such controller which can take care of all the three layers of control - upper level, lower level and actuator level. This integrated controller design is only possible with MPC due to its modular design concept.

The brake torques $T_{b_{\mathrm{ij}_{\mathrm{act}}}}$ represent the actual brake torques applied to the wheels i.e. the value after the brake actuator dynamics. Brake torques $T_{b_{\mathrm{ij}_{\mathrm{cal}}}}$ represents the values which are calculated before the effect of actuator dynamics. In reality with the VSC control, the control action is the brake pressure rate entering the brake actuators. Therefore the control action, apart from SWV (same as in bicycle model), are the brake torque rate change calculated before the actuator dynamics (Eq (3.46) - Eq (3.49)) to match the reality. It is the author's belief that by providing the actuator dynamics, the controller shall have the knowledge of performance losses to be compensated in order to achieve the final brake torque value $T_{b_{\mathrm{ij}_{\mathrm{act}}}}$. And by knowing this, the controller can beforehand modulate the control action accordingly to attain the calculated $T_{b_{\mathrm{ij}_{\mathrm{act}}}}$ value.

3.5.2. Constraints (Additional)

As mentioned before, the constraints were modelled with the aim of capturing both the dynamics well. Hence, the constraint design here has been changed to inculcate the same apart from the mechanical and electrical capabilities of the actuators which remains as before. A total of 19 constraints were defined, all active while solving the optimization problem. The first 5 constraints are same as that of the previous two bicycle model based MPC control i.e. Eq (3.8) - Eq (3.12) and therefore have not been mentioned here. This is because the simulation vehicle remains the same and so does its actuator limits as well. The equations for all the remaining 14 constraints is defined in Eq (3.55) - Eq (3.68).

$$(\dot{v}_x - v_y r)^2 + (\dot{v}_y + v_x r)^2 \leq (\mu g)^2 \qquad friction\ circle \tag{3.55}$$

$$0 \leq T_{b_{\mathrm{fl}_{\mathrm{act}}}} \leq 4885.8\ Nm \qquad maximum\ \mathrm{fl}\ brake\ torque\ bound \tag{3.56}$$

$$0 \leq T_{b_{\mathrm{fr}_{\mathrm{act}}}} \leq 4885.8\ Nm \qquad maximum\ \mathrm{fr}\ brake\ torque\ bound \tag{3.57}$$

$$0 \leq T_{b_{\mathrm{rl}_{\mathrm{act}}}} \leq 1614.3\ Nm \qquad maximum\ \mathrm{rl}\ brake\ torque\ bound \tag{3.58}$$

$$0 \leq T_{b_{\mathrm{rr}_{\mathrm{act}}}} \leq 1614.3\ Nm \qquad maximum\ \mathrm{rr}\ brake\ torque\ bound \tag{3.59}$$

$$-7023.3\ Nm/s \leq \dot{T}_{b_{\mathrm{fl}_{\mathrm{act}}}} \leq 7023.3\ Nm/s \qquad maximum\ \mathrm{fl}\ brake\ torque\ rate\ bound \tag{3.60}$$

$$-7023.3\ Nm/s \leq \dot{T}_{b_{\mathrm{fr}_{\mathrm{act}}}} \leq 7023.3\ Nm/s \qquad maximum\ \mathrm{fr}\ brake\ torque\ rate\ bound \tag{3.61}$$

$$-5549.1\ Nm/s \leq \dot{T}_{b_{\mathrm{rl}_{\mathrm{act}}}} \leq 5549.1\ Nm/s \qquad maximum\ \mathrm{rl}\ brake\ torque\ rate\ bound \tag{3.62}$$

$$-5549.1\ Nm/s \leq \dot{T}_{b_{\mathrm{rr}_{\mathrm{act}}}} \leq 5549.1\ Nm/s \qquad maximum\ \mathrm{rr}\ brake\ torque\ rate\ bound \tag{3.63}$$

$$\left(F_{x_{\mathrm{fl}}}\right)^2 + \left(F_{y_{\mathrm{fl}}}\right)^2 \leq \left(\mu_{\mathrm{fl}} F_{z_{\mathrm{fl}}}\right)^2 \qquad kamm\ circle\ bound\ on\ \mathrm{fl}\ tire \tag{3.64}$$

$$\left(F_{x_{\mathrm{fr}}}\right)^2 + \left(F_{y_{\mathrm{fr}}}\right)^2 \leq \left(\mu_{\mathrm{fr}} F_{z_{\mathrm{fr}}}\right)^2 \qquad kamm\ circle\ bound\ on\ \mathrm{fr}\ tire \tag{3.65}$$

$$\left(F_{x_{\mathrm{rl}}}\right)^2 + \left(F_{y_{\mathrm{rl}}}\right)^2 \leq \left(\mu_{\mathrm{rl}} F_{z_{\mathrm{rl}}}\right)^2 \qquad kamm\ circle\ bound\ on\ \mathrm{rl}\ tire \tag{3.66}$$

$$\left(F_{x_{\mathrm{rr}}}\right)^2 + \left(F_{y_{\mathrm{rr}}}\right)^2 \leq \left(\mu_{\mathrm{rr}} F_{z_{\mathrm{rr}}}\right)^2 \qquad kamm\ circle\ bound\ on\ \mathrm{rr}\ tire \tag{3.67}$$

$$\frac{T_{b_{\mathrm{rl_{act}}}} + T_{b_{\mathrm{rr_{act}}}}}{T_{b_{\mathrm{fl_{act}}}} + T_{b_{\mathrm{fl_{act}}}} + \epsilon} \leq \frac{\frac{l_f}{L} + \frac{h_{\mathrm{cg}}(\dot{v}_x - v_y r)}{gL}}{1 - \frac{l_f}{L} - \frac{h_{\mathrm{cg}}(\dot{v}_x - v_y r)}{gL}} \qquad \text{EBD}\ curve\ constraint\ (\epsilon = 0.001) \tag{3.68}$$

Now, explaining the constraint formulation, Eq (3.55) is the friction circle constraint defined now instead of constraining a_y only. This is because since the control is integrated in nature, it can control both lateral and longitudinal dynamics and therefore accordingly, the working envelope should be defined for controller to know the vehicle limits. The value of μ on the RHS bound of g-g constraint is taken to be the minimum of all the four μ of each tire respectively. Usually, there are three strategies for taking friction coefficient value for the g-g diagram:

- Minimum of all the four μ values
- Maximum of all the four μ values
- Average of all the four μ values

All the three methods are an approximation and limits the performance of the actual vehicle. But to ensure that the vehicle remains stable at all times, a conservative working envelope approach is utilized here and the minimum value of μ is taken as the bound for g-g constraint. Safety and stability over performance is chosen here.

The tires practically also show a working envelope for better driving and efficient control. Therefore, four kamm circle constraints are defined for each tire separately so that the condition of tire saturation is either avoided or minimized. Ideally, based on the behaviour of the tire forces, the maximum tire force values are bounded by Friction ellipse, but an approximation is considered here to formulate the bound as a circle than an ellipse for ease in modelling the constraint.

The expression for tire forces remains the same as mentioned in Eq (3.50) - Eq (3.53) and Eq (3.54). To define the right hand side of the bound, i.e. the normal load on each tire $F_{z_{\mathrm{ij}}}$ respectively, Eq (D.34) - Eq (D.37) from Section D.2.2 of Appendix was referred. Making assumption that all the sprung and unsprung masses are lumped as total mass m, roll angle ϕ is small and that the dynamic terms of roll and pitch motion are ignored, only the contribution from the static terms were taken, giving the normal load bound for each tire as shown in Eq (3.73) - Eq (3.76).

$$F_{z_x} = \frac{m(\dot{v}_x - v_y r) h_{\mathrm{cg}}}{2L} \tag{3.69}$$

$$F_{z_{y_f}} = \frac{m(\dot{v}_y + v_x r)}{t_f}\left(\frac{l_r h_{\mathrm{rf}}}{L} + \frac{K_{\phi,f} h}{K_{\phi,f} + K_{\phi,r} - mgh}\right) \tag{3.70}$$

$$F_{z_{y_r}} = \frac{m(\dot{v}_y + v_x r)}{t_r}\left(\frac{l_f h_{\mathrm{rr}}}{L} + \frac{K_{\phi,r} h}{K_{\phi,f} + K_{\phi,r} - mgh}\right) \tag{3.71}$$

$$h = h_{\mathrm{cg}} - \frac{l_r h_{\mathrm{rf}} + l_f h_{\mathrm{rr}}}{L} \tag{3.72}$$

$$F_{z_{\mathrm{fl}}} = F_{z,g}^{\mathrm{rear}} - F_{z_x} - F_{z_{y_f}} \tag{3.73}$$

$$F_{z_{\mathrm{fr}}} = F_{z,g}^{\mathrm{rear}} - F_{z_x} + F_{z_{y_f}} \tag{3.74}$$

$$F_{z_{\mathrm{rl}}} = F_{z,g}^{\mathrm{front}} + F_{z_x} - F_{z_{y_r}} \tag{3.75}$$

$$F_{z_{\mathrm{rr}}} = F_{z,g}^{\mathrm{front}} + F_{z_x} + F_{z_{y_r}} \tag{3.76}$$

With Kamm circle defined, Eq (3.56) - Eq (3.63) define the brake actuator limits in terms of maximum brake torque and rates. Lastly, Eq (3.68) defines the front to rear brake torque distribution ratio based on EBD curve shown in Fig 3.5 for optimal brake torque distribution , with the constraint's RHS defining the equation to get the EBD curve [60]. In a straight-line driving, when a vehicle brakes, it pitches forward, increasing the normal load of the front tires. Therefore the ability of the front tires to generate brake force increases as compared to rear ones. Hence, usually in a straight-line driving, the front tires brake more than the rear tires. Since this was not modelled in the prediction model, an additional constraint, which is only activated during straight-line driving, was defined with ϵ in denominator to ensure mathematical infeasibility is avoided.

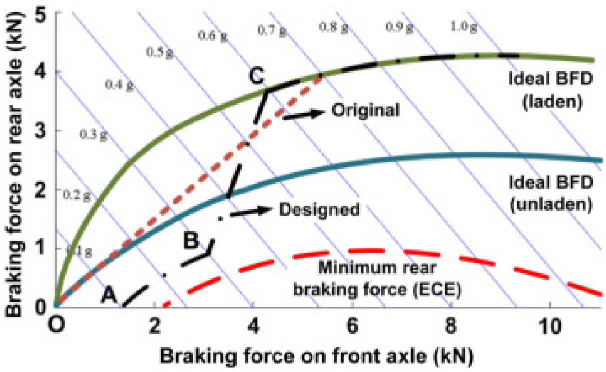

Figure 3.5: EBD curve for front-rear brake distribution by [11]

It is to be noted here that, the acceleration terms throughout the prediction model and constraints have not been kept constant along the prediction horizon. Instead dynamic equations $a_x = (\dot{v}_x - v_y r)$ and $a_y = (\dot{v}_y + v_u r)$ have been used based on the prediction model states defined so that along the prediction horizon, these values as well as the bounds in the constraints dynamically vary, making the predictions more accurate, leading to better control.

Finally, the cost function for this NMPC controller is modified due to change in the prediction model states. The formulation of cost function still uses 2-norm square method with terminal cost terms. The cost function thus defined is shown in Eq (3.77) and Eq (3.78). The reason to include the brake torques in the cost function is to ensure that minimum control action energy is utilized to perform the maneuver. This has been well explained in Section 5.5 of this report.

$$\begin{aligned} J_k = \sum_{i=1}^{N_p-1} \left[(X(k+i))^T Q_i (X(k+i)) + U(k+i-1)^T P_i U(k+i-1) \right] \\ + ((X(k+N_p))^T S_i (X(k+N_p)) \end{aligned} \tag{3.77}$$

$$X(k+i) = \begin{bmatrix} v_x(k+i) \\ \dot{\psi}(k+i) - r_{\text{ref}}(k+i) \\ \psi(k+i) - \psi_{\text{ref}}(k+i) \\ y_p(k+i) - y_{\text{ref}}(k+i) \\ \delta(k+i) \\ T_{b_{\text{fl}_{\text{act}}}}(k+i) \\ T_{b_{\text{fr}_{\text{act}}}}(k+i) \\ T_{b_{\text{rl}_{\text{act}}}}(k+i) \\ T_{b_{\text{rr}_{\text{act}}}}(k+i) \\ T_{b_{\text{fl}_{\text{cal}}}}(k+i) \\ T_{b_{\text{fr}_{\text{cal}}}}(k+i) \\ T_{b_{\text{rl}_{\text{cal}}}}(k+i) \\ T_{b_{\text{rr}_{\text{cal}}}}(k+i) \end{bmatrix}, \qquad U(k+i) = \begin{bmatrix} d_\delta(k+i) \\ d_{T_{b_{\text{fl}}}}(k+i) \\ d_{T_{b_{\text{fr}}}}(k+i) \\ d_{T_{b_{\text{rl}}}}(k+i) \\ d_{T_{b_{\text{rr}}}}(k+i) \end{bmatrix} \tag{3.78}$$

3.6. Summary

This chapter involved the complete formulation of all the three MPC controllers designed in this research. An extensive and detailed description of the prediction model and the constraints defined for each controller respectively was given. Reasoning for each constraint defined was explained along with equations used to defined the normal loads for kamm circle constraint and EBD curve. While the first two controllers involved the use of bicycle model as dynamic prediction model with SWV as control action, the third controller used planar car model formulations for its prediction model with control action both SWV and brake torque rates for each wheel, giving the final MIMO combined control.

4

Simulation Architecture

4.1. Introduction

This chapter provides the entire workflow of how the simulation was designed and implemented in Simulink with co-simulation architecture comprising three different softwares. Of the three layer control strategy, Chapter 3 covered the third layer i.e. the control architecture. This chapter will focus on the remaining two layers, decision making and reference trajectory. This will be followed by the formulation of single lane change maneuver that was performed in this research along with the KPI's defined for performance assessment. Finally, as seen in all the prediction models of the three controllers, the lateral control involves the use of tire cornering stiffness. The tire property analysis performed to get these cornering stiffness values will also be explained here.

4.2. Workflow

The co-simulation IPC architecture was used in this research to achieve results which are close representation of real-life scenarios. Fig 4.1 represents in-detail the simulation architecture designed in Simulink along with IPG CarMaker and ACADO as one framework to perform all the simulations accurately.

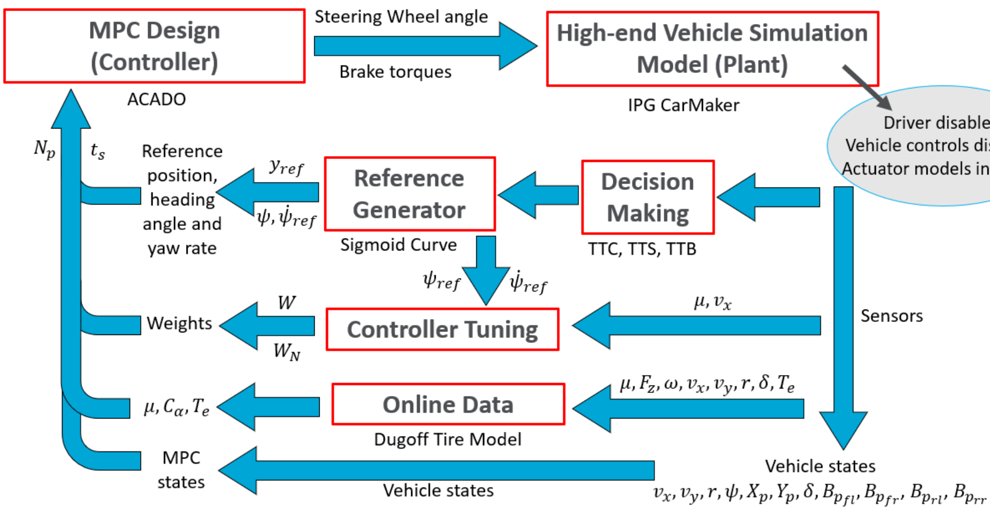

Figure 4.1: Simulation workflow architecture

To simply explain the structure, the first block is the 'Decision Making' where using parameters TTC, TTB, TTS defined in Section 4.3, the decision is made whether to steer or to brake. Once the decision, which in this research is steering, is made then the next step is to generate a reference trajectory. Here, a mathematical formulation using Sigmoid curve is used to get the reference position, heading angle and yaw rate and the equations used to formulate this curve is explained in Section 4.4. This reference information is then passed to the controller.

Now, apart from the reference values, the controller also needs certain other information before it solves the optimization problem, with the optimization settings already embedded in the 'Controller' block. The first thing is to get the updated information of all the states of the prediction model to know at current instant, what exactly are the parameter values of the vehicle. Thus, all these values are measured / estimated by vehicle sensors / estimators and passed to the controller.

Apart from the prediction model state's data, the controller designed also requires some additional data for the calculation of control action. In ACADO's language, this data is referred to as 'Online Data' which has been represented by the same name in Fig 4.1 as well. The three main parameters required as 'Online Data' are:

- Friction coefficient μ
- Tire's cornering stiffness C_α
- Wheel's drive torque T_e

There are estimators which can estimate and provide the value of friction coefficient for each wheel [61]. Using the engine output torque along with the gear reduction ratios, the drive torque at each wheel can also be estimated. To get the cornering stiffness, analysis on the tire property file was performed to generate a look-up table with inputs to the table being μ and F_{z_t}. And here, a Dugoff tire model was used to get the nonlinear fitted cornering stiffness values.

Lastly, the final information required by the controller is the tuning weights of the cost function. Here, a novel real-time cost function update method was designed by the author for improved performance. This update method is described in Chapter 5 and as seen from the workflow chart, requires only the reference yaw and yaw rate from reference generator to work. Once the controller's tuning parameters are set, they are passed on to the controller and the optimization problem is completely defined.

Based on the solution of the optimization problem, the desired control action is calculated and later converted using certain gains to SWA, SWV, SWAcc and final brake torques. This is then sent to the plant which is the multi-body Toyota vehicle modelled in IPG CarMaker. This vehicle model also contains the actuator dynamics very well to mimic the real-life dynamics of the overall vehicle. Naturally, an actuator is a mechanical or electrical component and therefore has certain design constraints and working limits in which it can work efficiently. Also, it is associated with wear and tear and performance losses which can affect vehicle control.

The steering actuator considered here is the state-of-the-art steering model developed by Toyota and used in their simulator. The brake actuators i.e. the calipers were modelled using a first order transfer function to capture the brake pressure build-up characteristics and associated delays. All the equations and in-depth explanation of the actuator dynamics have been documented in Section D.5 for better understanding. Now, once the control action is implemented on the vehicle via the actuators, the vehicle sensor then records the necessary information which is then used to calculate all the other parameters and MPC states defined above, thus closing the loop. Hence, it is clear that MPC is a closed-loop feedback controller and therefore has been modelled accordingly.

4.3. Decision Making

In this research, three basic decision making parameters Time To Collision (TTC), Time To Brake (TTB) and Time To Steer (TTS) were used mainly to decide the speed range in which the designed maneuver shall be performed. This is explained in Section 4.5. This section describes the equations used to calculate the decision making parameters.

TTC is defined as *"the time required for two vehicles to collide if they continue at their present speed and on the same path (i.e. same steering angle)"* [62]. This parameter clearly highlights the available time to avoid the otherwise imminent collision. Given the lead vehicle's longitudinal position and speed as $X_o(t)$ and $\dot{X}_o(t)$ respectively, l_e is the length of the subject vehicle and the subject vehicle's longitudinal position and speed as $X_e(t)$ and $\dot{X}_e(t)$, TTC can be calculated based on Eq (4.1) defined by [62].

$$TTC = \frac{X_o(t) - X_e(t) - l_e}{\dot{X}_e(t) - \dot{X}_o(t)} \quad \forall \;\; \dot{X}_e(t) > \dot{X}_o(t) \tag{4.1}$$

TTB denotes the remaining time until an emergency braking at maximum deceleration must be applied to avoid the collision by braking. It is the time when the braking needs to be commenced. Based on [63], TTB is calculated as shown in Eq (4.2).

$$TTB = -\frac{p_{x,\text{brake}}}{v_{x,0}} = \frac{v_{x,0}}{2a_{x,e}} \tag{4.2}$$

Here, $p_{x,\text{brake}}$ is the distance travelled by the subject vehicle once the brakes are applied, $v_{x,0}$ is the initial longitudinal velocity of the subject vehicle and $a_{x,e}$ is the longitudinal acceleration value of the subject vehicle.

Finally, TTS is the time at which steering needs to be commenced to avoid collision. Based on [63], TTS can be calculated using Eq (4.3).

$$TTS = \min\left(\sqrt{\frac{2}{a_{y,e}}\left(y_0 \pm \frac{w_e + w_o}{2}\right)}\right) \tag{4.3}$$

Here, $a_{y,e}$ is the lateral acceleration of the subject vehicle, y_0 is its initial lateral position, w_e is the lateral movement of the subject vehicle and w_o is lead vehicle's lateral movement.

It can be seen that the Eq (4.1) - Eq (4.3) are derived from the three Newton's Laws of Motion, thus considering the vehicle as point mass. Even though they are not accurate, the equations do give a decent idea about the situation of collision in general. Since decision making is not the key focus of this research, these point mass equations were sufficient to serve the purpose.

4.4. Reference Generator

The reference trajectory is an integral part of the path following controller. The accurate the reference generator formulation, the better and more realistic are the reference values leading to potential better control. But, in order to really asses the performance of the controllers designed, the idea was to not use a way-point generator that considers the vehicle dynamics in its formulation. Rather, a kinematic model using a mathematical equation was used to generate the reference path. By doing so, one can see the behaviour of controller in case the path is not dynamically feasible to be performed.

The vehicle certainly has certain performance limits as it is a mechanical machine after all. The idea was to remove these limitations by using a kinematic model which gives unrealistic path points, but to model the dynamics of the car wisely in the controller and see if the controller is able to understand the dynamics well and provide necessary control with a not-so-accurate reference trajectory.

A variety of kinematic trajectory models were found in the literature to get the desired reference points. These models have been well summarized by the author in the literature review report [36]. The main models found have been listed below but the reader is advised to refer [36] to understand the mathematical formulas behind the formulation. The kinematic reference generation models are:

- Sigmoid Curve
- n^{th} order polynomial curve using Way-point generator
- Geometrical Designing

In this research, Sigmoid curve was used to generate the reference trajectory curve. Since the maneuver to be performed is a single lane change, the trajectory will have two turning points. By theory, Sigmoid curve, due to its equation, gives the highest smoothness at those points (up to infinite order) and hence was chosen. Referring to [12], the formulations to define the Sigmoid curve is mentioned in Eq (4.4) - Eq (4.14).

$$C_1 = \log\left(\frac{B}{y_{\text{tol}}} - 1\right) \tag{4.4}$$

$$k_1 = \frac{(Bx_1)^2}{16} - \frac{(BC_2)^2}{16} \tag{4.5}$$

$$k_2 = -\frac{B^2 x_1 C_1}{8} - \frac{B y_1 x_1}{2} + \frac{B^2 x_1}{4} \tag{4.6}$$

$$k_3 = \frac{(BC_1)^2}{16} + y_1^2 + \frac{B^2}{4} + \frac{B y_1 C_1}{2} - B y_1 - \frac{B^2 C_1}{4} - C_2^2 \tag{4.7}$$

$$a = \frac{-k_2 + \sqrt{k_2^2 - 4k_1k_3}}{2k_1} \tag{4.8}$$

$$c = \frac{C_1}{a} \tag{4.9}$$

$$y_{\text{ref}} = \frac{B}{1 + e^{-a(x-c)}} \tag{4.10}$$

$$\frac{\partial y_{\text{ref}}}{\partial x} = \frac{aBe^{-a(x-c)}}{(1 + e^{-a(x-c)})^2} \tag{4.11}$$

$$\psi_{\text{ref}} = tan^{-1}\left(\frac{\partial y_{\text{ref}}}{\partial x}\right) \tag{4.12}$$

$$\kappa_1 = \frac{\left(\frac{\partial^2 y_{\text{ref}}}{\partial x^2}\right)}{\left(1 + \left(\frac{\partial y_{\text{ref}}}{\partial x}\right)^2\right)^{\frac{3}{2}}} \tag{4.13}$$

$$\dot{\psi}_{\text{ref}} = \kappa_1 v_x \tag{4.14}$$

Here, Eq (4.10) represents the sigmoid curve equation (a function of vehicle's longitudinal position x) used to give the reference lateral coordinates for path tracking. Eq (4.12) and Eq (4.14) provide the reference heading angle and yaw rate respectively to ensure that the vehicle tracks the reference by actually turning the car (Fig 4.2) and not just by skidding or drifting. It is essential to provide reference to both path and the way to track that path i.e. the yaw angle.

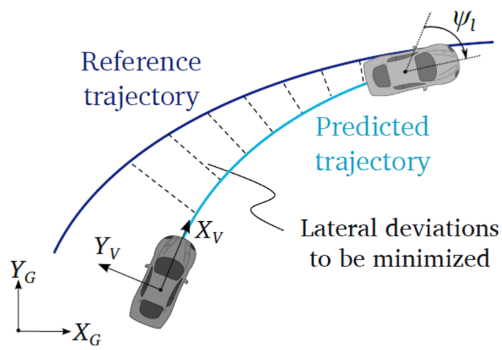

Figure 4.2: Vehicle tracking by turning and not skidding [8]

The notation B refers to lateral displacement to be achieved by the subject vehicle, a is the slope of the sigmoid curve, (x_1, y_1) are the coordinates of the obstacle vehicle's rear-left corner, y_{tol} is the initial lateral displacement of the subject vehicle at the beginning of the maneuver, C_2 is the pre-defined minimum length which is a tuning parameter and κ_1 is the trajectory curvature. The boundary conditions met by the sigmoid curve is defined below.

$$\begin{aligned} y_{\text{ref}}(0) &= y_{\text{tol}}, \\ y_{\text{ref}}(2c) &= B - y_{\text{tol}}, \end{aligned} \tag{4.15}$$

Once all the perimeters of the reference generator are defined accordingly to represent the desired maneuver to be performed, a representation of how the reference path looks when formulated by sigmoid curve is shown by dashed lines in Fig 4.3.

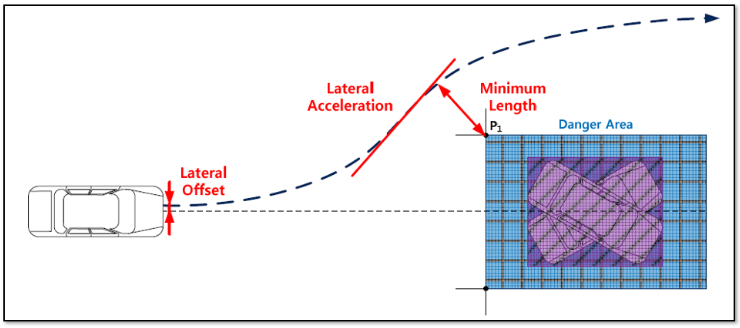

Figure 4.3: Reference trajectory by sigmoid curve [12]

4.5. Single lane change maneuver

The next step taken in the research was to finalize a maneuver that is evasive in nature to represent a rear-end collision scenario. But the issue was that there was no standard single lane change maneuver defined for assessment of evasive performance. All the standard organizations such as SAE, NHTSA, ISO and Euro NCAP were referred but none of them had an evasive maneuver defined as a standard test.

The idea was then to perform a literature survey and identify surrounding conditions in which the rear-end collision generally happens so that a similar scenario can be constructed in simulation environment as well. Based on this review, a NHTSA article [64] gave key insights into the real-life scenarios in which the rear-end collision is commonly seen. The NHTSA in [64] calls a rear-end crash, happened as a result of evasive action, by the term 'near-crash' with the formal definition being:

Near-Crash: Any circumstance that requires a rapid, evasive maneuver by the subject vehicle (or any other vehicle, pedestrian, cyclist, or animal) to avoid a crash. A rapid, evasive maneuver is defined as steering, braking, accelerating, or any combination of control inputs that approaches the limits of the vehicle's capabilities. As a guide, subject vehicle braking greater than 0.5g or steering input that results in a lateral acceleration greater than 0.4g to avoid a crash constitutes a rapid maneuver.

In their research, [64] collected the crash data of 100 different cars such as the timing and location of where drivers were looking, the timing of accelerator release and brake application, as well as the driver's time and force modulation of the brake pedal. This was then used to get further insight into the causes, characteristics, and potential countermeasures for rear-end crashes.

On analysing their result under varying event conditions, it was concluded that a rear-end collision mostly happens in a business/industrial area in daylight. The collision frequently happens on a straight road with no junctions, giving an idea about how the maneuver should be defined. It was observed that the near-end collision is mostly seen at straight line driving with constant speed. Thus, one can conclude that the potential maneuver for this thesis should be performed on a straight, non-junction road and should be designed such that the subject vehicle is driving straight at constant speed. A single lane change maneuver, which has been mostly found in the literature as well, covers all these conclusions and was therefore chosen as the maneuver for evasive action.

To design this maneuver with realistic parameters, the research from Ford Motors regarding evasive steering was referred [13]. In their controller design for evasive steering, [13] uses a single lane change maneuver as shown in Fig 4.4.

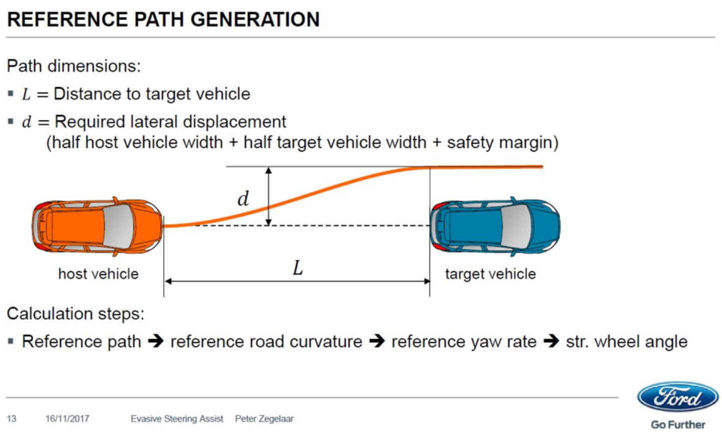

Figure 4.4: Single lane change maneuver [13]

Here, parameter d as shown in Fig 4.4 represents the total lateral displacement the SV has to traverse to change the lane and avoid the collision with LV. Parameter L of Fig 4.4 represents the relative longitudinal distance between the SV and LV at which the maneuver begins. Both these parameters are referred to as d_{ref} and L_{ref} respectively in this research. The values taken for both these parameters by [13] has been mentioned in Table 4.1.

S No.	Parameter	Value
1	d_{ref}	$2.5m$
2	L_{ref}	$30m$

Table 4.1: Maneuver settings by [13]

Thus, the SV initiates the maneuver when it is $30m$ away from LV and to avoid the collision, the SV has to traverse $2.5m$ to the left of the LV as shown in Fig 4.4, giving the evasive maneuver as a single lane change maneuver. Now, the only parameter remaining to define the maneuver fully is the SV's speeds at which the maneuver needs to be performed. To ensure that the maneuver remains evasive at all times, the formulas for TTC, TTB,and TTS were used to define the speed range based on varying road friction coefficient μ.

By assuming that the LV is at rest, the formulas for the *Decision Making* parameters were modified to the representation as shown in Eq (4.16) - Eq (4.18).

$$TTC_{\text{new}} = \frac{L_{\text{ref}}}{v_x} \tag{4.16}$$

$$TTB_{\text{new}} = \frac{v_x}{2a_{x_{\max}}} \tag{4.17}$$

$$TTS_{\text{new}} = \sqrt{\frac{2d_{\text{ref}}}{a_{y_{\max}}}} \tag{4.18}$$

Ensuring that the evasiveness of the maneuver is well-captured, the values of maximum achievable lateral and longitudinal acceleration for the SV were taken higher than the prescribed values mentioned by [64] in their definition of *near-crash*. The values thus taken were:

$$a_{x_{\max}} = 0.8\mu g \tag{4.19}$$

$$a_{y_{\max}} = 0.6\mu g \tag{4.20}$$

Hence, for a given μ, the SV's velocity v_x was varied and the three parameters were calculated. This was done for μ ranging from 0.1 till 1 with increments of 0.1. The plot obtained for the case of dry road i.e $\mu = 0.9$ is shown in this report in Fig 4.5 but the plot's trend remained the same for all other friction coefficients.

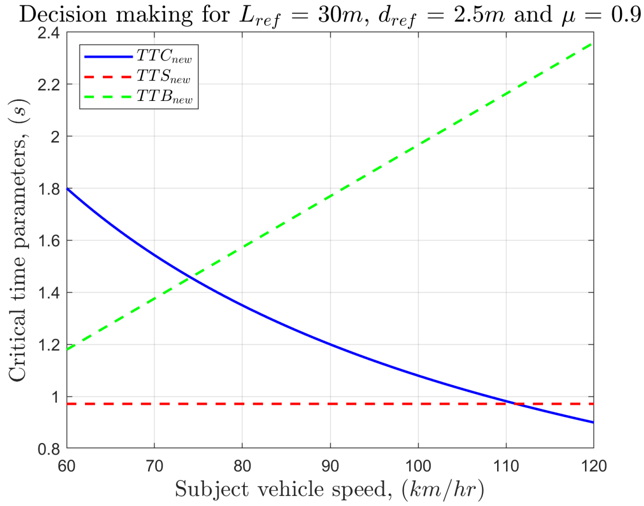

Figure 4.5: Decision making parameters for $\mu = 0.9$

It can be seen that for the same collision distance of $30m$, as the vehicle speed increases, the maneuver becomes more aggressive and therefore TTC_{new} value decreases. At the same time, the TTB_{new} increases with higher speeds because it will take more time for the car to come to full stop as the speed increases. Since the total lateral displacement is fixed at $2.5m$, the TTS_{new} value remains the same for all speeds. The area of the graph in Fig 4.5 in which the TTC_{new} line is above the TTB_{new} line is the region where the rear-end collision can be avoided by braking. The region where TTC_{new} line is between TTB_{new} and TTS_{new} are the vehicle speeds at the which the collision can be avoided only by steering. And the region where TTC_{new} is below both TTB_{new} and TTS_{new} is the area where the collision is imminent and cannot be avoided by steering as well. In this case, the best strategy is mitigate the effect of collision by braking hard and reducing vehicle speed.

Since the research focuses on steering to avoid the collision, the vehicle speeds where TTC_{new} line is between TTB_{new} and TTS_{new} were taken as the speeds at which the maneuver needs to be performed. Table 4.2 summarizes the speeds and the TTC_{new} values for all the friction coefficients. It can be clearly seen that as the friction coefficient decreases, the tires will have lesser grip and therefore the speeds at which the evasive maneuver can be performed also decreases. Also, the TTC values can be seen very small, with average around $1.5s$ highlighting that in fact the maneuver is aggressive and is a good representation for evasive action. The speeds here are derived purely using the theoretical point mass calculation and has no dynamic component of the vehicle. Thus, one cannot guarantee that the collision will be avoided at all speeds but these values gives a good ball-park of what speeds the maneuver should be performed.

S No.	μ	$v_{x_{\min}}$	$TTC_{\min}$	$v_{x_{\max}}$	$TTC_{\min}$
-	-	[km/hr]	[s]	[km/hr]	[s]
1	1	78	1.38	115	0.93
2	0.9	75	1.44	110	0.98
3	0.8	70	1.54	102	1.06
4	0.7	65	1.66	97	1.13
5	0.6	60	1.80	90	1.20
6	0.5	55	1.96	82	1.31
7	0.4	50	2.16	72	1.50
8	0.3	43	2.51	64	1.68
9	0.2	35	3.08	50	2.16
10	0.1	25	4.32	35	3.08

Table 4.2: Reference maneuver speed range and TTC values

In the simulations, the speeds were incremented with $5km/hr$ until the collision could not be avoided by the controller. Thus by defining all the key parameters, μ and vehicle speeds of maneuver, the single lane change maneuver was completely defined.

4.6. Manuever KPI's

The final step before the simulations were performed was to fix the KPI's based on which a quantitative and subjective evaluation of the controller's performance can be performed to make realistic conclusions. There were no standard list of KPI's found in the literature as the maneuver itself has no standardized formulation yet. To get meaningful set of KPI's that represent the controller's performance well, one parameter of the reference trajectory formulation was fixed by the author.

The parameter C_2 of the sigmoid curve represents the pre-defined minimum length to the LV as shown in Fig 4.3. The higher the value of C_2, the more steeper the sigmoid curve will become and the more evasive and aggressive the maneuver will become as now the vehicle will have to displace laterally the same amount in lesser time. Since the analysis is focused on evasive maneuvers, the value of C_2, which is a tuning parameter, was set to $5m$ by the author to generate an evasive reference trajectory as shown in Fig 4.6.

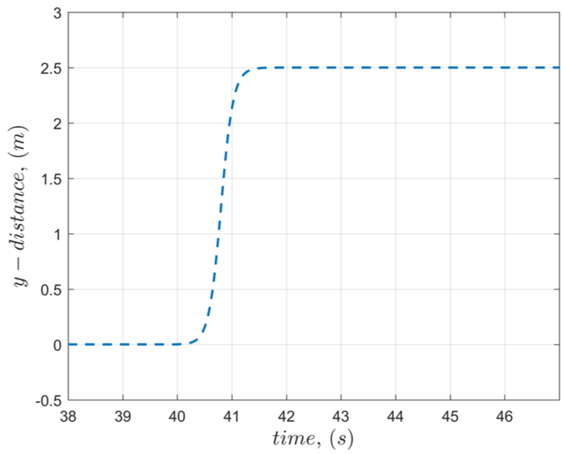

Figure 4.6: Reference trajectory with $C_2 = 5m$

By doing so, it was observed that the reference trajectory for the single lane change maneuver looked similar to that of a step response. And for the case of step response, there are well-defined KPI's to assess the performance as shown graphically in Fig 4.7.

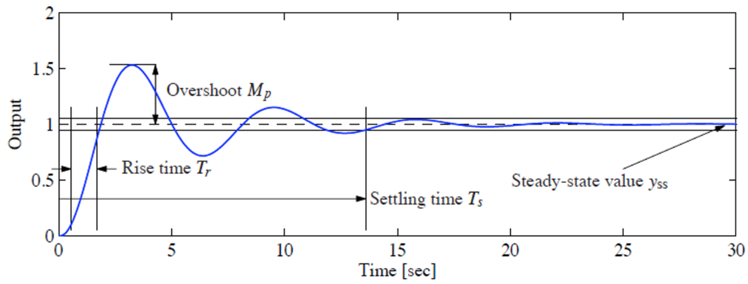

Figure 4.7: Step response KPI representation [14]

These four KPI's, highlighted in Fig 4.7 are:

- Overshoot (M_p): The maximum value of the output response minus the steady-state value of the response divided by the steady-state value of the response
- Rise Time (T_r): The time required for the output response to rise from 10% to 90% of the steady-state value
- Settling Time (T_s): The time output response takes to enter and remain within a 1% band centered around its steady-state value
- Steady-state value: The final output value of response, assuming it converges

In steady-state value, since the trajectory needs to be within 1% of reference value range, it physically means that a maximum deviation of $1cm$ is allowed. In all the simulations, the vehicle was well-within this bound and the steady state error was in few millimeters, which for a vehicle, is practically negligible. Hence, the KPI steady-state value was not reported in this research. Only the first three KPI's were used to assess the performance.

To purely assess the controller's tracking performance to the three reference values provided, the RMS error for all the three quantities was defined as shown in Eq (4.21) - Eq

(4.23). Here, RMS stands for Root Mean Square and is a quadratic formulation for measuring the average magnitude of the error. By squaring the error before they are averaged, the RMS ensures that large errors are given higher weight.

$$y_{\mathrm{RMS}} = \sqrt{\frac{1}{N}\sum_{i=1}^{N}\left(y_p(i) - y_{\mathrm{ref}}(i)\right)^2} \tag{4.21}$$

$$\psi_{\mathrm{RMS}} = \sqrt{\frac{1}{N}\sum_{i=1}^{N}\left(\psi(i) - \psi_{\mathrm{ref}}(i)\right)^2} \tag{4.22}$$

$$\dot{\psi}_{\mathrm{RMS}} = \sqrt{\frac{1}{N}\sum_{i=1}^{N}\left(\dot{\psi}(i) - \dot{\psi}_{\mathrm{ref}}(i)\right)^2} \tag{4.23}$$

The last KPI was define by the author and was called as Distance To Collision (DTC). DTC represents the lateral distance between the left-rear corner of LV and right-front corner of SV (for the case of left hand turn by SV) as shown in Fig 4.8. The red color vehicle represents the SV and the blue color vehicle represents the LV. The yellow arrow represents the DTC which gives an idea by how much lateral distance was the collision avoided. This safety distance gives an idea whether the collision was avoided or not, and in case if avoided, then by how much distance. Hence it is a relevant KPI for this research.

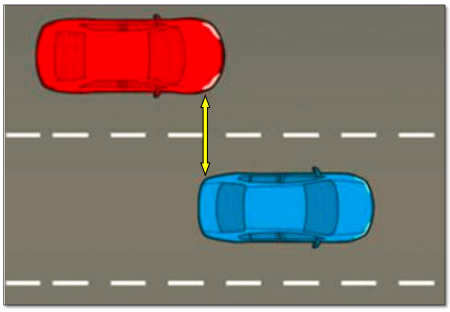

Figure 4.8: DTC graphical representation with yellow arrow

Thus in total, seven KPI's were defined for performance evaluation as listed below. An intuitive understanding would be that for a good performance, the DTC should be as high as possible and all other KPI should be as small as possible ensuring that collision is safely avoided, the trajectories are well tracked and the car quickly stabilized post lane change (which can be checked by settling time values).

- Overshoot M_p
- Settling Time T_s
- Rise Time T_r
- DTC
- RMS error for lateral position y_{RMS}
- RMS error for heading angle ψ_{RMS}
- RMS error for yaw rate $\dot{\psi}_{\mathrm{RMS}}$

4.7. Tire Cornering Stiffness

The second last section of this chapter gives an understanding regarding the method used to calculate the tire cornering stiffness $C_{\alpha_{\mathrm{ij}}}$ for each tire ij = (fl, fr, rl, rr) respectively. As seen in Eq (3.50) - Eq (3.53) and in all the three prediction models of controllers designed in Chapter 3, the tire's ability to generate lateral forces is directly proportional to the cornering stiffness. Since the maneuver designed involves lateral control, the correct estimation of the cornering stiffness is essential for the lateral force generation and lateral motion.

In literature, it is seen that a constant value for the front and rear tires respectively is taken. But here, the simulation architecture is designed in a generic way such that the controller works for varying vehicle speeds and friction coefficients. Hence the cornering stiffness can not be taken as a constant value but instead should varying according to the conditions.

It is generally seen that two parameters play a critical role in varying the tire's ability to generate forces- friction coefficient μ and tire normal load F_{z_t}. The higher the μ, more is tire-road adhesion and higher is the tire's ability to generate forces. Similarly, the higher the normal load on the tire, more is the effective capability of the tire to generate forces. This can be very well seen in the Kamm circle's equation in Eq (3.64) - Eq (3.64) where the bound on tire's forces are directly proportional to both μ and F_{z_t}.

To capture the tire's lateral behaviour well, the tire property file was analyzed extensively and a 2D look-up table was formulated. With an assumption that tire's camber angle is zero, the normal loads were varied from $1000N$ to $10{,}000N$,with an increment of $1000N$ at each instant. For each normal load value, μ was increased from 0.1 to 1 with increments of 0.1. These values were then given to the magic formula and offline simulations were performed to calculate the tire lateral forces in combined mode i.e. taking into account of wheel slip in both longitudinal (κ) and lateral (α) direction. Fig 4.9 shows the output for the case when F_{z_t} was set at $5000N$ with varying μ.

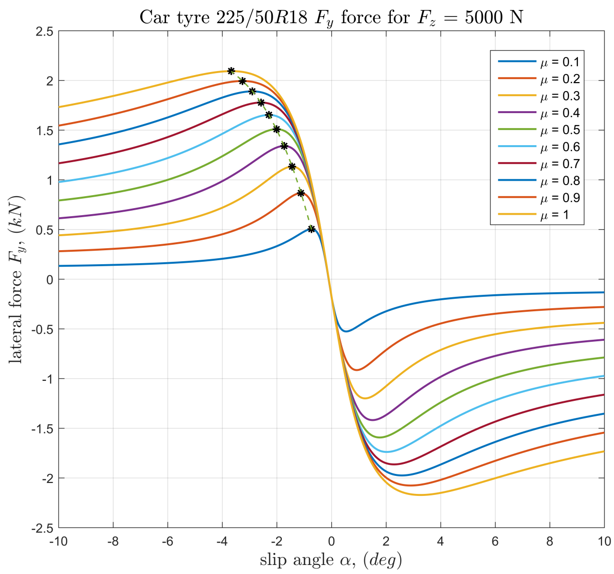

Figure 4.9: Tire lateral forces for $F_{z_t} = 5000N$

As seen in Fig 4.9, the tire lateral forces are increasing with increasing μ, with the black asterisk $'*'$ representing maximum force value. It can be seen that beyond $\alpha = \pm 4^o$, the tire forces saturate. And within $\alpha = \pm 2^o$, the tire shows a linear behaviour which can be approximated using the linear tire model equation (Eq (4.24)).

$$F_y = C_\alpha \alpha \tag{4.24}$$

So, to get the cornering stiffness, linearization of tire forces was performed in which the tire lateral forces were divided by the slip angle in the linear range of tire motion only. Later, a 1^{st} order polynomial was fitted for this data (because we are working in linear range) and using the average value the cornering stiffness values were estimated. Again for the case of $F_{z_t} = 5000N$, the linearization and polynomial fitting to estimate the cornering stiffness is shown in Fig 4.10.

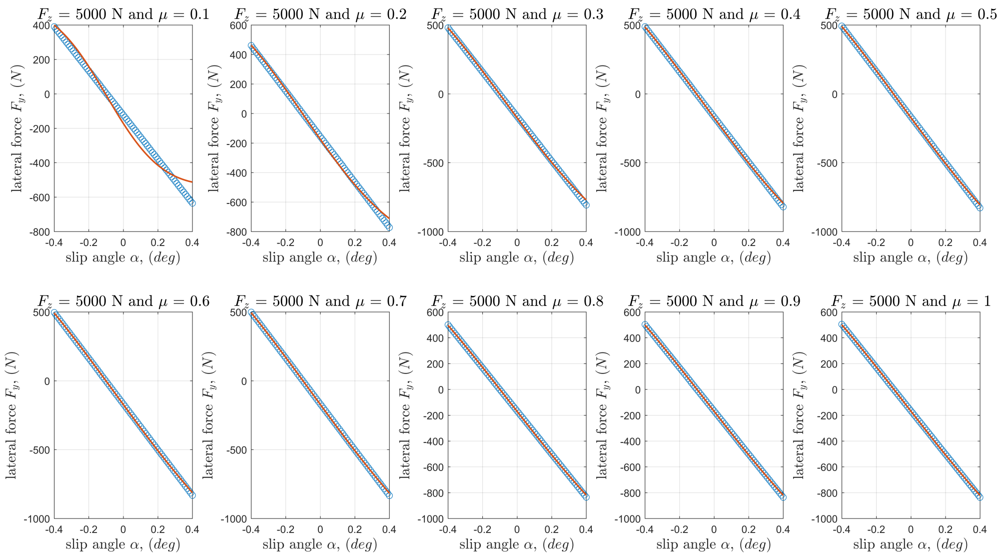

Figure 4.10: Tire Cornering stiffness C_α calculation

This curve fitting was performed for all other values of normal loads to generate the 2D look-up table. It is to be noted that the cornering stiffness calculated here only captures the linear regime of tire motion well. Later in Chapter 6, it will be shown how the nonlinear behaviour of the tire was captured in the cornering stiffness. But now, in principle, the tire forces should correctly be calculated for varying maneuver conditions.

4.8. Summary

This chapter gave a detailed workflow description regarding how the closed-loop simulation was set up and performed in Simulink. The two layers of the overall three-layer control, being the *Decision Making* and *Reference Generator* was explained. Formulas of TTC, TTB and TTS were described to decide whether to steer or to brake. Regarding the reference trajectory generation, a kinematic method using Sigmoid curve was used to get reference position, yaw angle and yaw rate respectively. The entire formulation of the sigmoid curve was summarized as well. The single lane change maneuver performed throughout the simulations was derived from Ford Motors and was explained along with the list of KPI's defined for controller's subjective performance assessment. Finally, the chapter concluded with a description of the method used to calculate tire's cornering stiffness value.

5

Controller Settings

5.1. Introduction

An integral feature of designing a MPC is to deal with various design and tuning parameters such that the performance can be improved and the desired objectives of superior tracking can be achieved. Before the simulation results are presented, it is necessary to describe and summarize all the design parameter values of MPC taken in this research while formulating the controller. The optimization settings of the MPC have already been described in Fig 2.3 of Chapter 2. This chapter focuses on explaining the thought process for designing the other tuning parameters of MPC such as sampling time t_s, prediction horizon N_p etc. The activation logic of the controller is described followed by the real-time cost function update scheme designed in this research. Lastly, the methodology used to tune the controller is explained and the chapter is concluded with a summary.

5.2. MPC Parameter Settings

One of the most critical parameter in designing a MPC controller is to decide how many seconds ahead the controller will predict in future. This is extremely important because the controller's performance directly depends on its future predictions. A thumb rule in this aspect is that:

Theoretically, the more the MPC can predict in future, more improved will its performance gradually become.

Therefore, ideally, one would like to predict infinitely to get the best performance. But an important constraint to this theory is the high computation time of MPC. Considered as a disadvantage of this scheme, an MPC formulation involves multiple equations in its prediction model, followed by constraint equations, future predictions and online solution to the optimization problem, making MPC computationally expensive. It is to be ensured that the designed controller's computation time should be low so that the control action calculated can be implemented in real-time and the effect of computational delays can be minimized. Hence, there is a fine line for a controller designer to decide between longer future predictions and lesser computation time.

The amount to predict in future is a numerical multiplication of two parameters, the sampling time of the controller and the prediction horizon of the controller. Carefully choosing these two values will ensure that both the desired objectives are successfully met. In literature, there is no golden rule for choosing t_s and N_p and it is completely left to controller designer to fix these values.

The MPC controller was designed with a mindset that it will be implemented in the vehicle as an ECU, connected with other vehicle ECU's and communicating with them through standard communication protocols. A standard ECU design has certain input ports to receive necessary vehicle information after which it processes them in the ECU logic designed (in this case, the MPC controller) following which the control signal commands are sent to vehicle actuators.

As explained in Section 4.2, the MPC controller requires certain information as input too in order to formulate and solve the optimization problem. Therefore, the idea was to analyze the ECU Can-bit sheet of the simulation vehicle and check the update time of each of these information signals required by the MPC. If the sampling time of the MPC ECU is higher than the maximum update time of that respective signal, then one can guarantee that at each sampling instant of the controller, the MPC will have all the necessary information it requires in its formulation.

The major signals that were analyzed were the vehicle acceleration terms, yaw rate, brake pressure and reference trajectory signals. These are the major external signals computed outside the MPC ECU and would be required by MPC at each sample. On performing the analyses, it was found that the maximum update time of one of the above mentioned signal was $0.032s$. Thus, the sampling time t_s of all the designed three MPC controllers was set to $0.035s$.

Now that one parameter was fixed, it was necessary to finalize the value of prediction horizon N_p to get the final prediction time of the controller. To do so, the MPC formulated using linear bicycle model was initially given a prediction horizon of 20 $samples$, thus giving a prediction of $0.7s$ as first guess. The idea was to increase the prediction horizon value further until the computation time increases the sampling time of the controller. Fig 5.1 represents the computation time of the controller for the case when the prediction were increased from 20 $samples$ till 50 $samples$. The KPI performance at each value of N_p is reported in Table 5.1.

S No. -	N_p -	M_p [%]	T_s [s]	T_r [s]	y_{RMS} [%]	ψ_{RMS} [%]	$\dot{\psi}_{\mathrm{RMS}}$ [%]	DTC [m]
1	20	27.41	6.20	0.44	11.30	98.07	526.28	0.47
2	30	28.6	5.55	0.43	9.22	85.4	473.07	0.56
3	40	26.22	5.71	0.44	9.00	83.55	467.66	0.58
4	50	25.03	5.66	0.45	7.94	80.16	465.28	0.60

Table 5.1: KPI performance with increasing N_p samples

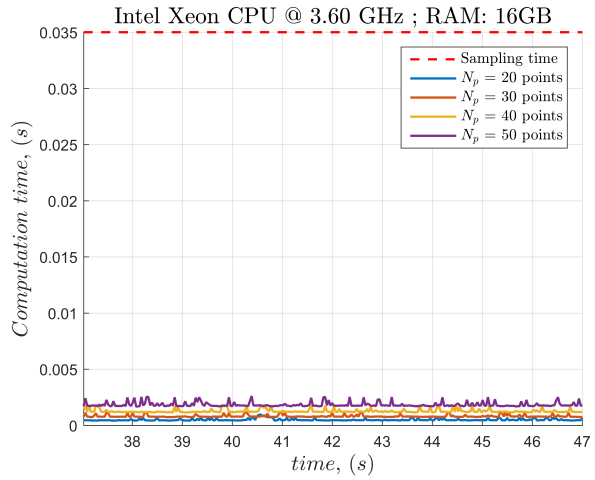

Figure 5.1: Linear bike MPC computation time for increasing N_p

The maneuver was performed at $\mu = 0.9$ with $v_x = 75\ km/hr$. It can be seen that as the number of predictions are increasing, the performance of the controller is also improving with reducing overshoot and RMS errors and increasing DTC values. At the same time, the computation time was also gradually increasing as a result of increasing computations. But, the computation time was still well below the t_s of MPC. It was seen that as the predictions gradually increased, the performance did improve but after a certain point, the performance improvement was not very significant. As can be seen in Table 5.1 from 30 to 50 $samples$, the improvements of all the KPI's is less than 3% with DTC increasing only by $0.02m$. Beyond 50 $samples$ the contribution towards performance improvement was negligible. Therefore N_p equal to 50 $samples$ was fixed for both linear and nonlinear bicycle model MPC, giving a prediction time of $1.75s$.

For the case of Planar car model MPC controller, since the number of prediction model equations as well as the constraints are significantly higher than the bicycle model, it was noticed that a prediction time of $1.75s$ increased the computation time of the controller significantly (more than the sampling time) with real-time simulation speed reported at 0.7 times by IPG CarMaker. Since t_s cannot be changed as planar car MPC controller also requires the same reference signals and other vehicle states signals, the idea was to reduce the number of prediction samples until the controller becomes real-time capable. On doing so, it was seen that at $N_p = 30\ samples$, the real-time speed was reported at 1.7 times by IPG CarMaker with computation time, now mostly below the t_s line. Thus for the case of Planar car MPC model, the prediction time was set at $1.05s$, giving a decent 1 second prediction time in future. Table 5.2 summarizes the controller sampling time and prediction horizon parameters.

S No.	Prediction Model	t_s	N_p
-	-	[s]	-
1	Linear bicycle model	0.035	50
2	Nonlinear bicycle model	0.035	50
3	Planar car model	0.035	30

Table 5.2: Final MPC prediction time parameter settings

It is to be noted that one way to reduce the computation time is to reduce the control horizon N_c samples. But the author did not want to compromise with the future predictions and subsequent performance of the MPC control. Hence, the control horizon for all the three controllers was set equal to the value of prediction horizon i.e. $N_c = N_p$.

5.3. MPC Activation Logic

It is necessary for any controller to have an activation logic for successful takeover of the vehicle. Ideally, the way in which this co-simulation structure works together gives an understanding how the controller will be activated i.e. in the case when an object is detected. A vehicle has radar which is efficient in detecting objects in the longitudinal direction. The camera is good in lateral detection of the object and its corner points. In this research, the Toyota vehicle was equipped with a radar sensor of detection radius 200m.

In reality, the author believes that a certain TTC threshold will be defined by the OEM (say 5s). When the object in front is detected, the necessary data will be provided to the MPC ECU to control the car but no reference trajectory will be calculated. Instead, the driver will be given warnings to take-over the control of car and avoid collision. These warnings can be visual, audio or even haptic in nature. If the driver responds to these warnings, then the driver takes over of the vehicle and the automated control system stops working. But in case if the driver does not respond and the *Decision Making* subsystem notices that the TTC is equal or below the threshold value, then the automated control will take over the control of the car. The *Reference Generator* subsystem will get activated and a reference trajectory will be generated. As soon as this trajectory is provided to the controller, the evasive maneuver will begin and the collision will be avoided.

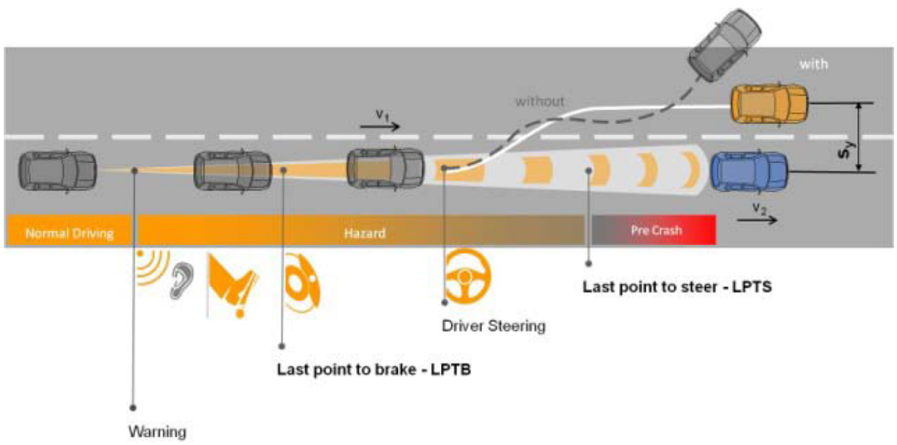

Figure 5.2: Realistic activation logic with warning and TTC monitoring [6]

But, since in this research it was already fixed that the maneuver begins when SV is 30m away from LV, no TTC threshold was defined. The way the automated control system works here is that as soon as the radar sensor detects the object vehicle in front, the controller starts to receive information of the vehicle's state but no active control is performed. As soon as the distance reduces from 200m to 30m, a constant reference trajectory is generated, making the value of trajectory generation flag from 0 to 1. As soon as this flag value becomes 1, the controller gets active, the cost function is updated with inclusion of reference values and the evasive maneuver begins. In this way, the controller is activated.

The activation method designed here is generic and practical too because in a real vehicle, the ECU's communicate and activate control subsystems via changing the value of flag indicator. These flags are variables defined to work like a switch to activate the systems. The same structure along with communication of all the three systems through flags is followed in this research also for controller's activation.

5.4. Cost Function Update

One of the contribution of this research was to design a simple but effective real-time cost function update method to improve the performance of the controller. The idea here was to ensure that according to the dynamics of the maneuver, the cost function should be updated such that all the necessary information of the dynamics is preserved in the cost function, while the rest is removed from it.

Looking at the reference trajectory of the maneuver as shown in Fig 4.6, the reference trajectory can be divided in three parts: part 1 is the straight line driving up to $40s$ mark, part 2 is the lane change maneuver which involves vehicle turning and laterally displacing, and finally part 3 is again the straight line driving where the car is not supposed to turn anymore but needs to drive straight again.

Now, in part 2, it is necessary that the cost function minimizes not only the lateral position error but also the yaw and yaw rate error as the car actually will make a turn here. But there is no need to minimize the yaw when the vehicle is straight line driving in part 1 and part 3. In these two parts of the maneuver, ψ_{ref} and $\dot{\psi}_{\text{ref}}$ is zero with y_{ref} being a constant value. Thus, in these parts, the only minimization term should be that of vehicle's y-position. If the cost function still has in its formulation, the minimization of ψ and $\dot{\psi}$, then the overall sensitivity of the cost function with respect to position error minimizes and the performance goes down.

The MPC understands what it needs to achieve based on the cost function formulated for its optimization problem. If for the case of straight line driving, the only term mentioned in the cost function is the lateral position, then the controller will clearly be able to understand what is being asked by it to do. A single term cost function clearly gives higher sensitivity to position tracking as compared to 3 parameter cost function. Hence, the idea was to update the cost function in real time based on the trajectory defined such that during straight line driving, the controller only minimizes the position, while in part 2, the controller minimizes all the three reference values.

To do so, only ψ_{ref} and $\dot{\psi}_{\text{ref}}$ values were used and a counter was set based on designed threshold value which was multiplied with the respective tuning value to vary the inclusion or exclusion of the respective state in the cost function. The algorithm defined is shown in Eq (5.1).

$$
\begin{aligned}
&\psi_{\min} = \psi_{\text{thr}}\\
&\dot{\psi}_{\min} = \dot{\psi}_{\text{thr}}\\
&\ \text{flag}_{\psi} = 0\\
&\ \text{flag}_{\dot{\psi}} = 0\\
&\quad \text{for}\ \ i = 1:1:N_p - 1\\
&\qquad \text{if}\ \ \|\psi_{\text{ref}}(i+1) - \psi_{\text{ref}}(i)\| \geq \psi_{\min}\ \ \text{or}\ \ \|\psi_{\text{ref}}(i)\| \geq \psi_{\min}\\
&\qquad\quad \text{flag}_{\psi} = \text{flag}_{\psi} + 1\\
&\quad\ \ \text{end}\\
&\qquad \text{if}\ \ \|\dot{\psi}_{\text{ref}}(i+1) - \dot{\psi}_{\text{ref}}(i)\| \geq \dot{\psi}_{\min}\ \ \text{or}\ \ \|\dot{\psi}_{\text{ref}}(i)\| \geq \dot{\psi}_{\min}\\
&\qquad\quad \text{flag}_{\dot{\psi}} = \text{flag}_{\dot{\psi}} + 1\\
&\quad\ \ \text{end}\\
&\ \ \text{end}
\end{aligned}
\tag{5.1}
$$

Firstly, a minimum threshold is defined for both ψ and $\dot{\psi}$. The threshold value represents a bound. If the ψ_{ref} and $\dot{\psi}_{\text{ref}}$ values are beyond this threshold value, it implies that the reference yaw values are significant and cannot be neglected, meaning that vehicle turning is critical and needs to be a part of the cost function. If the reference values are less than the threshold value, then vehicle yawing is not critical and hence can be neglected from the cost, making it a pure straight line driving cost function (for part 1 and part 3 of the maneuver). Thus, theoretically, the smaller the threshold value is chosen, more is the sensitivity of vehicle yaw and therefore longer is its presence in the cost function.

In this research, the threshold values for both the parameters ψ_{thr} and $\dot{\psi}_{\text{thr}}$ was taken as $10^{-5} rad$ and $10^{-5} rad/s$ respectively. This physically means that if the reference heading angle value is 0.005^o or less, it will be considered negligible and not considered in the cost function. For all the number of prediction horizons minus one, if the difference between the successive reference value is greater than the threshold value, it means that the amount of vehicle turn per sample difference is significant and cannot be neglected. This represents the case when the vehicle is making a turn.

But in case, if the vehicle, for example, makes a turn with constant ψ_{ref} value, (say 1^o), which is higher than the prescribed threshold value, then in that case the logic will fail as the difference will be less than threshold value. Thus, to cover the case of turning with constant yaw angle, the *or* condition was added which checks the absolute value of ψ_{ref}. Thus, both vehicle turning with constant and non-constant ψ_{ref} is covered. The same argument remains for $\dot{\psi}_{\text{ref}}$ as well.

The defined logic is consistent in its definition for both left and right turns and will also work in case a maneuver has multiple turns too. The output of this logic is the flag values flag_{ψ} and $\text{flag}_{\dot{\psi}}$ respectively. Fig 5.3 shows the graphical representation of these output values for the case of a single lane change maneuver.

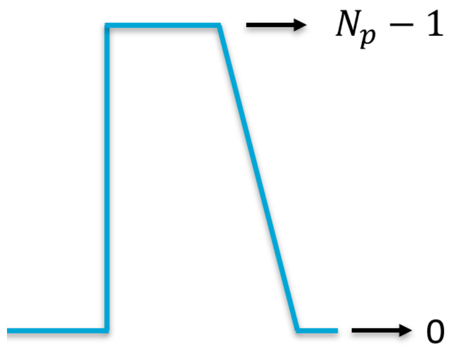

Figure 5.3: Graphical representation of variable flag_ψ and $\text{flag}_{\dot\psi}$

Starting from the left, the line representing value equal to zero represents the part 1 of the maneuver where only straight line driving is performed. Then as soon as part 2 begins of single lane change, the flag values increases, reaching maximum in case if all the reference values as well as their difference is higher than threshold value based on the logic defined above. Later, as the lane change maneuver is finishing and the reference trajectory is approaching towards the straight line again, the flag value gradually starts to decrease and goes to zero once the ψ_{ref} and $\dot\psi_{\text{ref}}$ values goes below the set threshold value, telling that the maneuver has entered to part 3 gradually.

This smooth transition is well captured in the logic which is critical as a sudden change of cost function definition may lead to jerky or abrupt changes in vehicle motion leading to poor performance and driver distress. Finally, to ensure that the controller understands this segregation of reference trajectory in three parts based on value of flag_ψ and $\text{flag}_{\dot\psi}$, these flag output values are then used in varying the tuning weights of the controller.

As seen in Eq (3.77) of the cost function, the states of the cost function are multiplied with the tuning weight matrix. If the respective term of the tuning weight matrix is made zero, the corresponding multiplied state to it gets removed from the cost function automatically. Therefore, since the major parameters to differentiate between turning and straight line driving is ψ and $\dot\psi$, the tuning weights of both these parameters were defined as shown in Eq (5.2).

$$
\begin{aligned}
Q_\psi = \frac{\text{flag}_\psi W_\psi}{N_p - 1}\ , \ Q_{\dot\psi} = \frac{\text{flag}_{\dot\psi} W_{\dot\psi}}{N_p - 1} \\
S_{\psi_N} = \frac{\text{flag}_\psi W_{\psi_N}}{N_p - 1}\ , \ S_{\dot\psi_N} = \frac{\text{flag}_{\dot\psi} W_{\dot\psi_N}}{N_p - 1}
\end{aligned}
\tag{5.2}
$$

Here, Q_ψ and $Q_{\dot\psi}$ represents the respective tuning terms corresponding to states ψ and $\dot\psi$ of the tuning matrix Q of Eq (3.77) while S_{ψ_N} and $S_{\dot\psi_N}$ represents the terminal tuning weight terms of the matrix S. Terms W_ψ and W_{ψ_N}represents the tuning value and terminal tuning value set for the state ψ based on reasoning given in Section 5.5. And terms $W_{\dot\psi}$ and $W_{\dot\psi_N}$represents the tuning value and terminal tuning value set for the state $\dot\psi$.

Thus, it can be seen in Eq (5.2) that the tuning values are multiplied with the respective state's flag values and are normalized by dividing the expression by the term $N_p - 1$. This ensures that if the turn is being performed, the tuning parameter set by the designer remains as it is (as the tuning value gets multiplied by 1) and the performance in not compromised. In the case when transition happens from part 2 to part 3, the tuning weights for ψ and $\dot{\psi}$ starts to reduce gradually, increasing the sensitivity towards position tracking after which the tuning term becomes zero and those respective states are disappeared form the cost function. The advantage of this real-time cost function update algorithm is shown in Fig 5.4 as compared to non-updated regular scheme shown in Fig 5.5. The maneuver was performed with planar car model MPC at μ=0.9 and v_x=75km/hr.

S No.	Overshoot	Settling Time	Rise Time	y_{RMS}	ψ_{RMS}	$\dot{\psi}_{RMS}$	DTC	$a_{y_{max}}$
-	[%]	[s]	[s]	[%]	[%]	[%]	[m]	[m/s^2]
1	0	3.8	0.56	4.86	65.40	391.02	0.61	5.06

(a) KPI performance

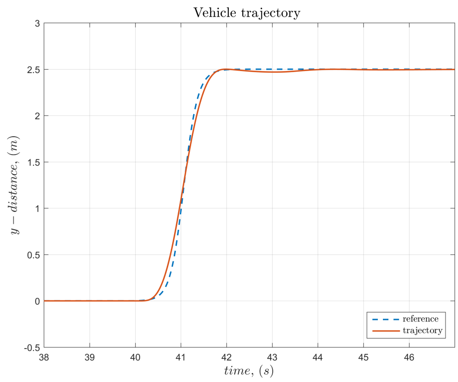

(b) Vehicle lateral position tracking

Figure 5.4: Performance with real-time updated cost function algorithm

S No.	Overshoot	Settling Time	Rise Time	y_{RMS}	ψ_{RMS}	$\dot{\psi}_{RMS}$	DTC	$a_{y_{max}}$
-	[%]	[s]	[s]	[%]	[%]	[%]	[m]	[m/s^2]
1	0	7.00	0.56	5.01	65.36	390.94	0.61	5.06

(a) KPI performance

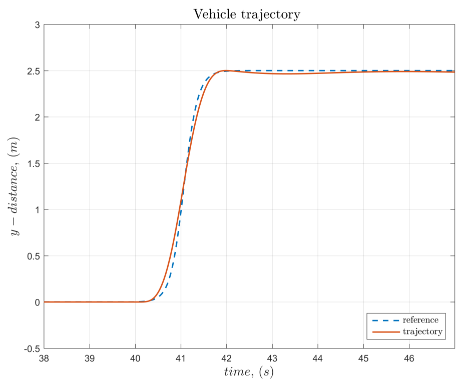

(b) Vehicle lateral position tracking

Figure 5.5: Performance without real-time update cost function algorithm

It is clearly seen that the performance by the algorithm has improved. During the turn in part 2 of the maneuver, the performance remains the same as seen by the KPI values DTC, Rise time, Overshoot and $a_{y_{max}}$. This was expected as in part 2 all the three reference values are passed to the cost function. Once part 2 of the maneuver is over and part 3 commences, it can be seen in Fig 5.5b that without the cost function update, the vehicle takes longer time to converge to the reference value. This is clearly highlighted in KPI value of Settling time shown in Fig 5.5a. But, with the cost function update, the sensitivity of position tracking increases during part 3 of the maneuver, as a result of which the vehicle quickly converges to the reference trajectory as shown in Fig 5.4b. Fig 5.4a proves this improvement in performance with KPI value of Settling time decreasing from $7s$ to now $3.80s$. Since now the position tracking has improved, the KPI value of y_{RMS} also highlights the same.

This proves that this cost function update scheme provides the necessary improvement in performance of the controller. The idea of breaking the trajectory in 3 parts makes it convenient for the designer to define modular cost functions and tune accordingly to extract maximum performance out of the controller. Another advantage of this scheme in terms of vehicle dynamics is reported in Section 5.5. It is to be noted here that only the states ψ and $\dot{\psi}$ were chosen in the cost function update and their subsequent tuning weights were modified. The vehicle's lateral position y_p was not used in this algorithm and its tuning weight was never made to zero because, predominantly the tracking controller's primary job is to track the reference to the best of its abilities. Thus, position error has to always be there in the cost function at all times.

5.5. Controller Tuning

The last section of this chapter deals with the controller tuning, which is an extremely important part of MPC designing process to get desired performance. Each controller, be it PID or LQR needs to be tuned efficiently to ensure that good performance is achieved. Specific to the case of MPC, tuning is considered one of the issues of MPC as it involves tuning a lot of parameters which might become cumbersome and complex to understand. A good example of this complexity is the planar car MPC model designed in this research which involves tuning of 35 parameters apart from other settings. In Section 5.2, three parameters (t_s, N_p and N_c) were tuned and the final values were reported in Table 5.2. Here, all the tuning parameters are not reported for each controller but instead the thought process behind tuning these parameters will be explained.

The process of tuning involved firstly to finalize which states are required in the cost function and which can be omitted. By doing so, the tuning parameter associated with that state also becomes zero and need not to be tuned further, thereby reducing few parameters. Once decided, the next step in the tuning was to vary the weights according to the desired tracking performance required to be achieved. Therefore, the tuning logic used for LQR control was also used here in which the tuning weight W_ϵ is calculated based on below-mentioned Eq 5.3.

$$W_\epsilon = \frac{1}{\text{desired error value between state } (\epsilon - \epsilon_{\mathrm{ref}})} \tag{5.3}$$

One would always want the error between the states to be as small as possible. This practically implies that smaller is the value of desired error, higher is the value of tuning weight. This in turn means that the higher the tuning weight, more is the emphasis given to that state by the controller for error minimization with respect to other states. Thus, generally, the tuning logic is such that for tuning the states in the cost function, the tuning weight is generally set to a higher value to minimize the error as much as possible, leading to good controller performance.

At the same time, the tuning weight for the control action also uses the same formula (Eq (5.3)). It is necessary to include the control action in the cost function as the amount of control action calculated is incurred as control energy cost which also needs to be minimized. The control action in a vehicle, be it steering or braking is applied via the actuators which are mechanical components and have a certain bound on their service life after which the performance starts to degrade. By calculating excessive control action, these actuators might get over-used and their service life will reduce quickly leading to maintenance costs and other repair costs. Therefore, it is essential to have the control action also in the cost function so that optimal control action value is calculated to achieve the desired result.

Generally, no reference values are calculated for the control action. It is the job of the controller to calculate the most suitable value and therefore in the cost function, the reference value for the control action is given as zero. If the same ideology of state's tuning weight is followed, a higher tuning weight to the control action will imply that the control action should be as close to zero as possible. This is practically incorrect as a zero control action will bring no control to vehicle dynamics. Therefore, in the case of control action, a higher error term is given to the denominator of Eq (5.3). By this way, the controller is told to not follow the reference zero value and instead calculate the desired value for minimization of state's error. at the same time, the error value is not given too high as control energy is also significant for actuator life.

In all the test cases, with all the three controllers, the tuning process started with defining the error value for state tracking to 0.01 meaning the tuning weight for all the cost function states (including the terminal states) was set initially set to 100. This for instance, practically means that an error of $1cm$ is tolerable with respect to reference position tracking which is a decent guess as in practice an error of $1cm$ for a vehicle is small and almost negligible. And for the control action, the initial value given to error was 0.1 giving a tuning weight of 10. It is to be noted that the tuning matrices are always diagonal matrices so that each parameter along the diagonal corresponds to the respective state for which it has been defined only. There are generally no cross-coupling of states in cost function and to ensure that, the non-diagonal terms of the tuning matrices were set to zero.

Once a ball-park value for the tuning weight was given, the idea was now to start fine tuning the controller. This was done via simulation based fine tuning approach in which one tuning parameter was varied at a time and the corresponding simulation's KPI values were analysed and compared with the previous simulation to get an understanding of how the controller is behaving with changes to tuning parameters i.e. changes to cost function. This was tedious and time-consuming effort but it gave some ideas while tuning about how the parameters were affecting the cost function and overall optimization problem.

Since the maneuver is performed for various speeds and for various values of μ, the controller was fine tuned for each speed values and for each value of μ. Doing so, certain patterns emerged while tuning the controller which are mentioned below.

- Increasing the terminal position tracking tuning weight S_{y_N} lead to corner cutting

- Increasing value of yaw rate tuning weight $Q_{\dot{\psi}}$ improved the overall reference tracking performance
- Reducing tuning weight of wheel angle Q_δ improved tracking performance
- For a fixed μ value with increasing maneuver speeds, the tracking was improved by increasing the weights of wheel angle and wheel velocity (Q_δ and $R_{\dot{\delta}}$), and by reducing the weight of lateral position Q_y
- Decreasing the tuning parameter of control action brake torque rate $R_{\dot{T}_{b_{\mathrm{fl}}}}$, $R_{\dot{T}_{b_{\mathrm{fr}}}}$, $R_{\dot{T}_{b_{\mathrm{rl}}}}$, $R_{\dot{T}_{b_{\mathrm{rr}}}}$ and keeping other tuning parameters constant lead to increase in overshoot

All these conclusion were made by carefully analyzing the KPI values and accordingly the controllers were fine tuned. Now to end this section, the final states chosen for each controller is mentioned.

MPC - Linear Bicycle Model

Out of the 7 prediction model states of the linear bicycle model, the ones chosen for the cost function formulation were $\dot{\psi}$, ψ, y_p and δ. Since the control action here is only steering and no brake action is performed, it is of no use to minimize the error for state v_x. The same argument goes for vehicle's longitudinal position x_p. Also, vehicle yawing is more critical during lateral control as compared to state v_y. Thus, by eliminating 3 of the total 7 states, 6 tuning parameters were eliminated from the cost function as well. Apart from the first three states which are must for lateral control, wheel angle δ was also kept in the cost function along with the control action $\dot{\delta}$. This was done because, practically to laterally displace $2.5m$, a car does not need to turn SWA by 200^o. The ideal situation will be to turn the SWA by minimum amount possible and achieve the desired output. This can be practically told to the controller by penalizing the SWA (in the form of wheel angle δ) apart from control action $\dot{\delta}$ so that minimum actuator wear is achieved.

MPC - Nonlinear Bicycle Model

The cost function defined for the nonlinear bike remains the same as that of the linear bicycle model as shown in Eq (3.15) - Eq (3.16). This is because here, the control action and desired output of lateral control remains the same, the only difference being the ability to capture the nonlinear dynamics of model and tire.

MPC - Planar Car Model

The planar car model has the ability to brake as well as steer. Therefore, in the cost function, the states apart from $\dot{\psi}$, ψ, y_p and δ also included longitudinal velocity v_x. But this state was only included in the case of pre-braking maneuver scenario shown in Chapter 6 in which the reference generator gave a non-zero reference longitudinal velocity $v_{x_{\mathrm{ref}}}$. Apart from this, in all other maneuver scenarios, the reference generator does not provide any $v_{x_{\mathrm{ref}}}$ value and hence in all those cases the state v_x was omitted from cost function formulation by giving setting its tuning weight zero.

Also, the 8 brake torque states and 4 brake torque rate control actions were also included in the cost function because of the same reason to utilize the actuator action as minimum as possible for future cost saving. Another reason to include the brake torques in the cost function was to ensure that the brake torques go to zero once part 3 of the maneuver begins.

As part 2 of the maneuver is completed, to reduce actuator wear and for maneuver requirement in general, the brake torques after part 2 of the maneuver should go to zero. Since the control action is brake torque rate, it was seen that the controller post part 2 of the maneuver, makes the brake control action equal to zero. Due to this, the brake torque values were remaining constant throughout. By including these 8 brake torque states in the cost function only during part 3 (post maneuver straight line driving) of the maneuver, the brakes were now also made to go to zero apart from usual control action. In other parts of the maneuver, these 8 states were not added to the cost function by setting their tuning weight as zero.

This is the reason why the cost function of Planar car MPC controller has a peak as seen in Fig 5.6a. The plots are of the same maneuver performed in Section 5.4. The maneuver begins at around $40s$ mark and the cost function there is non-zero as expected as seen in Fig 5.6b. But once the maneuver is over, these 8 brake torque states are added to cost function and a high weight is given to force them to go to zero quickly. Thus, the cost value suddenly jumps but gradually then goes to zero. Fig 5.6c and Fig 5.6d shows the brake torques going to zero now.

But, if a constant cost function is kept at all times and the 8 brake torque signals are not added later to cost function, then the cost function achieved is shown in Fig 5.7a. It can be seen that no peak is observed here meaning that the controller's cost function is not changed and the brake torques are not added in cost function's states. As a result, the brake torque values remained constant after part 2 of the maneuver as shown in Fig 5.7b. Because the controller makes the control action go to zero automatically as per the maneuver design, the brake torque remains constant as a result. Hence, both real time cost function update method via designed algorithm Section 5.4 and tuning parameter's variation in values together provides the necessary robustness and improvement in performance.

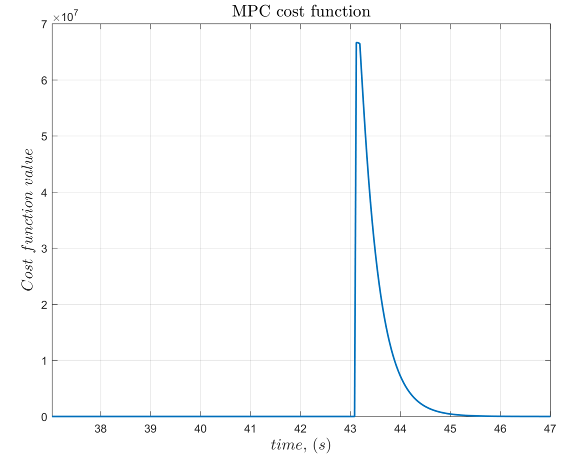

(a) Entire maneuver's cost function

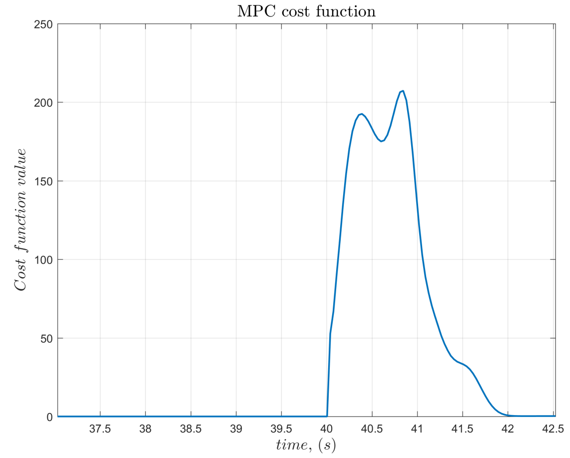

(b) Part 2 maneuver's cost function

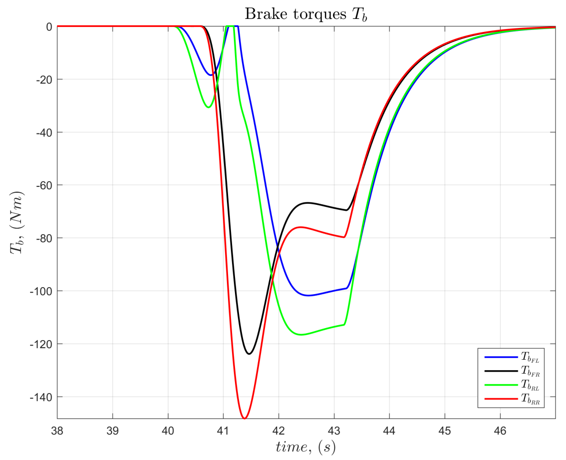

(c) Brake torque T_b

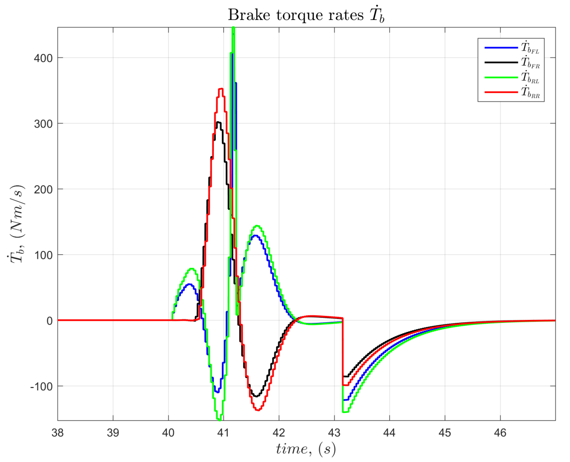

(d) Brake torque rates $\dot{T}_b$

Figure 5.6: NMPC - Planar car model with real-time cost update performance

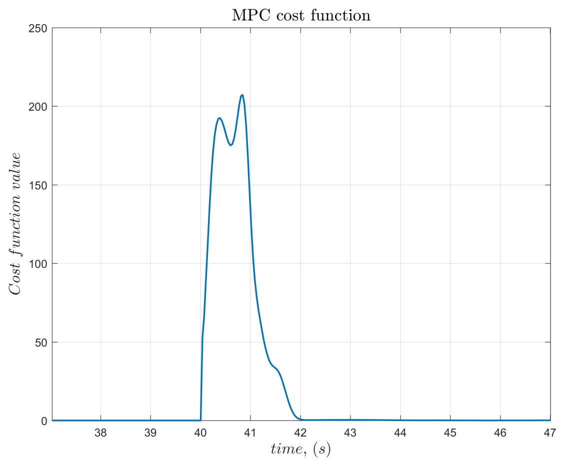

(a) Cost function

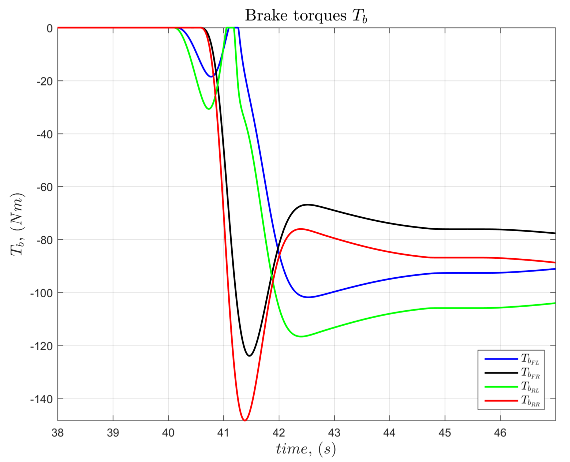

(b) Brake torques T_b

NMPC - Planar car model without real-time cost update performance

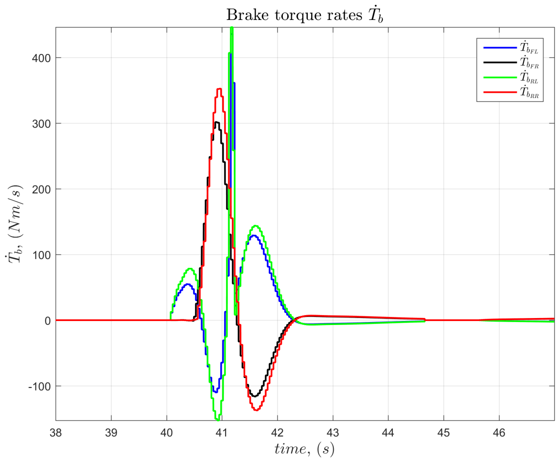

(c) Brake torque rates $\dot{T}_b$

Figure 5.7: NMPC - Planar car model without real-time cost update performance

This is again a big advantage of the real-time cost function update method. The modular cost function design can allow to break the maneuver in parts and tell the controller exactly what needs to be achieved in each part. By smartly dividing the maneuver in three parts, one can use the reference signals to vary the cost function in real-time and get the desired action achieved by the controller. If not for this update scheme, the brake torques would never go to zero. Therefore, this scheme is not only helpful in improving performance as shown in Section 5.4, but also ensures that the actuator wear is minimized and the car drives in a normal behaviour.

5.6. Summary

This chapter focused on all the key elements designed methodologically to ensure that superior performance from the controllers formulated can be achieved. Can-bit sheet analysis and simulation based method was deployed to fix the prediction time of the three controllers to ensure real-time feasibility is guaranteed at all times. The activation logic this control scheme was discussed in which the entire subsystem synchronisation of the three-layer control architecture was explained using the concept of pre-defined TTC threshold value. The implementation of designed activation logic in this research was then explained. The penultimate topic of this chapter involved the in-depth explanation of novel real-time cost function update algorithm designed to improve controller's overall tracking performance and simulation results were shown to highlight the same. Lastly, the chapter concluded by defining the LQR error based technique along with simulation and KPI study based methodology used to fine-tune the three controllers for further tracking performance improvements.

6

Controller Performance

6.1. Introduction

This chapter contains all the simulation results and performance plots to make conclusive observations based on subjective analysis of all the results. The simulation results for all the three controllers for all the scenarios defined are presented here along with comparison plots to make conclusion about the controller's performance. An analysis of controller's performance with and without constraints modelled is also shown following which the summary concludes this chapter.

6.2. Different maneuver scenarios

In order to asses the controller's performance, a variety of scenarios with different speed range and friction coefficient values were analysed. The controllers and simulation design was constructed in a generic way such that it can handle all these variations well. Also, the controller was not designed only for evasive control but has the capability to perform all the maneuvers At the same time, it was essential to assess the robustness of the controller. Therefore, scenarios with sensor information delay, lateral wind disturbances and varying normal loads via addition of passengers were also modeled to check controller's performance with parameter variations. The variety of scenarios are defined in total 5 sets.

The normal load here in the scenarios refers to variation in sprung mass of the vehicle. In reality, the car will have passengers sitting in it at random locations and it is expected that the controller should be able to deal with this variation and perform the maneuver successfully. In this research, four passengers were made to sit in the car at various random locations as shown in Fig 6.1.

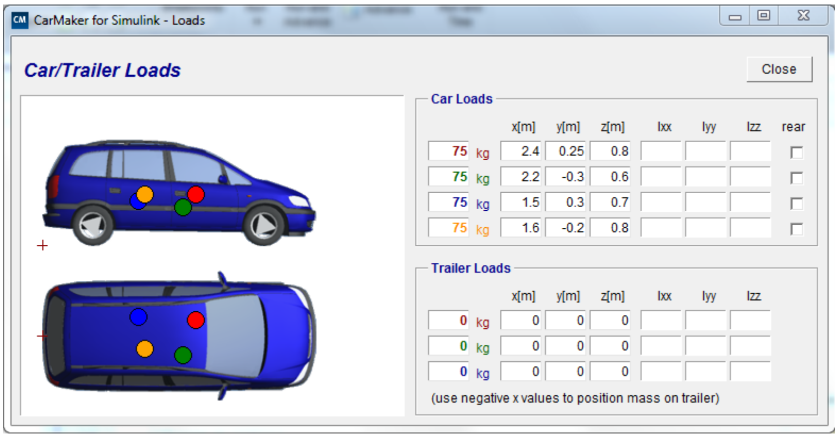

Figure 6.1: Location of passengers sitting in the vehicle

As an assumption, the weight of the passenger was assumed to be $75kg$. In total, four passengers were added to the car in the same order as shown in top view of Fig 6.1. Starting from front left i.e. the driver, then front right, rear left and finally rear, all being positioned one by one in the car. Thus, the total mass of the vehicle was gradually increased by $75kg$ till $300kg$. One can vary these positions as well and check the robustness for all cases. Here, the positions were randomly fixed based on intuitive understanding.

Set 1 - varying v_x

The first set of scenarios involves variation in vehicle speeds for a set road friction coefficient value. These speed range were calculated based on explanation given in Section 4.5. Table 6.1 provides all the scenarios. In all of them, no lateral wind is given as external disturbance and no passenger is made to sit i.e. the car is empty.

Case -	μ -	v_x [km/hr]
1	0.9 (dry road)	75
	0.9	80
	0.9	85
	0.9	90
	0.9	95
	0.9	100
2	0.6 (wet road)	70
	0.6	75
	0.6	80
	0.6	85
	0.6	90
3	0.3 (snow)	45
	0.3	50
	0.3	55
	0.3	60
	0.3	64

Table 6.1: Maneuver with varying velocity scenarios

Set 2 - varying μ
The second set of scenarios involves variation in values of μ for given set speeds as shown in Table 6.2. Here also, the external wind speed is zero and no passenger is sitting in the car.

Case. -	μ -	v_x [km/hr]
1	0.5	80
	0.6	80
	0.7	80
	0.8	80
	0.9	80
	1	80
2	0.3	60
	0.4	60
	0.5	60
	0.6	60

Table 6.2: Maneuver with varying μ scenarios

Set 3 - varying normal load
The third set of scenarios involves variation in values of normal load of the vehicle for a fixed value of μ and v_x as shown in Table 6.3. One by one, all four passengers are made to sit and the robustness of the controller to parameter variations is assessed. In this case too, the wind speed is set to zero.

Case -	μ -	v_x [km/hr]	Normal load [kg]
1	0.9	90	0
	0.9	90	75
	0.9	90	150
	0.9	90	225
	0.9	90	300
2	0.6	80	0
	0.6	80	75
	0.6	80	150
	0.6	80	225
	0.6	80	300
3	0.3	60	0
	0.3	60	75
	0.3	60	150
	0.3	60	225
	0.3	60	300

Table 6.3: Maneuver with varying normal load scenarios

Set 4 - varying wind velocity v_w

This set of scenarios involves variation of external lateral wind speeds v_w for a fixed value of μ and v_x as shown in Table 6.4. The wind is modelled to flow only in south direction, directly opposing the vehicle as it turns left (towards the north direction) according to the maneuver defined. By doing so, the idea is to completely oppose the motion of vehicle with wind and assess robustness of the controller with respect to external unmodelled disturbance. In this case, the car is empty, no passenger is sitting inside.

Case	μ	v_x	v_w
-	-	[km/hr]	[km/hr]
1	0.9	90	0
	0.9	90	10
	0.9	90	30
	0.9	90	50
	0.9	90	70
2	0.6	80	0
	0.6	80	10
	0.6	80	30
	0.6	80	50
	0.6	80	70
3	0.3	60	0
	0.3	60	10
	0.3	60	30
	0.3	60	50
	0.3	60	70

Table 6.4: Maneuver with varying wind speed scenarios

Set 5 - varying maneuver's aggressiveness

The fifth set of scenarios highlights the ability of the controller to handle various dynamic scenarios ranging from evasive action to normal single lane change maneuver. To achieve this, the parameter C_2 in the sigmoid curve was decreased gradually, By doing so, the slope of the trajectory was gradually reduced, making the reference trajectory less aggressive. Table 6.5 contains all the scenarios modelled for this case. The wind speed is zero and no passenger is sitting in the car.

Case	μ	v_x	C_2
-	-	[km/hr]	[m]
1	0.9	90	5
	0.9	90	4
	0.9	90	3
	0.9	90	2
	0.9	90	1
	0.9	90	0.5

Table 6.5: Maneuver with varying C_2 scenarios

6.3. Simulation Results and Comparison

6.3.1. Set 1 Scenarios - varying v_x

In this section, only the plots relevant to the Set 1 scenarios (constant μ with varying velocities) have been reported. All the plots of the simulation are attached in the Appendix. The tracking plots for Set 1 - Case 1 using a LMPC: Linear Bicycle Model is shown in Fig 6.2.

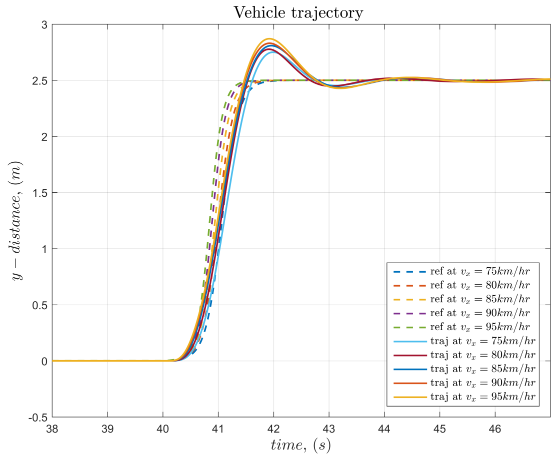

(a) Lateral position y_p

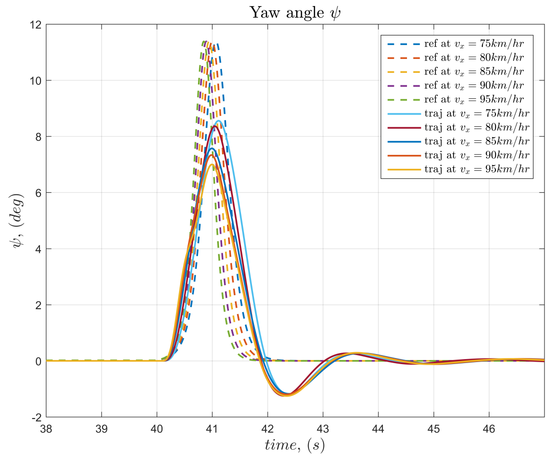

(b) Yaw angle ψ

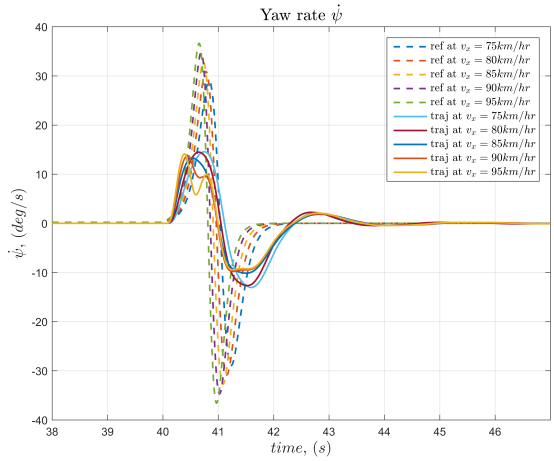

(c) Yaw rate $\dot{\psi}$

S No. -	v_x [km/hr]	M_p [%]	T_s [s]	T_r [s]	y_{RMS} [%]	ψ_{RMS} [%]	$\dot{\psi}_{RMS}$ [%]	DTC [m]
1	75	25.03	5.66	0.45	7.94	80.16	465.28	0.60
2	80	27.66	5.62	0.44	8.89	83.13	500.50	0.55
3	85	30.86	6.35	0.46	11.32	95.38	560.09	0.42
4	90	32.99	6.32	0.45	13.32	103.50	631.20	0.30
5	95	37.03	7.00	0.45	16.54	119.12	734.22	0.14

(d) KPI performance

Figure 6.2: MPC - Linear bicycle model simulation result: $\mu = 0.9$

It can be seen that for the same μ, as the vehicle speeds are increasing, the maneuver is becoming more aggressive. This was seen with reducing TTC values in Table 4.2. Thus, to cover the same lateral distance in reduced time, the vehicle needs to laterally traverse even more quickly than before. This effect is realized by the reference generator as well and that is why we see all the three reference trajectories shifting towards left side as the vehicle speeds increases. And because of the same reason, we see increase in value of $\dot{\psi}_{\text{ref}}$ with increasing speeds. Finally, it can be seen that due to using a kinematic reference generator, the ψ_{ref} and $\dot{\psi}_{\text{ref}}$ values are high and unrealistic for vehicle to follow at such speeds. This is the reason why the RMS error values of both these quantities are so high.

Now, the biggest issue noticed here was the high overshoot seen in all the trajectories with values around 30% (as seen in Fig 6.2d) meaning that the vehicle was overshooting the step value by 30cm. This can be very dangerous because the SV may collide with the vehicles coming from the opposite lane. The reason why this overshoot was occurring was due to the use of a linear tire model. A linear bicycle model is suitable to handle situations which fall in the linear regime of motion. This model uses a linear tire force model to estimate the cornering stiffness. But the maneuver designed forces the vehicle to go in the nonlinear regime of motion which a linear bicycle model is not designed to account for.

Therefore, to remove this overshoot, the idea was to use a nonlinear tire model which can capture the nonlinear tire dynamics well so that effective control is obtained. To do so, Dugoff tire model, explained in Section 3.3, was used to estimate the nonlinear cornering stiffness C_α^{non}. Instead of using the linearised value of C_α, the Dugoff tire formula was used and a fitted nonlinear cornering stiffness of the form shown in Eq (6.1) was now used as online data and passed to the controller. The Dugoff tire model's tuning parameter e_r was set to 0.05.

$$C_{\alpha_{\text{ij}}}^{\text{non}} = \frac{C_{\alpha_{\text{ij}}}}{1-\kappa_{\text{ij}}} f(\lambda) \tag{6.1}$$

In order to capture the nonlinear vehicle dynamics behaviour, the idea was to use a nonlinear bicycle model as the next MPC controller. By capturing all the relevant dynamics of vehicle and tire now, it was expected that the overshoot should reduce and the vehicle would still be able to avoid the collision. The tracking plots for Set 1 - Case 1 using a NMPC: Nonlinear Bicycle Model is shown in Fig 6.3. It can be seen that the overshoot has significantly reduced now. Thus, the Dugoff tire model did capture the dynamics well and the controller was able to provide the necessary control. But, the DTC values relatively decreased as compared to that of the linear bicycle model MPC.

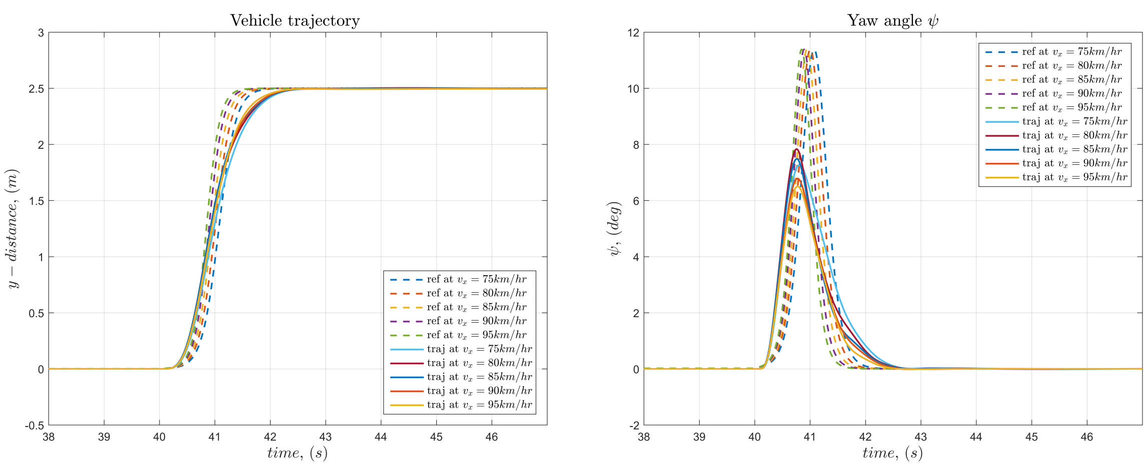

(a) Lateral position y_p

(b) Yaw angle ψ

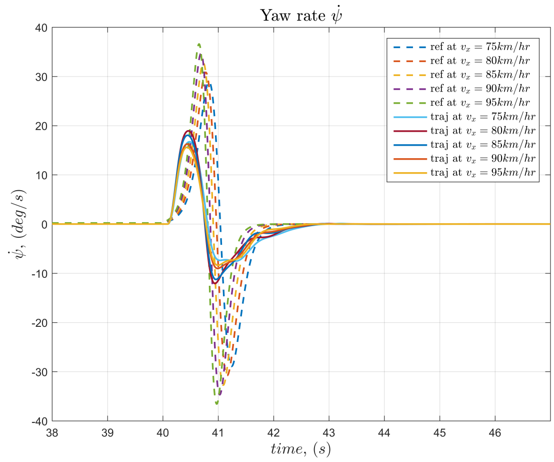

(c) Yaw rate $\dot{\psi}$

S No.	v_x	M_p	T_s	T_r	y_{RMS}	ψ_{RMS}	$\dot{\psi}_{RMS}$	DTC
-	[km/hr]	[%]	[s]	[s]	[%]	[%]	[%]	[m]
1	75	0.29	2.45	0.88	10.45	121.28	625.61	0.49
2	80	0.21	2.49	0.90	10.32	125.45	669.52	0.47
3	85	0.00	2.48	0.88	9.35	106.85	599.14	0.41
4	90	0.00	2.39	0.83	11.25	94.27	569.19	0.26
5	95	0.00	2.38	0.76	13.39	90.16	574.36	0.15

(d) KPI performance

Figure 6.3: MPC - Nonlinear bicycle model simulation result: $\mu = 0.9$

To improve the performance further, integrated brake and steering control was designed. The differential braking should provide an extra yaw moment which in principle should give better tracking and higher DTC values as compared to previous two bicycle based MPC control strategies. This performance improvement Fig 6.4 shows the tracking plots for Set 1 - Case 1 using a NMPC: Planar car Model.

It can be seen that as the maneuver becomes more aggressive, the controller responds to it by shifting the vehicle trajectory towards left. But as seen from the yaw angle plot (Fig 6.4b), the ability of the vehicle to yaw reduces with increasing speeds. This is very natural due to the vehicle dynamics, as the maneuver's speed is increasing, the ability to generate lateral forces will decrease leading to less turning of vehicle. This is very well captured in the KPI values (Fig 6.4d), which, apart from DTC, are gradually increasing. The DTC on the other hand is decreasing. But despite such aggressive action, it was the first time that the collision was avoided even at $100km/hr$ by this controller. With both the bicycle model based MPC controllers, the vehicle could only avoid the crash till $95km/hr$ only.

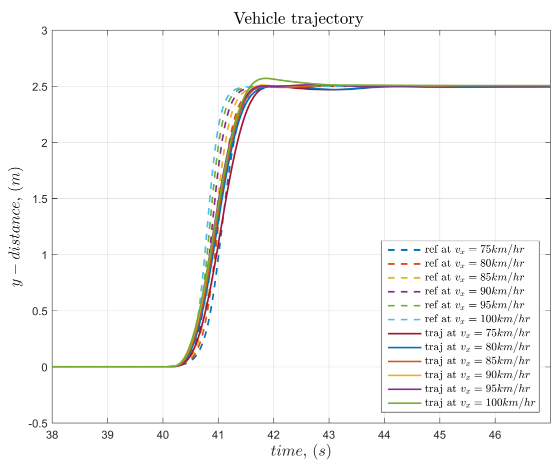

(a) Lateral position y_p

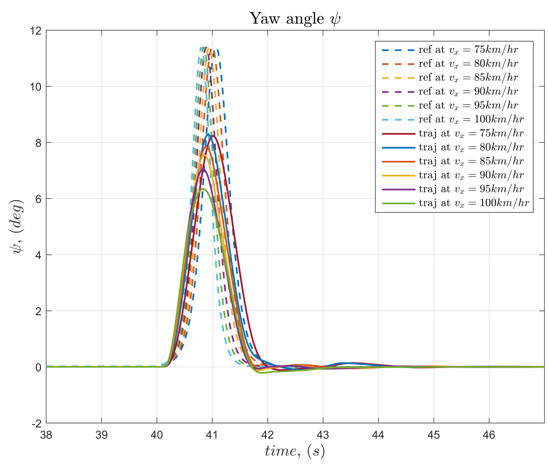

(b) Yaw angle ψ

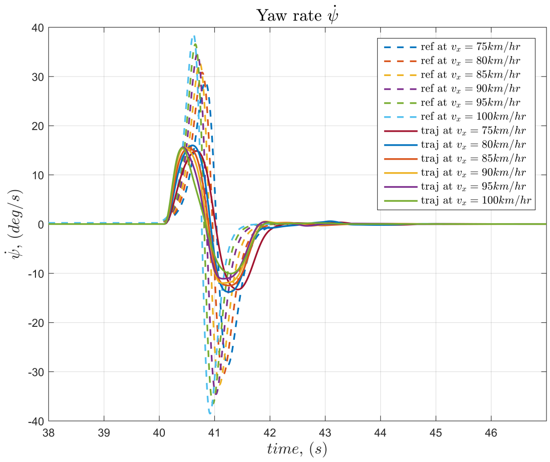

(c) Yaw rate $\dot{\psi}$

S No.	v_x	M$_p$	T$_s$	T$_r$	y$_{\mathrm{RMS}}$	ψ_{RMS}	$\dot{\psi}_{\mathrm{RMS}}$	DTC
-	[km/hr]	[%]	[s]	[s]	[%]	[%]	[%]	[m]
1	75	0.00	3.80	0.56	4.86	65.40	391.02	0.61
2	80	0.29	3.77	0.55	5.02	68.17	400.62	0.59
3	85	1.03	3.18	0.54	5.90	69.45	459.94	0.50
4	90	1.34	3.10	0.53	7.37	71.30	500.64	0.41
5	95	1.45	3.08	0.54	10.22	77.13	557.86	0.28
6	100	7.01	3.30	0.53	14.20	91.92	651.99	0.09

(d) KPI performance

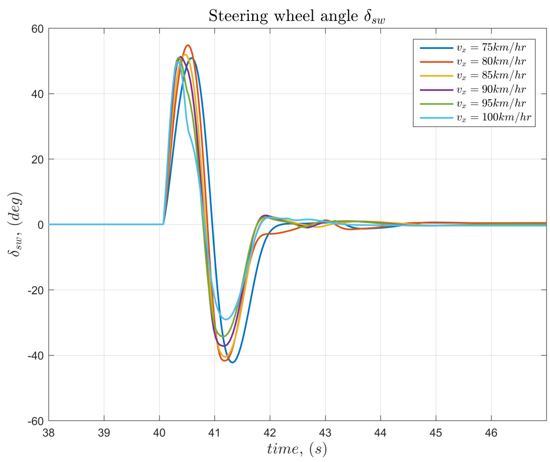

(e) SWA

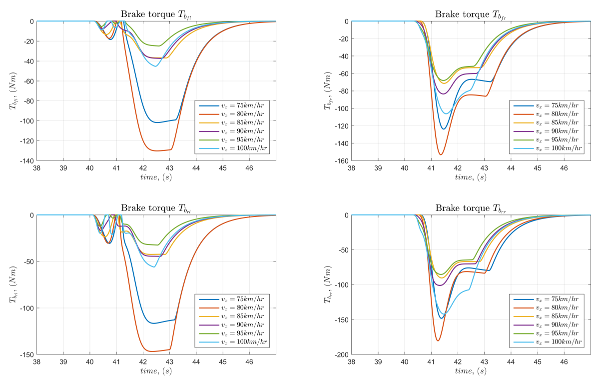

(f) Brake Torques T_b

Figure 6.4: MPC - Planar car model simulation result: $\mu = 0.9$

The integrated action of steering and braking is shown in Fig 6.4e and Fig 6.4f. The differential braking is well seen here with the left brakes braking first for left turn. Then the right brakes brake for the right turn and simultaneously left brakes torque reduces. Lastly, the controller modulates the brakes individually along with SWA to ensure car remains stable post maneuver and drives in straight-line with negligible overshoot. The control action plots SWV and $\dot{T}_b$ rate are attached in Appendix. So, one can now clearly see that the Planar car MPC controller gives the highest DTC values among all the controllers meaning that it performs the best in avoiding the collision. This comparative analysis is shown in Fig 6.5a - Fig 6.5g in which all the KPI values of all the three controllers have been plotted.

It can be seen that the Planar Car MPC based controller gives the lowest tracking error values for all the three reference signal. Its step input based KPI's are also on the lower side, if not the lowest and at the same time the DTC value is highest of all the three control strategies. The fact that rise time values are on an average $0.53s$ for the integrated MPC scheme shows that the reaction times of controller is superior as compared to a driver. This shows that autonomous design of controller for evasive action provides quick and active control.

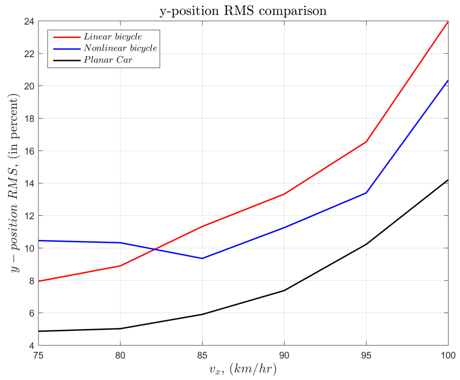

(a) y_{RMS}

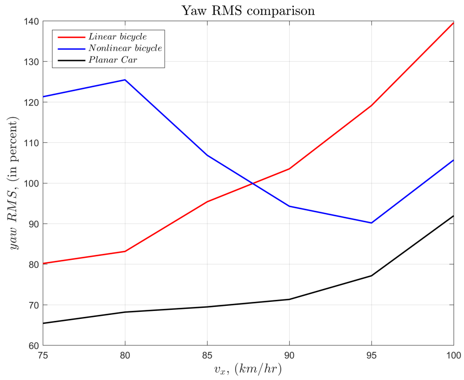

(b) ψ_{RMS}

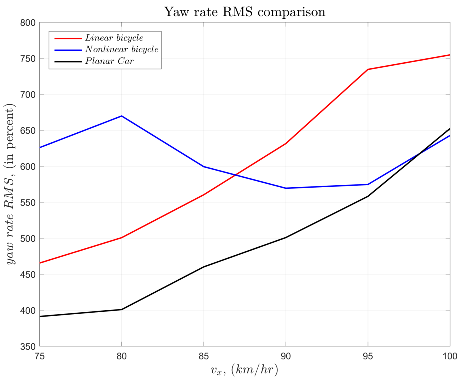

(c) $\dot{\psi}_{\text{RMS}}$

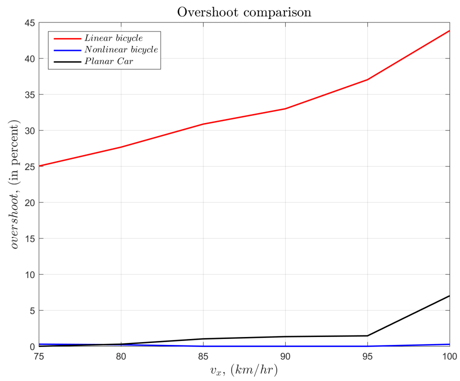

(d) Overshoot M_p

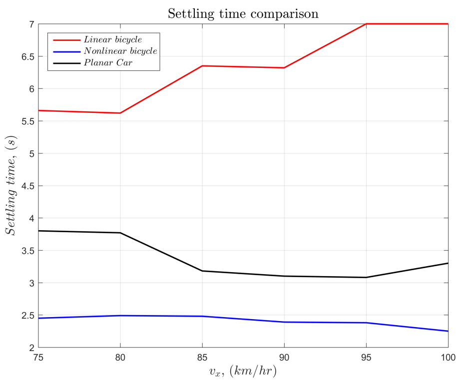

(e) Settling time T_s

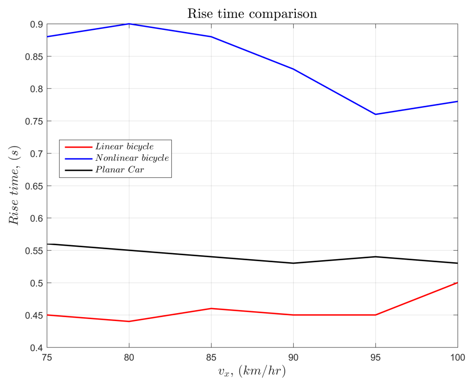

(f) Rise time T_r

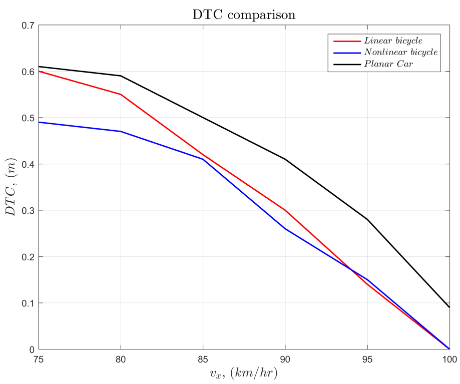

(g) DTC

Figure 6.5: KPI comparison for $\mu = 0.9$

The integrated control scheme has outperformed other two control scheme and provides the best performance of all. This is again very well understood in Fig 6.6a - Fig 6.6d for one scenario just to show how the trajectories look once they are compared together. It can be seen that with the integrated control scheme, not only has the overshoot reduced as compared to linear bicycle model, but the ability of the vehicle to yaw has increased leading to better tracking as compared to both the other control strategies.

The comparison performance for individual controller's trajectories is not reported for all cases here as the plots look very similar. The basic understanding behind how the pictorial representation of the quantitative KPI values looks like is presented for this case. Thus, the performance improvement can be better understood.

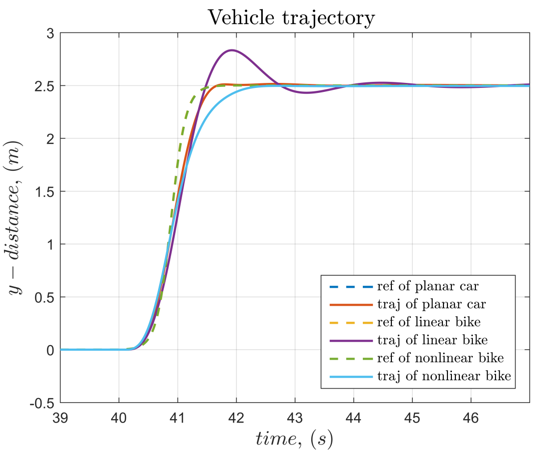

(a) Lateral position y_p

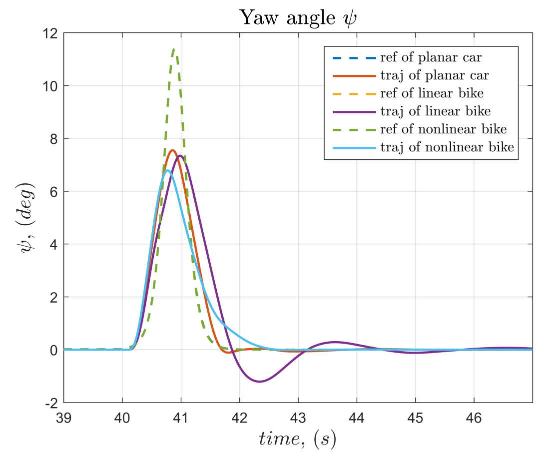

(b) Yaw angle ψ

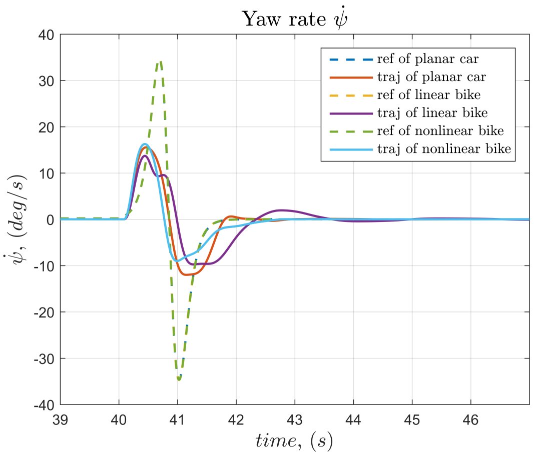

(c) Yaw rate $\dot{\psi}$

S No.	MPC model	M_p	T_s	T_r	y_{RMS}	ψ_{RMS}	$\dot{\psi}_{RMS}$	DTC
-	-	[%]	[s]	[s]	[%]	[%]	[%]	[m]
1	Linear bicycle	32.99	6.32	0.45	13.32	103.50	631.20	0.30
2	Nonlinear Bicycle	0.00	2.39	0.83	11.25	94.27	569.19	0.26
3	Planar car	1.34	3.10	0.53	7.37	71.30	500.64	0.41

(d) KPI performance

Figure 6.6: Performance comparison for the case: $\mu = 0.9$ and $v_x = 90 km/hr$

For the Set 1 - Case 2 and Set 1 - Case 3 scenarios, the maneuver plots remained very much similar in dynamics and therefore have been attached in the Appendix. But the KPI comparison plots are shown below to compare performance. It can be seen that similar trends for all KPI's with low values via Planar car MPC but high DTC values are seen in all the scenarios. The integrated controller outperforms the other two controllers at all speeds and at all road surface types, giving the best performance of all.

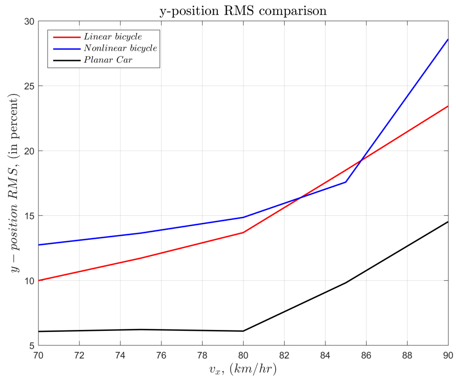

(a) y_{RMS}

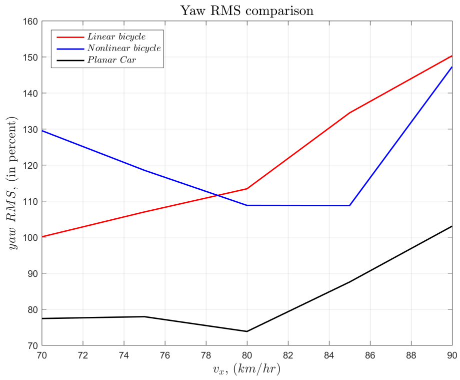

(b) ψ_{RMS}

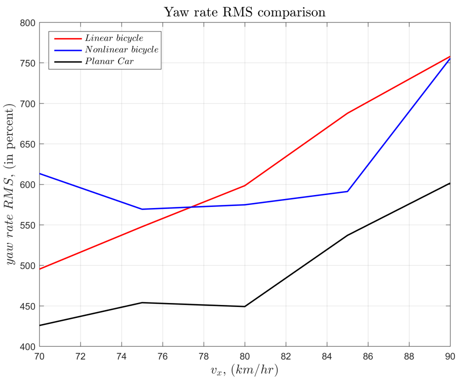

(c) $\dot{\psi}_{\text{RMS}}$

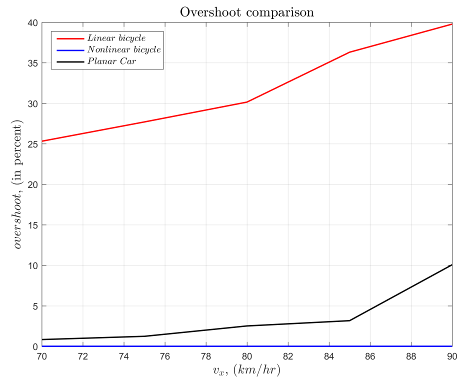

(d) Overshoot M_p

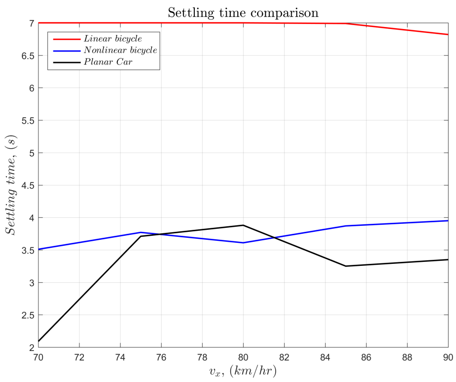

(e) Settling time T_s

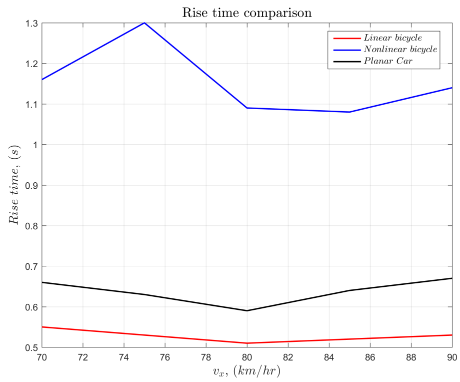

(f) Rise time T_r

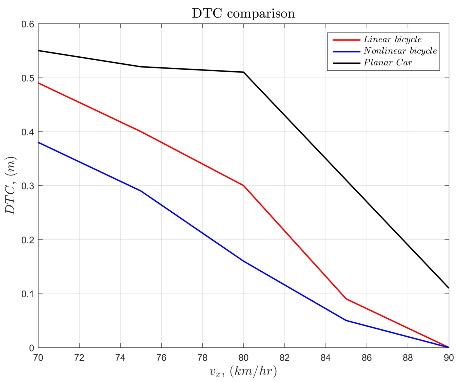

(g) DTC

Figure 6.7: KPI comparison for Set 1 - Case 2 scenarios: $\mu = 0.6$

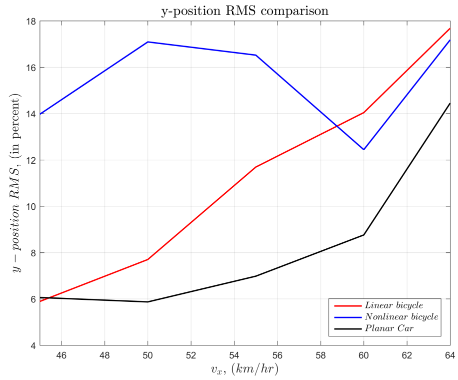

(a) y_{RMS}

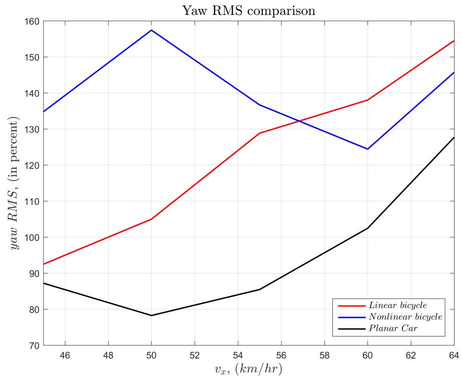

(b) ψ_{RMS}

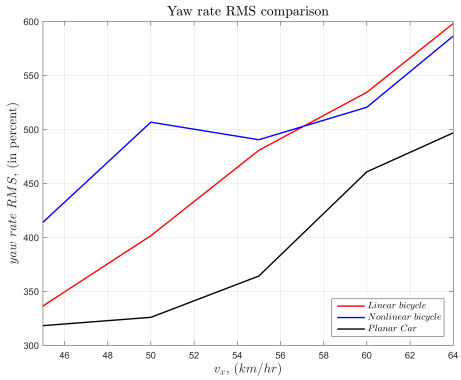

(c) $\dot{\psi}_{\text{RMS}}$

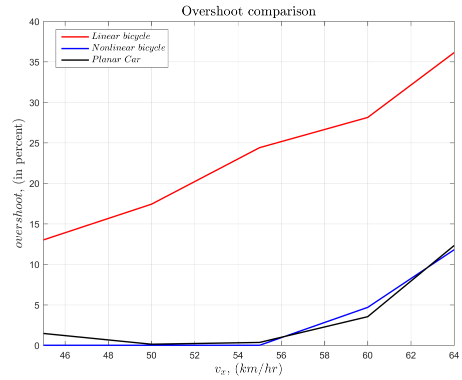

(d) Overshoot M_p

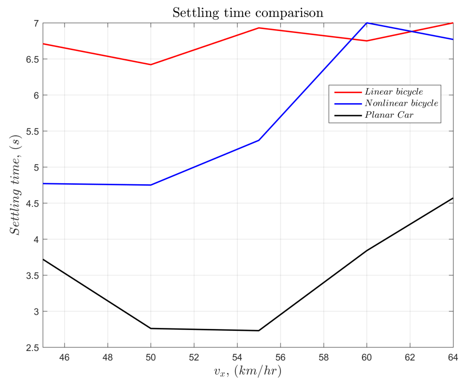

(e) Settling time T_s

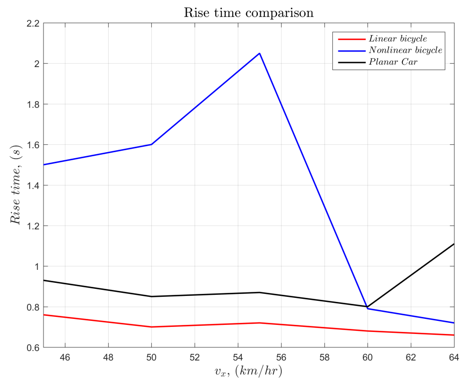

(f) Rise time T_r

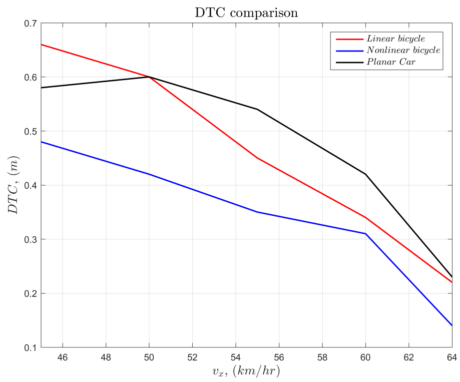

(g) DTC

Figure 6.8: KPI comparison for Set 1 - Case 3 scenarios: $\mu = 0.3$

6.3.2. Set 2 Scenarios - varying μ

This section involves the simulation results for the Set 2 scenarios (constant velocities with varying μ). The aim over here is to validate whether the control can work with varying road conditions and changing tire grip. The simulation plots for Set 2 - Case 1 with the use of Linear bicycle model have been reported in Fig 6.9.

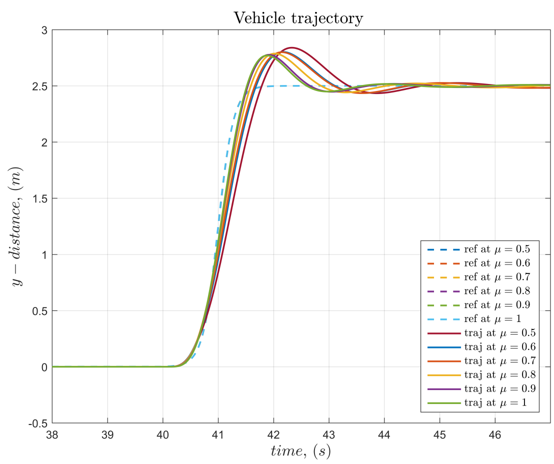

(a) Lateral position y_p

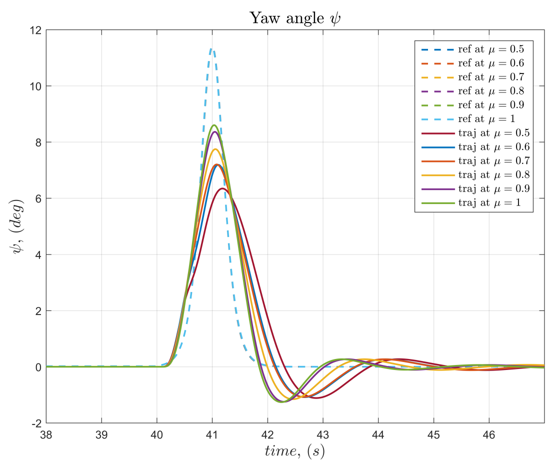

(b) Yaw angle ψ

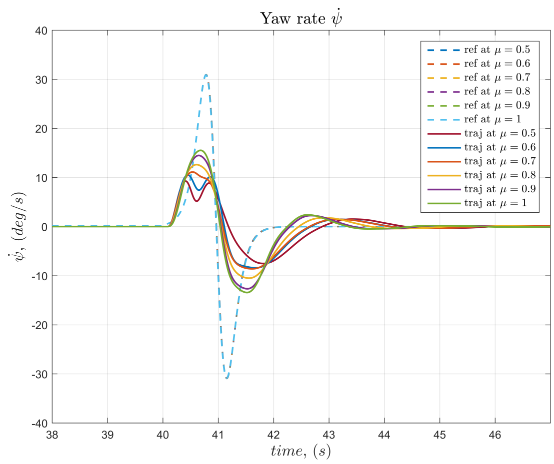

(c) Yaw rate $\dot{\psi}$

S No. -	μ -	M_p [%]	T_s [s]	T_r [s]	y_{RMS} [%]	ψ_{RMS} [%]	$\dot{\psi}_{RMS}$ [%]	DTC [m]
1	0.5	33.96	7.00	0.55	18.32	138.20	659.13	0.10
2	0.6	30.15	7.00	0.51	13.68	113.41	598.31	0.30
3	0.7	29.97	7.00	0.51	12.61	106.77	569.52	0.35
4	0.8	28.73	6.39	0.47	10.39	94.13	534.14	0.47
5	0.9	27.66	5.62	0.44	8.89	83.13	500.50	0.55
6	1	27.05	5.38	0.43	8.32	78.26	478.96	0.59

(d) KPI performance

Figure 6.9: MPC - Linear bicycle model simulation result: $v_x = 80 km/hr$

It can be seen that for the constant velocity case, the reference trajectory remains the same even though the friction coefficient is increasing. The ability of the vehicle to perform the same maneuver with increasing μ should improve but this is not seen in the kinematic reference trajectory. But, being so, this trajectory method was purposefully chosen as explained before to see if the controller is able to improve performance with a constant trajectory. And it can be seen that with increasing μ, the grip is improving and therefore the performance of the same maneuver is improving with vehicle trajectories shifting towards the left, closer to the reference (Fig 6.9a).

This is clearly highlighted with increasing yaw angle values as seen in Fig 6.9b as well as earlier yaw with peak shifting towards left. And the KPI values represent this phenomenon well with increasing DTC and decreasing RMS error values as the grip improves, showing that the vehicle dynamics are well captured here and the performance of the controller is improving with improving road conditions. And as expected, a high overshoot was again witnessed in this case. By using Nonlinear bicycle model with Nonlinear Dugoff tire model, Fig 6.10 represents the simulation results for same scenario performed.

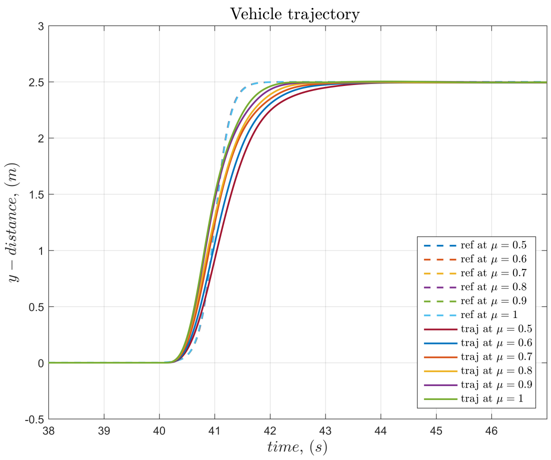

(a) Lateral position y_p

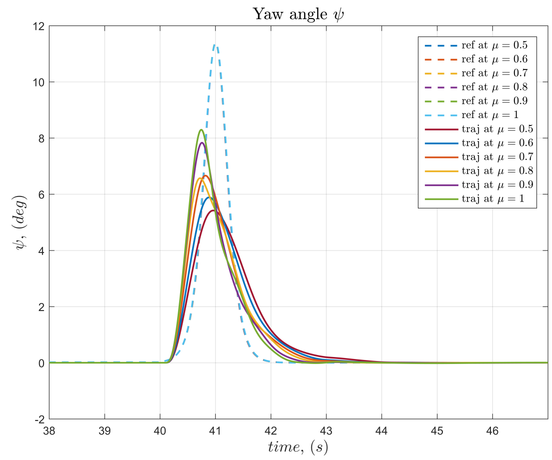

(b) Yaw angle ψ

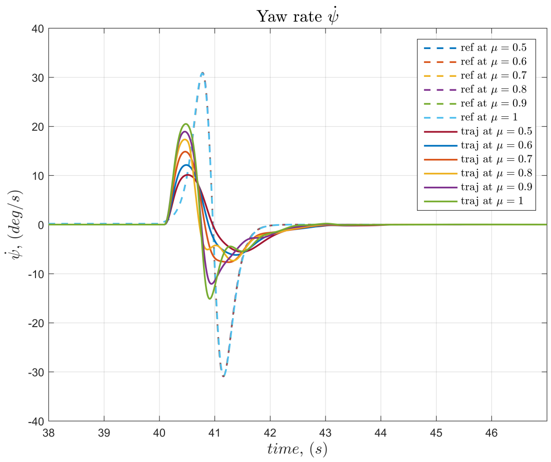

(c) Yaw rate $\dot{\psi}$

S No. -	μ -	M_p [%]	T_s [s]	T_r [s]	y_{RMS} [%]	ψ_{RMS} [%]	$\dot{\psi}_{RMS}$ [%]	DTC [m]
1	0.5	0.00	3.93	1.20	18.91	115.02	583.85	0.02
2	0.6	0.00	3.61	1.09	14.85	108.79	574.68	0.16
3	0.7	0.00	3.25	1.05	11.46	108.22	579.65	0.32
4	0.8	0.00	2.80	0.97	11.20	119.72	670.22	0.35
5	0.9	0.21	2.49	0.90	10.32	125.45	669.52	0.47
6	1	0.35	2.24	0.82	10.33	131.61	728.69	0.50

(d) KPI performance

Figure 6.10: MPC - Nonlinear bicycle model simulation result: $v_x = 80 km/hr$

Now the overshoot is reduced. The same behaviour of improving tracking performance is seen here as well clearly visible in all the figures. But it was observed that the DTC value now have gone down compared to the Linear Bicycle model MPC. This suggests a compromise that by reducing overshoot, one has to do with performance. But still, the collision was avoided at all μ values and the controller could capture the vehicle dynamics well. In order to further improve the performance and not make any comprise with safety distance, the Planar car model integrated MPC scheme was implemented to perform the same set of scenarios and the simulation results are presented in Fig 6.11.

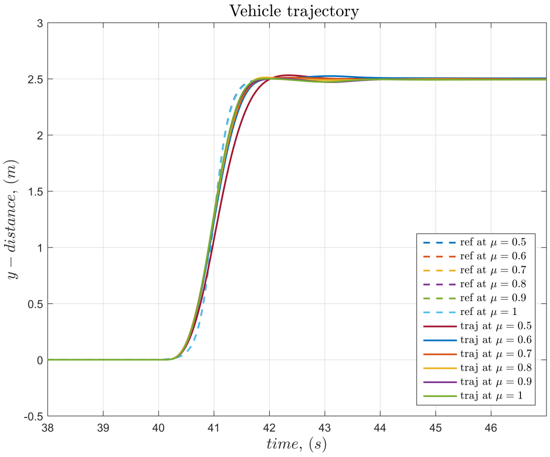

(a) Lateral position y_p

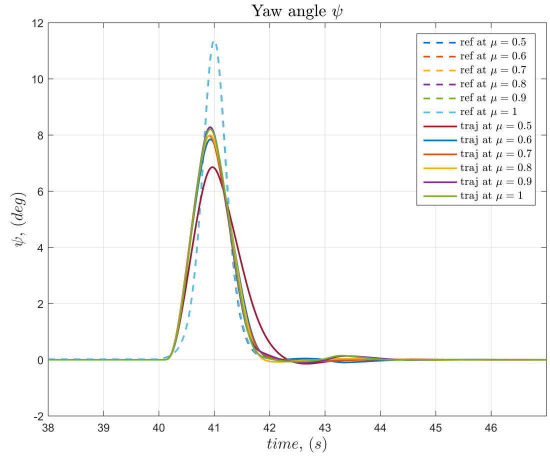

(b) Yaw angle ψ

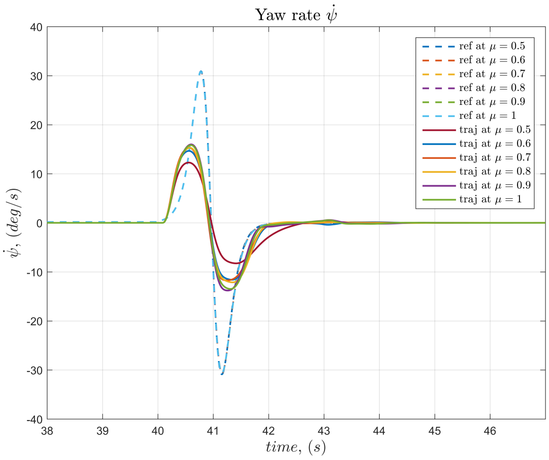

(c) Yaw rate $\dot{\psi}$

S No.	μ	M_p	T_s	T_r	y_{RMS}	ψ_{RMS}	$\dot{\psi}_{RMS}$	DTC
-	-	[%]	[s]	[s]	[%]	[%]	[%]	[m]
1	0.5	3.20	2.88	0.68	10.13	89.51	511.44	0.31
2	0.6	2.51	3.88	0.59	6.09	73.82	449.05	0.51
3	0.7	1.10	2.58	0.58	5.68	75.49	444.10	0.55
4	0.8	1.24	3.37	0.55	5.31	72.30	440.86	0.57
5	0.9	0.29	3.77	0.55	5.02	68.17	400.62	0.59
6	1	0.09	3.63	0.54	4.96	68.25	412.86	0.60

(d) KPI performance

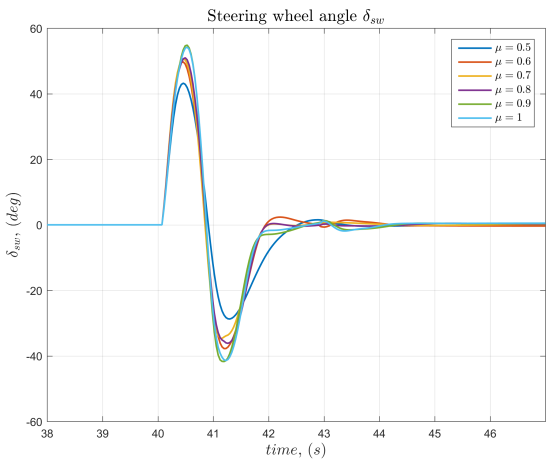

(e) SWA

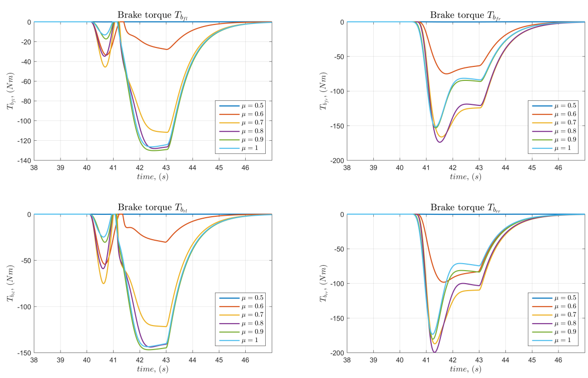

(f) Brake Torques T_b

Figure 6.11: MPC - Planar car model simulation result: $v_x = 80 km/hr$

It can be seen that the Planar car model MPC provides the best performance in terms of small overshoot, lowest RMS error values and highest DTC values. This controller's performance at low μ values is better than the other two strategies which suggests that the controller works well even in low μ conditions. The increasing SWA in Fig 6.11e shows how the controller is able to improve the tracking performance with increasing μ. And the assistance by the differential braking (Fig 6.11f) is very well coordinated along with steering by the controller to further improve the tracking.

A comparative analysis of all the KPI's for the Set 2 - Case 1 scenarios for all the three controllers is shown in Fig 6.12.It can be clearly seen that the integrated Planar car MPC control outperforms other two control strategies. The RMS error obtained from it is the least of all in all the scenario cases and the step input KPI's are also on the lower side. Lastly, the collision avoidance performance w.r.t. DTC values is seen best with Planar car MPC model, providing the best collision avoidance control in all scenarios.

Figure 6.13 represents the KPI performance for the Set 2 - Case 2 scenarios in which the vehicle is made in to drive in snow to wet road conditions at $60km/hr$. As can be seen, for Set 2 - Case 2 scenarios too, the Planar car MPC provided the least RMS error values and highest DTC values in general. This is enough evidence to conclude that for all range of speeds and for all range of μ values, the integrated Planar car MPC control scheme gives the best evasive action performance over the other two control strategies. The essential dynamics are well captured in this scheme and maximum safety is provided at all times by the integrated MPC control.

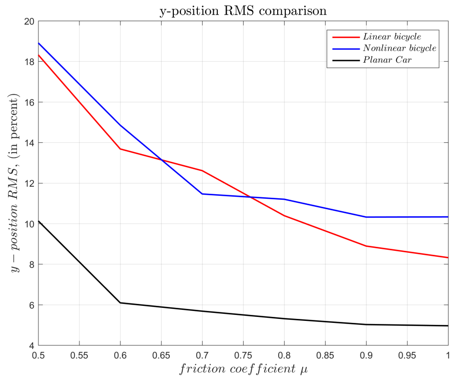

(a) y_{RMS}

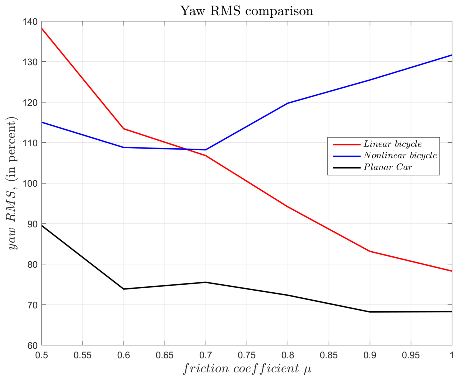

(b) ψ_{RMS}

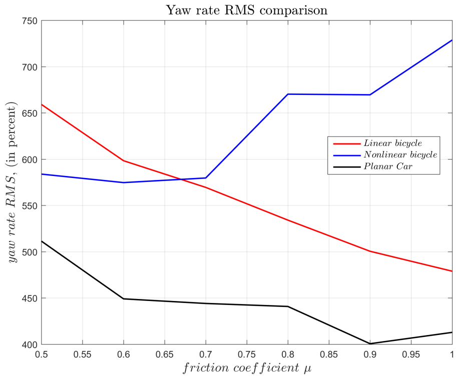

(c) $\dot{\psi}_{\mathrm{RMS}}$

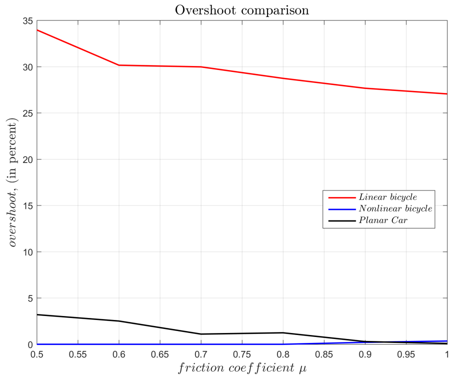

(d) Overshoot M_p

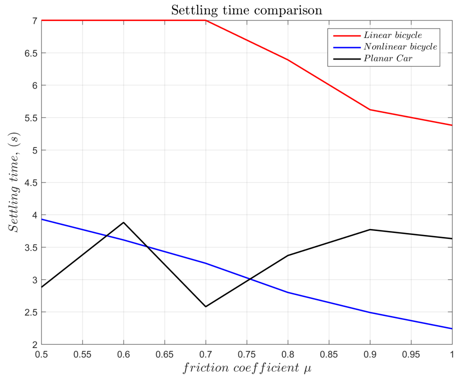

(e) Settling time T_s

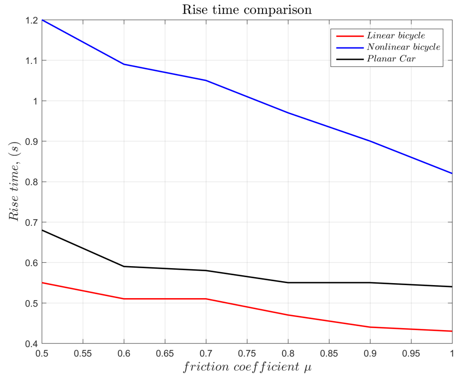

(f) Rise time T_r

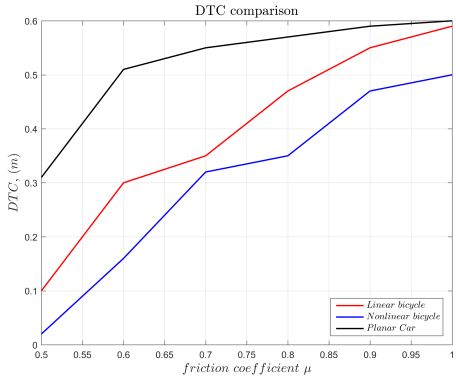

(g) DTC

Figure 6.12: KPI comparison for Set 2 - Case 1 scenarios: $v_x = 80 km/hr$

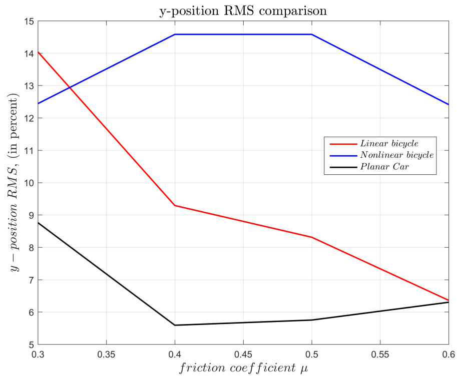

(a) y_{RMS}

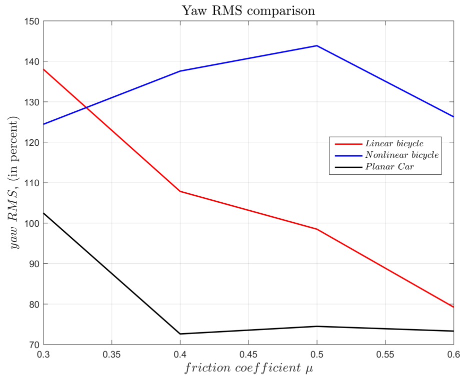

(b) ψ_{RMS}

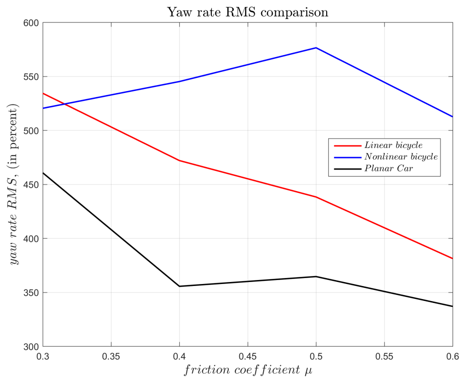

(c) $\dot{\psi}_{\text{RMS}}$

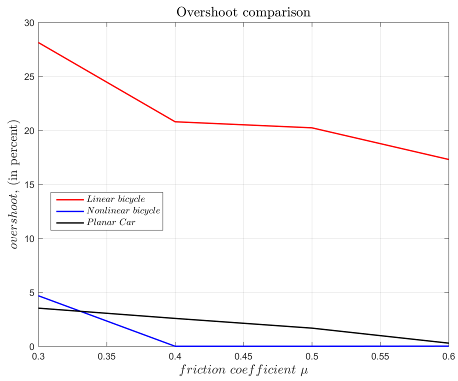

(d) Overshoot M_p

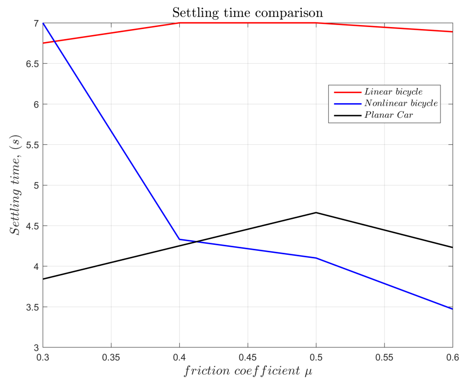

(e) Settling time T_s

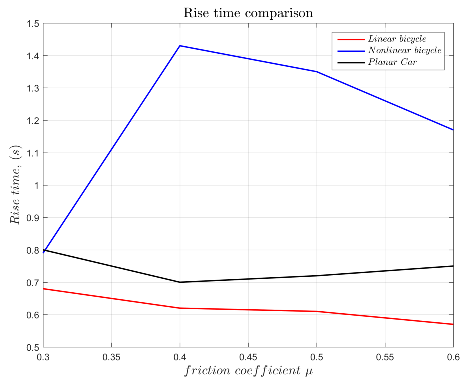

(f) Rise time T_r

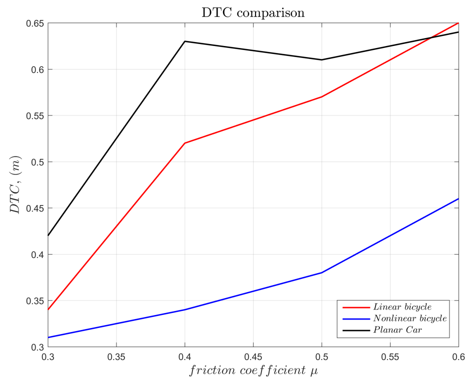

(g) DTC

Figure 6.13: KPI comparison for Set 2 - Case 2 scenarios: $v_x = 60 km/hr$

6.3.3. Set 3 Scenarios - varying normal load

Now that the final control scheme was chosen, it was necessary to analyze the robustness of Planar car model based MPC control scheme. The following sections evaluates this performance in particular. To have a pure robustness analysis, in all the scenarios now, the tuning parameter of the controller were kept the same, only external loads and wind speeds were varied. This section provides the analysis of controller's performance to increasing normal load of the car. By adding passengers one by one as shown in Fig 6.1, the controller's tracking performance for Set 3 - Case 1 is shown in Fig 6.14.

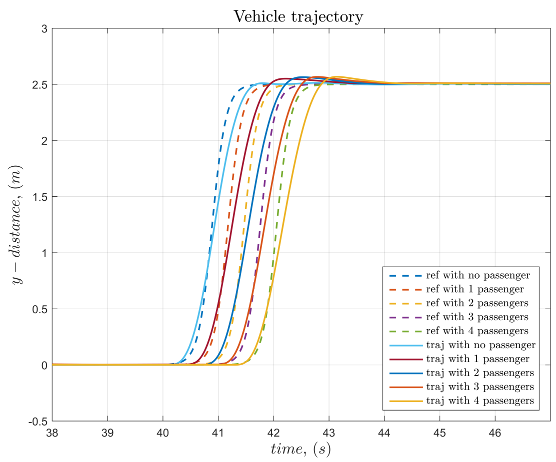

(a) Lateral position y_p

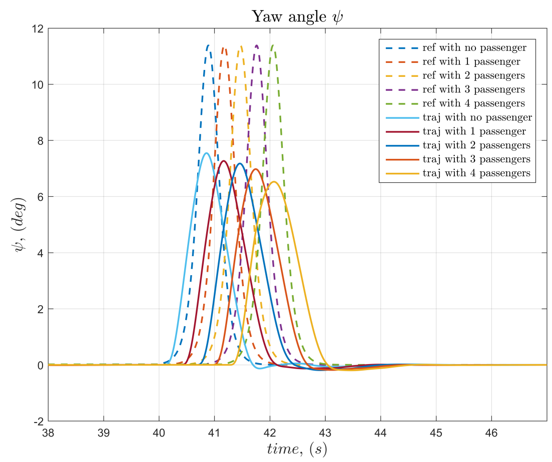

(b) Yaw angle ψ

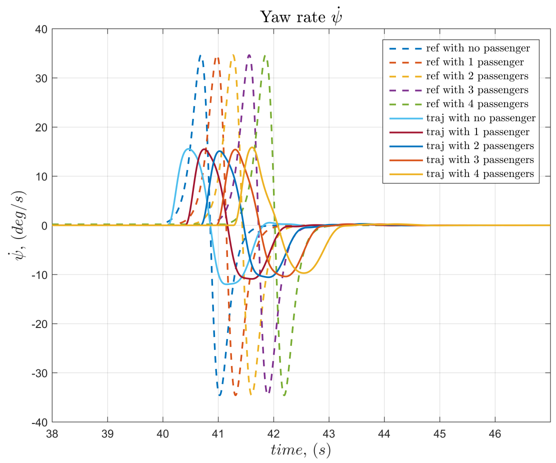

(c) Yaw rate $\dot{\psi}$

S No. -	$F_{z_{passenger}}$ [kg]	M_p [%]	T_s [s]	T_r [s]	y_{RMS} [%]	ψ_{RMS} [%]	$\dot{\psi}_{RMS}$ [%]	DTC [m]
1	0	1.34	3.10	0.53	7.37	71.30	500.64	0.41
2	75	5.00	4.63	0.53	9.36	76.16	528.23	0.33
3	150	6.37	3.01	0.53	9.73	78.82	539.42	0.31
4	225	6.60	4.48	0.54	9.86	82.46	563.42	0.31
5	300	6.67	3.04	0.56	12.35	91.68	612.30	0.20

(d) KPI performance

Figure 6.14: MPC - Planar car Set 3 - Case 1 simulations: $\mu = 0.9$, $v_x = 90 km/hr$

As the normal load of the car is increasing, the aerodynamic drag forces are also increasing. As a result, the vehicle was taking a longer time to reach the starting point of the maneuver i.e. the set point where the SV is $30m$ away from LV. This is the reason why the same maneuver is beginning at varying time values. It was explained in Section 5.3 that instead of setting a minimum TTC threshold value, here the maneuver is defined such that the reference trajectory is calculated when there is a distance of $30m$ between LV and SV, and the same is reflected in the simulation results seen above.

Now, it can be seen that with increasing load, the parameter uncertainty is increasing due to varying CoG positions, roll and pitch center, normal load on each wheel etc. Due to this, the performance of the controller is compromised as seen in the KPI values in Fig 6.14d. But for all the cases, the collision was successfully avoided. Even with such variations, the maximum overshoot was reported at 6.67% but the collision was avoided with still a safety margin of $0.2m$.

The plots for SWA and T_b for this case is not shown here as the dynamic phenomenon of steering and differential braking remains the same. But these plots along with all the other plots have been attached in the Appendix. Now, Fig 6.15 and Fig 6.16 shows the performance of the controller in wet and snow road conditions respectively.

Based on the KPI values for both the cases, it can be concluded that for all different road scenarios, the controller is robust to changing uncertain parameter values and is able to avoid the collision successfully.

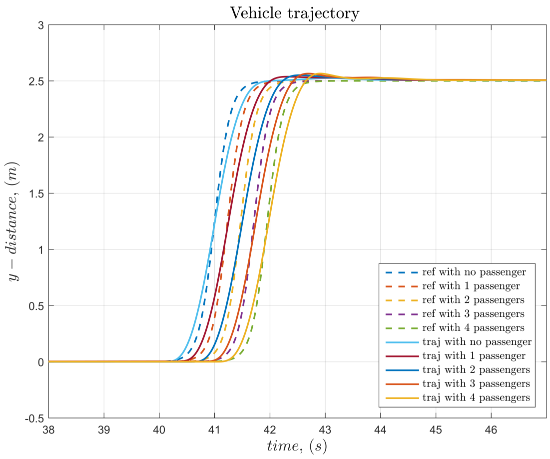

(a) Lateral position y_p

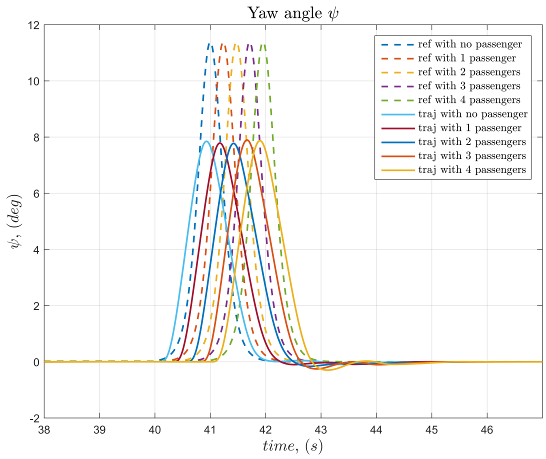

(b) Yaw angle ψ

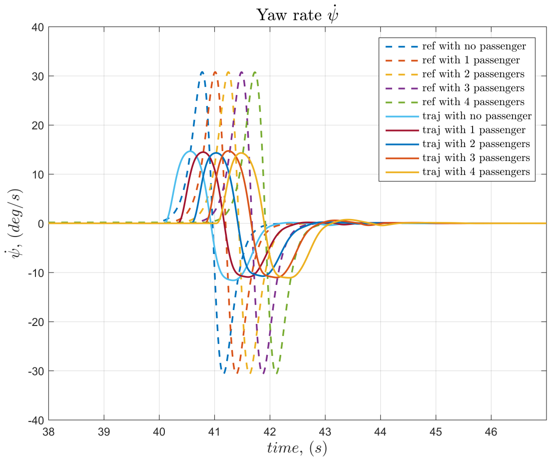

(c) Yaw rate $\dot{\psi}$

S No. -	$F_{z_{\text{passenger}}}$ [kg]	M$_p$ [%]	T$_s$ [s]	T$_r$ [s]	y_{RMS} [%]	ψ_{RMS} [%]	$\dot{\psi}_{\text{RMS}}$ [%]	DTC [m]
1	0	2.51	3.88	0.59	6.09	73.82	449.05	0.51
2	75	3.72	4.12	0.57	6.34	74.45	457.16	0.50
3	150	5.09	4.46	0.57	6.71	74.44	460.00	0.47
4	225	6.47	4.21	0.54	6.62	72.81	457.77	0.48
5	300	6.52	3.92	0.54	6.35	74.74	463.33	0.50

(d) KPI performance

Figure 6.15: MPC - Planar car Set 3 - Case 2 simulations: $\mu = 0.6$, $v_x = 80km/hr$

It was observed in a few scenarios of Set 3 - Case 3 (Fig 6.16) that the controller countersteers for a fraction of second to ensure vehicle stability. But the author believes that this performance can be improved with better tuning of the tuning parameters.

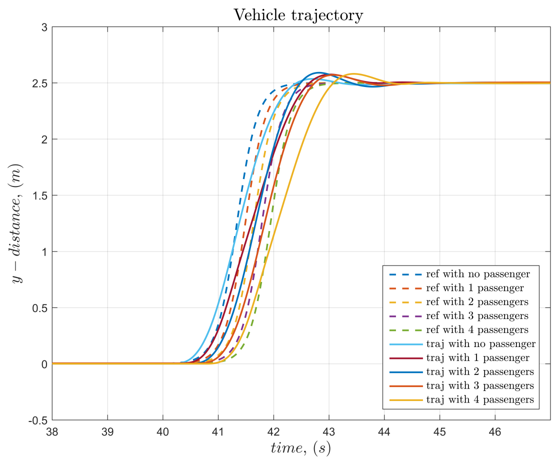

(a) Lateral position y_p

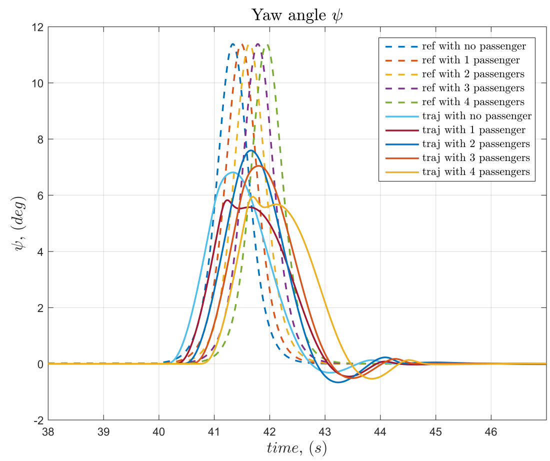

(b) Yaw angle ψ

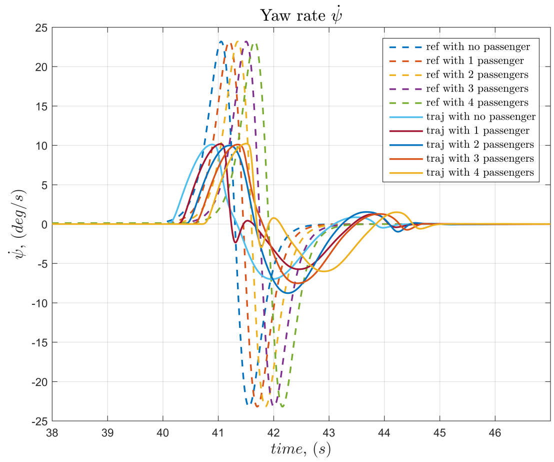

(c) Yaw rate $\dot{\psi}$

S No. -	$F_{z_{\text{passenger}}}$ [kg]	M_p [%]	T_s [s]	T_r [s]	y_{RMS} [%]	ψ_{RMS} [%]	$\dot{\psi}_{\text{RMS}}$ [%]	DTC [m]
1	0	3.53	3.84	0.80	8.76	102.46	460.61	0.42
2	75	7.48	3.50	0.88	13.57	135.58	562.74	0.23
3	150	9.03	3.98	0.68	7.01	91.16	428.69	0.52
4	225	7.07	3.86	0.74	8.32	99.68	454.20	0.44
5	300	8.01	3.77	0.86	13.71	134.33	564.74	0.22

(d) KPI performance

Figure 6.16: MPC - Planar car Set 3 - Case 3 simulations: $\mu = 0.3$, $v_x = 60 km/hr$

6.3.4. Set 4 Scenarios - varying wind velocity v_w

This section covers the Set 4 scenarios related to varying wind speeds to further asses the robustness of Planar car model based MPC control scheme. The performance of controller to parameter uncertainty was evaluated above, now external disturbance is given in the form of lateral wind opposing the vehicle's left turn to see if the controller is able to avoid the collision in such case. Fig 6.17 shows the performance of controller for Set 4 - Case 1 scenarios, designed on dry road.

The wind speed was given about $3s$ before the start of the maneuver to check how quickly can the controller respond to it and control the car. Later, throughout the maneuver, the wind speed acts in the south direction and finally once the steady state is reached, the wind disturbance is removed and it is checked how the controller behaves to this variation. Here also, the reference trajectory remains the same for all cases and controller's performance is purely analyzed.

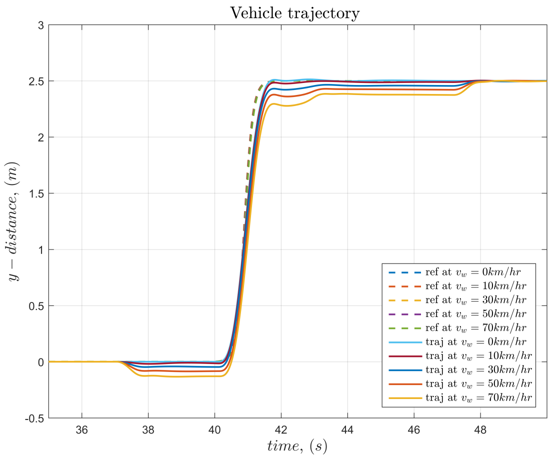

(a) Lateral position y_p

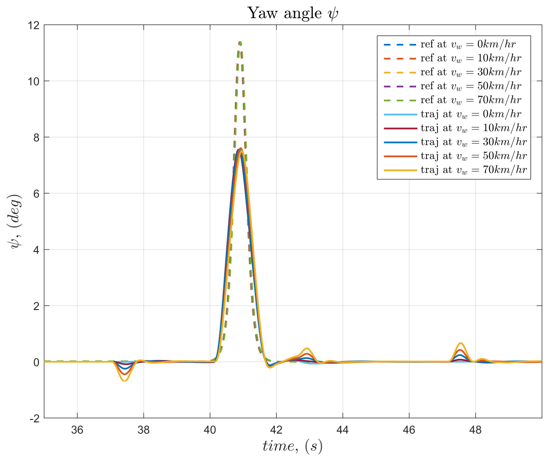

(b) Yaw angle ψ

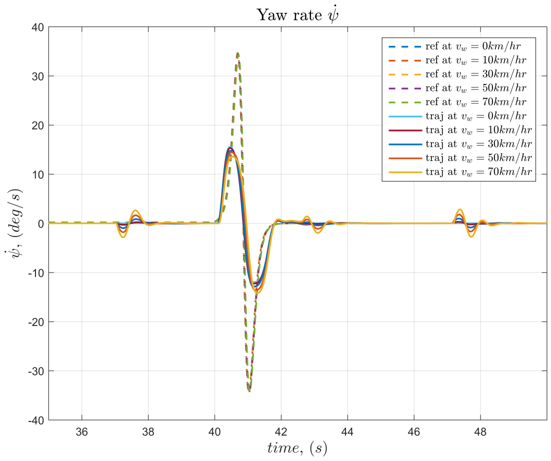

(c) Yaw rate $\dot{\psi}$

S No.	v_w	M_p	T_s	T_r	y_{RMS}	ψ_{RMS}	$\dot{\psi}_{RMS}$	DTC	D_{off}
-	[km/hr]	[%]	[s]	[s]	[%]	[%]	[%]	[m]	[m]
1	0	1.34	3.10	0.53	5.71	55.24	387.90	0.41	0.00
2	10	0.29	7.34	0.54	6.12	54.70	386.41	0.39	0.01
3	30	0.08	7.72	0.58	7.75	53.94	384.16	0.35	0.04
4	50	0.18	7.83	0.64	11.22	53.45	394.12	0.26	0.08
5	70	0.11	8.06	1.95	15.21	56.21	411.01	0.18	0.12

(d) KPI performance

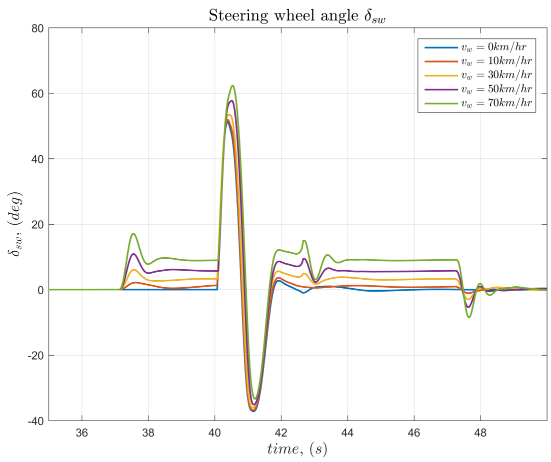

(e) SWA

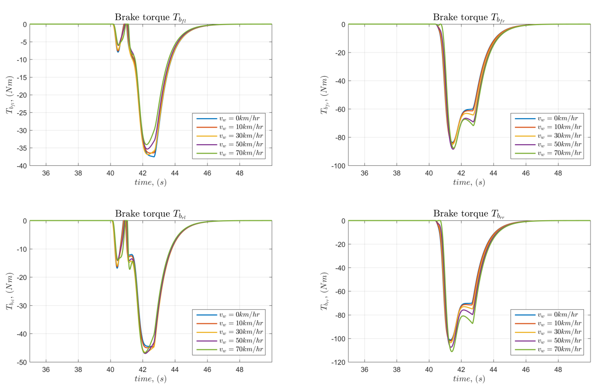

(f) Brake Torques T_b

Figure 6.17: MPC - Planar car Set 4 - Case 1 simulations: $\mu = 0.9$, $v_x = 90km/hr$

It can be seen that as soon as the wind disturbance begins, the car shifts from the reference trajectory. But, with the controller active, it is able to understand this external disturbance effect based on vehicle states passed to its prediction model. This can be seen with increasing non-zero cost function value in Fig 6.18b as v_w increases. As a result, the controller reacts to this opposing effect of the wind and increases the SWA (Fig 6.17e) with synchronized differential braking to avoid the collision. In the straight line driving as well, the SWA increases with increasing v_w speeds to counter the external effect and reduce the offset from trajectory.

Defining D_{off} as the offset distance between reference trajectory and the vehicle trajectory at time equal to $46s$, maximum value of $0.12m$ was observed. Considering wind speed of $70km/hr$ is relatively high, the performance of the controller is very good in limiting the offset to such small value. The controller is also able to perform the maneuver and avoid the collision successfully in all cases. And once the wind disturbance is removed, the controller automatically brings the vehicle back to reference trajectory value.

It is to be noted that during straight-line driving, only SWA corrections are used and not brake torques. It is theoretically possible that by differential braking, the offset value can further be reduced, but the implementation will not be suitable. This is because if the wind speeds are lasting for a long time, one cannot expect to brake the whole time continuously. Doing so will not only lead to actuator wear and reduced brake service life but will also affect the longitudinal dynamics with reducing speeds. Therefore this performance compromise was made with realistic implementation mindset and only SWA corrections were used to reduce the offset.

As seen in all the scenarios, the collision was successfully avoided and the controller ensured that the vehicle remains stable in all the conditions. The small offset seen in the cost function (Fig 6.18b) shows that the controller understands the presence of external wind disturbance and is indeed able to react to it. But the offset does not goes to zero which suggests that the robustness performance can still be improved.

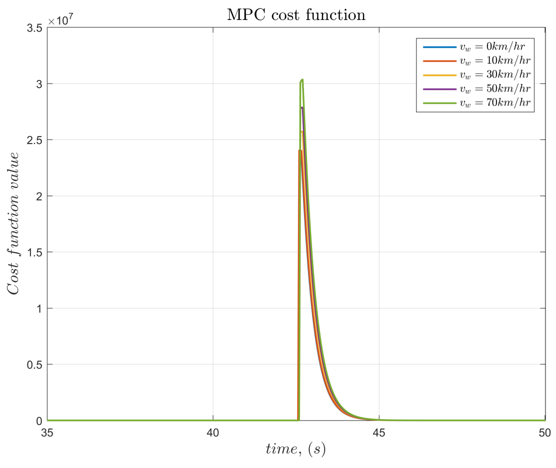

(a) Cost function

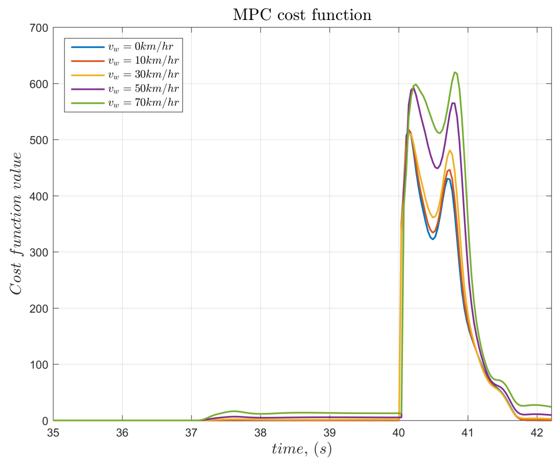

(b) Cost function

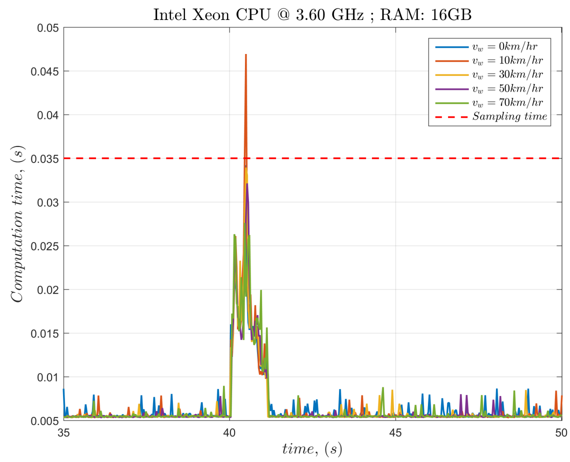

(c) Computation time

Figure 6.18: MPC - Planar car Set 4 - Case 1 simulations: $\mu = 0.9$, $v_x = 90km/hr$

The computation time (Fig 6.18c) is also below the sampling time of the controller to highlight real-time feasibility even in extreme conditions. The occasional peaks are seen as a result of constraints becoming active and varying the ASM solutions to solve the OCP, leading to more computation time to solve the optimization problem. Therefore, after all the analysis, it can be clearly seen that the controller is able to respond to varying external disturbance scenarios effectively using the same formulation and tuning parameters, highlighting its robustness. This effect is consistent in wet and snow road conditions as shown in Fig 6.19 and Fig 6.20 respectively. The oscillations in Fig 6.20e are seen as a result of aggressive tuning (i.e. high value of tuning weights) and can be eliminated by changing the tuning parameters.

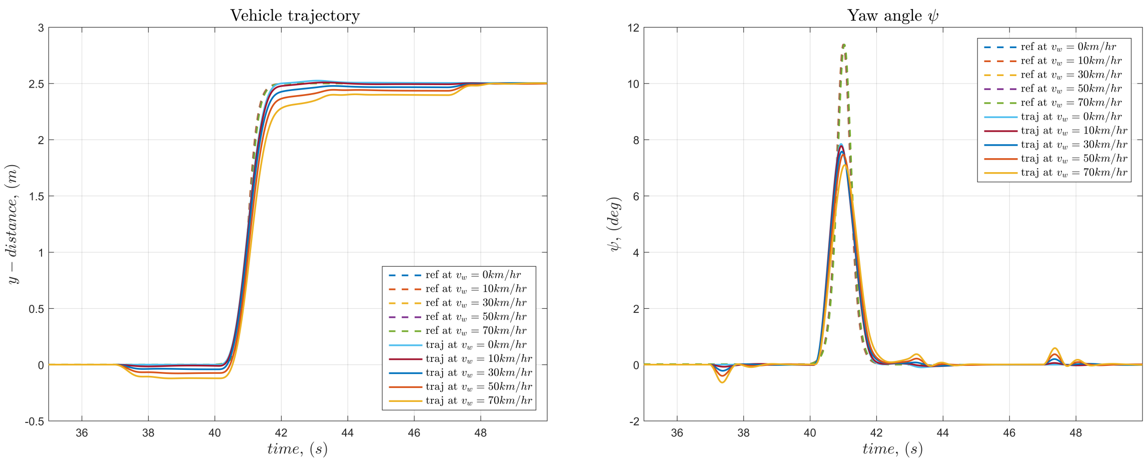

(a) Lateral position y_p

(b) Yaw angle ψ

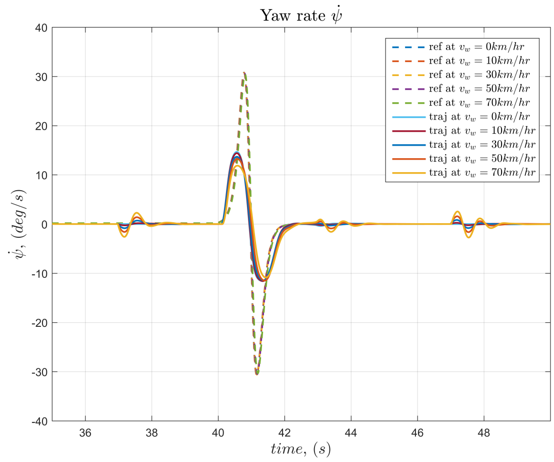

(c) Yaw rate $\dot{\psi}$

S No.	v_w [km/hr]	M_p [%]	T_s [s]	T_r [s]	y_{RMS} [%]	ψ_{RMS} [%]	$\dot{\psi}_{RMS}$ [%]	DTC [m]	D_{off} [m]
-									
1	0	2.51	3.88	0.59	4.72	57.19	347.92	0.51	0.00
2	10	0.89	2.44	0.61	5.03	57.30	349.36	0.48	0.01
3	30	0.29	7.51	0.68	6.64	58.47	355.43	0.42	0.03
4	50	0.03	7.99	0.84	9.80	58.00	359.60	0.32	0.06
5	70	0.30	8.10	1.90	14.22	63.98	384.29	0.20	0.10

(d) KPI performance

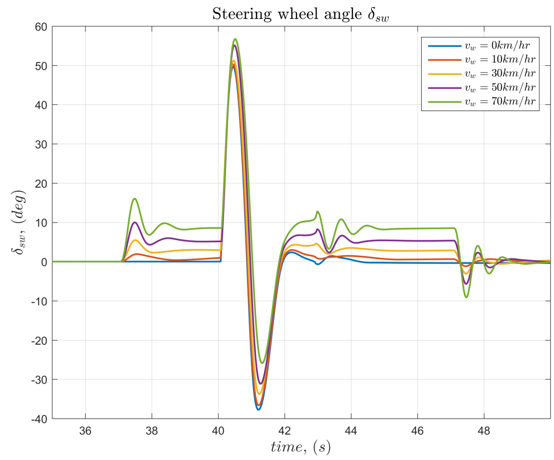

(e) SWA

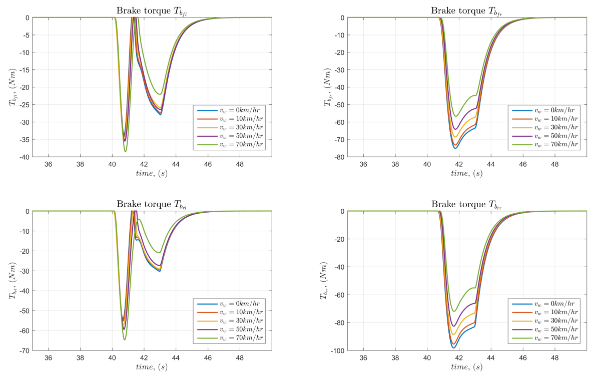

(f) Brake Torques T_b

Figure 6.19: MPC - Planar car Set 4 - Case 2 simulations: $\mu = 0.6$, $v_x = 80km/hr$

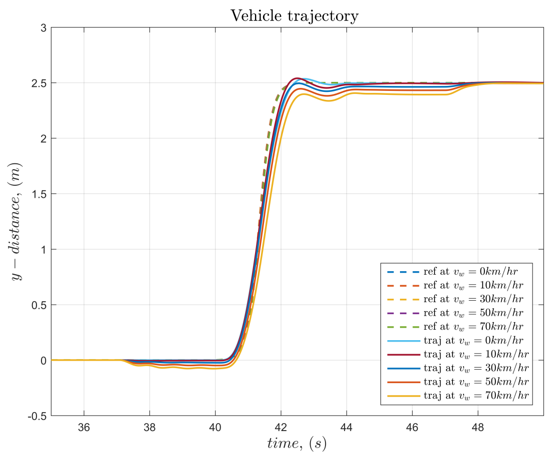

(a) Lateral position y_p

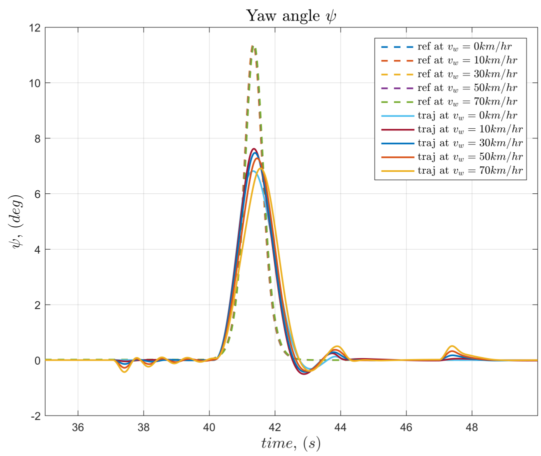

(b) Yaw angle ψ

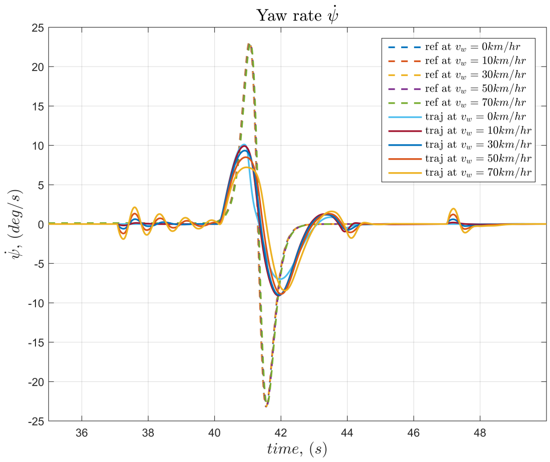

(c) Yaw rate $\dot{\psi}$

S No.	v_w	M$_p$	T$_s$	T$_r$	y$_{\text{RMS}}$	ψ_{RMS}	$\dot{\psi}_{\text{RMS}}$	DTC	D$_{\text{off}}$
-	[km/hr]	[%]	[s]	[s]	[%]	[%]	[%]	[m]	[m]
1	0	3.53	3.84	0.80	6.79	79.37	356.83	0.42	0.00
2	10	3.99	4.85	0.70	5.25	67.43	323.03	0.52	0.01
3	30	0.00	7.70	0.74	6.65	70.42	332.08	0.46	0.04
4	50	0.00	8.03	0.80	9.73	78.30	355.91	0.35	0.07
5	70	0.00	8.22	0.90	14.60	95.44	403.67	0.18	0.11

(d) KPI performance

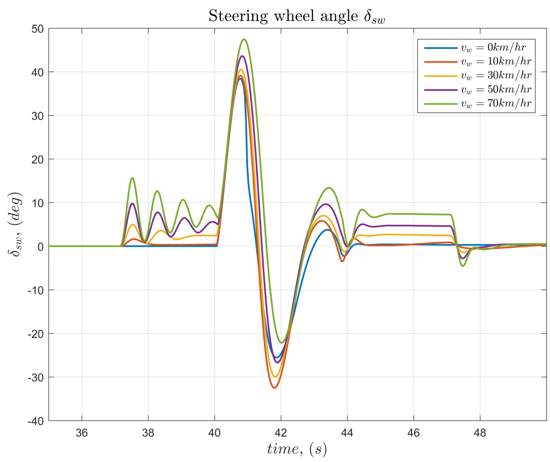

(e) SWA

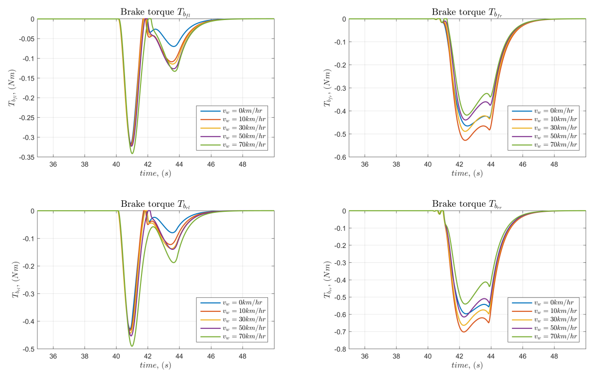

(f) Brake Torques T_b

Figure 6.20: MPC - Planar car Set 4 - Case 3 simulations: $\mu = 0.3$, $v_x = 60km/hr$

6.3.5. Set 5 Scenarios - varying maneuver's aggressiveness

It was mentioned before that the control design is generic in nature and not just limited to evasive maneuvers. This set of scenarios proves this. Fig 6.21 represents the single lane change maneuver performed with varying trajectory's minimum length parameter C_2. It can be clearly seen that the controller is able to track all the trajectories well with KPI values of the three RMS errors indicating that the performance is improving as the maneuver is becoming less aggressive. The same maneuver which was evasive and was performed with $a_{y_{\max}} = 5.83m/s^2$ is now normal lane change and is performed accordingly with $a_{y_{\max}} = 0.77m/s^2$. Here also, the tuning weights have been kept the same for all scenarios to purely assess the controller's performance for varying scenarios but with same formulation.

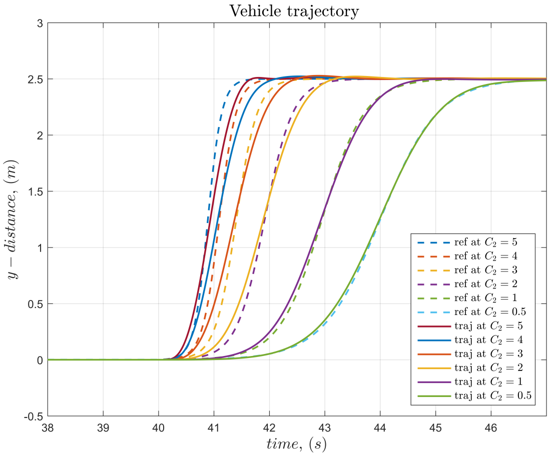

(a) Lateral position y_p

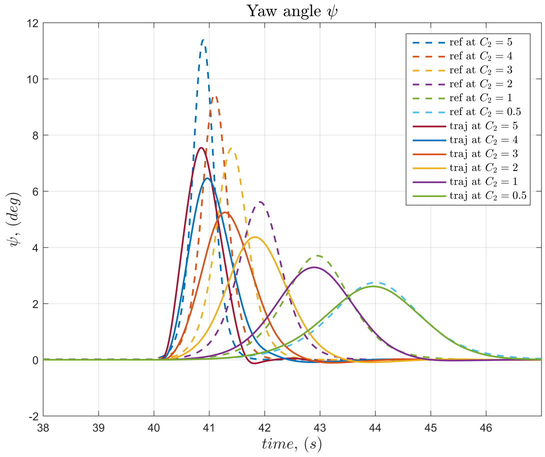

(b) Yaw angle ψ

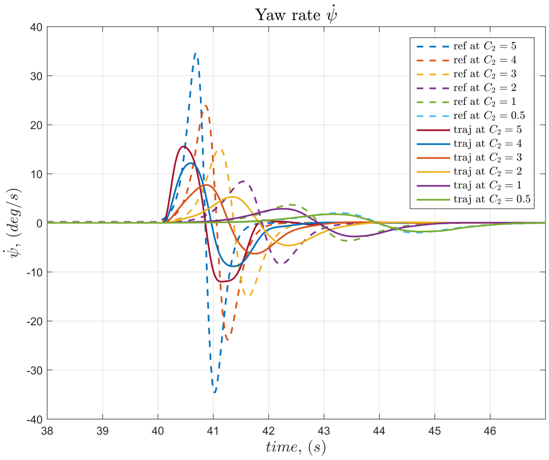

(c) Yaw rate $\dot{\psi}$

S No.	C_2	M_p	T_s	T_r	y_{RMS}	ψ_{RMS}	$\dot{\psi}_{RMS}$	$a_{y_{max}}$
-	-	[%]	[s]	[s]	[%]	[%]	[%]	[m/s^2]
1	5	1.34	3.10	0.53	7.37	71.30	500.64	5.83
2	4	2.25	3.11	0.66	6.46	72.91	389.33	4.78
3	3	2.78	3.47	0.77	6.38	56.82	252.89	3.18
4	2	2.12	4.04	0.89	4.69	33.58	121.79	2.22
5	1	0.00	5.01	1.18	2.44	13.48	36.04	1.23
6	0.5	0.00	5.75	1.49	1.37	6.52	12.20	0.77

(d) KPI performance

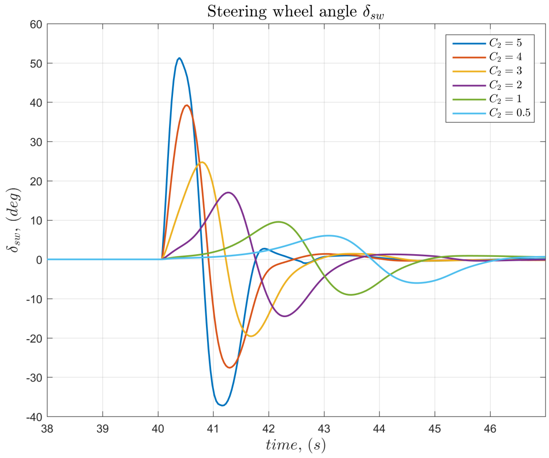

(e) SWA

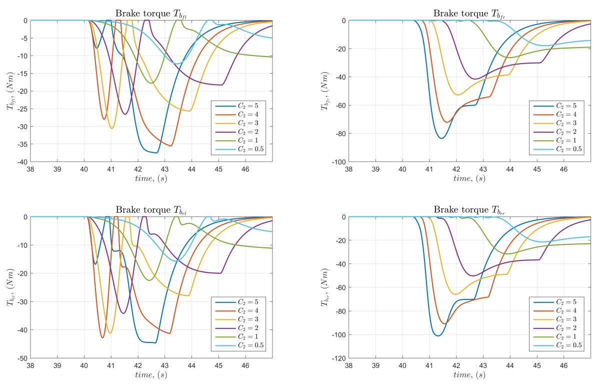

(f) Brake Torques T_b

Figure 6.21: MPC - Planar car Set 5 - Case 1 simulations: $\mu = 0.9$, $v_x = 90 km/hr$

This shows that the controller is capable to perform all dynamic range of maneuvers from normal lane change to evasive lane change in one control scheme. It is able to calculate and modulate the SWA and brake torque values according to the requirements of the maneuver successfully. This shows that it is the reference trajectory which makes the scenario evasive or non-evasive. The controller works with the aim of following the reference signal as well as it can under all circumstances. This proves that the designed controller is generic in design concept and can handle scenarios with varying dynamic requirements efficiently and autonomously.

6.4. Additional Scenarios

To further test the integrated NMPC controller's robustness in certain real-life scenarios, four more set of maneuvers were performed. The first two maneuvers involve friction jump during the maneuver and the next two set of maneuvers involve braking the car earlier before the collision and then perform the lane change maneuver to improve the collision avoidance performance. Three of these maneuvers have been are reported below.

6.4.1. Low to High μ jump

This scenario involves friction jump in the middle of maneuver to asses if the controller is able to react to this change in road conditions or not. The scenario involves SV's speed set at 80km/hr with no normal load and no wind disturbances present. The vehicle is driven initially at $\mu = 0.6$ (wet road) and during the middle of lane change maneuver (part 2 of the maneuver), the road friction is increased and set at $\mu = 1$ (dry road). Fig 6.22 shows the controller's performance for this scenario.

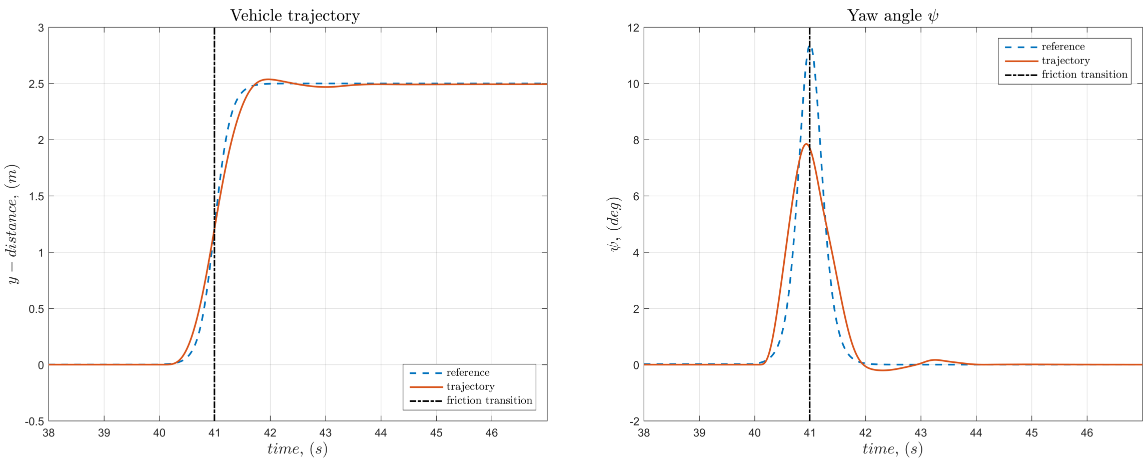

(a) Lateral position y_p (b) Yaw angle ψ

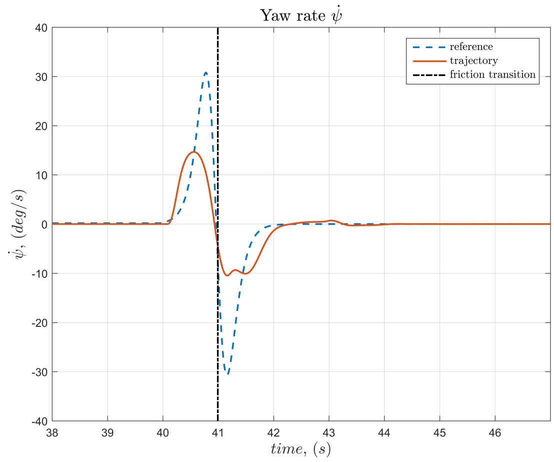

(c) Yaw rate $\dot{\psi}$

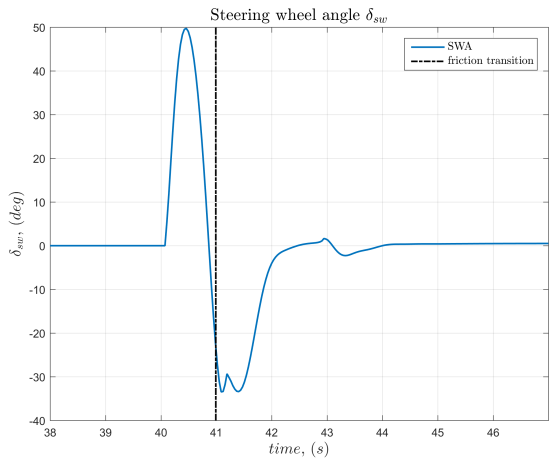

(d) SWA

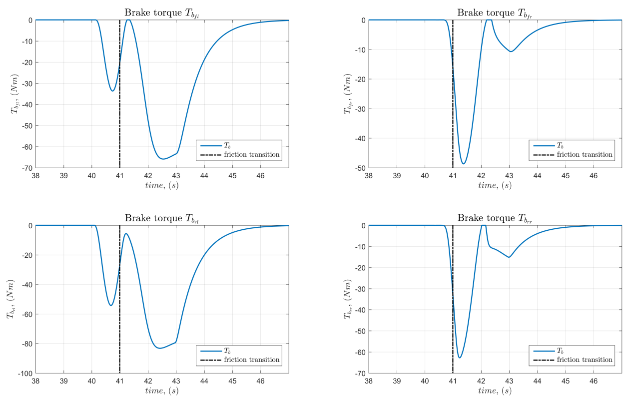

(e) Brake Torques T_b

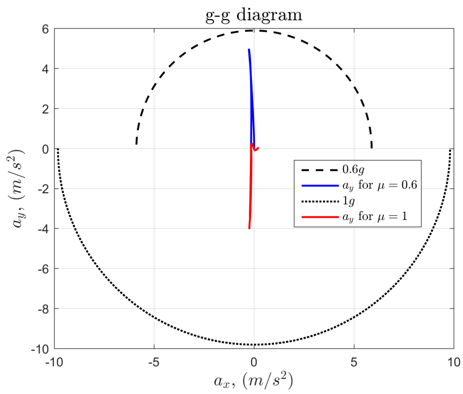

(f) g-g diagram

Figure 6.22: MPC - Planar car model μ jump simulations: $\mu = 0.6$ to $\mu = 1$

The black 'dash-dotted' line in all the figure represent the point at which the μ-jump happens. It can be seen that the vehicle is able to successfully avoid the collision (DTC = 0.51 m) and keeps the vehicle stable. The g-g diagram is constructed in two halves here. The first part with low μ has the circle with smaller radius and the subsequent acceleration values obtained are highlighted as well. Post μ-jump, the bound on the g-g constraint increases to 1 and so circle with higher radius represents this increase in bound. Hence the g-g circle is not just one circle of constant radius. The friction jumps to different values and so the g-g diagram has two circles now to show the same. The same argument hold true for the kamm circle as well.

6.4.2. High to Low μ jump

This scenario is the opposite of the previous μ-jump scenario. Here the maneuver begins at high μ conditions ($\mu = 1$) and during the middle of the maneuver, the friction coefficient is reduced to $\mu = 0.6$. The rest of the conditions and vehicle speed of $v_x = 80 km/hr$ remains the same here as well. Fig 6.23 shows the controller's performance for this scenario.

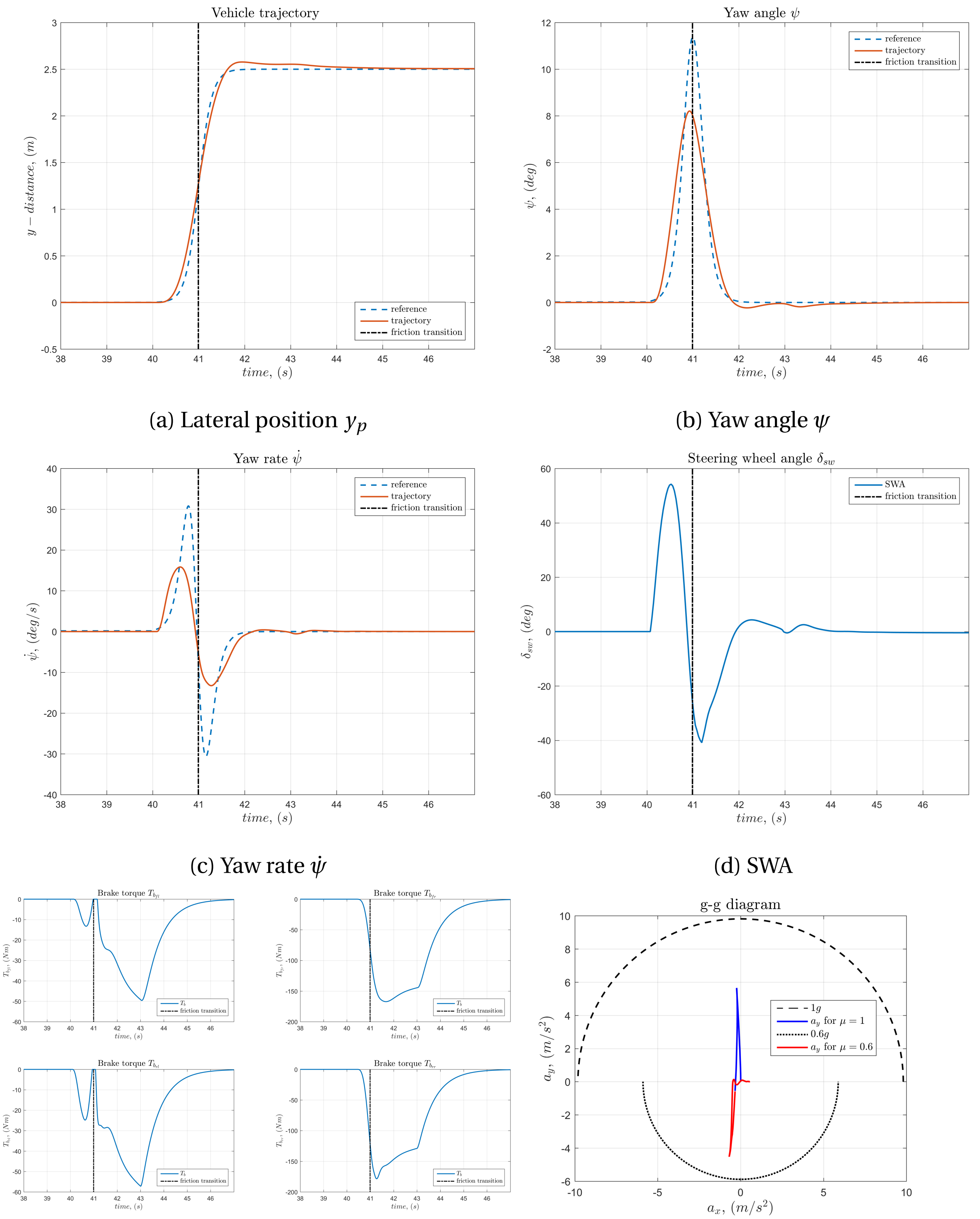

(a) Lateral position y_p (b) Yaw angle ψ

(c) Yaw rate $\dot{\psi}$ (d) SWA

(e) Brake Torques T_b (f) g-g diagram

Figure 6.23: MPC - Planar car model μ jump simulations: $\mu = 1$ to $\mu = 0.6$

It is seen here that when jumped to lower μ values, the performance deteriorate with overshoot increasing to 7.82% as compared to 3.67% in the low to high μ-jump case. The reason for this deterioration can be that at high μ, the controller is able to generate high tire forces and therefore relatively high control action can be given for vehicle control. But with a sudden μ drop, the tire's traction limits reduces and the performance ability of the vehicle gets limited due to this. Hence, a performance deterioration was expected here but still, the vehicle control is effective in keeping the vehicle stable at all times. This effect is also seen in the plots for brake torques. As soon as the μ value decreases post jump, the controller brakes more as compared to previous case. This ensures that with sudden drop in μ and similar lateral force requirements, the controller not only provides vehicle motion stability with more braking, but also perfectly differential brakes so that maneuver performance is not compromised significantly.

Here, two cases were shown to demonstrate the controller's ability to handle μ jump scenario but the controller is designed to handle μ jump scenario for different μ values as well.

6.4.3. Pre-Braking

The final scenario designed highlights the capability of an integrated control scheme. It was seen in Fig 6.4 that at speed of $100 km/hr$, the vehicle avoided the collision with DTC value of $0.09m$ only. In the designed maneuver, the trajectory is only generated when SV is $30m$ away from LV, even though the LV has already been detected. But in real-life, instead of waiting for $30m$, once the LV is detected and the possibility of potential collision scenario is observed (due to decreasing TTC value), ideally the vehicle will start to decelerate to increase the chances of collision avoidance. This deceleration will continue until a set TTC threshold value is reached after which the maneuver shall be performed.

The advantage of using an integrated control scheme is that only one controller is capable to perform both braking and steering action simultaneously. The controller designed is capable of both differential braking and straight-line braking. To show this, a scenario was modeled on $\mu = 0.9$ with $v_x = 100 km/hr$. Two seconds before the SV performs the lane change maneuver, a reference longitudinal velocity with decreasing speeds is calculated by the reference generator block and sent to the controller via its cost function. The tuning weight for the state v_x was set to 100 to include this reference in the cost function and the vehicle is supposed to straight-line brake and decelerate before it begins to turn.

Fig 6.24 shows the controller's performance for this maneuver. It can be seen in Fig 6.24e that the controller first brakes in straight-line with front torque values higher than rear and SWA kept at zero. Then the same controller performs lane change maneuver as seen with non-zero SWA plot in Fig 6.24d. The highlight of this maneuver is the fact that as soon as the vehicle starts to turn, the controller is able to modulate the brake torques from straight-line braking to differential braking automatically to improve the tracking performance.

As seen with the left turn first, both the left side brakes brake more compared to right side brakes to get the extra counter-clockwise yaw moment. And when the right turn is performed, the brake torques are modulated again and now both the right side brakes more along with decrease in brake torques of the left side brake to get the extra clockwise yaw-moment. Later the vehicle travels in straight line with brake torques and SWA, both going to zero. This combined maneuver is very well illustrated in the g-g diagram in Fig 6.24f where both effects of a_x and a_y are captured.

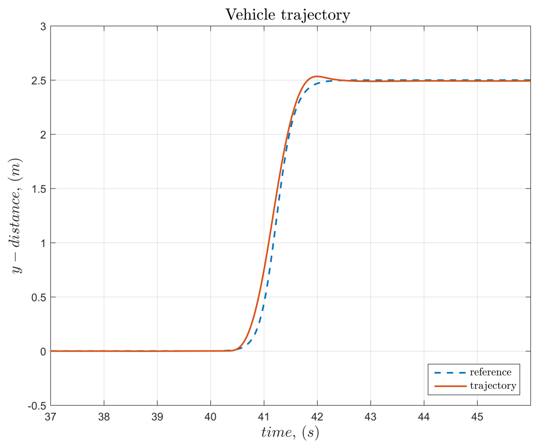

(a) Lateral position y_p

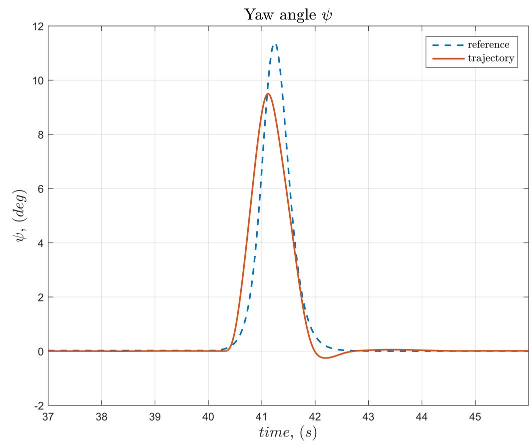

(b) Yaw angle ψ

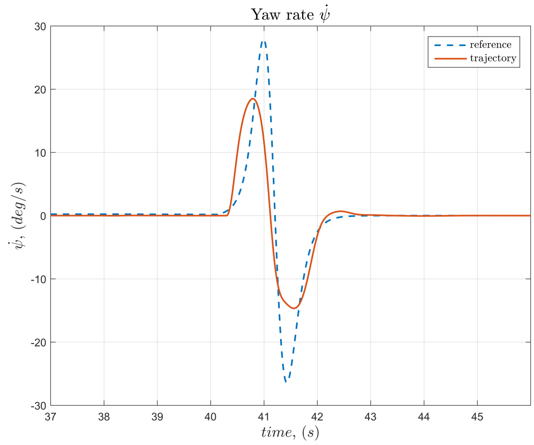

(c) Yaw rate $\dot{\psi}$

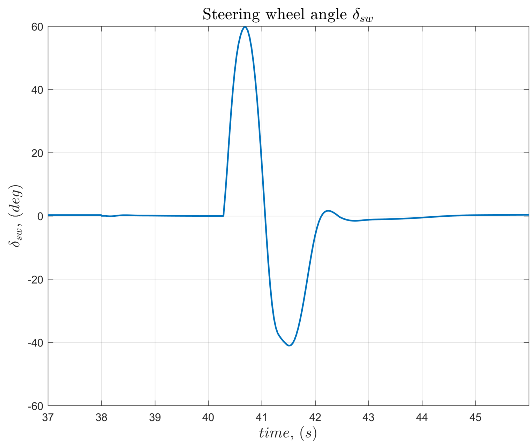

(d) SWA

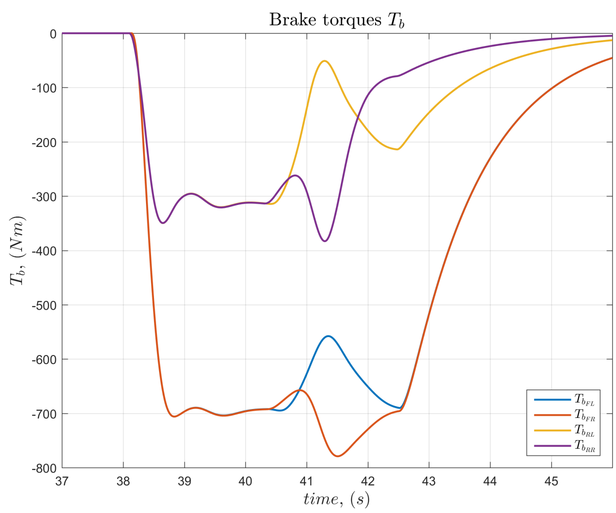

(e) Brake Torques T_b

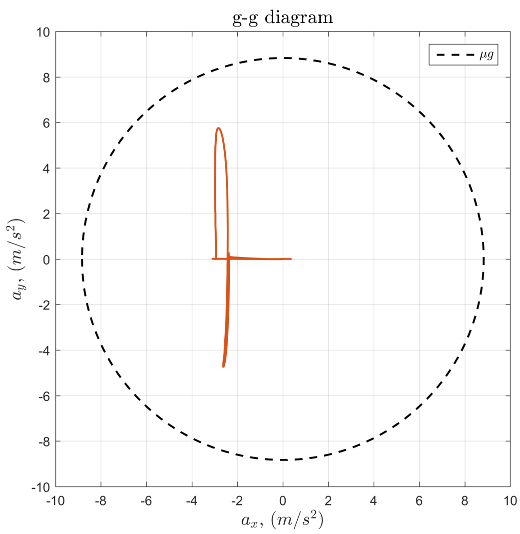

(f) g-g diagram

Figure 6.24: MPC - Planar car model pre-braking simulation result

By decelerating before the maneuver begins, the vehicle speed decreases as a result of which the ability of the car to turn increases. This is seen in the trajectory plots where now the car can yaw more than 9^o and is able to follow the trajectory better as a result of which the TTC value now is $0.8m$ as compared to $0.09m$ before. Also, by designing two separate controllers for longitudinal and lateral control, the vehicle dynamics coupling is lost and performance is deteriorated. But by using a combined integrated control technique, this coupling is well preserved in the controller and better performance is now achieved.

The same maneuver was performed in the presence of external wind speed $v_w = 50km/hr$ and it was seen that the controller is able to steer and straight line differential brake simultaneously to reduce the wind offset and follow the longitudinal reference successfully. The results have been reported in the Appendix.

This gives the final conclusion that the MPC with planar car model is capable to work wit varying road and surrounding conditions at all the varying range of speeds successfully. The controller captures the dynamics of the vehicle well and avoids the collision successfully in all the scenarios. The controller is robust to external wind disturbance, normal load variation and sensor delays as well. In all the simulations performed in this research, the simulation time was set at $0.001s$ while the sampling time of the controller was $0.035s$. The controller was therefore provided with the information of vehicle states and trajectory values with a delay of 34 samples and still the controller was able to perform the desired maneuver efficiently, highlighting further its robust performance.

6.5. Effect of Constraints and Actuator Dynamics

The trajectory tracking plots showed that the vehicle control was indeed able to track the reference successfully in all conditions. But one needs to ensure that the vehicle during the maneuver remains in the working region and that the vehicle dynamics are respected at all times. To ensure this , constraints were defined in the MPC Planar car model controller. In this section, the effect of those constraints in controlling the vehicle dynamics accurately is shown. Also, the improvement in performance as a result of addition of brake actuator dynamics in the prediction model of MPC - Planar car model will be shown.

6.5.1. β - $\dot{\beta}$ Phase plane

The evasive maneuvers if not performed properly may lead to unstable cases where the vehicle might spin out. To ensure, this does not happen Eq (3.9) and Eq (3.10) were defined as constraints. For Set 1 - Case 1, Fig 6.25 shows the phase space diagram of the vehicle during the maneuver. It can be seen that the vehicle remains in the set envelope area (shown by black dashed lines) at all times and the vehicle never goes unstable as the phase space converges to zero always.

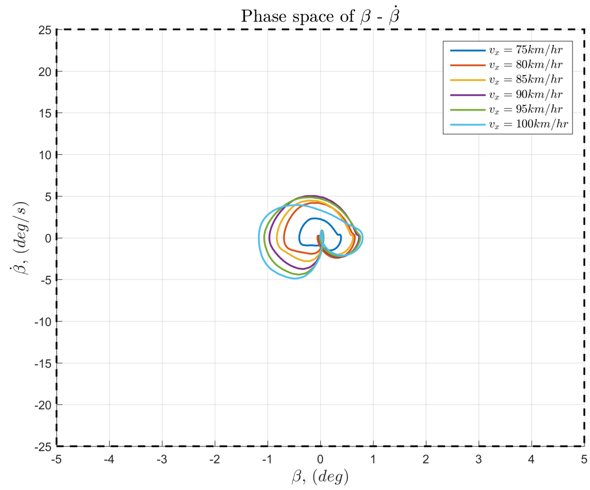

Figure 6.25: β - $\dot{\beta}$ Phase plane diagram for Set 1 - Case 1 scenarios

6.5.2. g-g diagram

The ability of the vehicle to accelerate in both directions is limited by the bound μg. This envelope was defined as a constraint in Eq (3.55) in the MPC formulation. For Set 1 - Case 1, Fig 6.26 shows the g-g diagram, also called as friction circle, obtained. It can be seen that the maneuver is performed within the set working envelope and the constraint is always satisfied. The vertical lines indicate that the majority of the maneuver involved lateral travel and the longitudinal dynamics did not alter much. This is exactly what was desired by the controller. By braking too much, one may reduce the potential of lateral tire force generation. The extra yaw by differential braking should improve the performance but at the same time should not dominate the majority of maneuver.

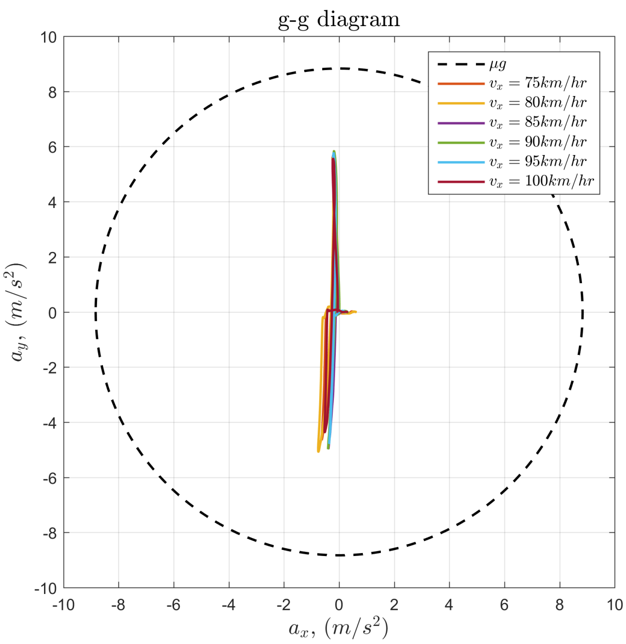

Figure 6.26: g-g diagram for Set 1 - Case 1 scenarios

6.5.3. Kamm circle

The tire's working envelope was designed in the MPC controller using the Kamm circle equation as constraints for all the four tires as shown in Eq (3.64) - Eq (3.67) respectively. An ideal scenario would be the case when best performance is achieved with least tire and actuator wear to get longer service life. To ensure such objectives are achieved for the case of tire wear, a tire envelope was defined such that the maneuver is performed successfully while the tire forces are minimized as well.

To highlight this effect and the difference in tire force generation, an MPC controller was designed without the constraint of kamm circles in its formulation. It was seen that in Set 1 - Case 1 at higher speeds when more lateral forces are required to perform the maneuver, the front left tire forces generated were found outside the kamm circle envelope as shown in Fig 6.27. But with the use of these constraints, the controller was not only able to perform the same maneuver, but now was able to keep the tire forces in the working envelope, optimizing the tire force and improving the overall performance. This optimization in control action is well seen in all the tires as now the tire forces are more similar and well distributed as compared to random peak values seen in Fig 6.27a.

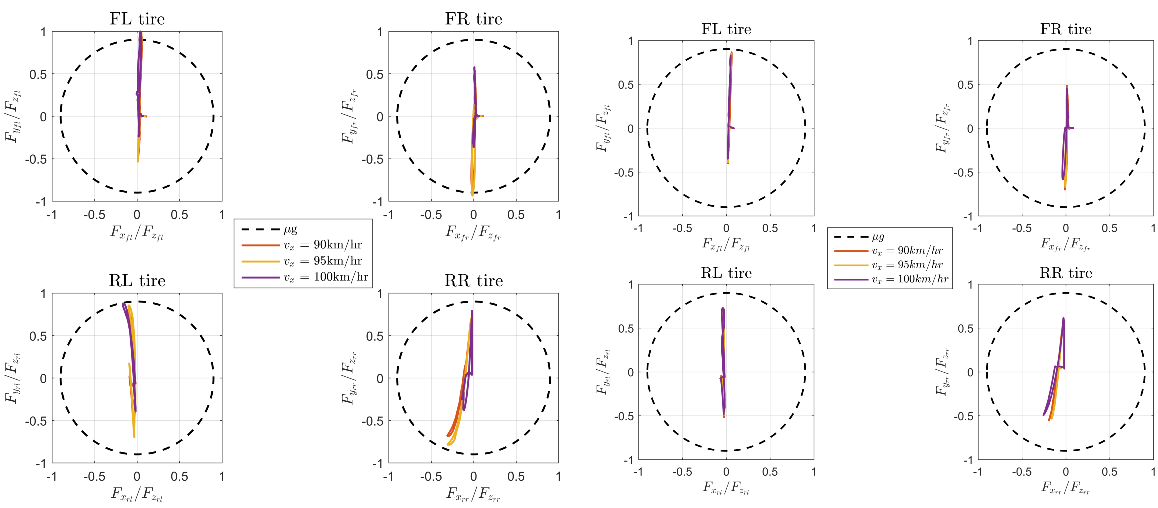

(a) Without the constraints

(b) With the constraints

Figure 6.27: Effect of Kamm circle tire constraints in Set 1 - Case 1 scenario

The above figure showed vertical lines meaning that the almost only vehicle lateral control was performed. To analyze the ability of the controller in the combined case if it can minimize forces and still give the desired vehicle control, the pre-braking maneuver was performed with and without the kamm circle constraints. The constraint as well as the NMPC Planar car model control is formulated such that it can handle the variations in longitudinal dynamics as well. By testing this, it was seen (in Fig 6.28a) that without the constraints, the tire forces were way outside the working envelope. But with the use of the constraints, all the tire forces worked in the domain defined and was able to give good performance as shown in Fig 6.24.

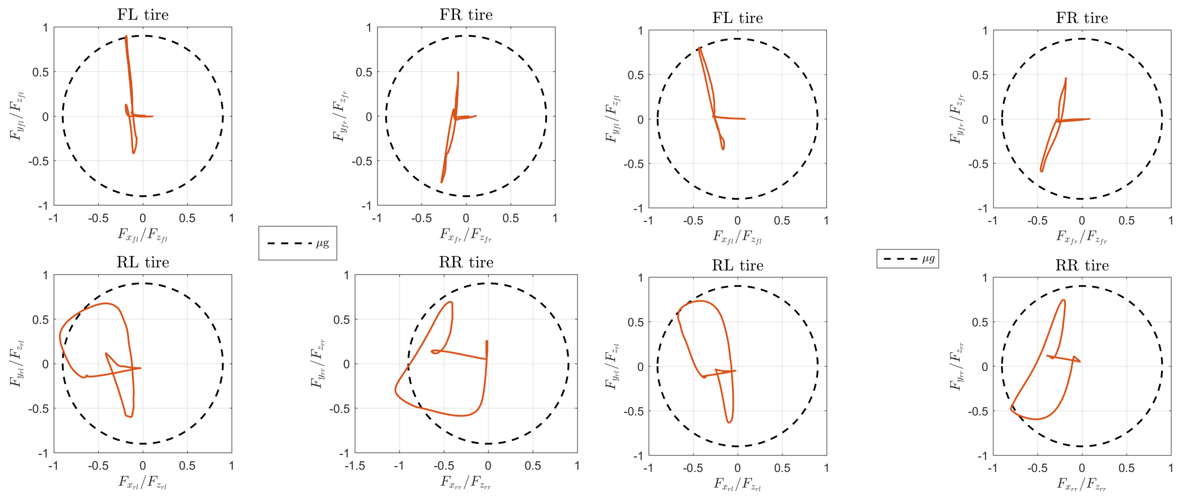

(a) Without the constraints (b) With the constraints

Figure 6.28: Effect of Kamm circle tire constraints in pre-braking scenario

This proves that the use of this constraint helps in minimizing the tire forces and still provides good control action. The working envelope defined is using a circle as an approximation. But better envelopes such as friction ellipse can be defined to mimic the real data and tire behaviour well.

6.5.4. EBD logic

This section gives an idea regarding the need of EBD logic equation, defined as a constraint in Eq (3.68) in the MPC scheme, to show how the performance was varied by this constraint. As explained in Fig 3.5 and the para above it, the ability of the front tires to generate longitudinal forces is higher than the rear tires due to weight transfer while pitching motion. When the pre-braking maneuver was performed in which straight-line braking was required, it was seen that without the EBD logic, the rear brakes were braking more than the front (Fig 6.29a).

This is logically incorrect. While the maneuver was performed successfully, the brake output was dynamically incorrect and was not acceptable. Also, the rear brakes should not lock first as the vehicle might spin out. The front needs to almost always brake more than the rear for safe and dynamically correct performance. To modulate this effect and let the controller know how the brake torques need to be distributed between the front and the rear brakes, the EBD constraint was defined. Fig 6.29b shows the response with the constraints.

The optimal brake distribution performance is now achieved due to the constraint. This constraint is only activated during the straight-line braking and now it is always ensured that optimally, the front will brake more than the rear brakes. It is seen in both figures that the total brake torques of all four wheels remain the same during straight-line braking, only the distribution ratio has changed to optimal value.

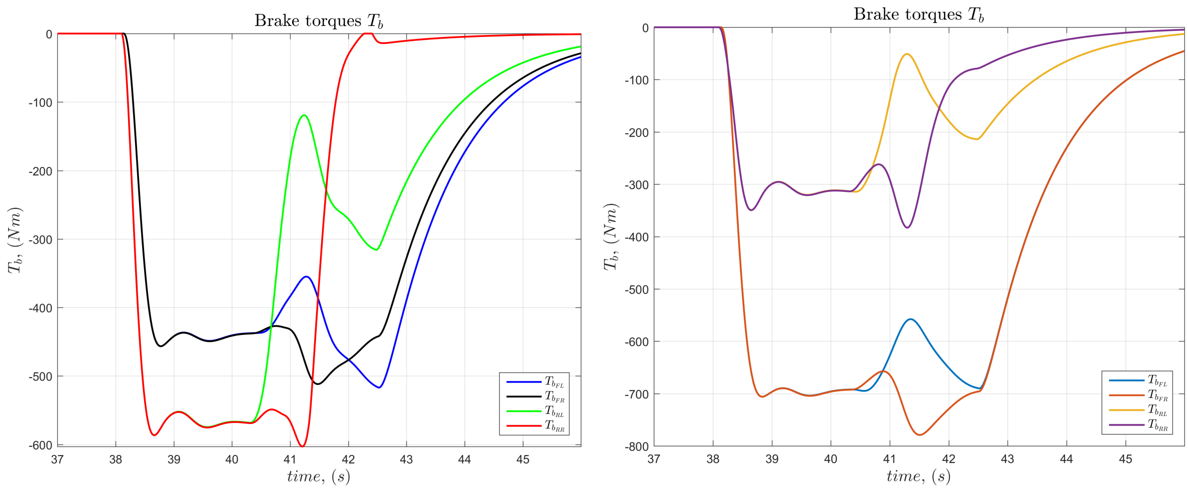

(a) Without the constraint

(b) With the constraint

Figure 6.29: Effect of EBD constraint in pre-braking scenario

6.5.5. Actuator dynamics in prediction model

One of the unique implementation in this scheme was to add the brake actuator dynamics in the prediction model of the MPC control. In a conventional hydraulic brake system, the pressure build up rate between the front and rear brakes is not the same. Explained in detail in Section D.5.2 of Appendix, the rear brakes in a conventional HAB system build brake pressure quicker than the front brakes. By providing this information in the prediction model of the controller (Eq (3.42) - Eq (3.45)), the calculation of brake torques by the controller show the similar effect as seen in Fig 6.30b. The rear brakes more than the front in the straight line braking due to more pressure build up.

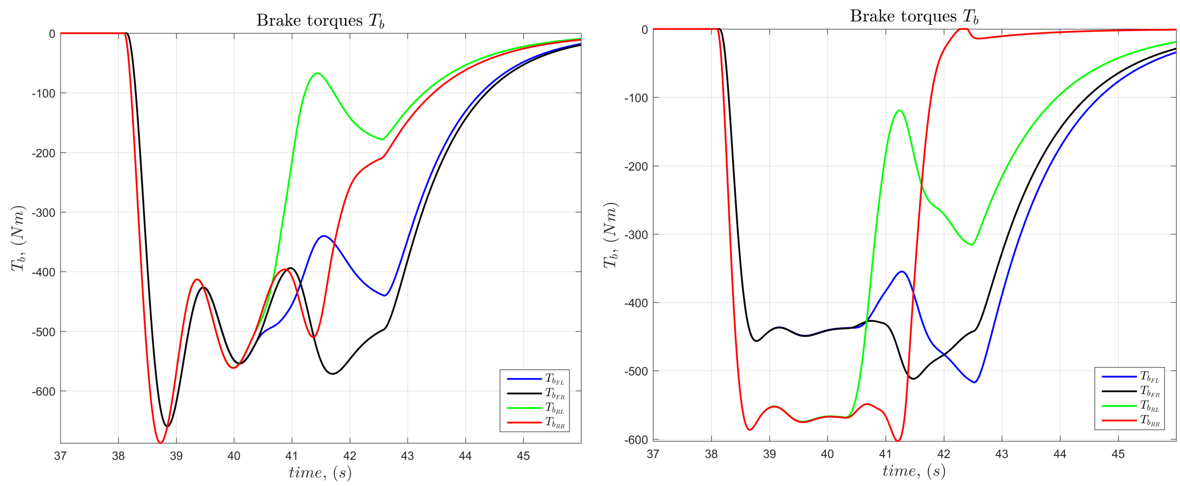

(a) Without the brake dynamics

(b) With the brake dynamics

Figure 6.30: Effect of brake dynamics in the prediction model

Without the implementation of the brake dynamics in prediction model, the controller does not have this pressure build up information anymore and so it builds equal pressure in all four wheels as seen in Fig 6.30a with almost equal brake torques for front and rear brakes respectively. Performance wise, not much difference was observed and hence has not been reported her. But providing this extra information ensures that the brake actuators naturally perform the way they are designed to be and that the brake actuator wear is reduced. This can provide advantages such as reduced service cost and longer brake life in future.

It is to be noted that in Fig 6.30, the EBD constraint was disabled throughout the maneuver. This was done so that the brake torque calculation is not affected by other constraints but is only studied and analyzed by the predictions made via prediction model equations.

6.6. Summary

In this chapter, all the list of scenarios that were performed were documented as sets and cases. Later, all the simulation results, KPI values and comparative study's conclusions were reported. It was seen that the integrated MPC using Planar car model as its prediction model outperformed the bicycle model based MPC schemes in all the varying μ and v_x scenarios and gave the best performance with highest DTC values and lowest RMS error values. The controller was robust to sensor information delay, normal load variation, external wind disturbance and friction jump as well and avoided the rear-end collision in all theses cases.

The effect of constraints in ensuring that the vehicle works withing the designed working envelope was then analysed and it was found that kamm circle and g-g diagram did ensure this well. The EBD logic ensured that the front tires would brake more than the rear tires in straight-line braking. The controller was also robust to tracking a kinematic reference at all times but the issue of pre-tracking behaviour was noticed which has been explained in the Appendix to be caused as a result of incorrect reference information calculation along the horizon by the Reference Generator. Despite this, the tracking was good and the successful coordination of steering and braking was achieved by the integrated MPC control at all times.

7

Conclusion and Recommendations

7.1. Summary and Conclusion

The aim of this research was to design a controller that can successfully avoid a rear-end collision and guarantee vehicle stability and passenger safety at all times. Three autonomous MPC based control schemes were developed and an evasive single lane change maneuver was performed under varying speeds and varying road friction conditions. It was seen that among the three MPC controllers, the combined steering and braking based MPC control using Planar car as its prediction model gave the best performance under all scenarios and outperformed the other two control strategies.

It was concluded in the literature review that an integrated control action of steering and braking in principle should provide good evasive action. But it was seen that very few research was done in the domain of integrated control. The current trend of vehicle control which has been actively researched involves the use of a hierarchical control of the following structure (Fig 7.1) involving the below-mentioned stages [65].

- Vehicle Dynamics Control
- Force and Moment Distribution
- Wheel Control
- Actuator Control

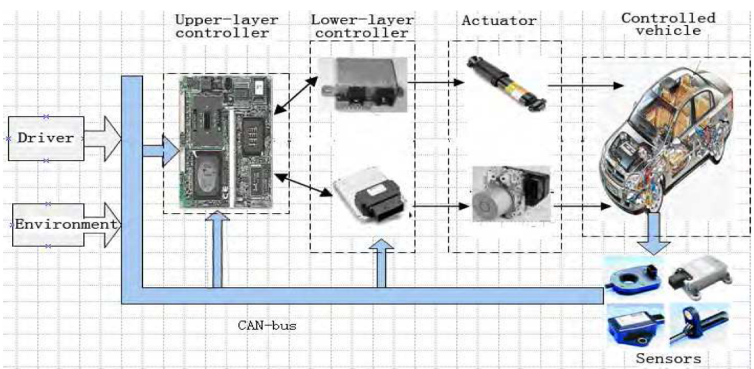

Figure 7.1: Hierarchy control by [15]

A vehicle's motion is always coupled in both the lateral and longitudinal direction. But a hierarchical control strategy divides these two motions and calculates separate control action for each dynamics with a hope that when this control action is applied tot the car, it will be able to take care of both the dynamics. To give away with this uncertainty and contribute to the domain of vehicle control, an active research was done on designing an integrated control that provides a coupled control action and guarantees that the vehicle control is robust and efficient for all lateral and longitudinal cases.

To achieve this target, a unique MPC formulation was designed to ensure that the coupled dynamics are well captured for superior control. This controller's formulation involved the use of Planar car model in its prediction model to capture the nonlinear coupled dynamics of the vehicle. The brake actuator dynamics was also captured in the prediction model to ensure that actuators are optimally used and their service life is not compromised. Constraints were designed to ensure that the control action given is within the mechanical and electrical capability of the actuator dynamics.

Also, it was necessary to develop a working envelope in which the vehicle remains stable at all times. This envelope was designed in such a manner that it covered both the dynamics so that the performance is not limited and the controller in principle can work in different scenarios. Therefore, for the first time in MPC control design, nonlinear constraints of g-g diagram, kamm circle and EBD curve logic were formulated. This in principle allowed the controller to perform maneuvers and effectively control the vehicle in both linear and nonlinear regime of motion.

To highlight this, a single lane change maneuver was performed with varying road and surrounding conditions at varying vehicle speeds. The controller was also tested for robustness with external wind disturbances parameter uncertainties in the form of external loads and sensor information delay. The maneuver design covered scenarios ranging from normal lane change to evasive maneuver. It was seen that the integrated nonlinear MPC control was able to control the car in all the scenarios effectively and ensured that the rear-end collision was avoided at all times. The ability of the controller to simultaneously steer and brake (differential and straight line both) in a synchronized manner autonomously provided the best control among all the three MPC controllers designed in this research.

The controller's parameters and OCP solver settings were designed to ensure that the controller is works in real-time and in principle is ready for actual implementation. This real-time feasibility is proven via the computation time plots attached in the Appendix for all the three controllers. This gives the motivation that an integrated MPC control has the ability to control a vehicle actively at all times in all the scenarios. It paves way for new area of research that gives way to hierarchical control and uses one controller for all situations, a "One for all" control strategy.

To conclude, an optimal control with the ability to predict in future to apply necessary action for real time control, MPC is an ideal candidate for vehicle control. The control strategy modelled in this research has the ability to steer and brake together and control vehicle in all dynamic scenarios. This controller is robust, real-time implementable, autonomous in nature and reduces vehicle control complexity found with hierarchical control implementation. With an aim to achieve a SAE Level 5 vehicle, it is necessary that the vehicle is capable of autonomous driving in all conditions and it is the author's belief that with this MPC based integrated control strategy, the dream of producing a fully automated passenger car is now firmly within our grasp.

7.2. Recommendations and future work

During this research, a lot of learning was done and many issues were tackled. But there is always scope for improvement and this research work is no exception to it. Below mentioned points are few of the recommendations the author would like to give as future work to further improve the controller design and its performance.

- **Use of sophisticated reference trajectory generation methods** - This research involved the use of a kinematic reference generator using a mathematical equation. Sophisticated reference generators which considers vehicle dynamics in its formulation should be used to get an improved performance and ease the MPC tuning process [66]

- **Designing a real-time MPC tuning algorithm** - The performance of the controller significantly changes if the sensitivity to each parameter in the cost function changes. This is controlled by the tuning matrix containing the tuning weights for each and every state. By designing a real-time tuning algorithm that can update the tuning parameters at each sample, the performance can be further enhanced.

  In this research, constant tuning parameters are given. An effort was made in defining exponentially increasing tuning weights for the scenario of wind disturbance. It was seen that as the weights increased, the tracking was improved with offset value D_{off} decreasing even more, improving the controller's robustness. Since the formulation of this tuning scheme could not be made generic, the idea of real-time tuning was dropped. But the effects seen on the performance certainly proved the hypothesis that real-time tuning can significantly improve the performance.

  Also, the method of tuning weights can also be used to ensure that MPC remains stable at all times. Explained well in [67], an exponential weighing scheme is used in the cost function to ensure that the calculated Hessian matrix of the QP problem is always stable. In this strategy, the tuning weights are varying along the horizon with tracking sensitivity decreasing as the horizon progresses. Eq (7.1) shows the modified cost function of the OCP.

$$\begin{aligned} \min \ J_1 = \int_0^{T_p} \left[e^{-2\alpha\tau} x(t_i+\tau)^T Q x(t_i+\tau) + e^{-2\alpha\tau} \dot{u}(\tau)^T R \dot{u}(\tau) \right] d\tau \\ \text{subject to} \\ \dot{x}(t_i+\tau) = Ax(t_i+\tau) + B\dot{u}(\tau) \end{aligned} \tag{7.1}$$

  Here, T_p is the entire prediction time, Q and R are the tuning weights and $\alpha \geq 0$ is a constant tuning parameter. This OCP is similar to the OCP of the form shown in Eq (7.2).

$$
\begin{aligned}
\min\ J_1 = \int_0^{T_p} \left[x_\alpha(t_i+\tau)^T Q x_\alpha(t_i+\tau) + \dot{u}_\alpha(\tau)^T R \dot{u}_\alpha(\tau)\right] d\tau \\
\text{subject to} \\
\dot{x}_\alpha(t_i+\tau) = (A-\alpha I)\, x_\alpha(t_i+\tau) + B\dot{u}_\alpha(\tau) \\
\text{where} \\
x_\alpha(t_i+\tau) = e^{-\alpha\tau} x(t_i+\tau) \ \text{ and } \ \dot{u}_\alpha(\tau) = e^{-\alpha\tau}\dot{u}(\tau)
\end{aligned}
\tag{7.2}
$$

This shows that by defining a constant α that is always positive, one can make the unstable poles of matrix A stable. This allows to eliminate any ill-conditioned matrix defined for optimization problem and stability of the system can be guaranteed at all times. This approach was tried in this research but it was noticed that by varying the tuning parameters along the prediction horizon, the computation time of the MPC significantly increased and real-time feasibility was compromised. But it is believed with future advancements in technology, computation time will not be an issue and this method will provide the MPC stability, which otherwise is theoretically hard to prove and still remains an open-end research topic.

- **Use of better tire models** – In this research, a Dugoff tire model was used to calculate the cornering stiffness of the tire. Since tire lateral force is the most important quantity to have a successful lateral vehicle control, estimating accurately the value of cornering stiffness is extremely important. Using more sophisticated tire models such as magic formula can further provide improvement in the controller's performance.

- **Inclusion of wheel slip dynamic equations** – The integrated MPC control design ignores the roll and pitch control which is a decent assumption considering small roll values achieved in this scenario as seen in the Appendix plots. But the other assumption of not considering longitudinal wheel slip in the formulation can be an issue. Because the control action is brake torques, a condition of wheel locking is possible. In this research, it is assumed that the vehicle already has ABS implemented and so if such high torque values are calculated by the controller which induces condition of wheel lock, the ABS will become active and will vary the torque values to ensure that such situation is avoided.

  But, by adding the dynamic equations of wheel slip for each wheel respectively as shown in Eq (7.3), the MPC controller will then become capable of handling even the wheel lock condition and the use of ABS controller will be limited or redundant. This again improves the claim of "One for all" control strategy. But this will increase the computation time and tuning weights so the design needs to be carefully analysed.

$$
\dot{\kappa}_{\mathrm{ij}} = \frac{1}{v_x}\left(\frac{1-\kappa_{\mathrm{ij}}}{m} + \frac{r_{\mathrm{eff}}^2}{J_{\mathrm{yy_{ij}}}}\right) C_{\kappa_{\mathrm{ij}}}\kappa_{\mathrm{ij}} - \frac{r_{\mathrm{eff}}}{J_{\mathrm{yy_{ij}}} v_x}\left(T_{e_{\mathrm{ij}}} - T_{b_{\mathrm{ij_{act}}}}\right) \quad , \quad \mathrm{ij} = (\mathrm{fl}, \mathrm{fr}, \mathrm{rl}, \mathrm{rr}) \tag{7.3}
$$

- **Improvement in kamm circle formulation** – The kamm circle constraints defined used static normal load transfer terms and ignored the dynamics terms. Also, a circle was defined as an envelope instead of an ellipse which actually captures the tire dynamics well. It is believed that by adding these improvements in the formulation, the tire forces calculated will further improve the performance. Also, use of better tire models for lateral force estimation may improve the constraint's overall performance.

Before implementing the controller on a real vehicle, rigorous **testing** needs to be performed. It was always stressed in this research that the designed controller is generic in formulation and in principle has the ability to perform varying dynamics scenarios. But this was shown only with a single lane change maneuver. By **performing a variety of maneuvers** such as double lane change, mu-split or sine with dwell, the performance of the controller can further be analysed and improvements can be suggested to ensure that the controller works in all the environment.

This has to be accompanied with the **use of estimators** to estimate the information of the states required by the controller to effectively control the car. In reality, one cannot measure all the signals and need to estimate them accurately. This induces sensor noise and parameter uncertainty. By coupling the controller with these estimators, not only the robustness can be verified, but successful working will also provide a step further towards the real implementation on a vehicle.

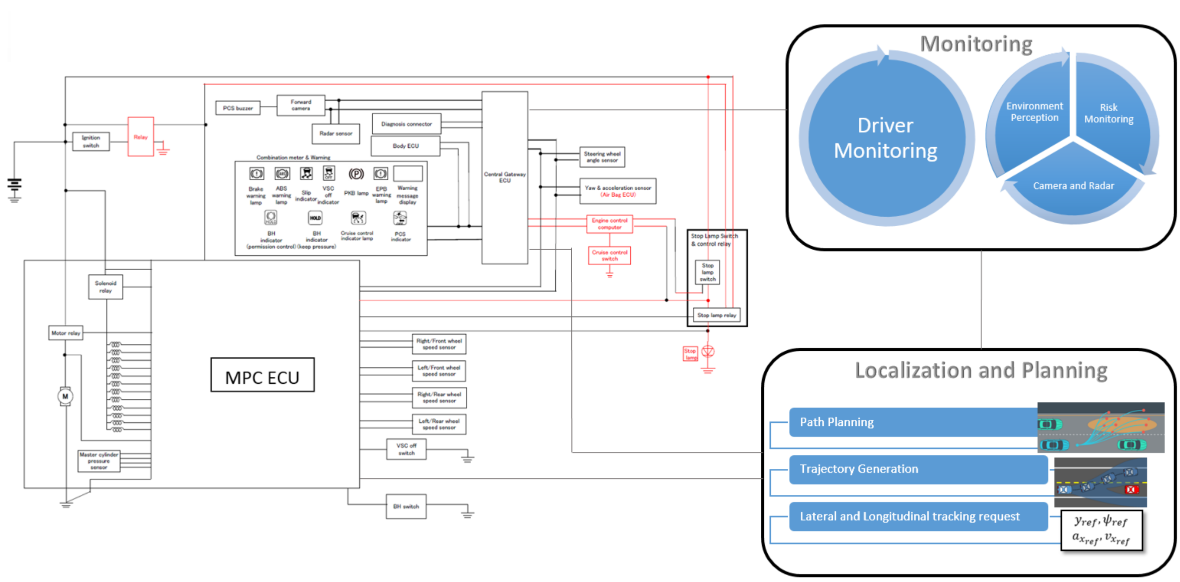

Figure 7.2: Controller's ECU integration

Lastly, the controllers are implemented on a vehicle in the form of an ECU. A unique controller as this would also require a specific and well-though architecture such that it can be integrated with other ECU's of the vehicle, communicating with them successfully and work efficiently to control the car. Thus, it is **necessary to think of an architecture in which this controller can be actually implemented on the vehicle**. Fig 7.2 is an illustration of one such architecture proposed by the author which can provide simple but efficient integration of controller in the car. With one ECU now for all control, the wire connections can be reduced, electrical requirement of the car can be optimized, debugging can be made easy and vehicle cost can be reduced. These advantages certainly provide the motivation to go for such control design and with current technological advancements taking place in automotive sector, this train of thought seems certainly achievable in the near future.

Bibliography

[1] M. Gerard, “Global chassis control and braking control using tyre forces measurements,” master thesis, Delft University of Technology, 2011.

[2] European Road Safety Observatory, “Annual accident report 2018,” tech. rep., European Commission, 2018.

[3] X. Wang, M. Zhu, M. Chen, and P. Tremont, “Drivers’ rear end collision avoidance behaviors under different levels of situational urgency,” *Transportation Research*, vol. Part C, pp. 419–433, August 2016.

[4] G. Markkula, O. Benderius, K. Wolff, and M. Wahde, “A review of near-collision driver behavior models,” *Human Factors*, vol. 54, no. 6, pp. 1117–1143, 2012. http://dx.doi.org/10.1177/0018720812448474.

[5] J. J. Scott and R. Gray, “Comparison of driver brake reaction times to multimodal rear-end collision warnings,” in *Proceedings of the Fourth International Driving Symposium on Human Factors in Driver Assessment, Training and Vehicle Design*, (Stevenson, Washington. Iowa City), pp. 285–291, Public Policy Center, University of Iowa, July 9-12 2007. https://doi.org/10.17077/drivingassessment.1251.

[6] A. Eckert, B. Hartmann, M. Sevenich, and P. E. Rieth, “Emergency steer & brake assist - a systematic approach for system integration of two complementary driver assistance systems.” 22nd International Technical Conference on the Enhanced Safety of Vehicles (ESV), 2011. Corporate Authors: National Highway Traffic Safety Administration.

[7] F. Pretagostini, *Anti-lock braking control design using a Nonlinear Model Predictive approach and wheel information.* PhD thesis, Delft University of Technology, Netherlands, 2018.

[8] S. D. Bruyne, *Model-based control of mechatronic systems.* PhD thesis, KU Leuven, December 2013.

[9] A. Hac and M. O. Bodie, “Improvements in vehicle handling through integrated control of chassis systems,” *Int. J. of Vehicle Autonomous Systems*, vol. 1, no. 1, pp. 83–110, 2002.

[10] H. Zhang and J. Wang, “Vehicle Lateral Dynamics Control Through AFS/DYC and Robust Gain-Scheduling Approach,” *IEEE Transactions on Vehicular Technology*, vol. 65, p. 489, 2016.

[11] C. Lv, H. Wang, and D. Cao, *Brake-Blending Control of EVs*, ch. 8, pp. 275–308. Modeling, Dynamics and Control of Electrified Vehicles, 2017.

[12] J. Choi, K. Kim, and K. Yi, "Emergency driving support algorithm with steering torque overlay and differential braking," *2011 14th International IEEE Conference on Intelligent Transportation Systems, Washington, DC, USA*, pp. 1433–1439, October 5-7 2011. doi:978-1-4577-2197-7/11/.

[13] P. Zegelaar, "For evasive steering assist 'steering you out of trouble'." 11th International IQPC Conference "Steering Systems" Berlin, November 2017.

[14] K. J. Aström and R. M. Murray, *Feedback Systems: An Introduction for Scientists and Engineers*. Princeton University Press, February 2009.

[15] W. Chen, H. Xiao, L. Liu, J. W. Zu, and H. Zhou, "Integrated control of vehicle system dynamics: Theory and experiment," in *Advances in Mechatronics* (P. H. Martinez-Alfaro, ed.), InTech, 2011.

[16] B. Shyrokau, "Planar model. lateral weight transfer. roll dynamic." Vehicle Dynamics A, Delft University of Technology, 2018.

[17] V. Patil, *Generic and complete vehicle dynamic models for open-source platforms*. PhD thesis, Delft University of Technology and Chalmers University of Technology, 2017.

[18] European Automobile Manufacturers Association, "Vehicles in use europe 2018," tech. rep., 2018. `https://www.acea.be/statistics/article/report-vehicles-in-use-europe-2018`.

[19] Hedges & Company, "U.S. vehicle registration statistics," 2019. `https://hedgescompany.com/automotive-market-research-statistics/auto-mailing-lists-and-marketing/`.

[20] National Highway Traffic Safety Administration, "2016 fatal motor vehicle crashes: Overview," tech. rep., U.S. Department of Transportation, October 2017. DOT HS 812 456.

[21] National Highway Traffic Safety Administration, "Table 99 - pedestrians killed or injured in single-vehicle crashes, by vehicle type and initial point of impact, 2016." `https://cdan.nhtsa.gov/tsftables/tsfar.htm#`.

[22] Y. Watanabe and S. Ito, "Influence of vehicle properties and human attributes on neck injuries in rear-end collisions," in *20th International Technical Conference on the Enhanced Safety of Vehicles (ESV)*, no. 07-0160, June 2007.

[23] M. Fausten, "Accident avoidance by evasive manoeuvres- Challenges and steps towards technical solution," 2010. Presentation on Vehicle Motion and Safety, Robert Bosch GmbH.

[24] Starline Safety, "Rear-end collisions still most common," October 2016. `https://www.tdmoes.com/rear-end-collisions-still-most-common/`.

[25] Insurance Information Institute, "Facts + statistics: Highway safety." `https://www.iii.org/fact-statistic/facts-statistics-highway-safety`.

[26] National Highway Traffic Safety Administration, "Table 29 - crashes by first harmful event, manner of collision, and crash severity, 2016." `https://cdan.nhtsa.gov/tsftables/tsfar.htm#`.

[27] Kearney Freeman Fogarty & Joshi, "Rear-end collisions are the most common type of car accident, and can cause serious injuries." `https://www.kffjlaw.com/library/a-few-facts-about-rear-end-collisions.cfm`.

[28] Gilreath & Associates, "Rear-end collisions: The most common type of auto accident in the U.S.," January 2013. `https://blog.sidgilreath.com/safety/rear-end-collisions-the-most-common-type-of-auto-accident-in-the-u-s.html`.

[29] Y. Belkadi and A. Campbell, "Naturalistic driver behaviour in response to the multi-sensory experience of rear-end collisions," in *Proceedings of the Human Factors and Ergonomics Society 2017 Annual Meeting*, 2017.

[30] J. J. Breuer, "Analysis Of Driver-Vehicle-Interaction In An Evasive Manoeuvre - Results of "Moose Test" Studies," no. 98-S2-W-35, 1998.

[31] N. Kuge, H. Ueno, H. Ichikawa, and K. Ochiai, "A study on the causes of rear-end collision based on an analysis of driver behavior," *JSAE - Society Automotive Engineers of Japan Review 16*, pp. 55–60, 1995.

[32] D. Shinar, *Psychology on the road : the human factor in traffic safety*. New York: John Wiley & Sons Inc, 1978.

[33] C. E. Beal and J. C. Gerdes, "Enhancing vehicle stability through model predictive control," ASME 2009 Dynamic Systems and Control Conference, January 2009. DOI: 10.1115/DSCC2009-2659.

[34] L. D. Adams, "Review of the literature on obstacle avoidance maneuvers: Braking versus steering," Tech. Rep. UMTRI-94- 19, The University of Michigan, Transportation Research Institute, Ann Arbor, Michigan 48 109-2 150, U.S.A., August 1994.

[35] European Road Safety Organisation, "Advanced driver assistance systems," tech. rep., European Commision, 2016.

[36] N. Chowdhri, "Vehicle evasive manoeuvre performance evaluation using active control techniques," tech. rep., Delft University of Technology, December 2018.

[37] L. Zhu, B. Shyrokau, B. Boulkroune, S. van Aalst, and R. Happee, "Performance benchmark of state-of-the-art lateral path-following controllers." 15th International Workshop on Advanced Motion Control, Tokyo, Japan, 2018.

[38] C. Ackermann, J. Bechtloff, and R. Isermann, "Collision avoidance with combined braking and steering," in *Springer Fachmedien Wiesbaden 2015* (P. Pfeffer, ed.), (6th International Munich Chassis Symposium 2015), pp. 199–213, 2015. doi:10.1007/978-3-658-09711-0_16.

[39] O. Mokhiamar and M. Abe, "Simultaneous optimal distribution of lateral and longitudinal tire forces for the model following control," *Journal of Dynamic Systems, Measurement, and Control by ASME*, vol. 126, pp. 753–763, December 2004. doi:10.1115/1.1850533.

[40] M. Jalali, S. Khosravani, A. Khajepour, S. Chen, and B. Litkouhi, "Model predictive control of vehicle stability using coordinated active steering and differential brakes," *IFAC Mechatronics: The Science of Intelligent Machines*, vol. 48, pp. 30–41, October 2017. `http://dx.doi.org/10.1016/j.mechatronics.2017.10.003`.

[41] P. Falcone, H. E. Tseng, F. Borrelli, J. Asgari, and D. Hrovat, "MPC-based yaw and lateral stabilisation via active front steering and braking," *Vehicle System Dynamics*, vol. 46, pp. 611–628, January 2009. `https://doi.org/10.1080/00423110802018297`.

[42] M. Choi and S. B. Choi, "MPC for vehicle lateral stability via differential braking and active front steering considering practical aspects," *Journal of Automobile Engineering*, vol. 230, no. 4, pp. 459–469, 2016. doi:10.1177/0954407015586895.

[43] H. Chen, S. Yu, X. Lu, F. Xu, T. Qu, and F. Wang, "Applying model predictive control in automotive," in *Proceesdings of the 10th World Congress on Intelligent Control and Automation, Beijing, China*, July 2012. doi:978-1-4673-1398-8/12.

[44] T. A. Johansen, "Chapter 1: Introduction to nonlinear model predictive control and moving horizon estimation."

[45] J. M. Maciejowski, *Predictive Control with Constraints*. Prentice Hall, Pearson Education, 2000.

[46] D. E. Seborg, T. F. Edgar, and D. A. Mellichamp, *Process Dynamics and Control*, ch. 20: Model Predictive Control, pp. 414–438.

[47] M. Vukov, A. Domahidi, H. J. Ferreau, M. Morari, and M. Diehl, "Auto-generated Algorithms for Nonlinear Model Predicitive Control on Long and on Short Horizons," in *Proceedings of the 52nd Conference on Decision and Control (CDC)*, 2013.

[48] R. Quirynen, M. Vukov, M. Zanon, and M. Diehl, "Autogenerating Microsecond Solvers for Nonlinear MPC: a Tutorial Using ACADO Integrators," *Optimal Control Applications and Methods*, 2014.

[49] M. Diehl, *Real-Time Optimization for Large Scale Nonlinear Processes*. PhD thesis, Ruprecht-Karls-Universität Heidelberg, 2001.

[50] J. Ferreau, H. Bock, , and M. Diehl, "An online active set strategy to overcome the limitations of explicit MPC," *Int. J. Robust Nonlinear Control*, vol. 18, pp. 816 – 830, 2008.

[51] P. Song, C. Zong, and M. Tomizuka, "Combined longitudinal and lateral control for automated lane guidance of full drive-by-wire vehicles," *SAE Int. J. Passeng. Cars – Electron. Electr. Syst*, vol. 8, no. 2, 2015. doi:10.4271/2015-01-0321.

[52] R. Hoppe, "Chapter 4 Sequential Quadratic Programming." Department of Mathematics, University of Houston, 2006.

[53] A. Geletu, “Quadratic programming problems - a review on algorithms and applications (Active-set and interior point methods).” Department of Simulation and Optimal Processes, Ilmenau University of Technology.

[54] R. Attia, R. Orjuela, and M. Basset, “Longitudinal control for automated vehicle guidance,” *The International Federation of Automatic Control*, October 2012.

[55] E. H. M. Lim and J. K. Hedrick, “Lateral and longitudinal vehicle control coupling for automated vehicle operation,” (San Diego, California), pp. 3676–3680, Proceedings of the American Control Conference, June 1999.

[56] J. He, D. A. Crolla, M. C. Levesley, and W. J. Manning, “Coordination of active steering, driveline, and braking for integrated vehicle dynamics control,” *J. Automobile Engineering*, vol. 220, pp. 1401 – 1421, 2006. DOI: 10.1243/09544070JAUTO265.

[57] European Council Service Framework Programme, “Electric-VEhicle Control of individual wheel Torque for On- and Off-Road Conditions (E-VECTOORC),” 2007 - 2013. European funded project, FP7.

[58] B. Shyrokau, D. Wang, K. H. D. Savitski, and v. Ivanov, “Vehicle motion control with subsystem prioritization,” *Mechatronics*, vol. 30, pp. 297–315, September 2015. `https://doi.org/10.1016/j.mechatronics.2014.11.004`.

[59] R. Rajamani, *Vehicle Dynamics and Control*. Springer, 2012. DOI 10.1007/978-1-4614-1433-9.

[60] B. Breuer and K. H. Bill, *Brake Technology Handbook*. SAE International, 2008.

[61] S. Kerst, B. Shyrokau, and E. Holweg, “Reconstruction of wheel forces using an intelligent bearing,” *AE Int. J. Passeng. Cars – Electron. Electr. Syst.*, vol. 9, no. 1, pp. 196–203, 2016. doi:10.4271/2016-01-0092.

[62] J. Hou, G. F. List, and X. Guo, “New algorithms for computing the time-to-collision in freeway traffic simulation models,” *Hindawi Publishing Corporation Computational Intelligence and Neuroscience*, vol. 2014, December 2014. `http://dx.doi.org/10.1155/2014/761047`.

[63] E. Coelingh, “Decision making and threat assessment for automotive collision avoidance.” interactIVe Summer School, July 2012.

[64] S. E. Lee, E. Llaneras, S. Klauer, and J. Sudweeks, “Analyses of rear-end crashes and near-crashes in the 100-car naturalistic driving study to support rear-signaling countermeasure development,” *USDOT/National Highway Traffic Safety Administration*, October 2007.

[65] Y. Hattori, E. Ono, and S. Hosoe, “Optimum vehicle trajectory control for obstacle avoidance problem,” *IEEE/ASME Transactions on Mechatronics*, vol. 11, pp. 507–512, October 2006.

[66] G. Schildbach, “A new nonlinear model predictive control algorithm for vehicle path tracking,” September 2016.

[67] L. Wang, "Model predictive control system design and implementation using MATLAB." Advances in Industrial Control, Springer, 2009. doi 10.1007/978-1-84882-331-0.

[68] H. B. Pacejka, *Tire and Vehicle Dynamics.* Butterworth-Heinemann, third edition ed., 2012.

[69] M. Damian, B. Shyrokau, A. Ocariz, and X. C. Akutain, "Torque control for more realistic hand-wheel haptics in a driving simulator." Driving Simulation Conference Europe, 2019.

[70] J. Zhou, J. Lu, and H. Peng, "Vehicle stabilisation in response to exogenous impulsive disturbances to the vehicle body," *Int. J. Vehicle Autonomous Systems*, vol. 8, no. 2/3/4, p. 242–262, 2010. DOI: 10.1504/IJVAS.2010.035798.

[71] R. Limpert, "Brake design and safety." Society of Automotive Engineers, July 1999.

A

LMPC - Linear Bicycle Model Plots

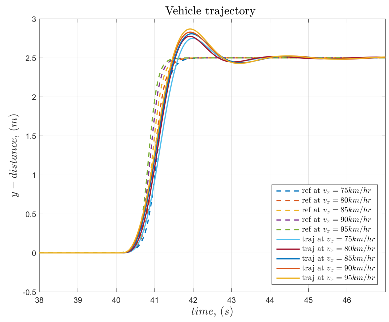

(a) Lateral position y_p

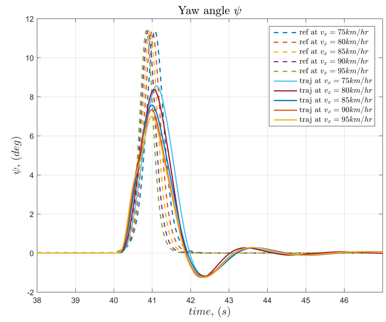

(b) Yaw angle ψ

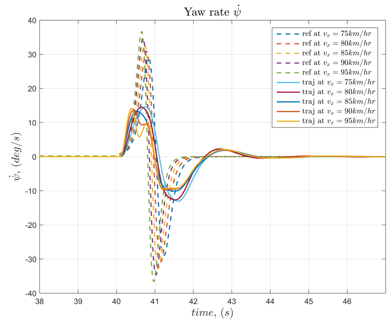

(c) Yaw rate $\dot{\psi}$

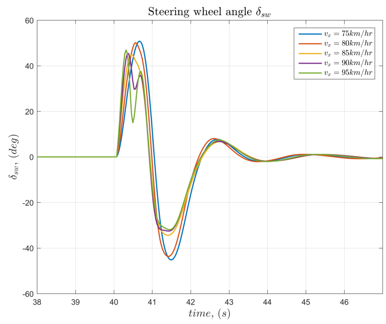

(d) SWA δ_{sw}

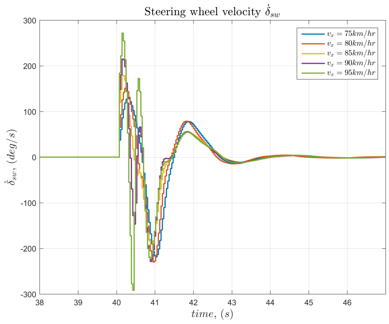

(e) SWV $\dot{\delta}_{\text{sw}}$

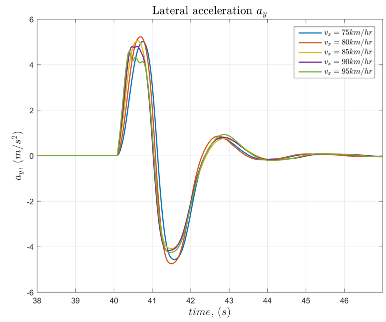

(f) Lateral acc. a_y

Simulation result for Set 1 - Case 1: $\mu = 0.9$

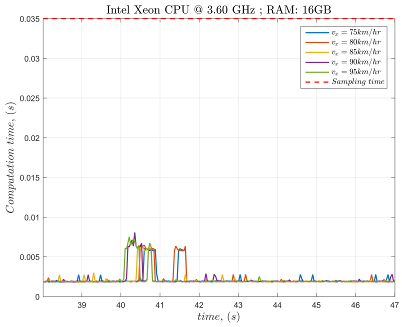

(g) Computation time

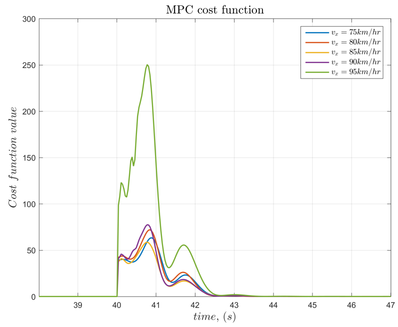

(h) Cost function value

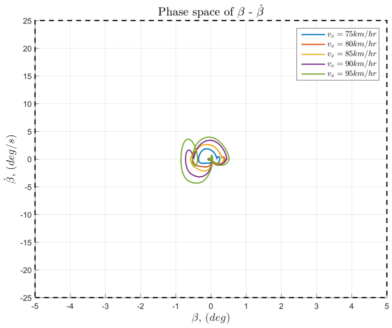

(i) β - $\dot{\beta}$ phase space

S No. -	v_x [km/hr]	M_p [%]	T_s [s]	T_r [s]	y_{RMS} [%]	ψ_{RMS} [%]	$\dot{\psi}_{RMS}$ [%]	DTC [m]
1	75	25.03	5.66	0.45	7.94	80.16	465.28	0.60
2	80	27.66	5.62	0.44	8.89	83.13	500.50	0.55
3	85	30.86	6.35	0.46	11.32	95.38	560.09	0.42
4	90	32.99	6.32	0.45	13.32	103.50	631.20	0.30
5	95	37.03	7.00	0.45	16.54	119.12	734.22	0.14

(j) KPI table

Figure A.1: Simulation result for Set 1 - Case 1: $\mu = 0.9$

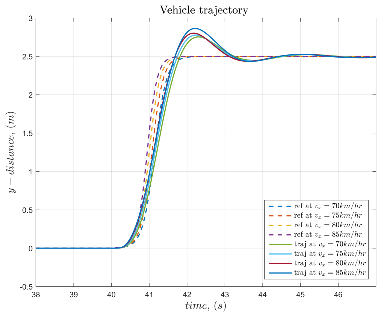

(a) Lateral position y_p

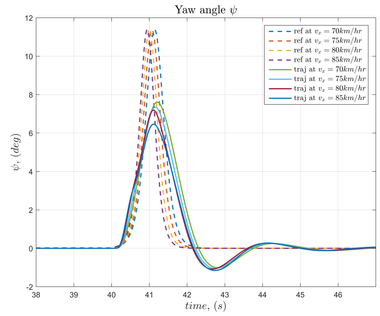

(b) Yaw angle ψ

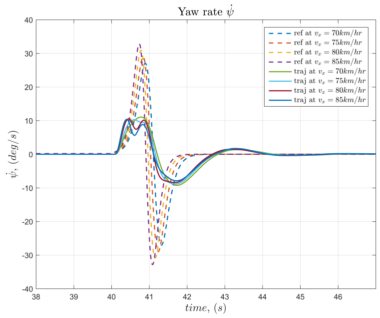

(c) Yaw rate $\dot{\psi}$

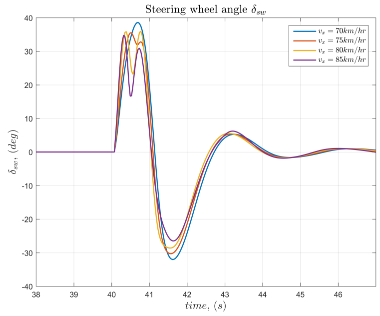

(d) SWA δ_{sw}

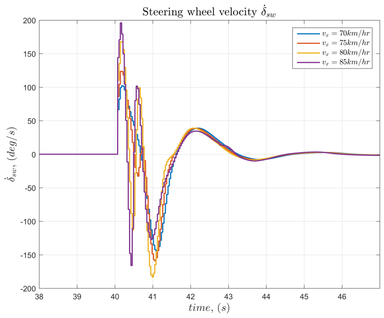

(e) SWV $\dot{\delta}_{\mathrm{sw}}$

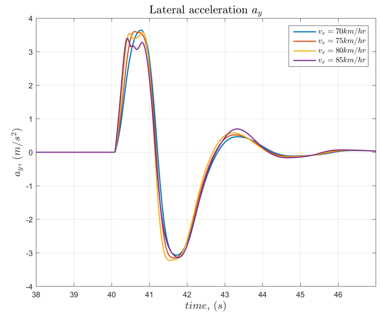

(f) Lateral acc. a_y

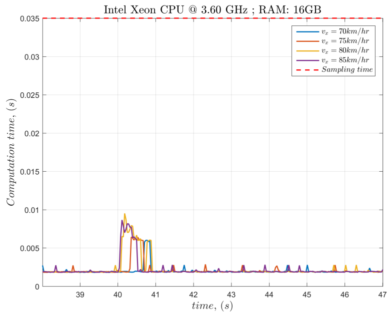

(g) Computation time

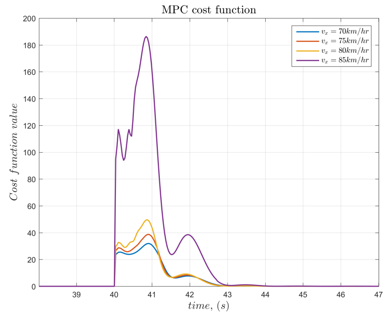

(h) Cost function value

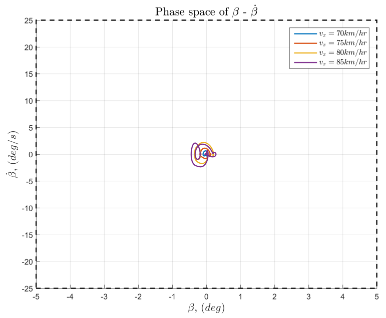

(i) β - $\dot{\beta}$ phase space

S No.	v_x	M_p	T_s	T_r	y_{RMS}	ψ_{RMS}	$\dot{\psi}_{RMS}$	DTC
-	[km/hr]	[%]	[s]	[s]	[%]	[%]	[%]	[m]
1	70	25.32	7.00	0.55	9.98	100.08	495.22	0.49
2	75	27.70	7.00	0.53	11.71	106.98	547.64	0.40
3	80	30.15	7.00	0.51	13.68	113.41	598.31	0.30
4	85	36.31	6.99	0.52	18.49	134.47	687.73	0.09

(j) KPI table

Figure A.2: Simulation result for Set 1 - Case 2: $\mu = 0.6$

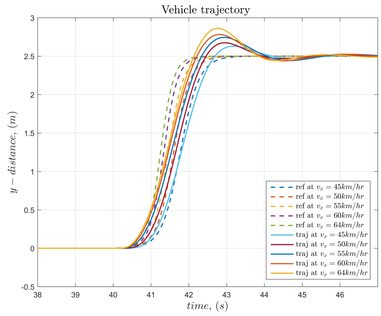

(a) Lateral position y_p

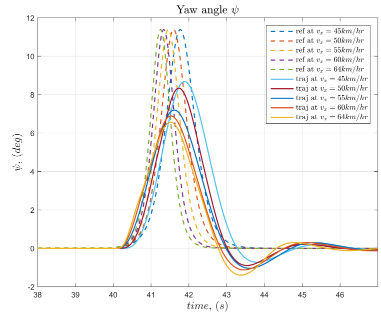

(b) Yaw angle ψ

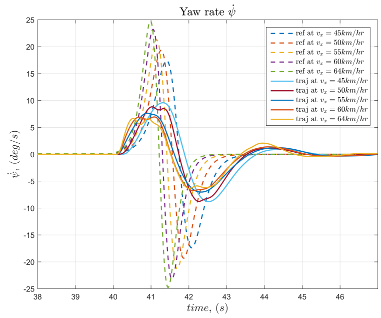

(c) Yaw rate $\dot{\psi}$

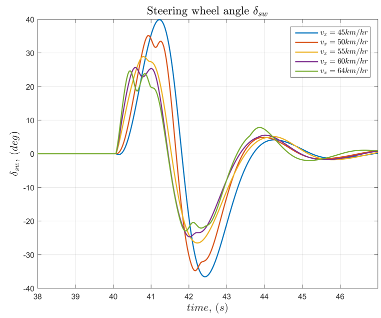

(d) SWA δ_{sw}

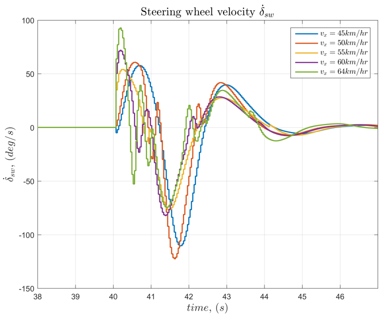

(e) SWV $\dot{\delta}_{\mathrm{sw}}$

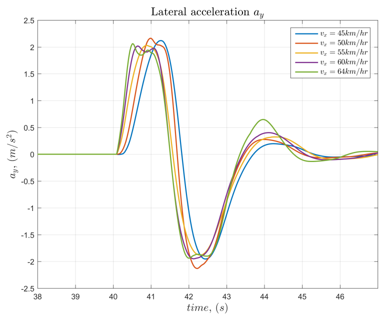

(f) Lateral acc. a_y

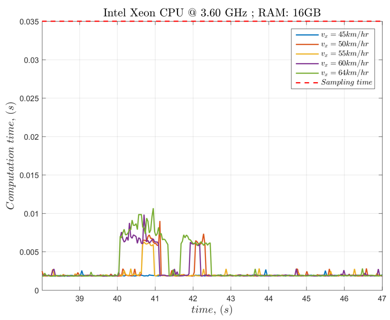

(g) Computation time

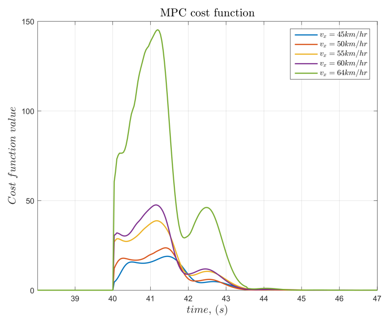

(h) Cost function value

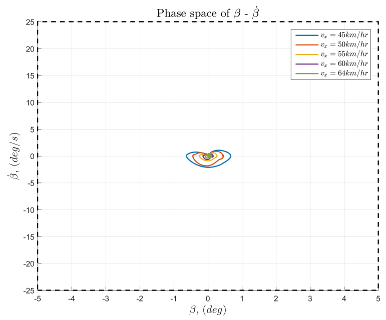

(i) β - $\dot{\beta}$ phase space

S No.	v_x	M_p	T_s	T_r	$\mathrm{y_{RMS}}$	ψ_{RMS}	$\dot{\psi}_{\mathrm{RMS}}$	DTC
-	[km/hr]	[%]	[s]	[s]	[%]	[%]	[%]	[m]
1	45	13.01	6.71	0.76	5.89	92.48	336.32	0.66
2	50	17.42	6.42	0.70	7.70	104.98	401.44	0.60
3	55	24.40	6.93	0.72	11.69	128.82	480.52	0.45
4	60	28.13	6.75	0.68	14.04	138.02	534.25	0.34
5	64	36.14	7.00	0.66	17.68	154.50	597.93	0.22

(j) KPI table

Figure A.3: Simulation result for Set 1 - Case 3: $\mu = 0.3$

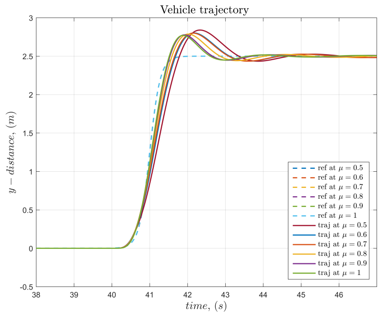

(a) Lateral position y_p

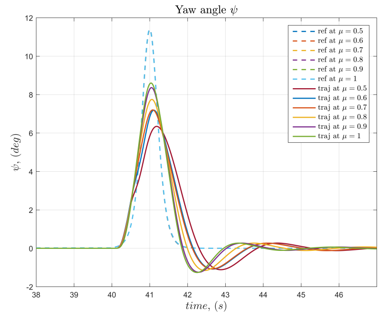

(b) Yaw angle ψ

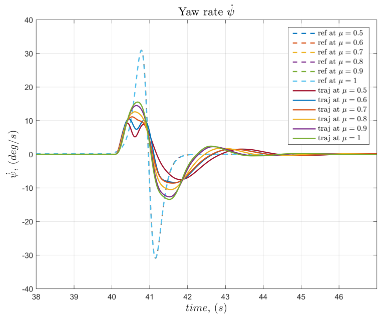

(c) Yaw rate $\dot{\psi}$

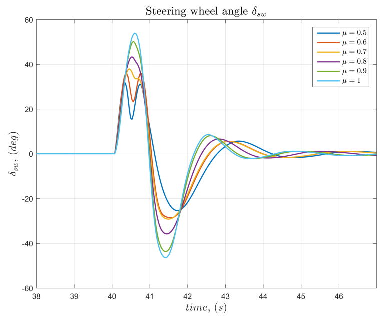

(d) SWA δ_{sw}

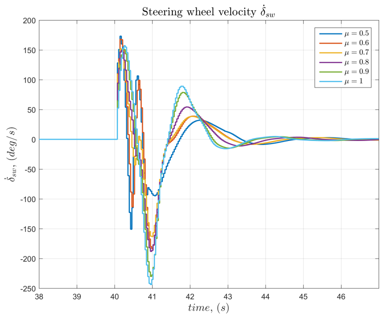

(e) SWV $\dot{\delta}_{\text{sw}}$

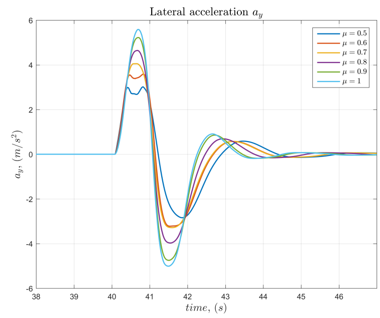

(f) Lateral acc. a_y

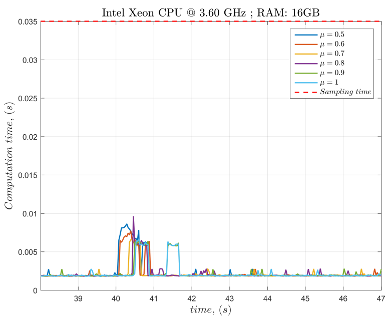

(g) Computation time

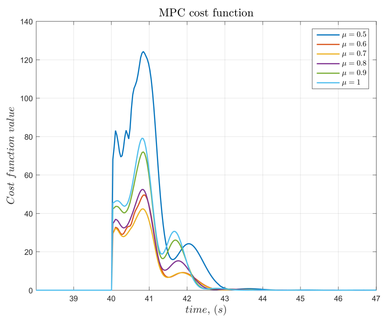

(h) Cost function value

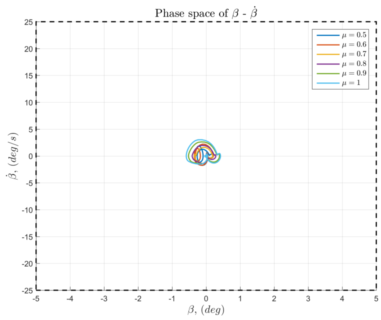

(i) β - $\dot{\beta}$ phase space

S No.	μ	M$_p$	T$_s$	T$_r$	y_{RMS}	ψ_{RMS}	$\dot{\psi}_{\text{RMS}}$	DTC
-	-	[%]	[s]	[s]	[%]	[%]	[%]	[m]
1	0.5	33.96	7.00	0.55	18.32	138.20	659.13	0.10
2	0.6	30.15	7.00	0.51	13.68	113.41	598.31	0.30
3	0.7	29.97	7.00	0.51	12.61	106.77	569.52	0.35
4	0.8	28.73	6.39	0.47	10.39	94.13	534.14	0.47
5	0.9	27.66	5.62	0.44	8.89	83.13	500.50	0.55
6	1	27.05	5.38	0.43	8.32	78.26	478.96	0.59

(j) KPI table

Figure A.4: Simulation result for Set 2 - Case 1: $v_x = 80 km/hr$

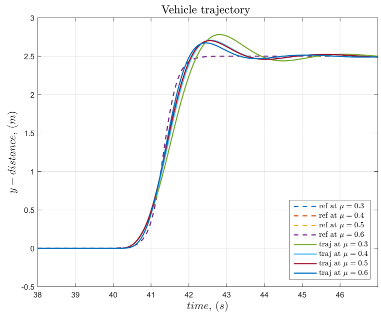

(a) Lateral position y_p

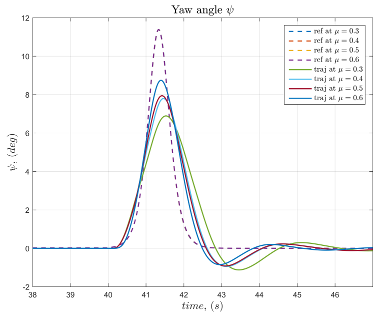

(b) Yaw angle ψ

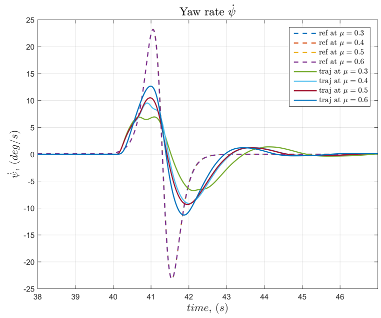

(c) Yaw rate $\dot{\psi}$

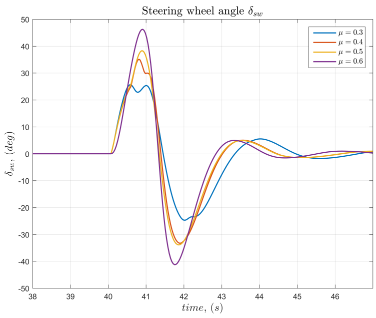

(d) SWA δ_{sw}

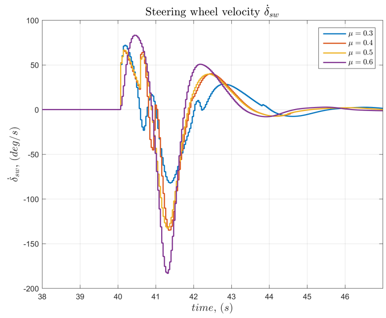

(e) SWV $\dot{\delta}_{\text{sw}}$

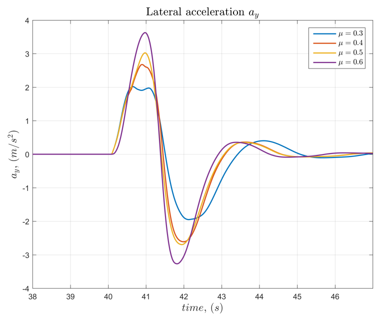

(f) Lateral acc. a_y

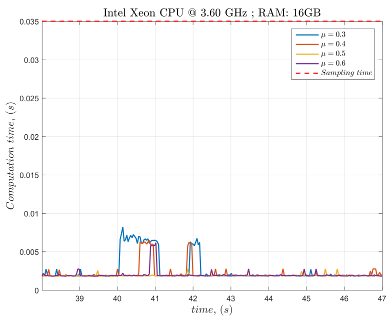

(g) Computation time

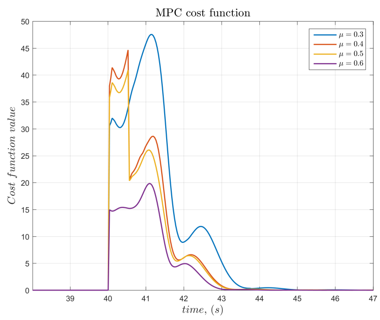

(h) Cost function value

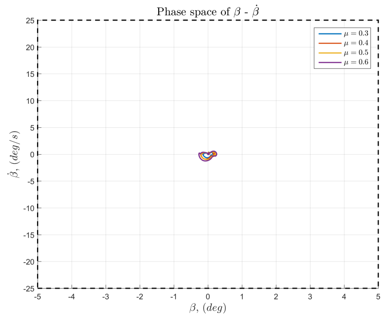

(i) β - $\dot{\beta}$ phase space

S No.	μ	M_p	T_s	T_r	y_{RMS}	ψ_{RMS}	$\dot{\psi}_{\text{RMS}}$	DTC
-	-	[%]	[s]	[s]	[%]	[%]	[%]	[m]
1	0.3	28.13	6.75	0.68	14.04	138.02	534.25	0.34
2	0.4	20.79	7.00	0.62	9.29	107.82	471.96	0.52
3	0.5	20.23	7.00	0.61	8.31	98.48	438.25	0.57
4	0.6	17.30	6.89	0.57	6.36	79.19	381.22	0.65

(j) KPI table

Figure A.5: Simulation result for Set 2 - Case 2: $v_x = 60 km/hr$

B

NMPC - Nonlinear Bicycle Model Plots

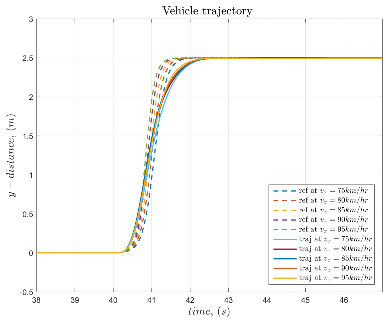

(a) Lateral position y_p

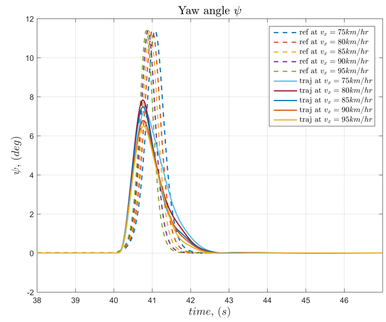

(b) Yaw angle ψ

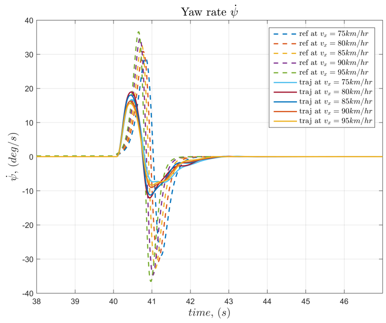

(c) Yaw rate $\dot{\psi}$

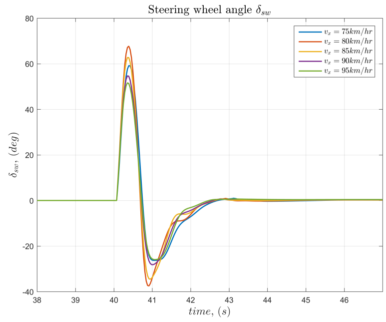

(d) SWA δ_{sw}

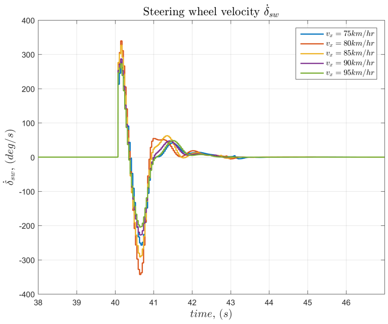

(e) SWV $\dot{\delta}_{\mathrm{sw}}$

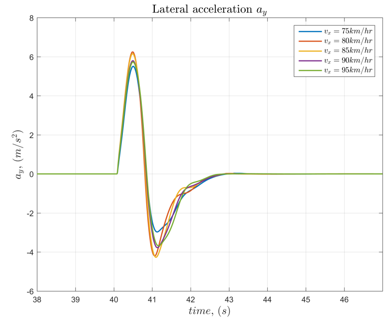

(f) Lateral acc. a_y

Simulation result for Set 1 - Case 1: $\mu = 0.9$

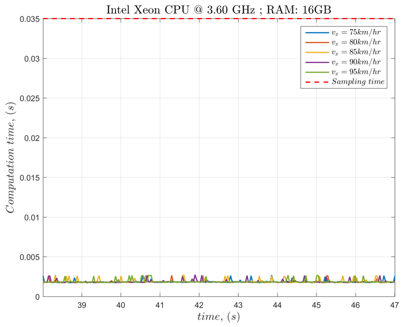

(g) Computation time

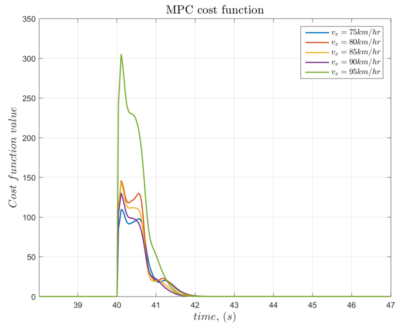

(h) Cost function value

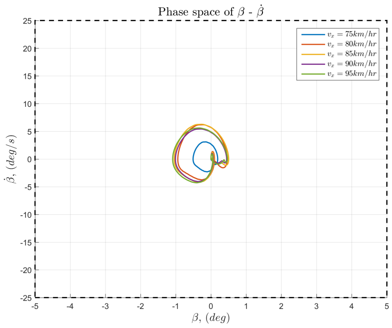

(i) β - $\dot{\beta}$ phase space

S No. -	v_x [km/hr]	M_p [%]	T_s [s]	T_r [s]	y_{RMS} [%]	ψ_{RMS} [%]	$\dot{\psi}_{RMS}$ [%]	DTC [m]
1	75	0.29	2.45	0.88	10.45	121.28	625.61	0.49
2	80	0.21	2.49	0.90	10.32	125.45	669.52	0.47
3	85	0.00	2.48	0.88	9.35	106.85	599.14	0.41
4	90	0.00	2.39	0.83	11.25	94.27	569.19	0.26
5	95	0.00	2.38	0.76	13.39	90.16	574.36	0.15

(j) KPI table

Figure B.1: Simulation result for Set 1 - Case 1: $\mu = 0.9$

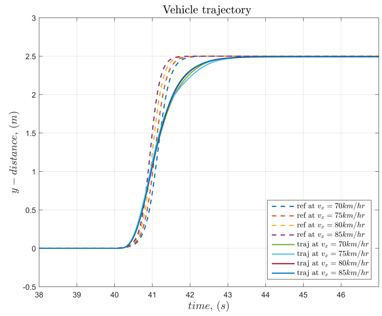

(a) Lateral position y_p

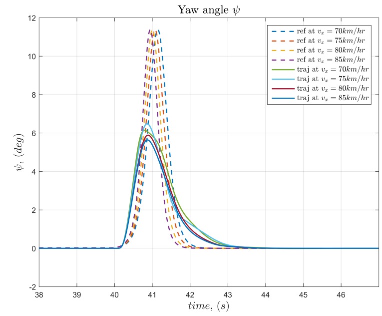

(b) Yaw angle ψ

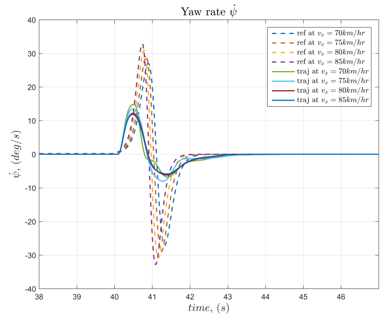

(c) Yaw rate $\dot{\psi}$

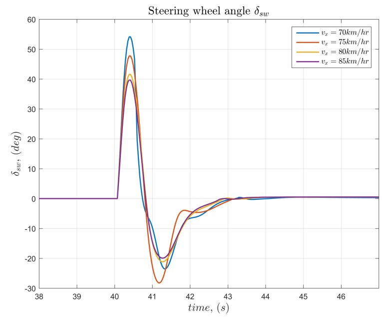

(d) SWA δ_{sw}

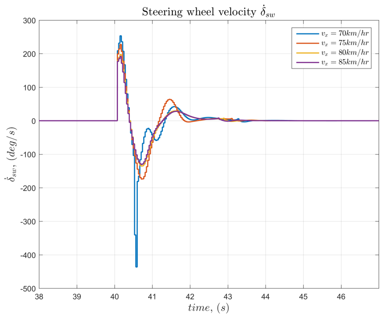

(e) SWV $\dot{\delta}_{\text{sw}}$

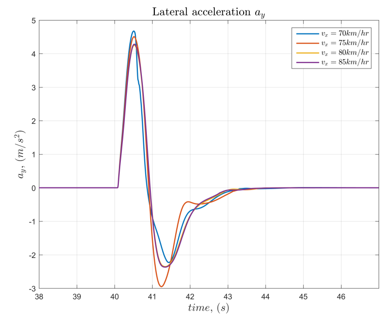

(f) Lateral acc. a_y

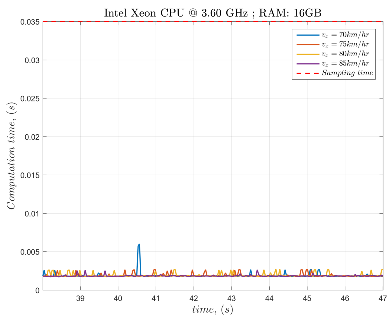

(g) Computation time

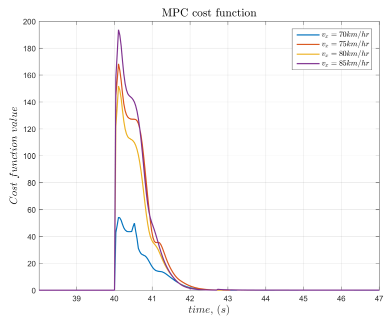

(h) Cost function value

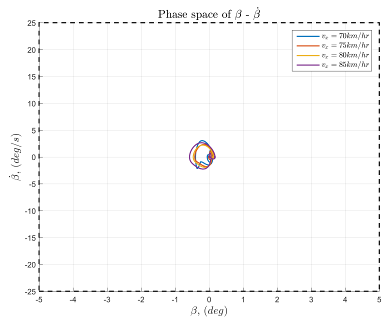

(i) β - $\dot{\beta}$ phase space

S No. -	v_x [km/hr]	M_p [%]	T_s [s]	T_r [s]	y_{RMS} [%]	ψ_{RMS} [%]	$\dot{\psi}_{RMS}$ [%]	DTC [m]
1	70	0.00	3.51	1.16	12.73	129.53	613.27	0.38
2	75	0.00	3.77	1.30	13.64	118.53	569.20	0.29
3	80	0.00	3.61	1.09	14.85	108.79	574.68	0.16
4	85	0.00	3.87	1.08	17.57	108.75	591.10	0.05

(j) KPI table

Figure B.2: Simulation result for Set 1 - Case 2: $\mu = 0.6$

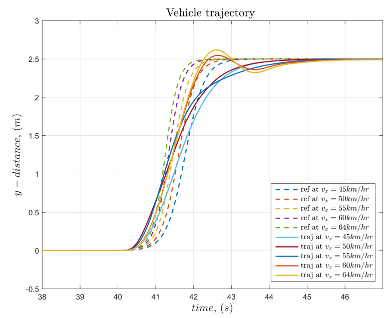

(a) Lateral position y_p

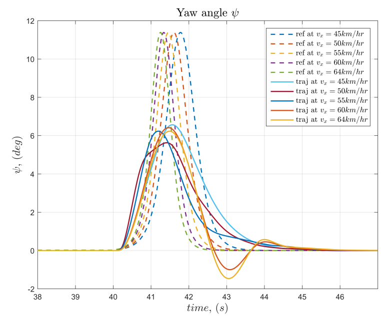

(b) Yaw angle ψ

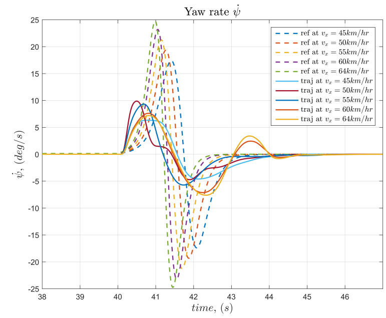

(c) Yaw rate $\dot{\psi}$

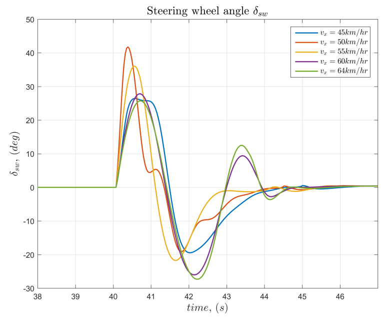

(d) SWA δ_{sw}

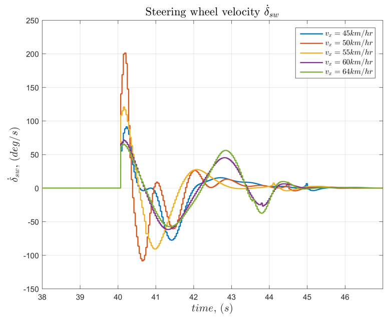

(e) SWV $\dot{\delta}_{\text{sw}}$

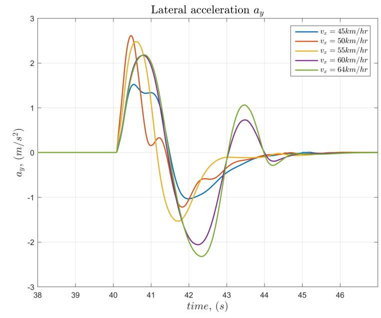

(f) Lateral acc. a_y

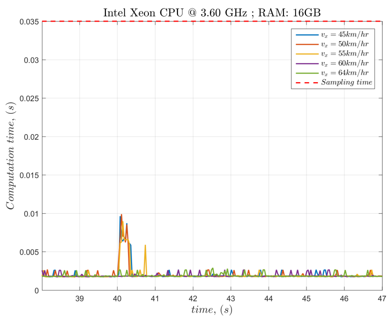

(g) Computation time

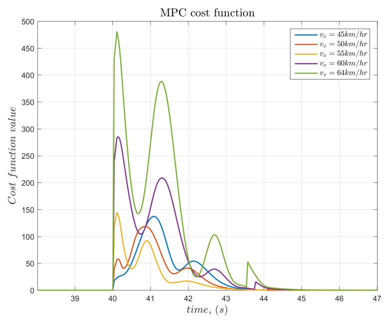

(h) Cost function value

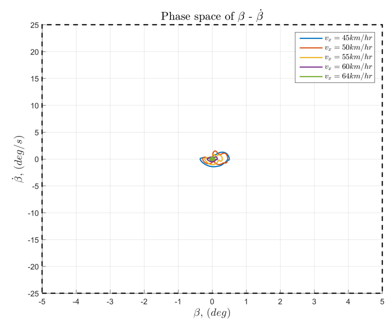

(i) β - $\dot{\beta}$ phase space

S No.	v_x	M_p	T_s	T_r	y_{RMS}	ψ_{RMS}	$\dot{\psi}_{\text{RMS}}$	DTC
-	[km/hr]	[%]	[s]	[s]	[%]	[%]	[%]	[m]
1	45	0.00	4.77	1.50	13.97	134.77	413.82	0.48
2	50	0.00	4.75	1.60	17.09	157.41	506.58	0.42
3	55	0.00	5.37	2.05	16.52	136.68	490.34	0.35
4	60	4.68	7.00	0.79	12.44	124.41	520.39	0.31
5	64	11.80	6.77	0.72	17.18	145.72	586.33	0.14

(j) KPI table

Figure B.3: Simulation result for Set 1 - Case 3: $\mu = 0.3$

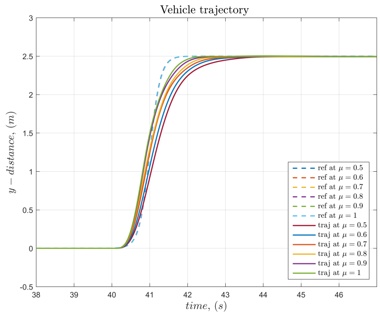

(a) Lateral position y_p

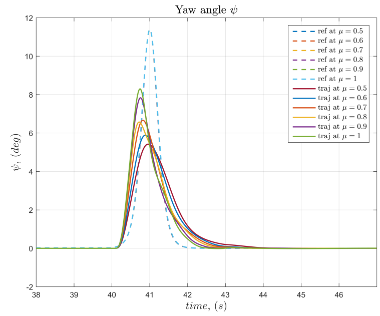

(b) Yaw angle ψ

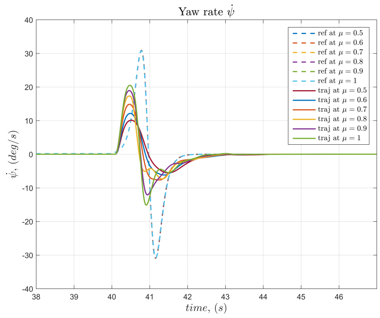

(c) Yaw rate $\dot{\psi}$

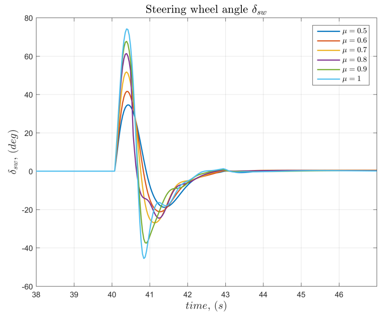

(d) SWA δ_{sw}

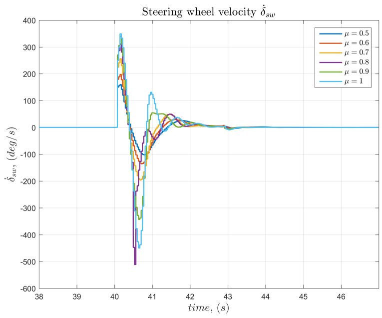

(e) SWV $\dot{\delta}_{\mathrm{sw}}$

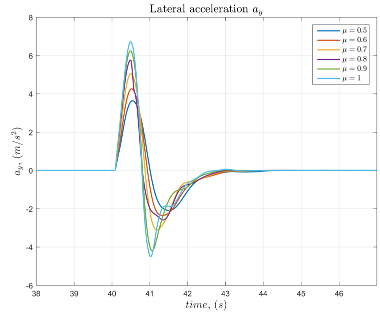

(f) Lateral acc. a_y

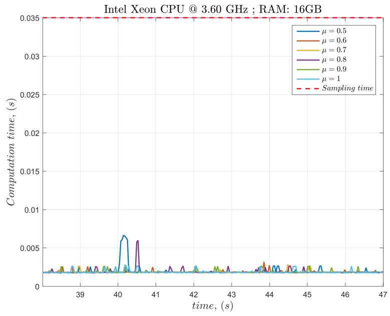

(g) Computation time

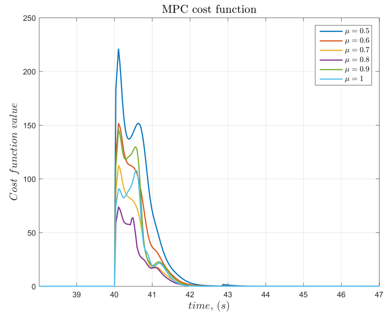

(h) Cost function value

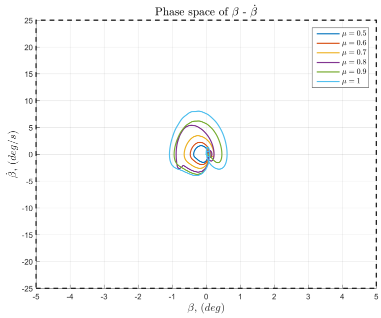

(i) β - $\dot{\beta}$ phase space

S No.	μ	M_p	T_s	T_r	y_{RMS}	ψ_{RMS}	$\dot{\psi}_{\mathrm{RMS}}$	DTC
-	-	[%]	[s]	[s]	[%]	[%]	[%]	[m]
1	0.5	0.00	3.93	1.20	18.91	115.02	583.85	0.02
2	0.6	0.00	3.61	1.09	14.85	108.79	574.68	0.16
3	0.7	0.00	3.25	1.05	11.46	108.22	579.65	0.32
4	0.8	0.00	2.80	0.97	11.20	119.72	670.22	0.35
5	0.9	0.21	2.49	0.90	10.32	125.45	669.52	0.47
6	1	0.35	2.24	0.82	10.33	131.61	728.69	0.50

(j) KPI table

Figure B.4: Simulation result for Set 2 - Case 1: $v_x = 80 km/hr$

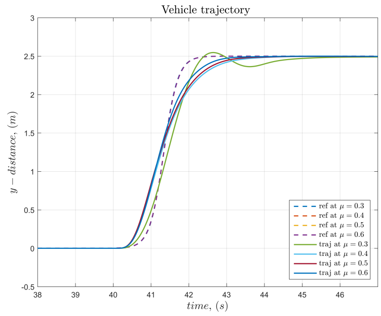

(a) Lateral position y_p

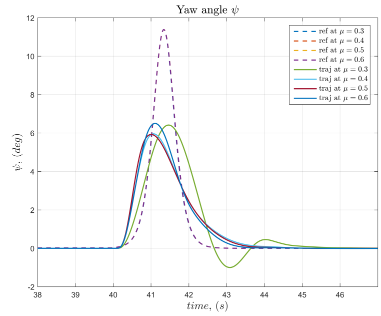

(b) Yaw angle ψ

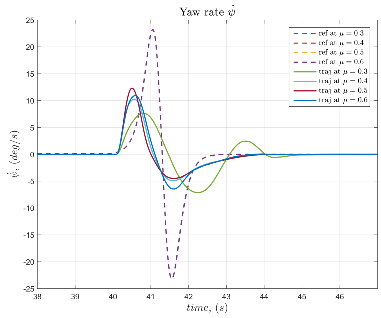

(c) Yaw rate $\dot{\psi}$

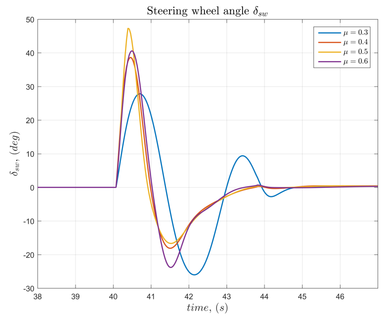

(d) SWA δ_{sw}

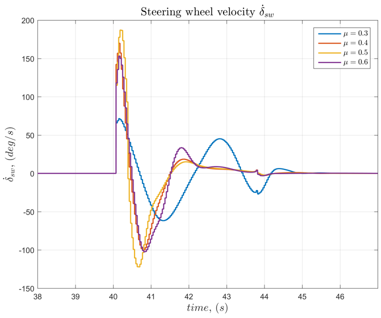

(e) SWV $\dot{\delta}_{\text{sw}}$

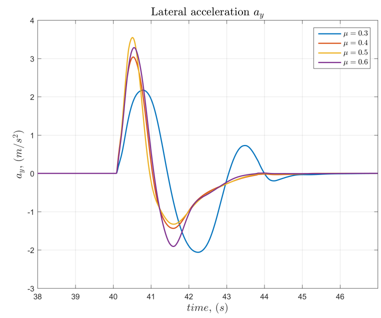

(f) Lateral acc. a_y

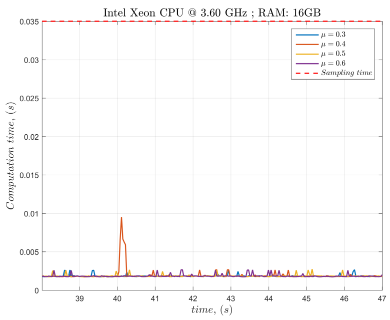

(g) Computation time

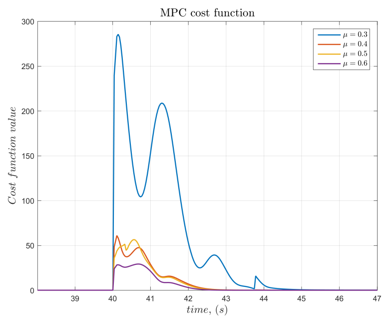

(h) Cost function value

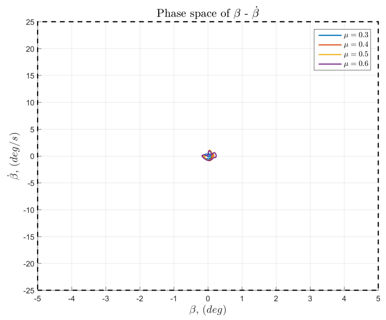

(i) β - $\dot{\beta}$ phase space

S No.	μ	M_p	T_s	T_r	y_{RMS}	ψ_{RMS}	$\dot{\psi}_{\text{RMS}}$	DTC
-	-	[%]	[s]	[s]	[%]	[%]	[%]	[m]
1	0.3	4.68	7.00	0.79	12.44	124.41	520.39	0.31
2	0.4	0.00	4.33	1.43	14.58	137.56	545.17	0.34
3	0.5	0.00	4.10	1.35	14.58	143.84	576.41	0.38
4	0.6	0.01	3.47	1.17	12.41	126.25	512.52	0.46

(j) KPI table

Figure B.5: Simulation result for Set 2 - Case 2: $v_x = 60 km/hr$

C

NMPC - Planar Car Model Plots

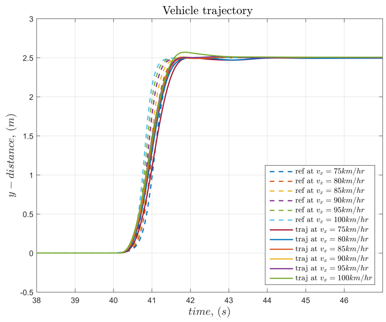

(a) Lateral position y_p

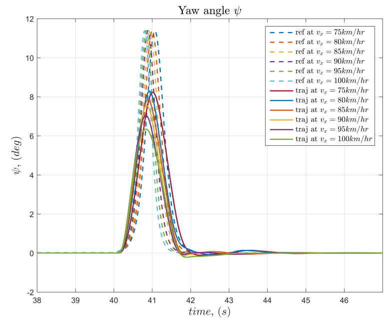

(b) Yaw angle ψ

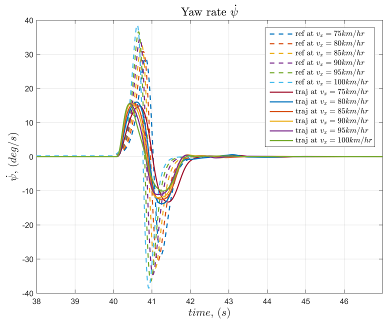

(c) Yaw rate $\dot{\psi}$

S No.	v_x	M_p	T_s	T_r	y_{RMS}	ψ_{RMS}	$\dot{\psi}_{RMS}$	DTC
-	[km/hr]	[%]	[s]	[s]	[%]	[%]	[%]	[m]
1	75	0.00	3.80	0.56	4.86	65.40	391.02	0.61
2	80	0.29	3.77	0.55	5.02	68.17	400.62	0.59
3	85	1.03	3.18	0.54	5.90	69.45	459.94	0.50
4	90	1.34	3.10	0.53	7.37	71.30	500.64	0.41
5	95	1.45	3.08	0.54	10.22	77.13	557.86	0.28
6	100	7.01	3.30	0.53	14.20	91.92	651.99	0.09

(d) KPI table

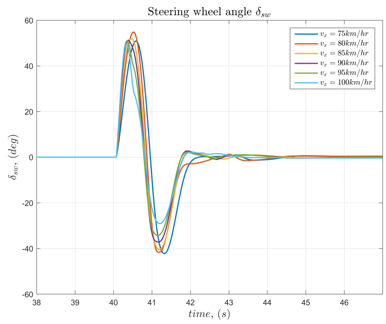

(e) SWA δ_{sw}

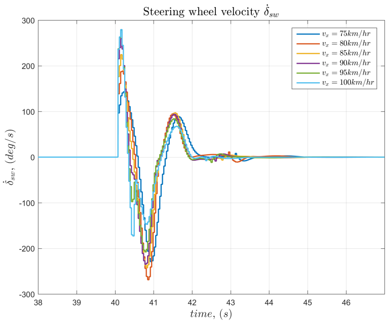

(f) SWV $\dot{\delta}_{\text{sw}}$

Simulation result for Set 1 - Case 1: $\mu = 0.9$

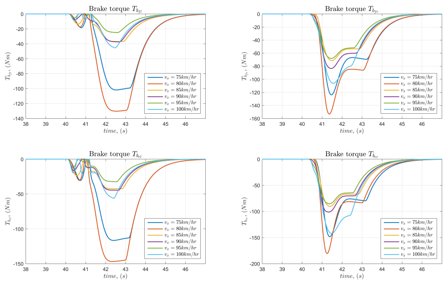

(g) Brake Torques T_b

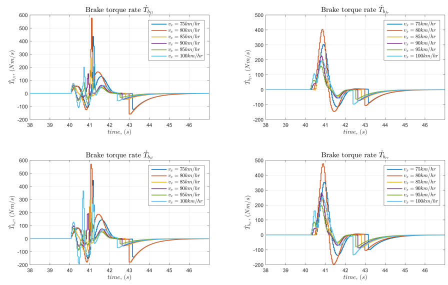

(h) Brake torque rates $\dot{T}_b$

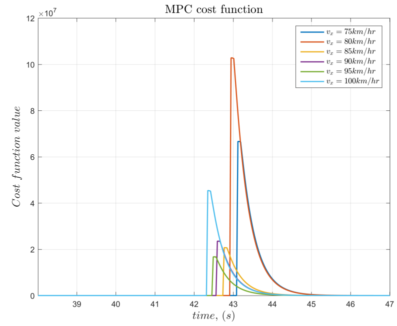

(i) Cost function value

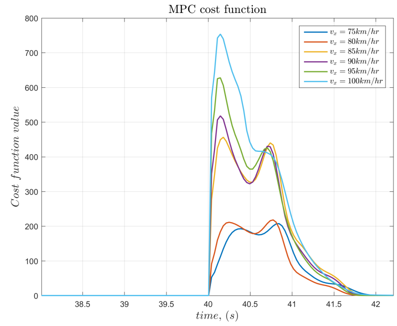

(j) Cost function value

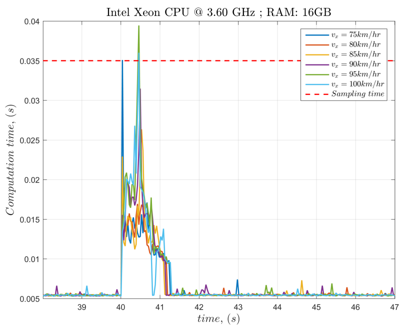

(k) Computation time

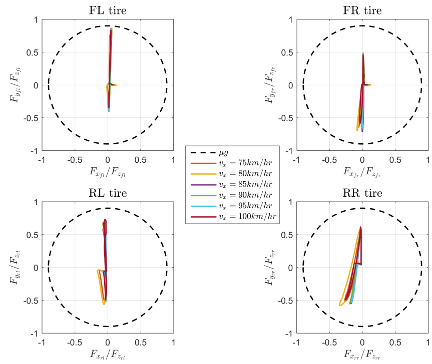

(l) Kamm Circle

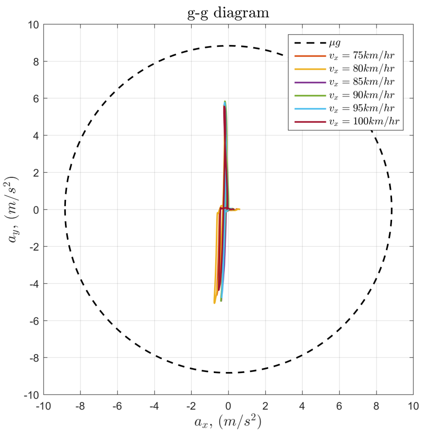

(m) g-g diagram

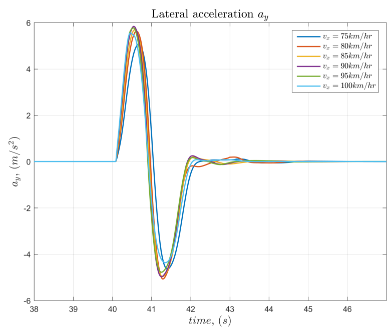

(n) Lateral acc. a_y

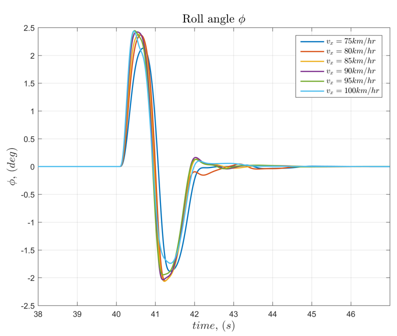

(o) Roll angle ϕ

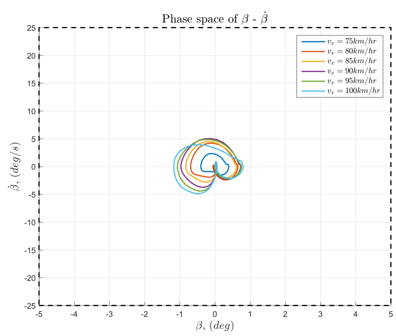

(p) β - $\dot{\beta}$ phase space

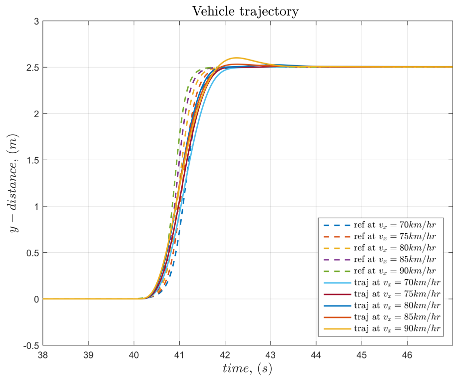

(a) Lateral position y_p

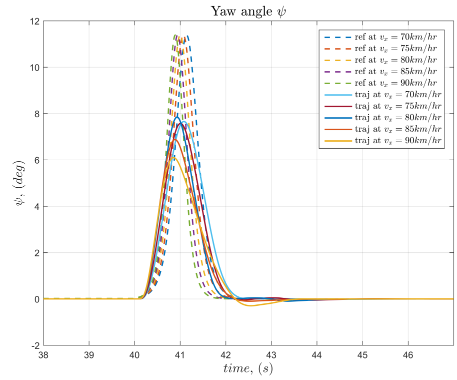

(b) Yaw angle ψ

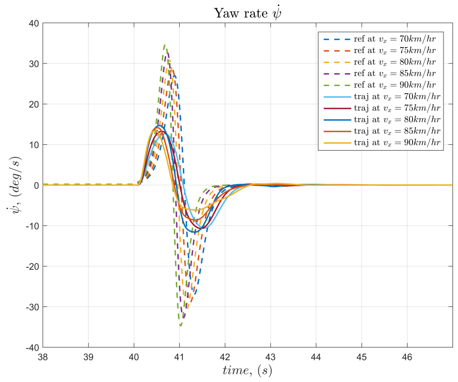

(c) Yaw rate $\dot{\psi}$

S No.	v_x	M_p	T_s	T_r	y_{RMS}	ψ_{RMS}	$\dot{\psi}_{\mathrm{RMS}}$	DTC
-	[km/hr]	[%]	[s]	[s]	[%]	[%]	[%]	[m]
1	70	0.83	2.09	0.66	6.06	77.41	425.69	0.55
2	75	1.23	3.71	0.63	6.21	77.92	453.85	0.52
3	80	2.51	3.88	0.59	6.09	73.82	449.05	0.51
4	85	3.16	3.25	0.64	9.81	87.54	536.96	0.31
5	90	10.07	3.35	0.67	14.52	103.04	601.45	0.11

(d) KPI table

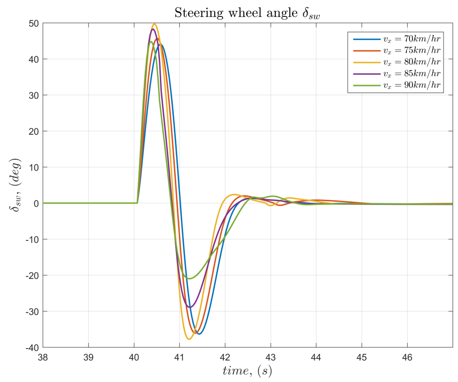

(e) SWA δ_{sw}

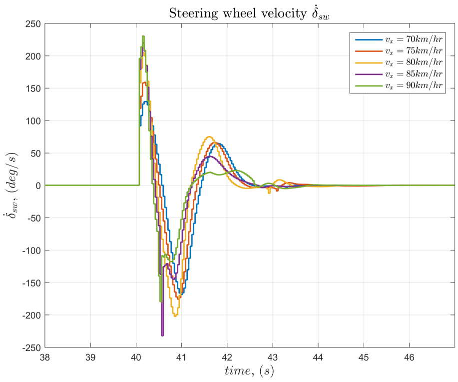

(f) SWV $\dot{\delta}_{\text{sw}}$

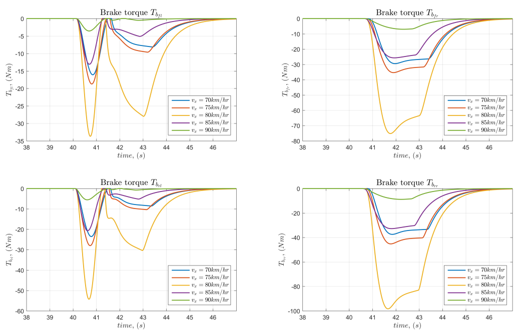

(g) Brake Torques T_b

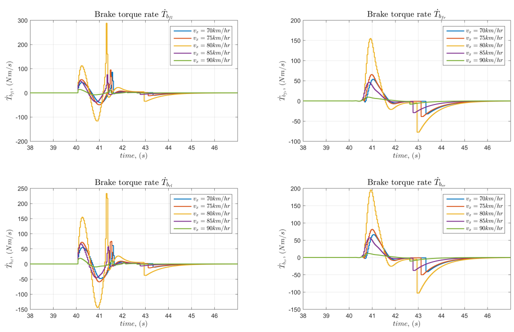

(h) Brake torque rates $\dot{T}_b$

Simulation result for Set 1 - Case 2: $\mu = 0.6$

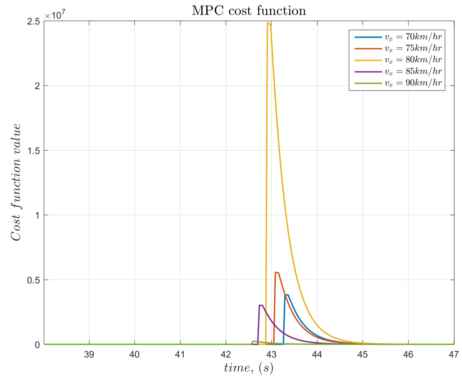

(i) Cost function value

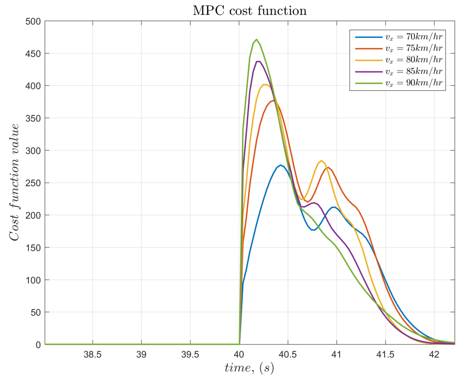

(j) Cost function value

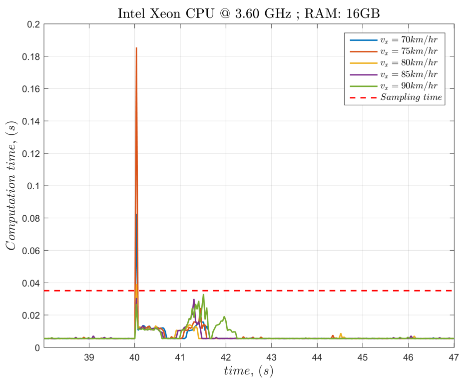

(k) Computation time

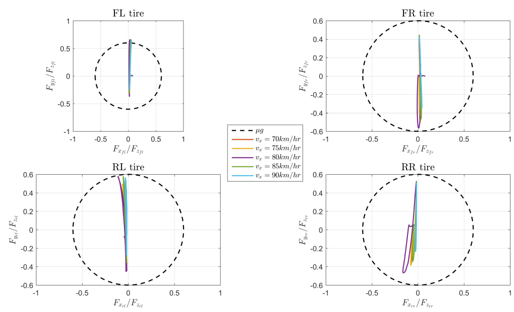

(l) Kamm Circle

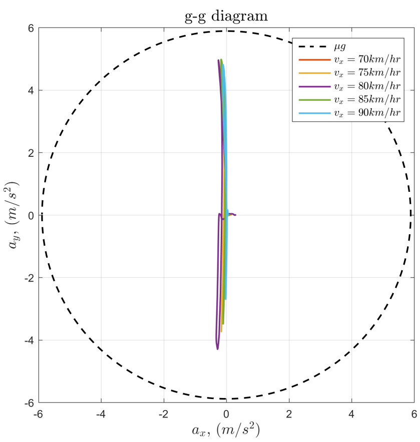

(m) g-g diagram

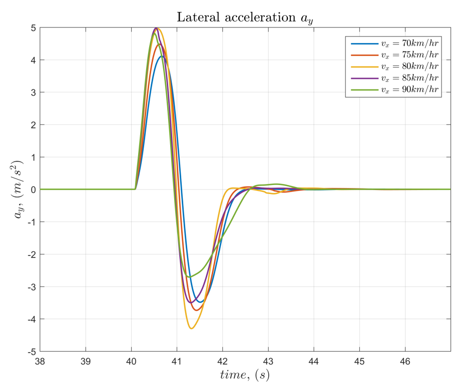

(n) Lateral acc. a_y

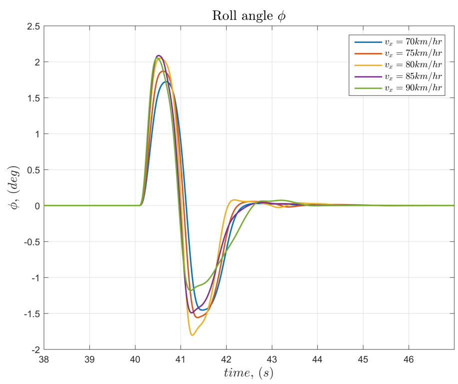

(o) Roll angle ϕ

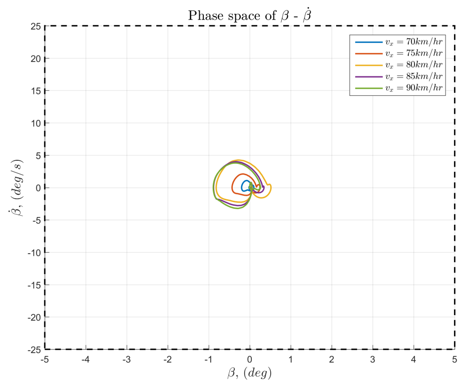

(p) β - $\dot{\beta}$ phase space

Figure C.2: Simulation result for Set 1 - Case 2: $\mu = 0.6$

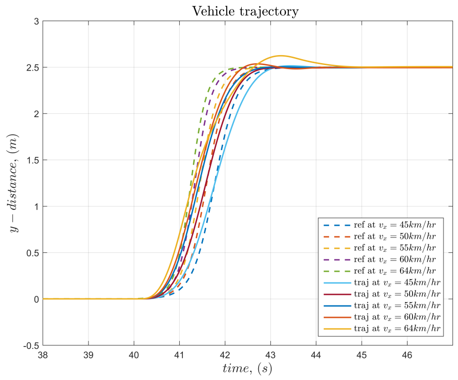

(a) Lateral position y_p

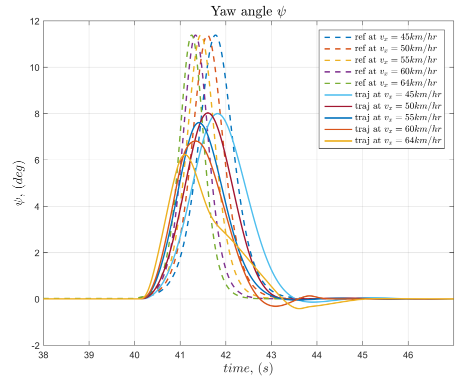

(b) Yaw angle ψ

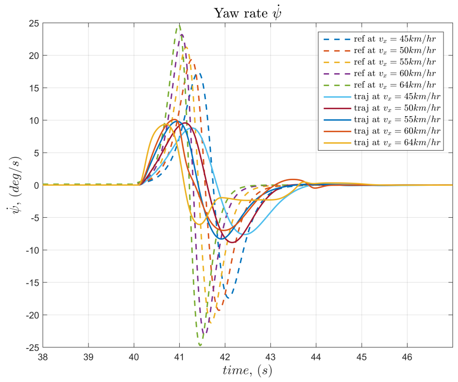

(c) Yaw rate $\dot{\psi}$

S No.	v_x	M_p	T_s	T_r	y_{RMS}	ψ_{RMS}	$\dot{\psi}_{RMS}$	DTC
-	[km/hr]	[%]	[s]	[s]	[%]	[%]	[%]	[m]
1	45	1.46	3.72	0.93	6.06	87.21	318.16	0.58
2	50	0.13	2.76	0.85	5.87	78.25	325.87	0.60
3	55	0.35	2.73	0.87	6.98	85.45	364.09	0.54
4	60	3.53	3.84	0.80	8.76	102.46	460.61	0.42
5	64	12.32	4.57	1.11	14.45	127.68	496.68	0.23

(d) KPI table

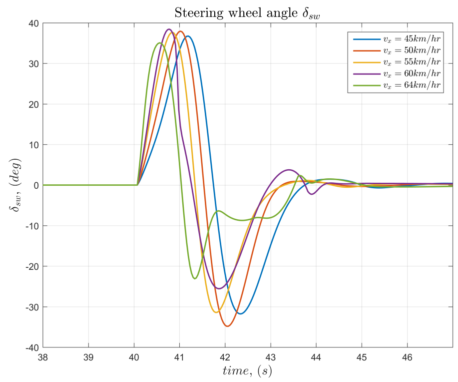

(e) SWA δ_{sw}

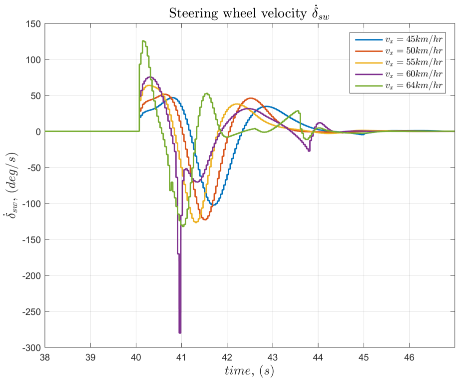

(f) SWV $\dot{\delta}_{\text{sw}}$

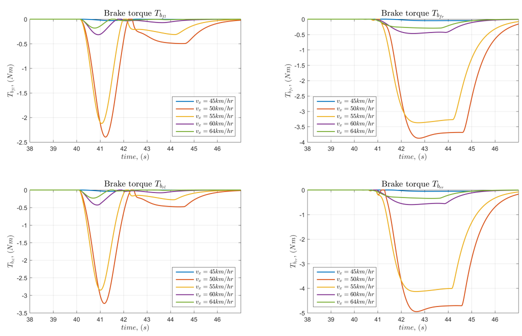

(g) Brake Torques T_b

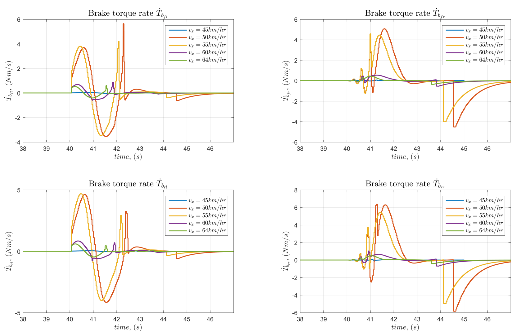

(h) Brake torque rates $\dot{T}_b$

Simulation result for Set 1 - Case 3: $\mu = 0.3$

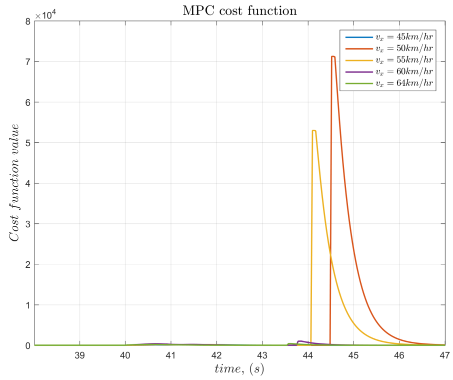

(i) Cost function value

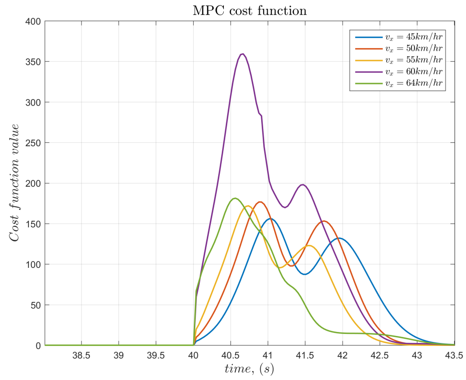

(j) Cost function value

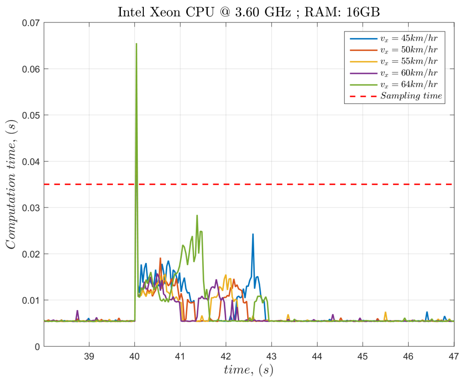

(k) Computation time

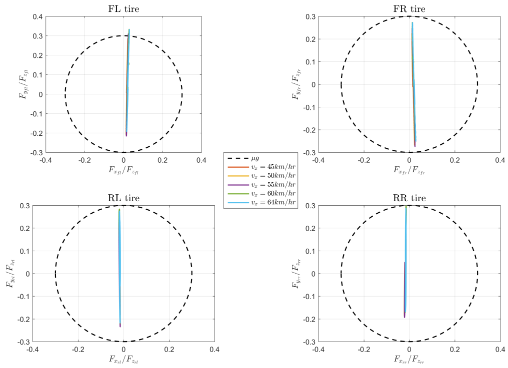

(l) Kamm Circle

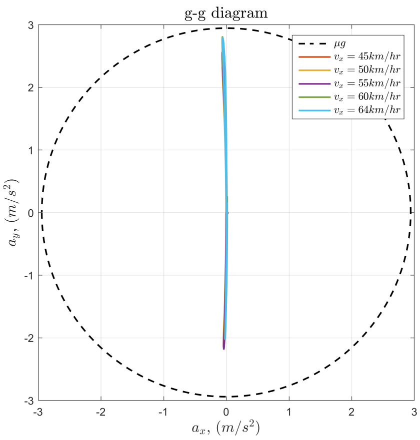

(m) g-g diagram

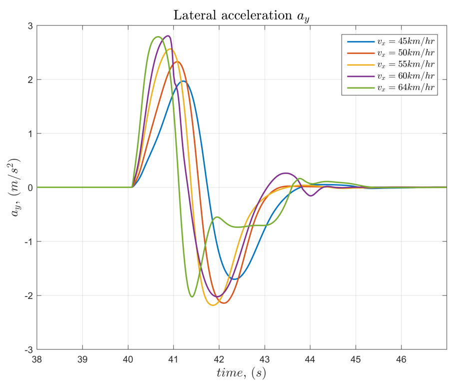

(n) Lateral acc. a_y

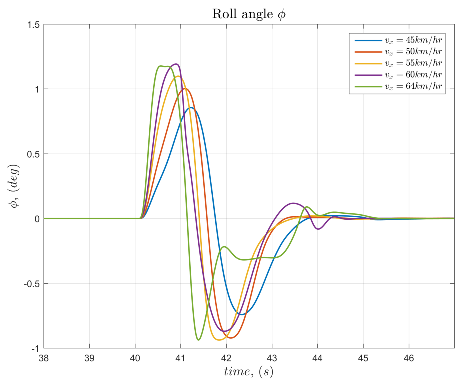

(o) Roll angle ϕ

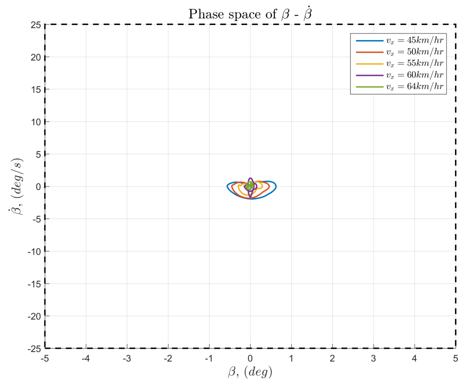

(p) β - $\dot{\beta}$ phase space

Figure C.3: Simulation result for Set 1 - Case 3: $\mu = 0.3$

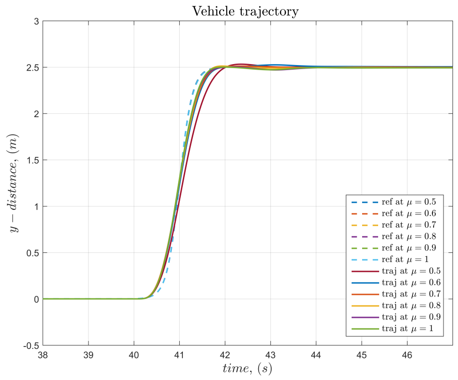

(a) Lateral position y_p

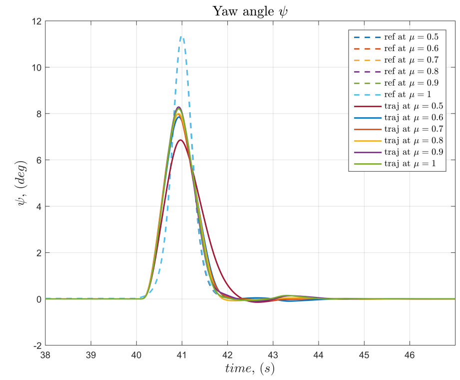

(b) Yaw angle ψ

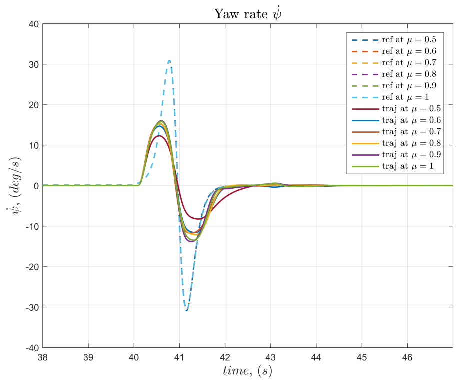

(c) Yaw rate $\dot{\psi}$

S No.	μ	M_p	T_s	T_r	y_{RMS}	ψ_{RMS}	$\dot{\psi}_{RMS}$	DTC
-	-	[%]	[s]	[s]	[%]	[%]	[%]	[m]
1	0.5	3.20	2.88	0.68	10.13	89.51	511.44	0.31
2	0.6	2.51	3.88	0.59	6.09	73.82	449.05	0.51
3	0.7	1.10	2.58	0.58	5.68	75.49	444.10	0.55
4	0.8	1.24	3.37	0.55	5.31	72.30	440.86	0.57
5	0.9	0.29	3.77	0.55	5.02	68.17	400.62	0.59
6	1	0.09	3.63	0.54	4.96	68.25	412.86	0.60

(d) KPI table

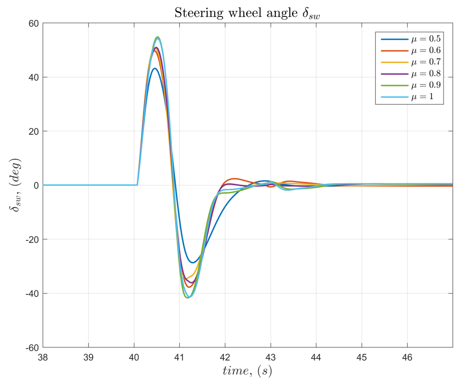

(e) SWA δ_{sw}

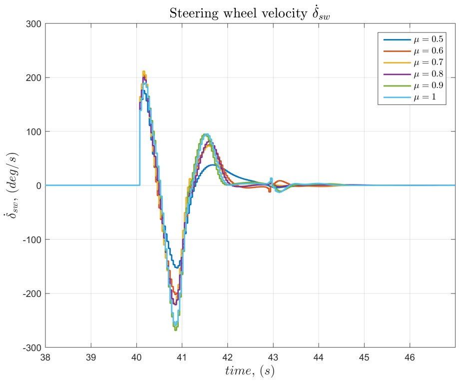

(f) SWV $\dot{\delta}_{sw}$

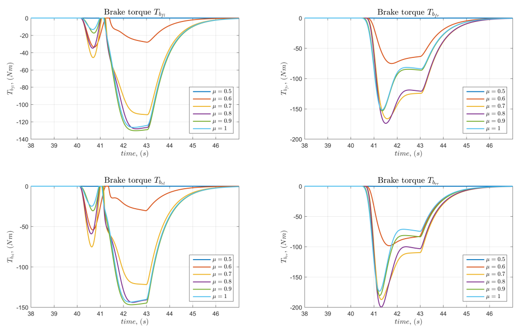

(g) Brake Torques T_b

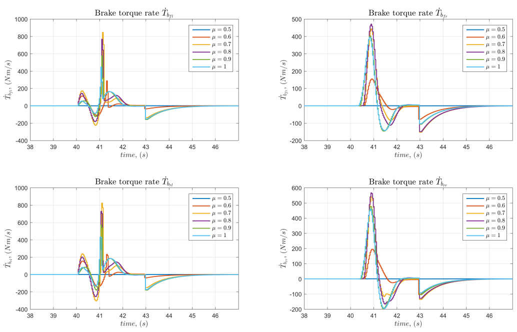

(h) Brake torque rates $\dot{T}_b$

Simulation result for Set 2 - Case 1: $v_x = 80 km/hr$

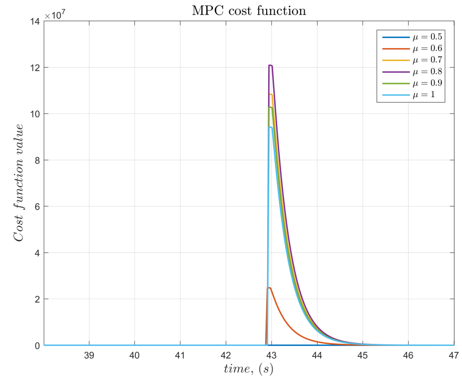

(i) Cost function value

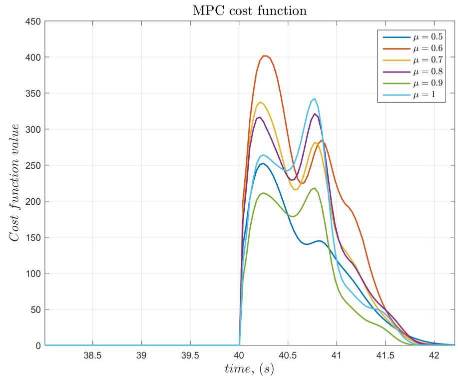

(j) Cost function value

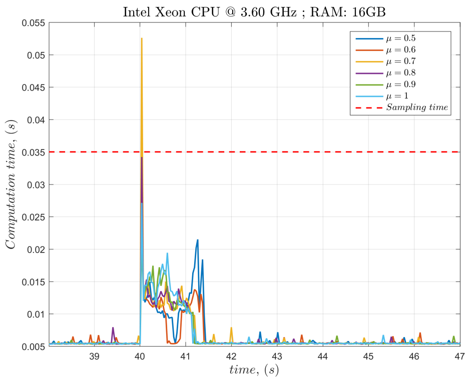

(k) Computation time

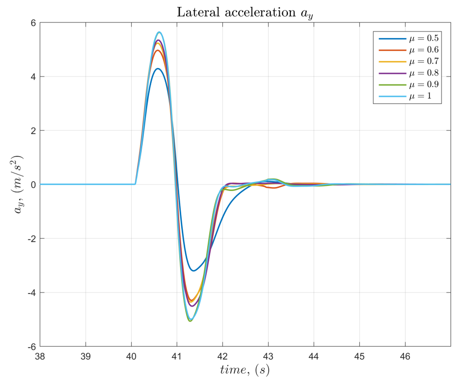

(l) Lateral acc. a_y

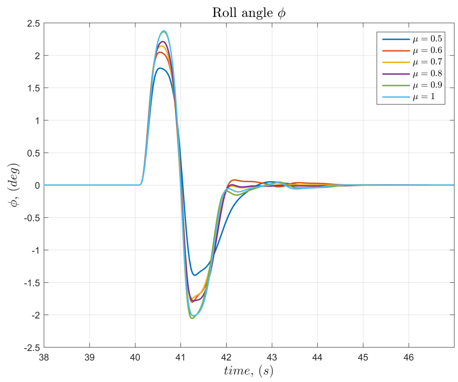

(m) Roll angle ϕ

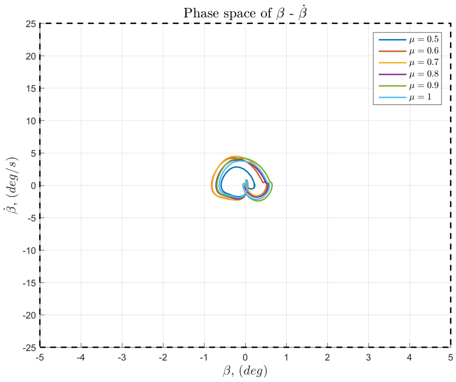

(n) β - $\dot{\beta}$ phase space

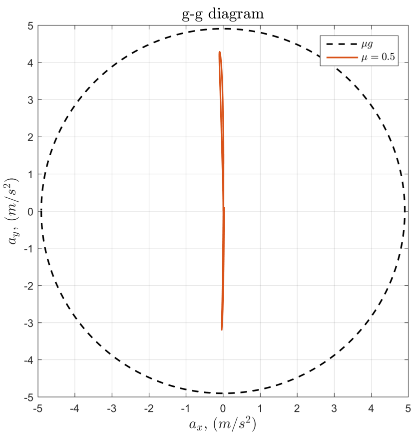

(o) g-g diagram: $\mu = 0.5$

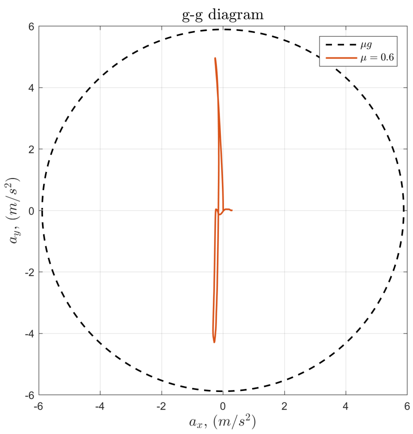

(p) g-g diagram: $\mu = 0.6$

Simulation result for Set 2 - Case 1: $v_x = 80 km/hr$

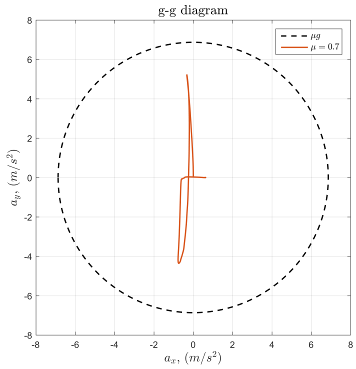

(q) g-g diagram: $\mu = 0.7$

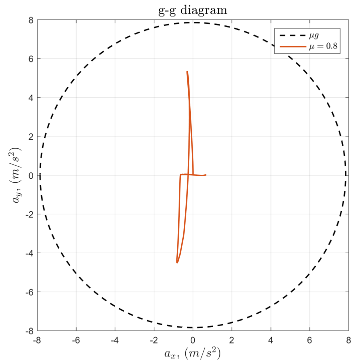

(r) g-g diagram: $\mu = 0.8$

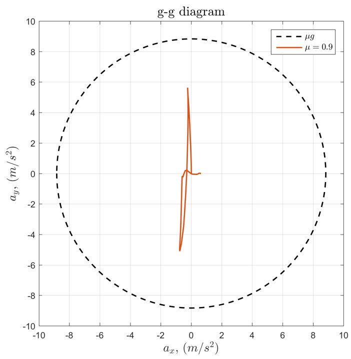

(s) g-g diagram: $\mu = 0.9$

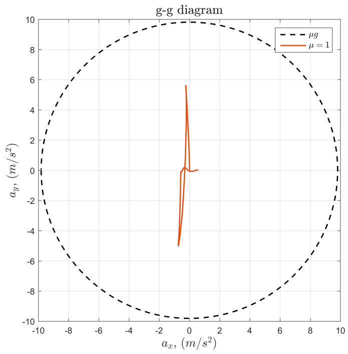

(t) g-g diagram: $\mu = 1$

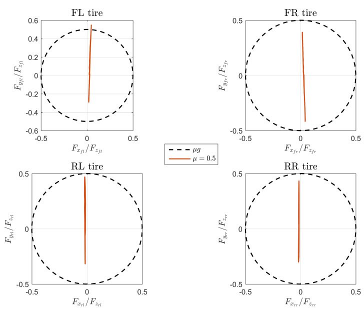

(u) Kamm circle: $\mu = 0.5$

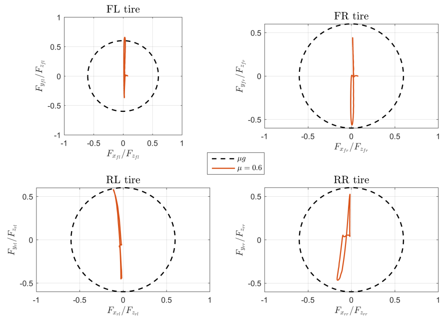

(v) Kamm circle: $\mu = 0.6$

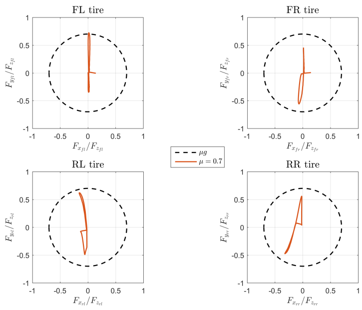

(w) Kamm circle: $\mu = 0.7$

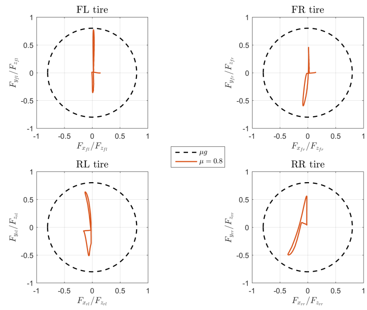

(x) Kamm circle: $\mu = 0.8$

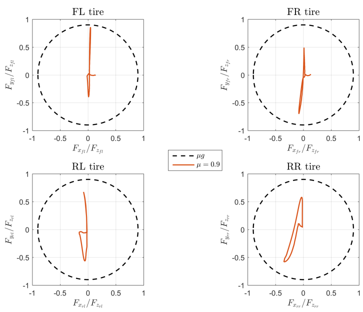

(y) Kamm circle: $\mu = 0.9$

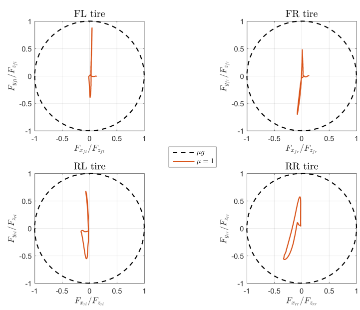

(z) Kamm circle: $\mu = 1$

Figure C.4: Simulation result for Set 2 - Case 1: $v_x = 80 km/hr$

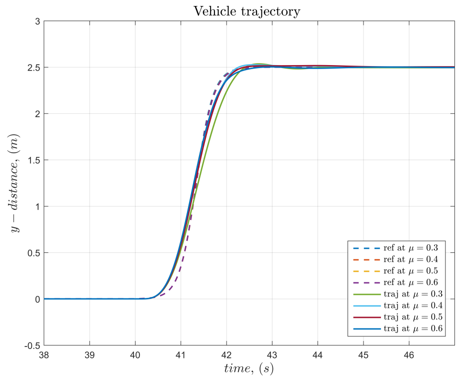

(a) Lateral position y_p

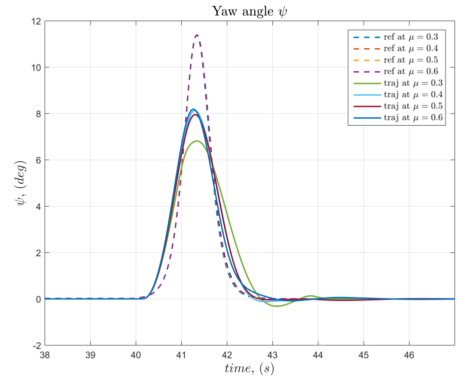

(b) Yaw angle ψ

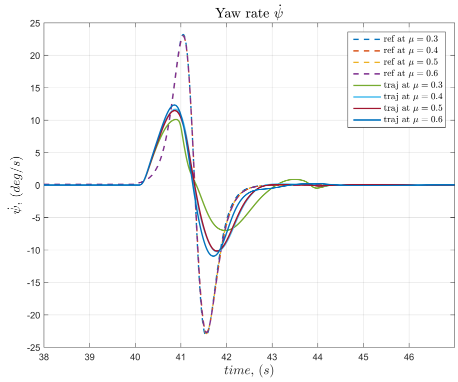

(c) Yaw rate $\dot{\psi}$

S No.	μ	M_p	T_s	T_r	y_{RMS}	ψ_{RMS}	$\dot{\psi}_{RMS}$	DTC
-	-	[%]	[s]	[s]	[%]	[%]	[%]	[m]
1	0.3	3.53	3.84	0.80	8.76	102.46	460.61	0.42
2	0.4	2.58	4.25	0.70	5.59	72.57	355.51	0.63
3	0.5	1.68	4.66	0.72	5.75	74.44	364.55	0.61
4	0.6	0.29	4.23	0.75	6.30	73.27	336.93	0.64

(d) KPI table

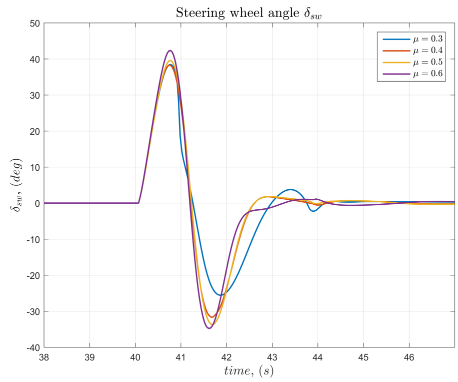

(e) SWA δ_{sw}

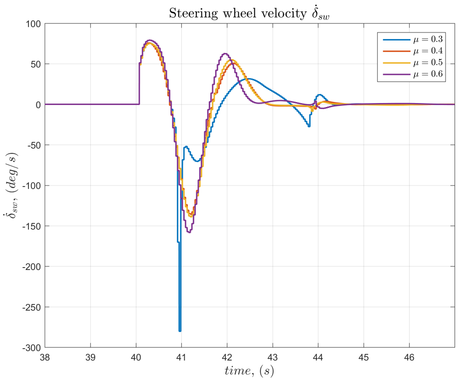

(f) SWV $\dot{\delta}_{\text{sw}}$

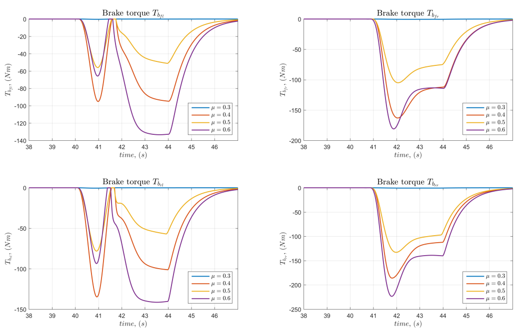

(g) Brake Torques T_b

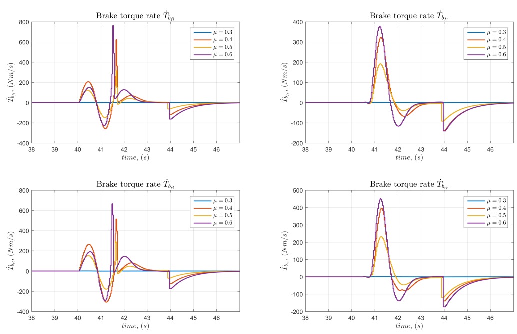

(h) Brake torque rates $\dot{T}_b$

Simulation result for Set 2 - Case 2: $v_x = 60 km/hr$

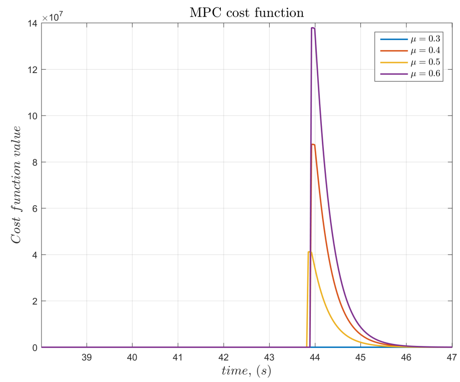

(i) Cost function value

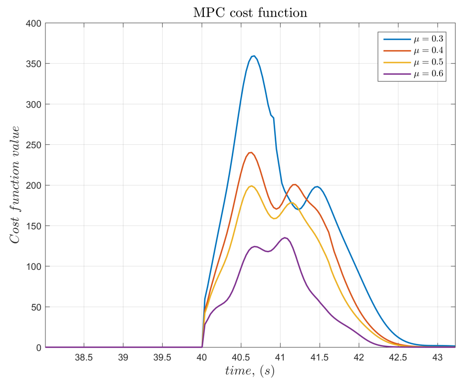

(j) Cost function value

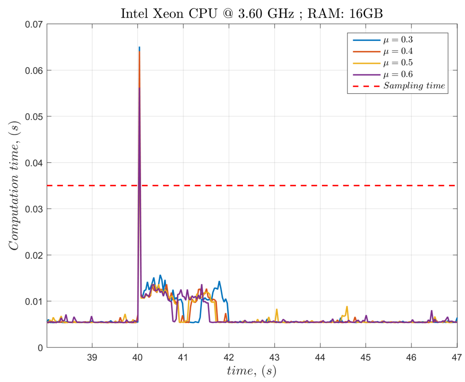

(k) Computation time

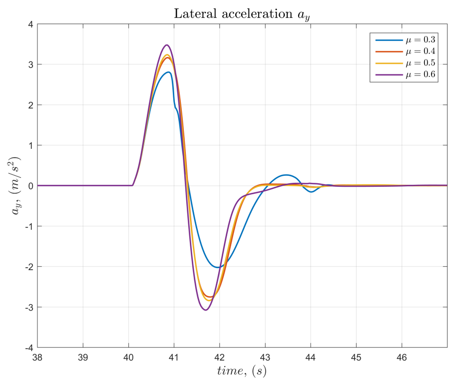

(l) Lateral acc. a_y

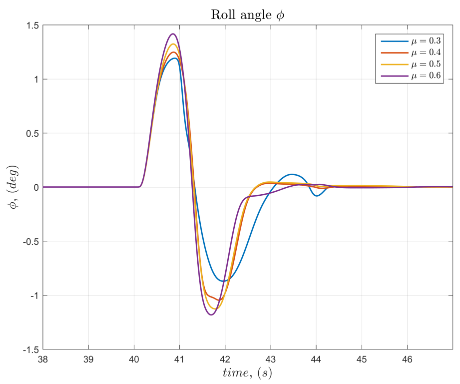

(m) Roll angle ϕ

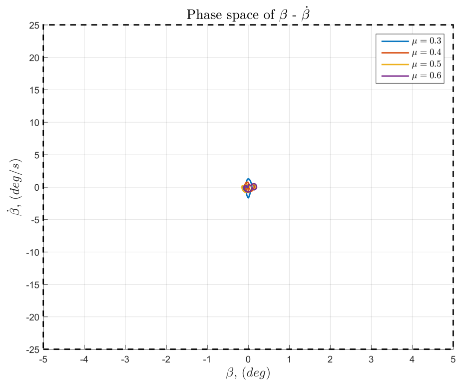

(n) β - $\dot{\beta}$ phase space

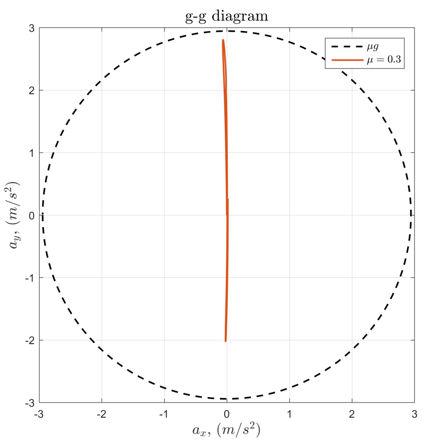

(o) g-g diagram: $\mu = 0.3$

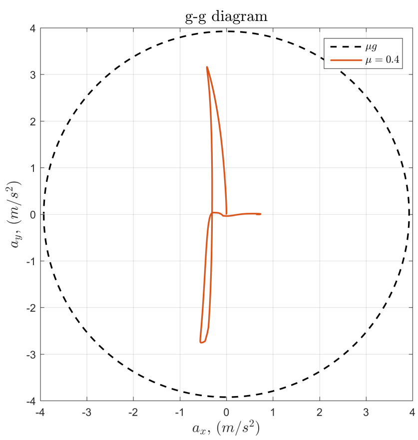

(p) g-g diagram: $\mu = 0.4$

Simulation result for Set 2 - Case 2: $v_x = 60 km/hr$

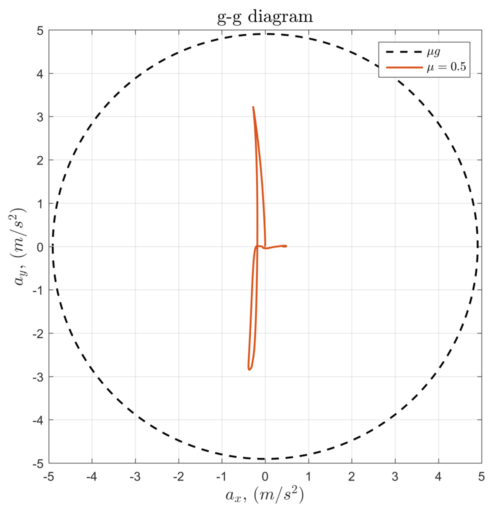

(q) g-g diagram: $\mu = 0.5$

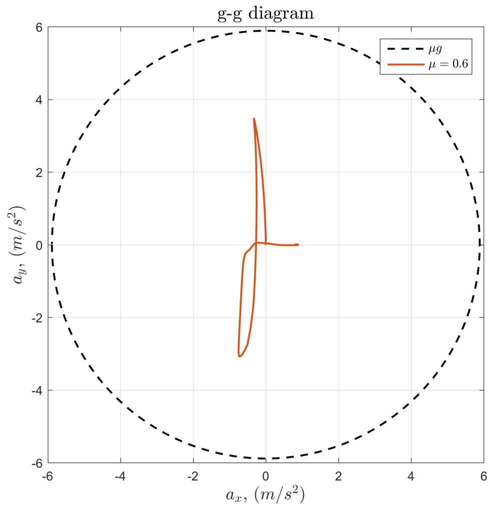

(r) g-g diagram: $\mu = 0.6$

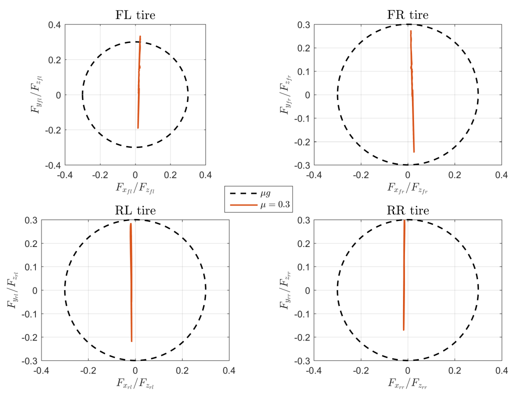

(s) Kamm circle: $\mu = 0.3$

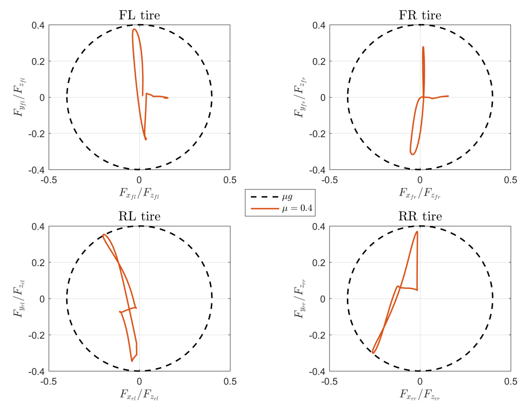

(t) Kamm circle: $\mu = 0.4$

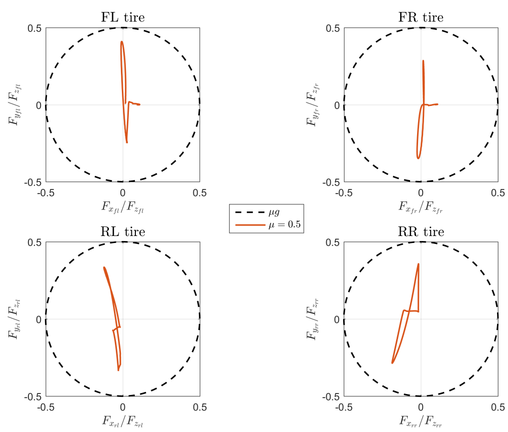

(u) Kamm circle: $\mu = 0.5$

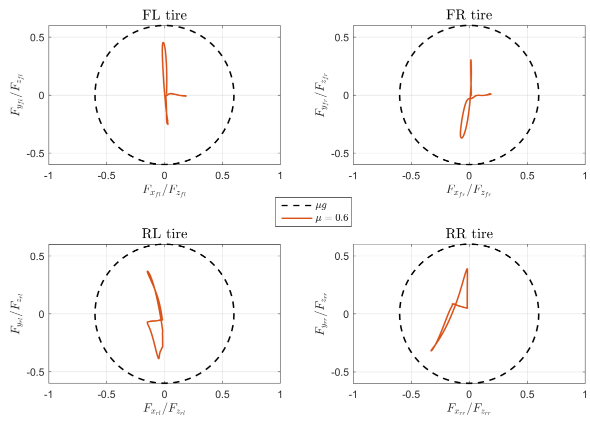

(v) Kamm circle: $\mu = 0.6$

Figure C.5: Simulation result for Set 2 - Case 2: $v_x = 60km/hr$

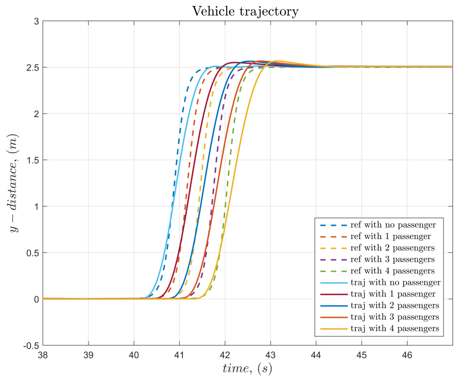

(a) Lateral position y_p

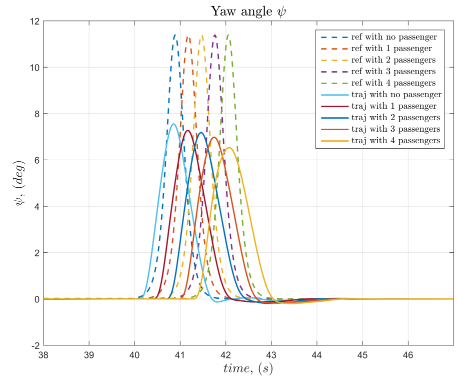

(b) Yaw angle ψ

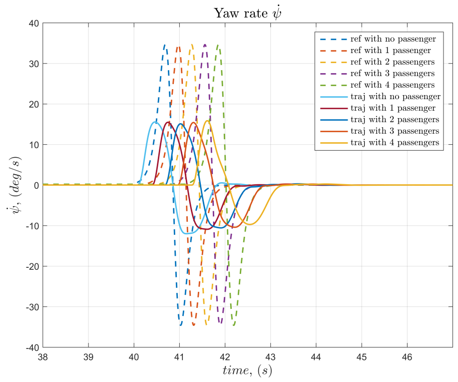

(c) Yaw rate $\dot{\psi}$

S No.	$F_{z_{\text{passenger}}}$	M_p	T_s	T_r	y_{RMS}	ψ_{RMS}	$\dot{\psi}_{\text{RMS}}$	DTC
-	[kg]	[%]	[s]	[s]	[%]	[%]	[%]	[m]
1	0	1.34	3.10	0.53	7.37	71.30	500.64	0.41
2	75	5.00	4.63	0.53	9.36	76.16	528.23	0.33
3	150	6.37	3.01	0.53	9.73	78.82	539.42	0.31
4	225	6.60	4.48	0.54	9.86	82.46	563.42	0.31
5	300	6.67	3.04	0.56	12.35	91.68	612.30	0.20

(d) KPI table

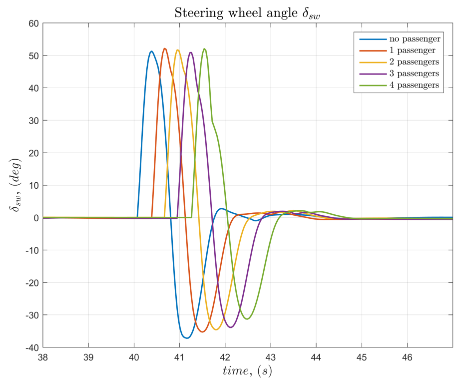

(e) SWA δ_{sw}

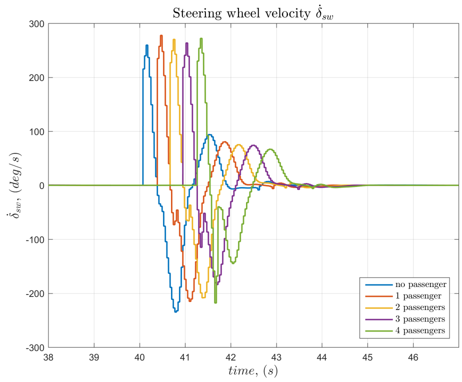

(f) SWV $\dot{\delta}_{\text{sw}}$

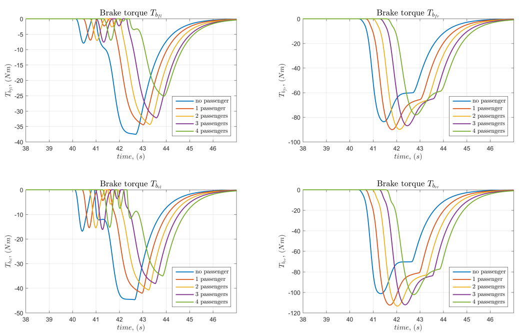

(g) Brake Torques T_b

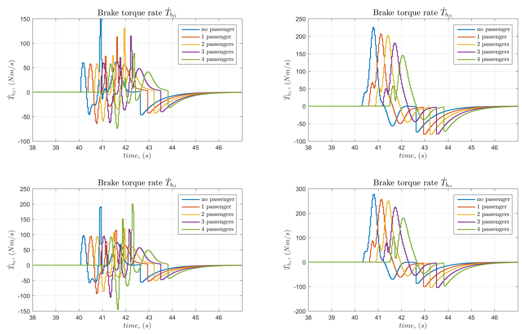

(h) Brake torque rates $\dot{T}_b$

Simulation result for Set 3 - Case 1: $\mu = 0.9$, $v_x = 90 km/hr$

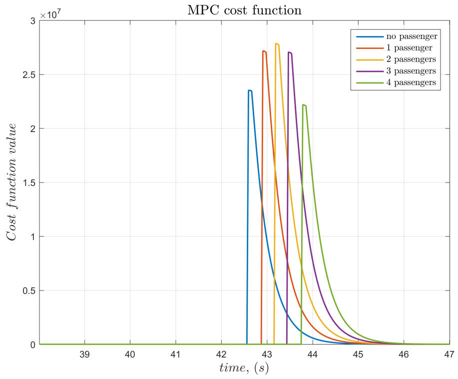

(i) Cost function value

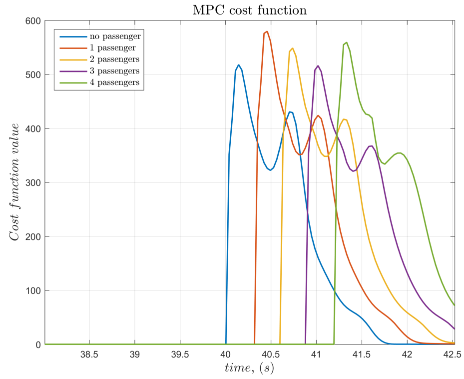

(j) Cost function value

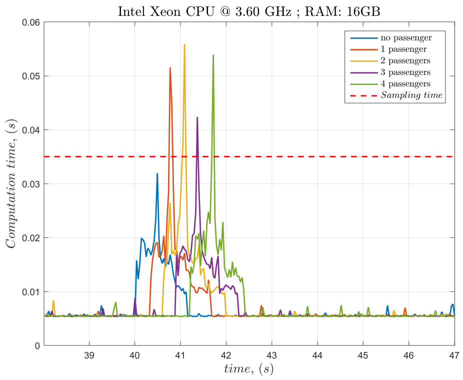

(k) Computation time

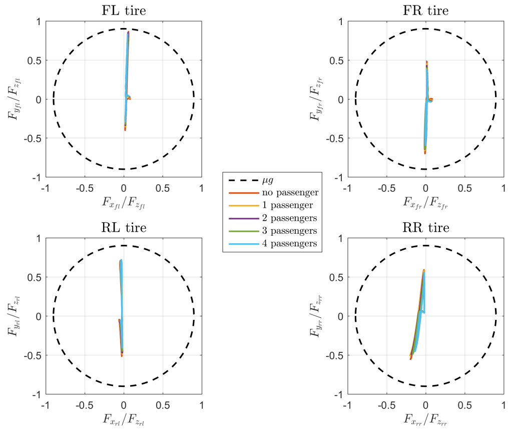

(l) Kamm Circle

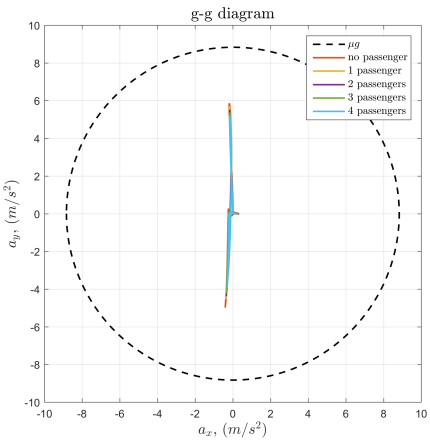

(m) g-g diagram

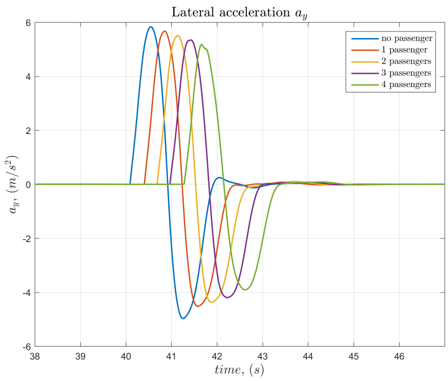

(n) Lateral acc. a_y

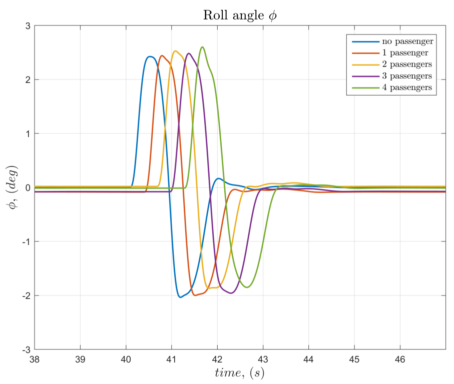

(o) Roll angle ϕ

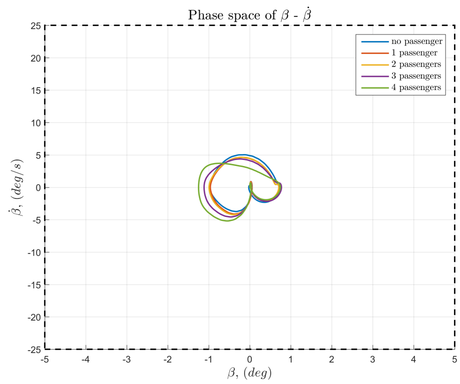

(p) β - $\dot{\beta}$ phase space

Figure C.6: Simulation result for Set 3 - Case 1: $\mu = 0.9$, $v_x = 90 km/hr$

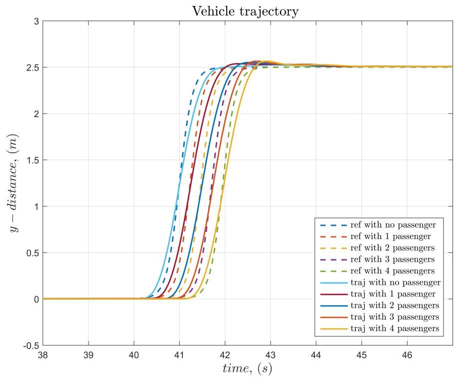

(a) Lateral position y_p

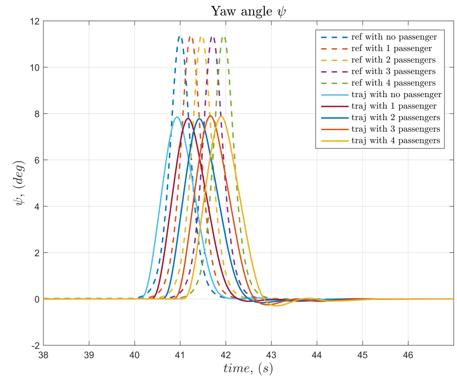

(b) Yaw angle ψ

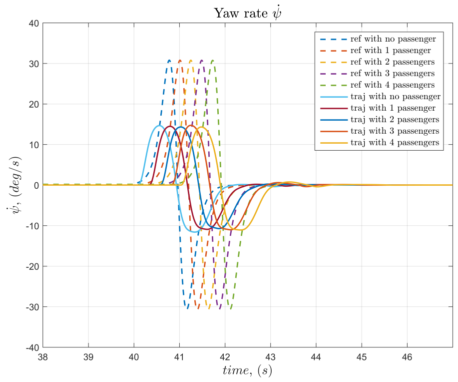

(c) Yaw rate $\dot{\psi}$

S No.	$F_{z_{\text{passenger}}}$	M_p	T_s	T_r	y_{RMS}	ψ_{RMS}	$\dot{\psi}_{\text{RMS}}$	DTC
-	[kg]	[%]	[s]	[s]	[%]	[%]	[%]	[m]
1	0	2.51	3.88	0.59	6.09	73.82	449.05	0.51
2	75	3.72	4.12	0.57	6.34	74.45	457.16	0.50
3	150	5.09	4.46	0.57	6.71	74.44	460.00	0.47
4	225	6.47	4.21	0.54	6.62	72.81	457.77	0.48
5	300	6.52	3.92	0.54	6.35	74.74	463.33	0.50

(d) KPI table

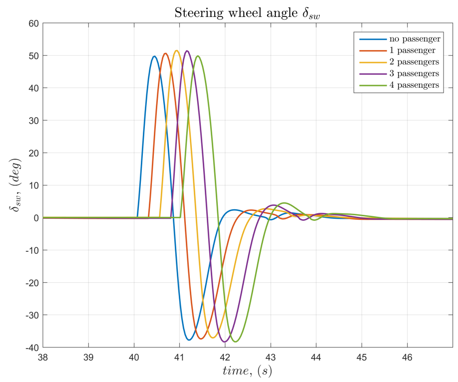

(e) SWA δ_{sw}

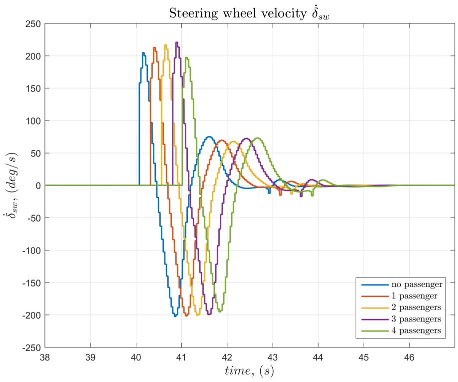

(f) SWV $\dot{\delta}_{\text{sw}}$

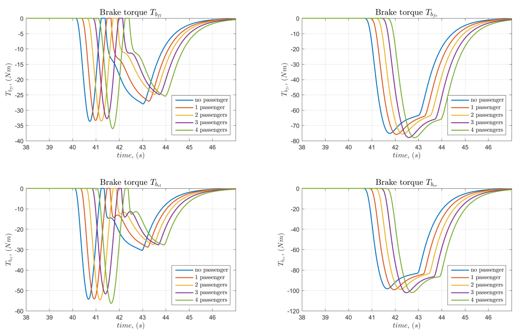

(g) Brake Torques T_b

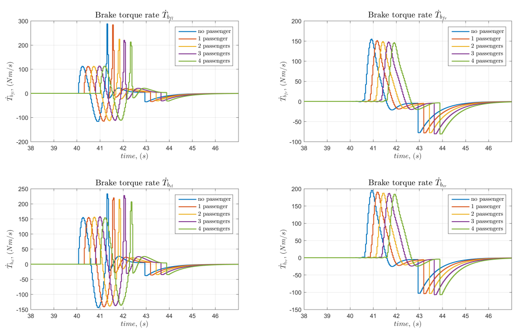

(h) Brake torque rates $\dot{T}_b$

Simulation result for Set 3 - Case 2: $\mu = 0.6$, $v_x = 80 km/hr$

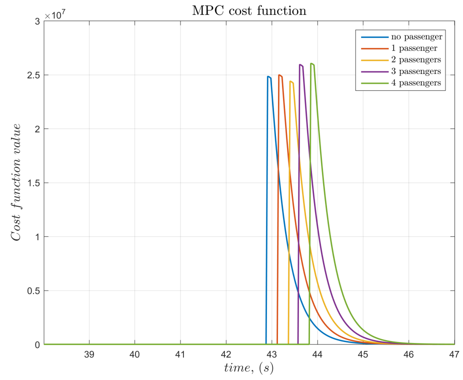

(i) Cost function value

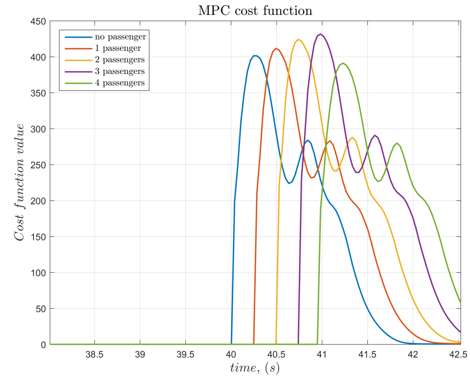

(j) Cost function value

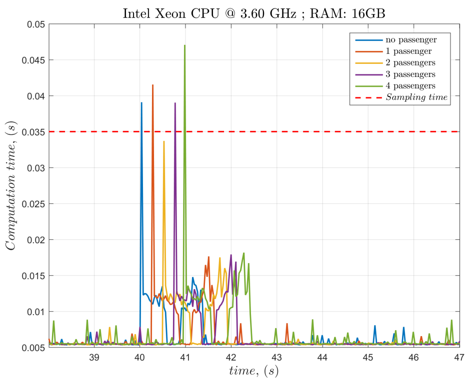

(k) Computation time

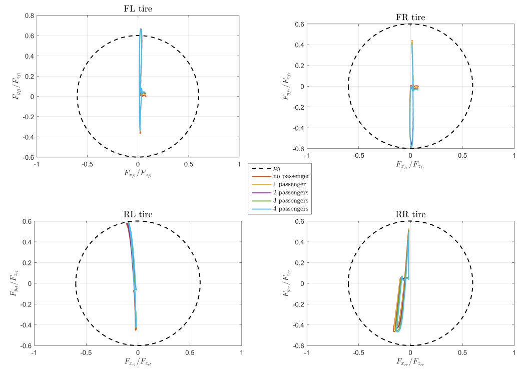

(l) Kamm Circle

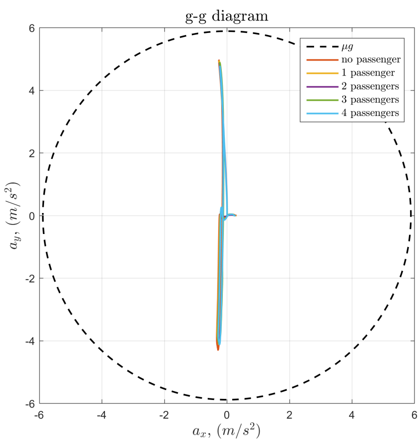

(m) g-g diagram

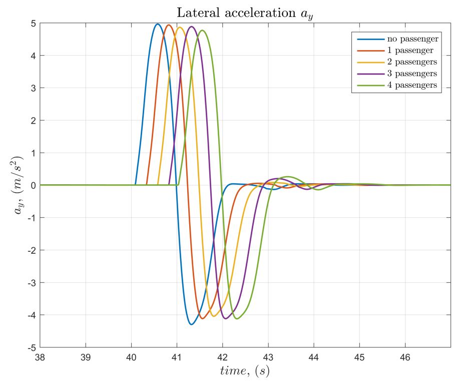

(n) Lateral acc. a_y

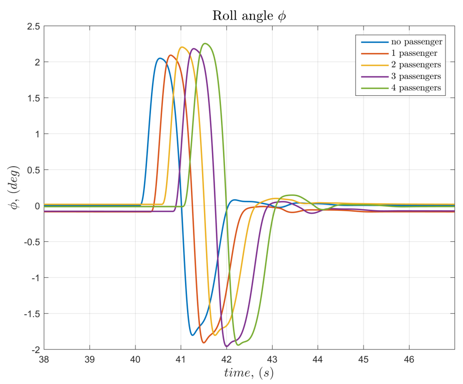

(o) Roll angle ϕ

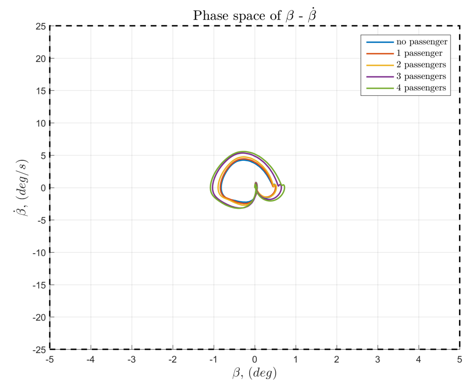

(p) β - $\dot{\beta}$ phase space

Figure C.7: Simulation result for Set 3 - Case 2: $\mu = 0.6$, $v_x = 80 km/hr$

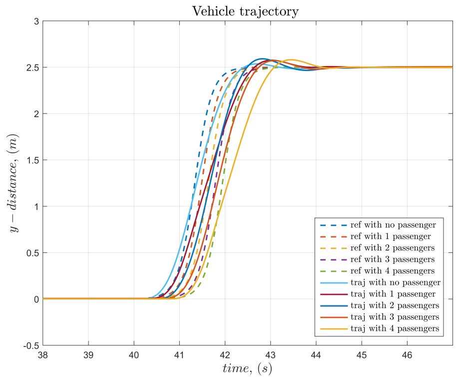

(a) Lateral position y_p

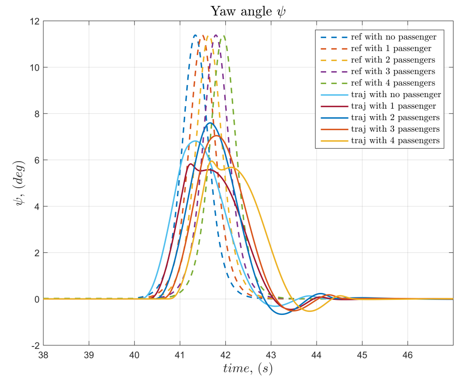

(b) Yaw angle ψ

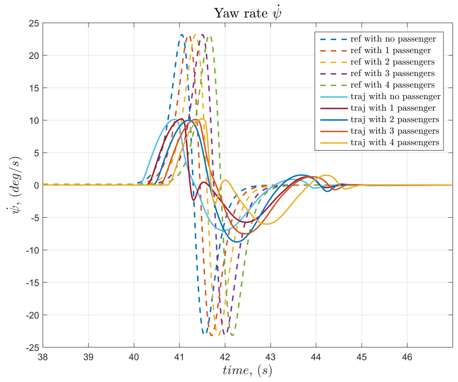

(c) Yaw rate $\dot{\psi}$

S No. -	$F_{z_{\text{passenger}}}$ [kg]	M_p [%]	T_s [s]	T_r [s]	$\mathrm{y}_{\mathrm{RMS}}$ [%]	ψ_{RMS} [%]	$\dot{\psi}_{\mathrm{RMS}}$ [%]	DTC [m]
1	0	3.53	3.84	0.80	8.76	102.46	460.61	0.42
2	75	7.48	3.50	0.88	13.57	135.58	562.74	0.23
3	150	9.03	3.98	0.68	7.01	91.16	428.69	0.52
4	225	7.07	3.86	0.74	8.32	99.68	454.20	0.44
5	300	8.01	3.77	0.86	13.71	134.33	564.74	0.22

(d) KPI table

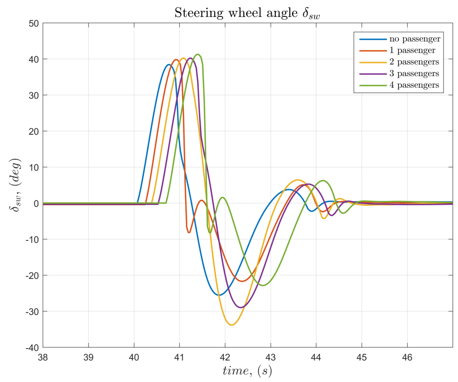

(e) SWA δ_{sw}

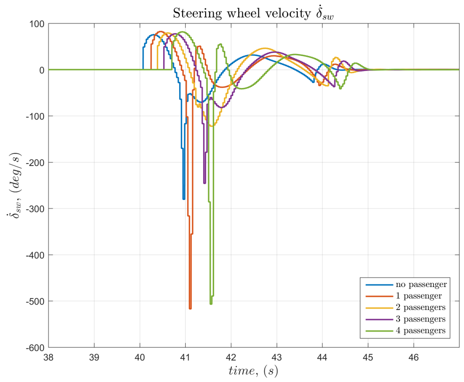

(f) SWV $\dot{\delta}_{\text{sw}}$

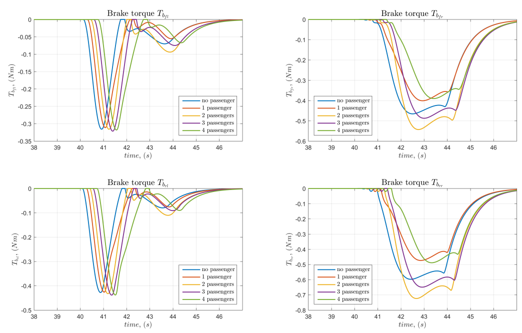

(g) Brake Torques T_b

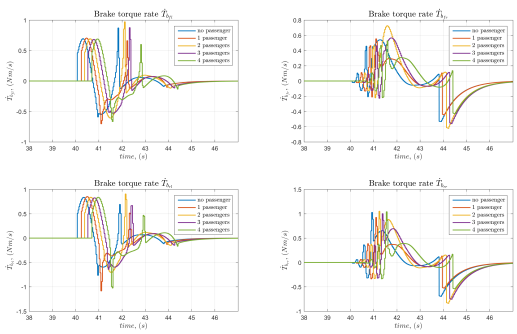

(h) Brake torque rates $\dot{T}_b$

Simulation result for Set 3 - Case 3: $\mu = 0.3$, $v_x = 60 km/hr$

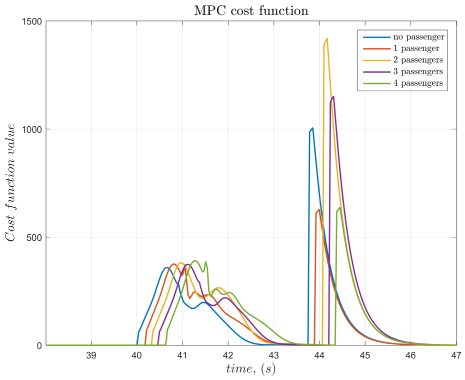

(i) Cost function value

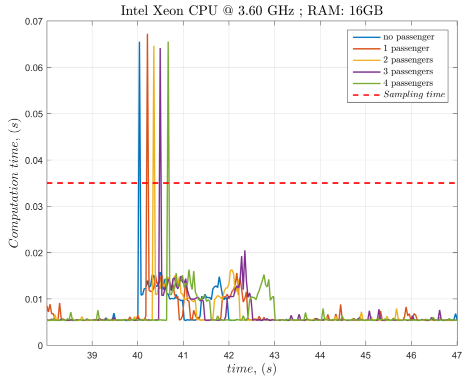

(j) Computation time

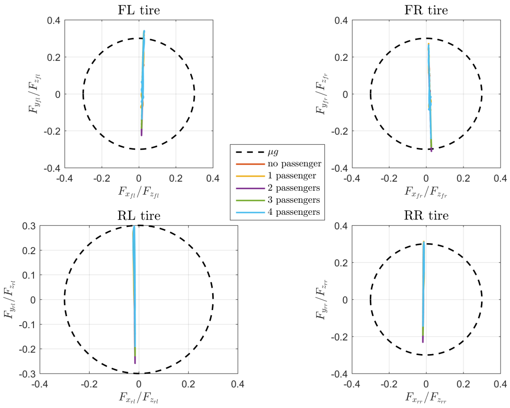

(k) Kamm Circle

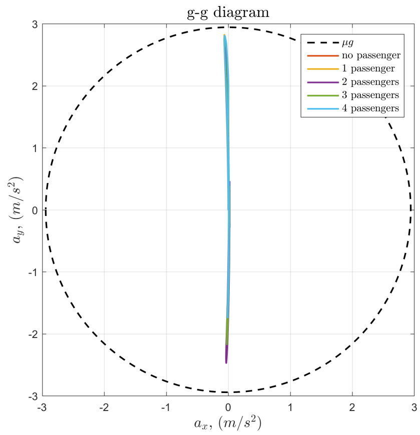

(l) g-g diagram

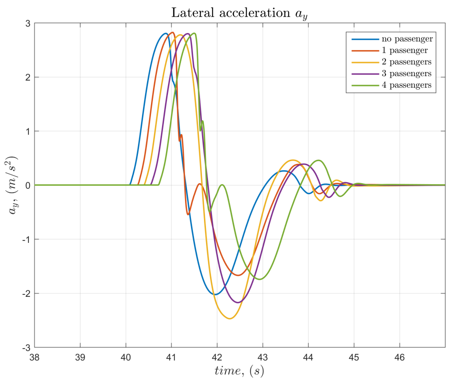

(m) Lateral acc. a_y

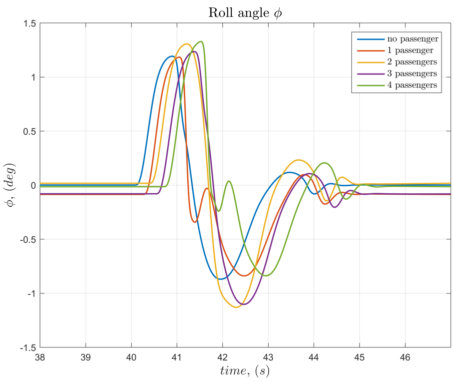

(n) Roll angle ϕ

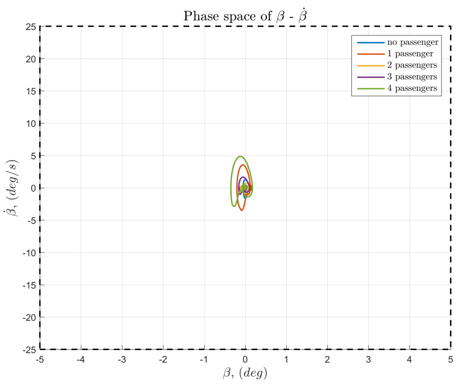

(o) β - $\dot{\beta}$ phase space

Figure C.8: Simulation result for Set 3 - Case 3: $\mu = 0.3$, $v_x = 60 km/hr$

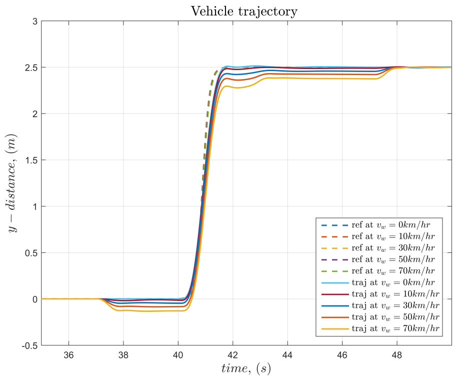

(a) Lateral position y_p

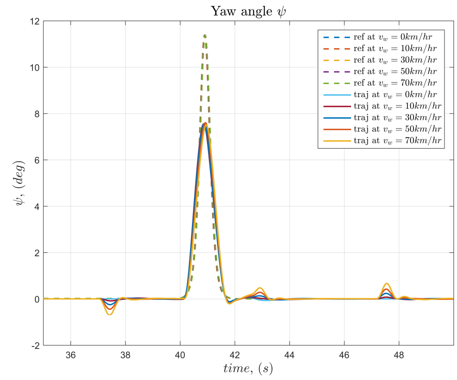

(b) Yaw angle ψ

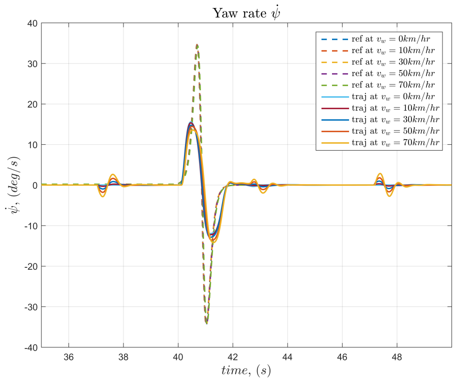

(c) Yaw rate $\dot{\psi}$

S No.	v_w	M_p	T_s	T_r	y_{RMS}	ψ_{RMS}	$\dot{\psi}_{RMS}$	DTC	D_{off}
-	[km/hr]	[%]	[s]	[s]	[%]	[%]	[%]	[m]	[m]
1	0	1.34	3.10	0.53	5.71	55.24	387.90	0.41	0.00
2	10	0.29	7.34	0.54	6.12	54.70	386.41	0.39	0.01
3	30	0.08	7.72	0.58	7.75	53.94	384.16	0.35	0.04
4	50	0.18	7.83	0.64	11.22	53.45	394.12	0.26	0.08
5	70	0.11	8.06	1.95	15.21	56.21	411.01	0.18	0.12

(d) KPI table

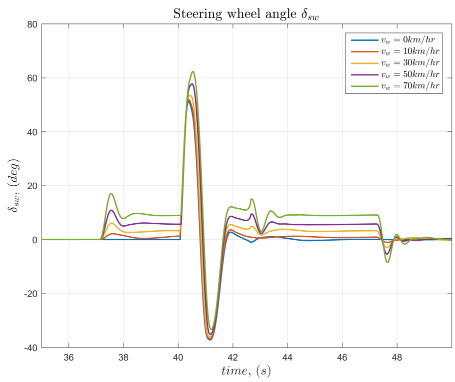

(e) SWA δ_{sw}

(f) SWV $\dot{\delta}_{\text{sw}}$

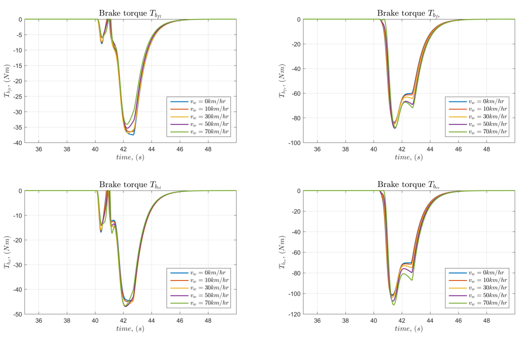

(g) Brake Torques T_b

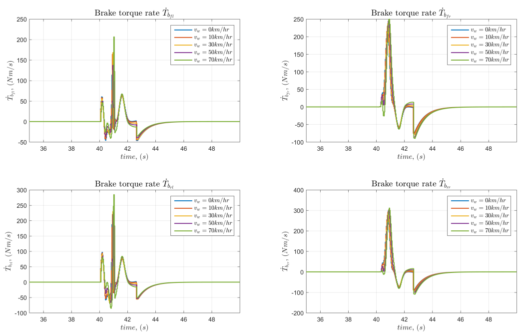

(h) Brake torque rates $\dot{T}_b$

Simulation result for Set 4 - Case 1: $\mu = 0.9$, $v_x = 90km/hr$

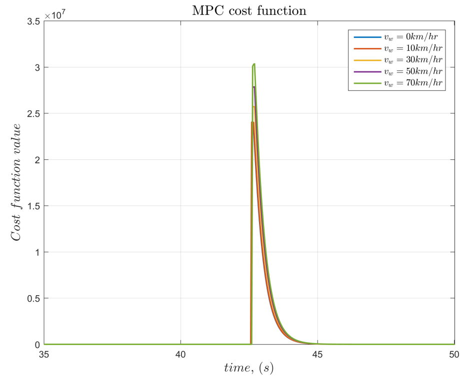

(i) Cost function value

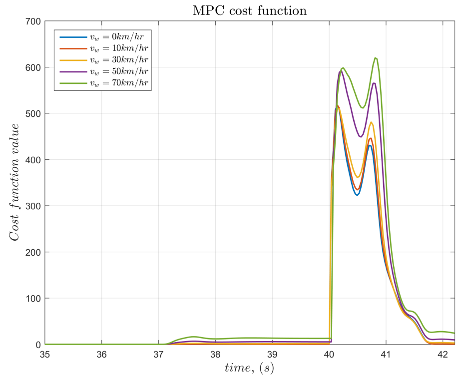

(j) Cost function value

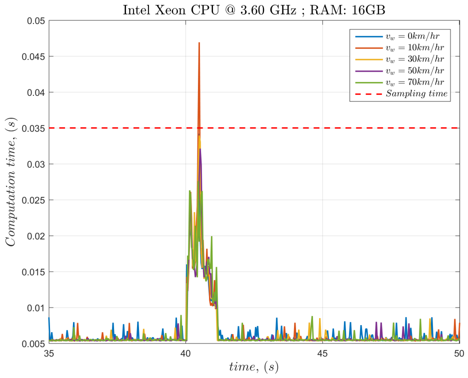

(k) Computation time

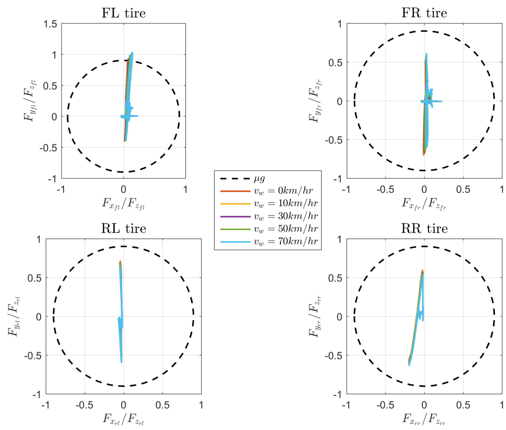

(l) Kamm Circle

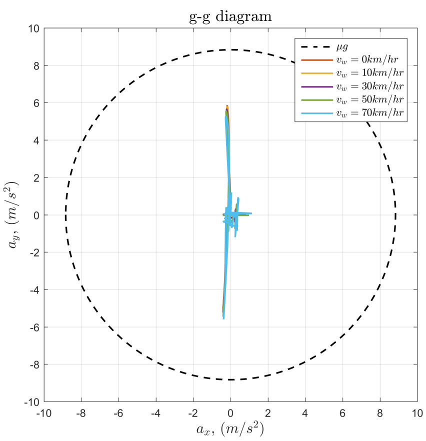

(m) g-g diagram

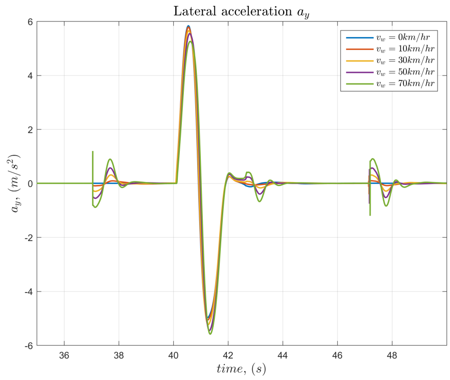

(n) Lateral acc. a_y

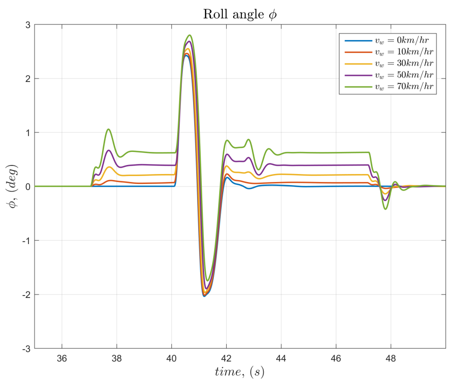

(o) Roll angle ϕ

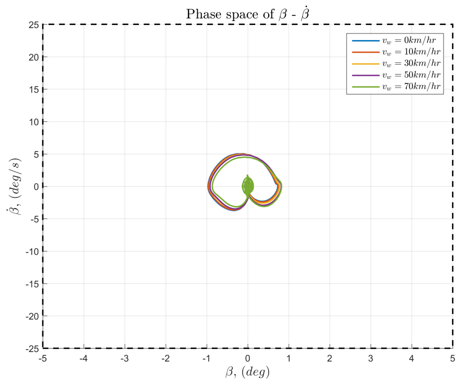

(p) β - $\dot{\beta}$ phase space

Figure C.9: Simulation result for Set 4 - Case 1: $\mu = 0.9$, $v_x = 90km/hr$

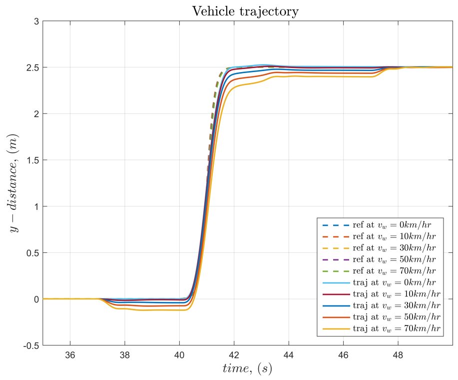

(a) Lateral position y_p

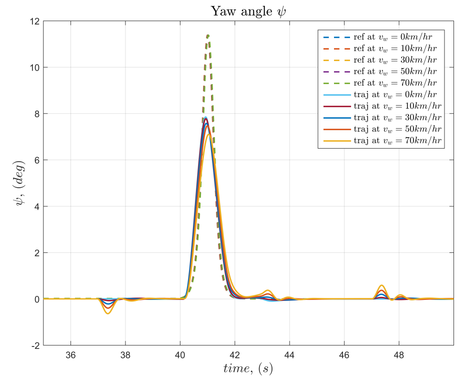

(b) Yaw angle ψ

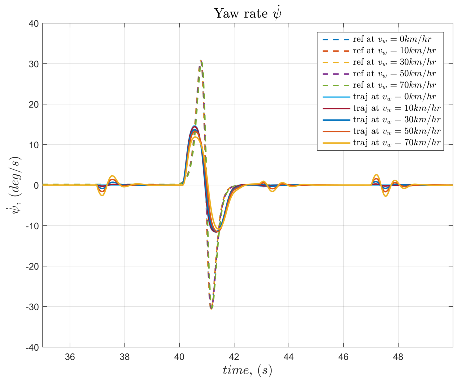

(c) Yaw rate $\dot{\psi}$

S No.	v_w	M_p	T_s	T_r	y_{RMS}	ψ_{RMS}	$\dot{\psi}_{RMS}$	DTC	D_{off}
-	[km/hr]	[%]	[s]	[s]	[%]	[%]	[%]	[m]	[m]
1	0	2.51	3.88	0.59	4.72	57.19	347.92	0.51	0.00
2	10	0.89	2.44	0.61	5.03	57.30	349.36	0.48	0.01
3	30	0.29	7.51	0.68	6.64	58.47	355.43	0.42	0.03
4	50	0.03	7.99	0.84	9.80	58.00	359.60	0.32	0.06
5	70	0.30	8.10	1.90	14.22	63.98	384.29	0.20	0.10

(d) KPI table

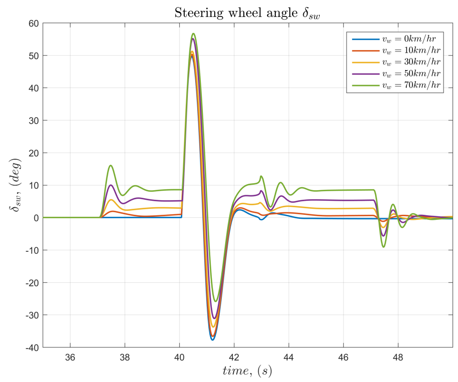

(e) SWA δ_{sw}

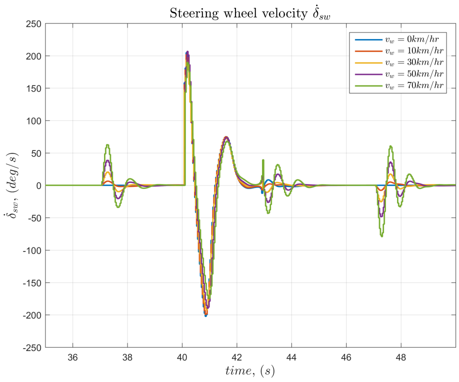

(f) SWV $\dot{\delta}_{\text{sw}}$

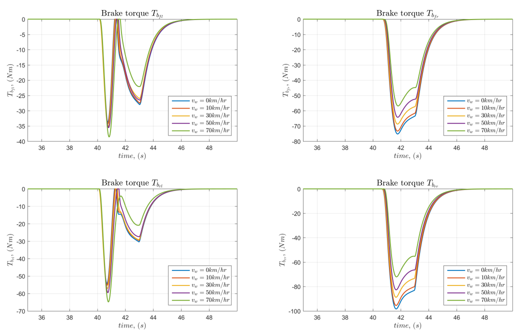

(g) Brake Torques T_b

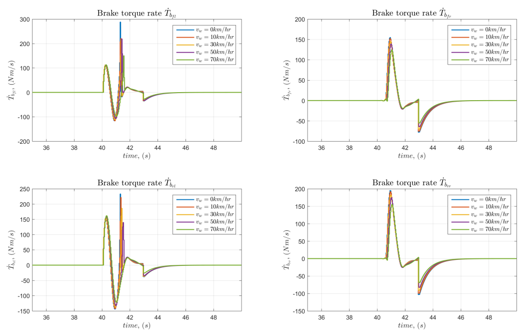

(h) Brake torque rates $\dot{T}_b$

Simulation result for Set 4 - Case 2: $\mu = 0.6$, $v_x = 80 km/hr$

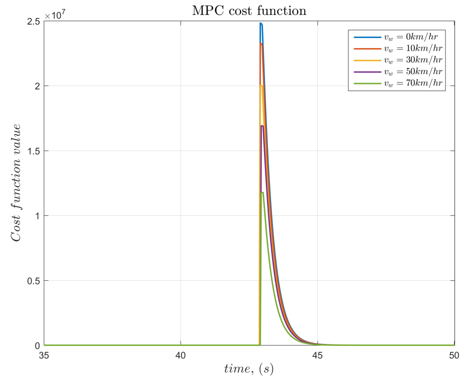

(i) Cost function value

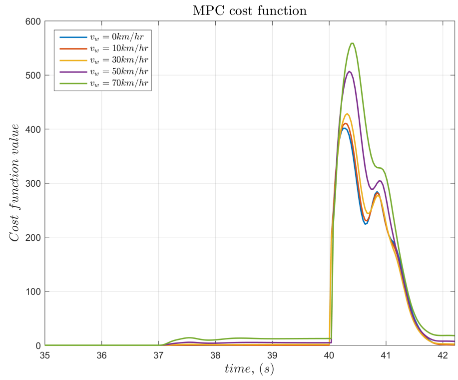

(j) Cost function value

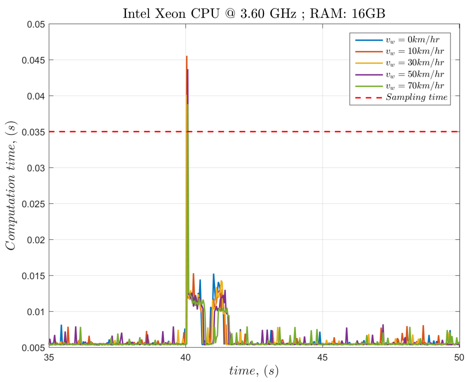

(k) Computation time

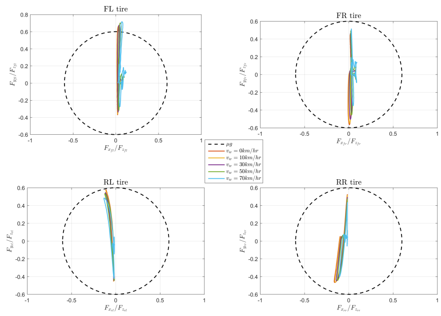

(l) Kamm Circle

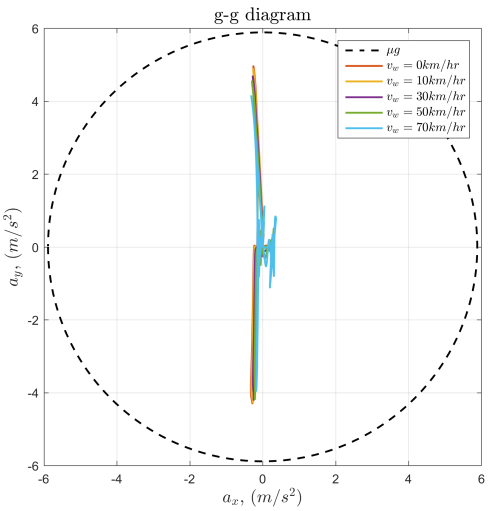

(m) g-g diagram

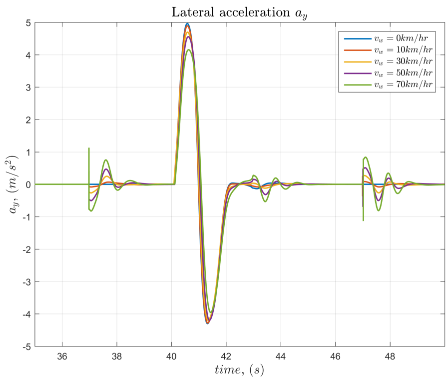

(n) Lateral acc. a_y

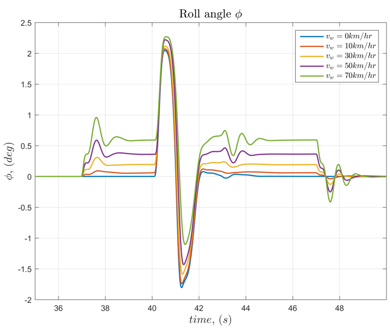

(o) Roll angle ϕ

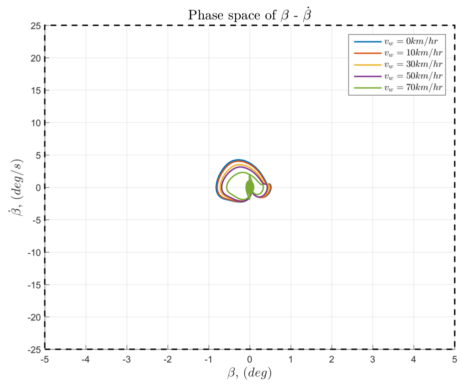

(p) β - $\dot{\beta}$ phase space

Figure C.10: Simulation result for Set 4 - Case 2: $\mu = 0.6$, $v_x = 80km/hr$

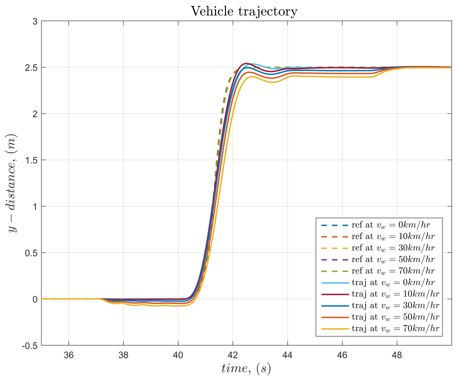

(a) Lateral position y_p

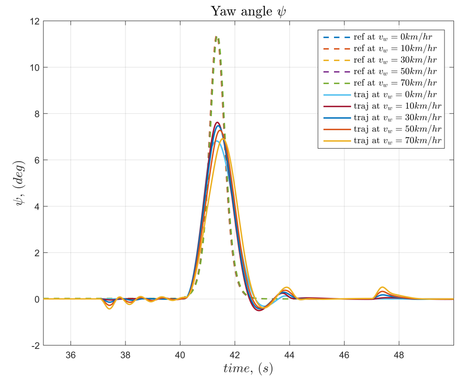

(b) Yaw angle ψ

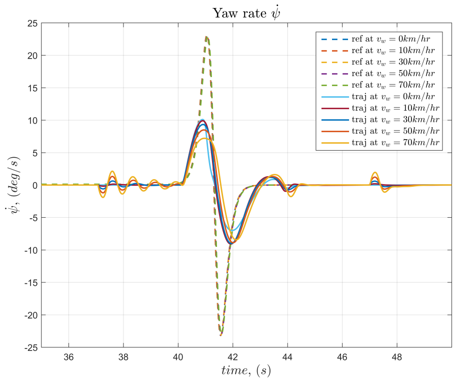

(c) Yaw rate $\dot{\psi}$

S No.	v_w	M_p	T_s	T_r	y_{RMS}	ψ_{RMS}	$\dot{\psi}_{RMS}$	DTC	D_{off}
-	[km/hr]	[%]	[s]	[s]	[%]	[%]	[%]	[m]	[m]
1	0	3.53	3.84	0.80	6.79	79.37	356.83	0.42	0.00
2	10	3.99	4.85	0.70	5.25	67.43	323.03	0.52	0.01
3	30	0.00	7.70	0.74	6.65	70.42	332.08	0.46	0.04
4	50	0.00	8.03	0.80	9.73	78.30	355.91	0.35	0.07
5	70	0.00	8.22	0.90	14.60	95.44	403.67	0.18	0.11

(d) KPI table

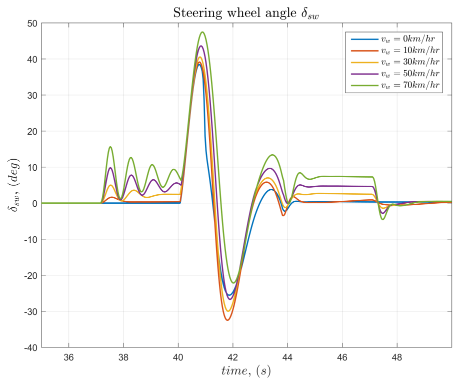

(e) SWA δ_{sw}

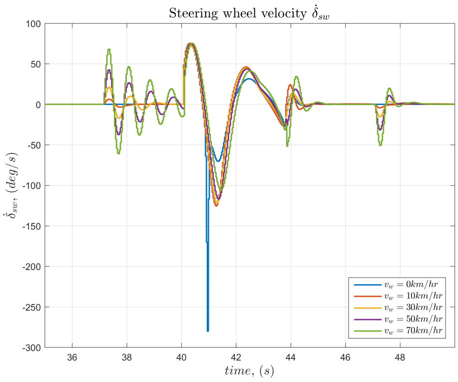

(f) SWV $\dot{\delta}_{\mathrm{sw}}$

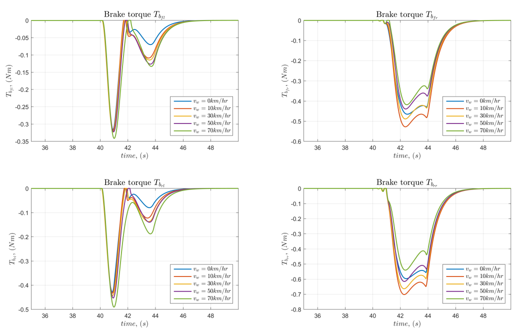

(g) Brake Torques T_b

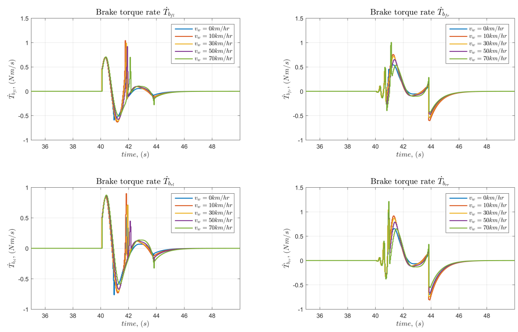

(h) Brake torque rates $\dot{T}_b$

Simulation result for Set 4 - Case 3: $\mu = 0.3$, $v_x = 60 km/hr$

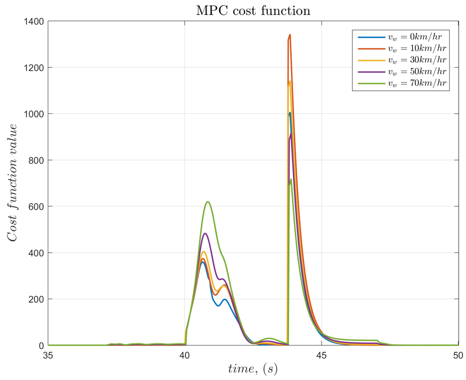

(i) Cost function value

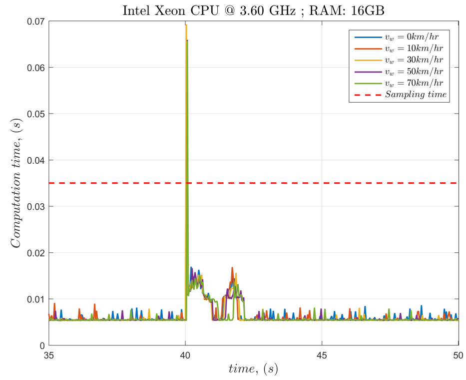

(j) Computation time

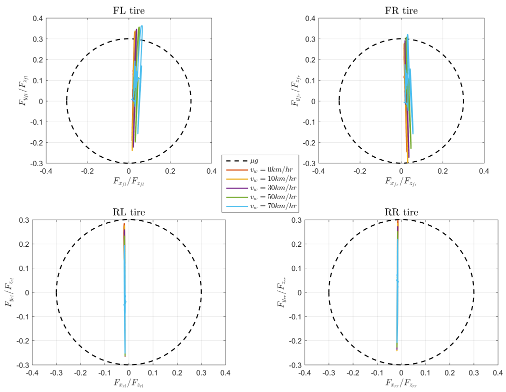

(k) Kamm Circle

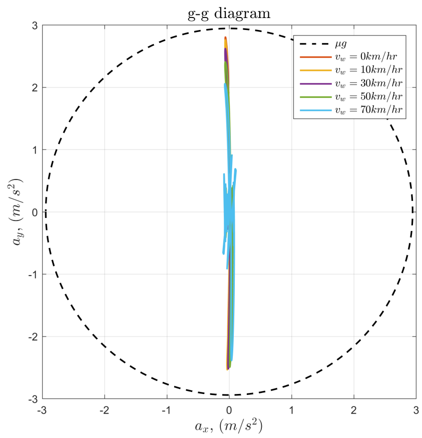

(l) g-g diagram

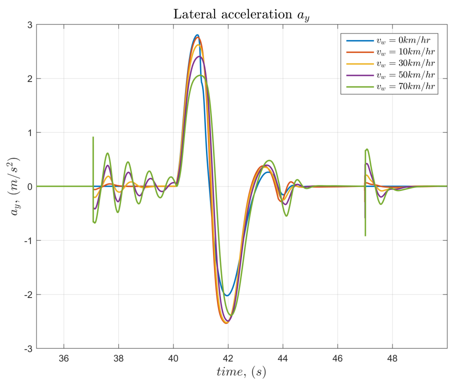

(m) Lateral acc. a_y

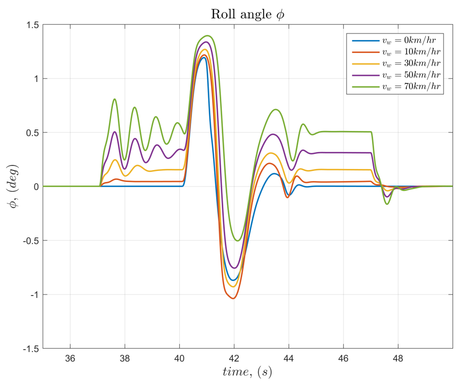

(n) Roll angle ϕ

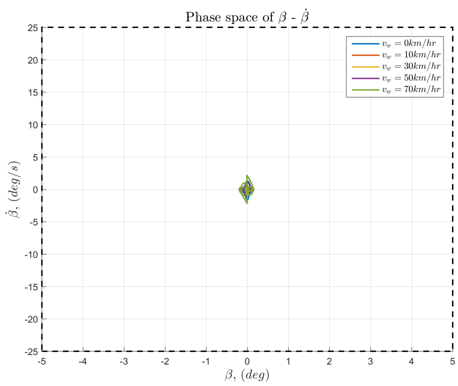

(o) β - $\dot{\beta}$ phase space

Figure C.11: Simulation result for Set 4 - Case 3: $\mu = 0.3$, $v_x = 60km/hr$

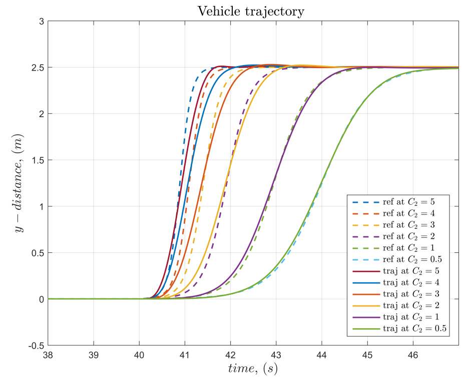

(a) Lateral position y_p

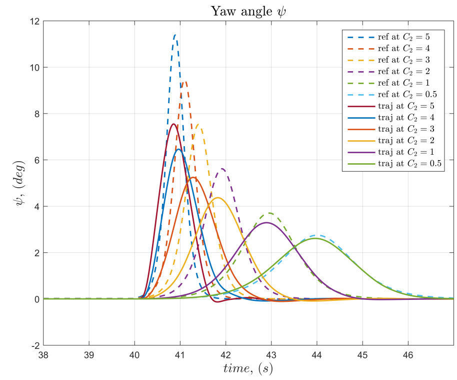

(b) Yaw angle ψ

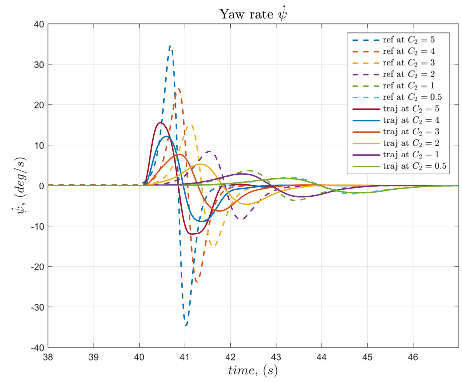

(c) Yaw rate $\dot{\psi}$

S No.	C_2	M_p	T_s	T_r	y_{RMS}	ψ_{RMS}	$\dot{\psi}_{RMS}$	$a_{y_{max}}$
-	-	[%]	[s]	[s]	[%]	[%]	[%]	[m/s^2]
1	5	1.34	3.10	0.53	7.37	71.30	500.64	5.83
2	4	2.25	3.11	0.66	6.46	72.91	389.33	4.78
3	3	2.78	3.47	0.77	6.38	56.82	252.89	3.18
4	2	2.12	4.04	0.89	4.69	33.58	121.79	2.22
5	1	0.00	5.01	1.18	2.44	13.48	36.04	1.23
6	0.5	0.00	5.75	1.49	1.37	6.52	12.20	0.77

(d) KPI table

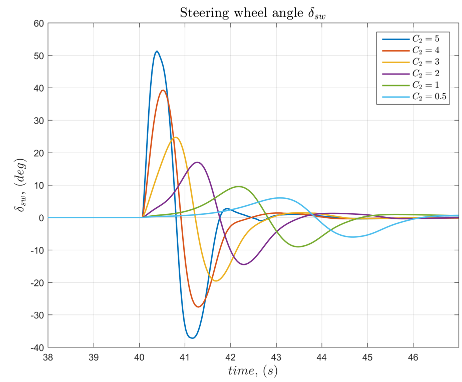

(e) SWA δ_{sw}

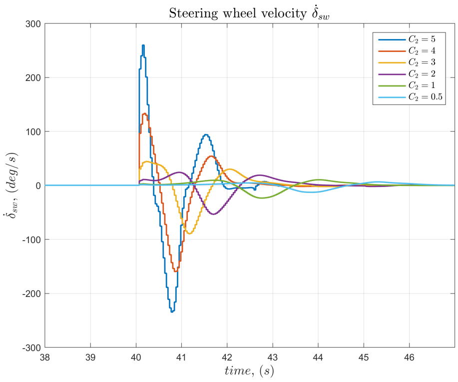

(f) SWV $\dot{\delta}_{\text{sw}}$

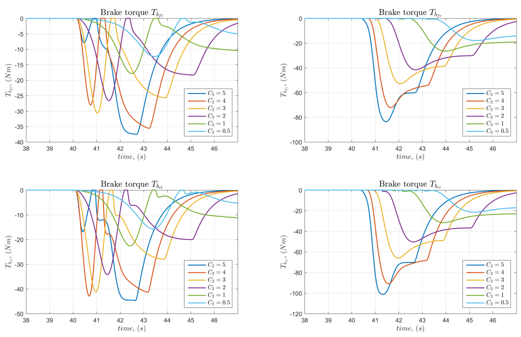

(g) Brake Torques T_b

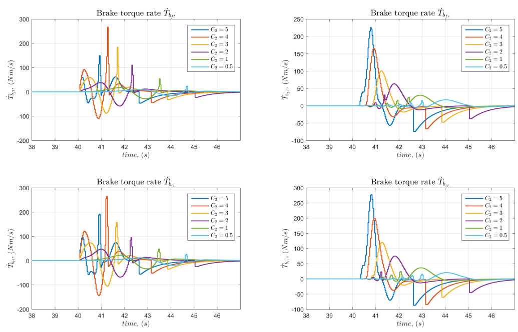

(h) Brake torque rates $\dot{T}_b$

Simulation result for Set 5 - Case 1: $\mu = 0.9$, $v_x = 90 km/hr$

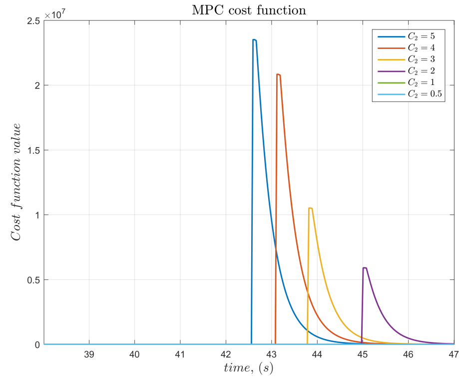

(i) Cost function value

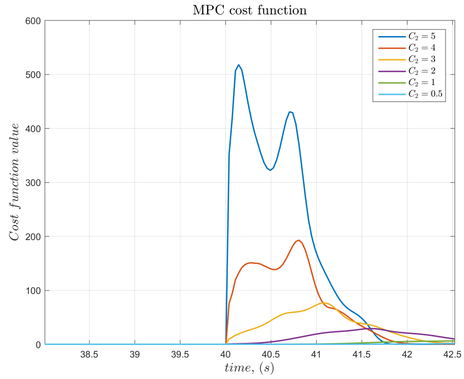

(j) Cost function value

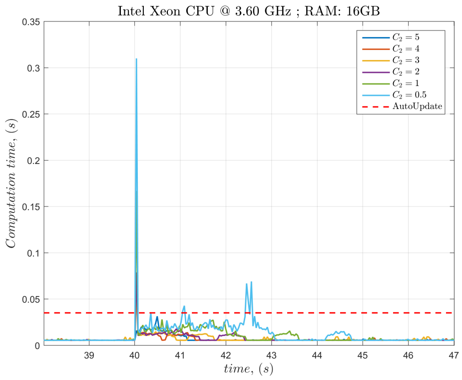

(k) Computation time

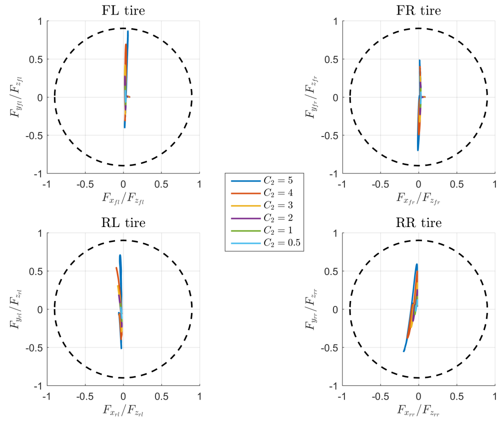

(l) Kamm Circle

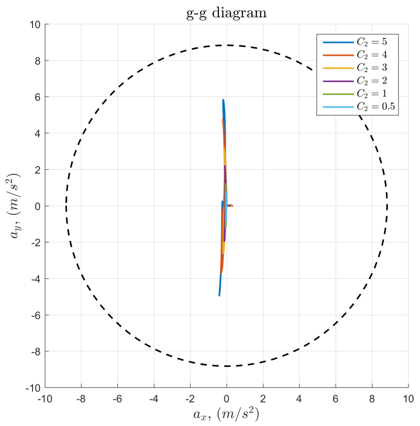

(m) g-g diagram

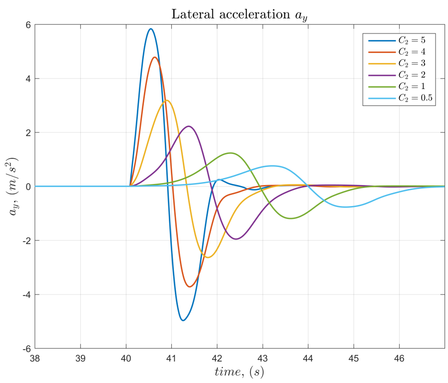

(n) Lateral acc. a_y

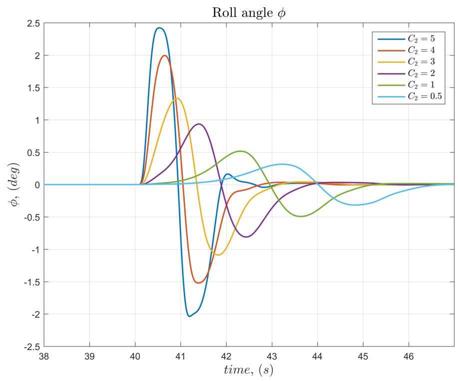

(o) Roll angle ϕ

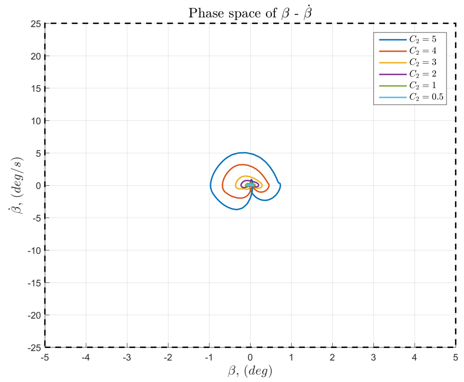

(p) β - $\dot{\beta}$ phase space

Figure C.12: Simulation result for Set 5 - Case 1: $\mu = 0.9$, $v_x = 90 km/hr$

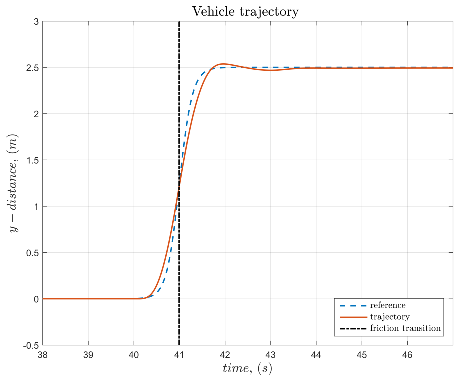

(a) Lateral position y_p

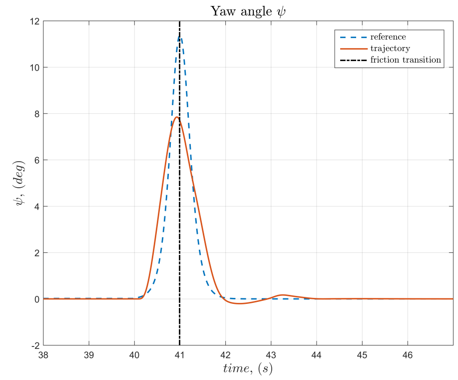

(b) Yaw angle ψ

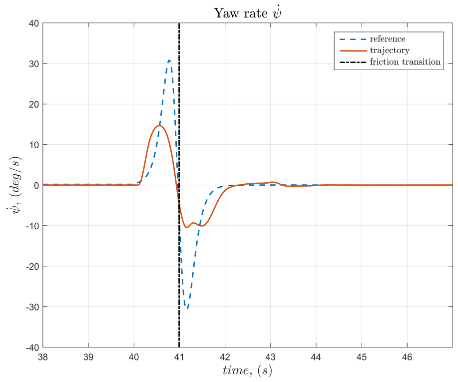

(c) Yaw rate $\dot{\psi}$

S No.	M_p	T_s	T_r	y_{RMS}	ψ_{RMS}	$\dot{\psi}_{RMS}$	DTC	$a_{y_{max}}$
-	[%]	[s]	[s]	[%]	[%]	[%]	[m]	[m/s^2]
1	3.67	3.67	0.57	6.05	76.98	464.86	0.51	4.96

(d) KPI table

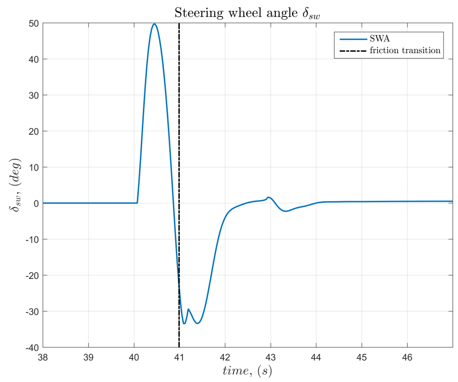

(e) SWA δ_{sw}

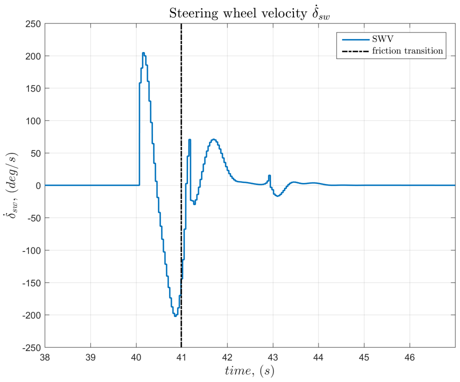

(f) SWV $\dot{\delta}_{\text{sw}}$

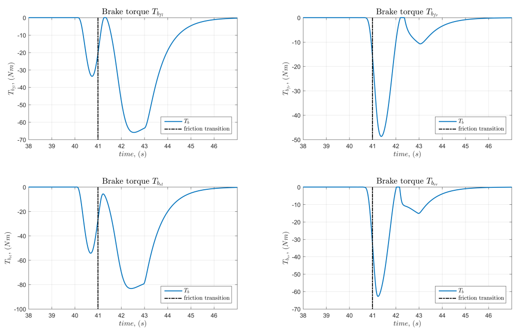

(g) Brake Torques T_b

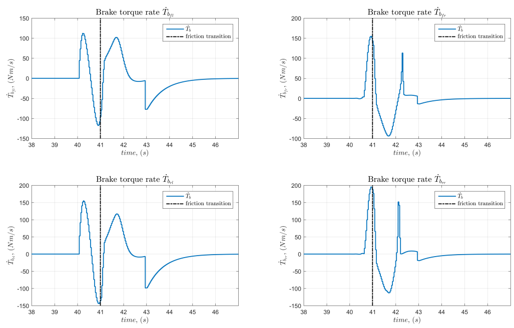

(h) Brake torque rates $\dot{T}_b$

Simulation result for Low to High μ jump: $v_x = 80 km/hr$

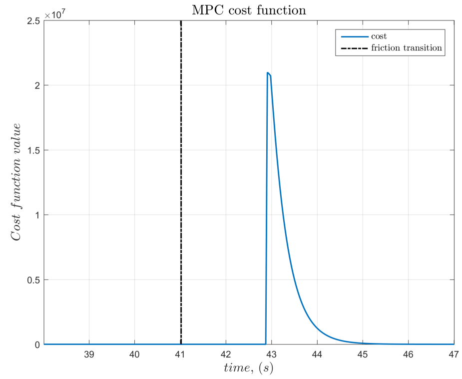

(i) Cost function value

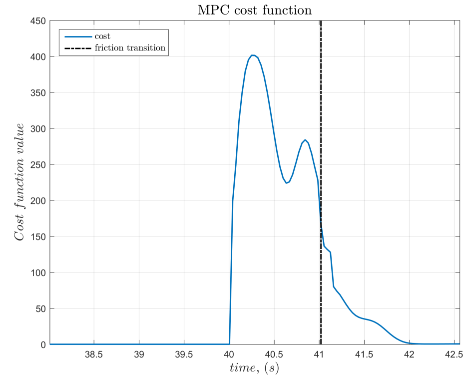

(j) Cost function value

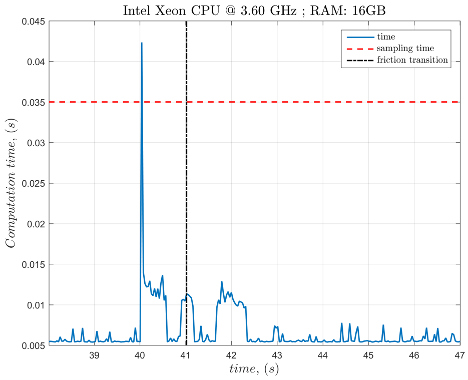

(k) Computation time

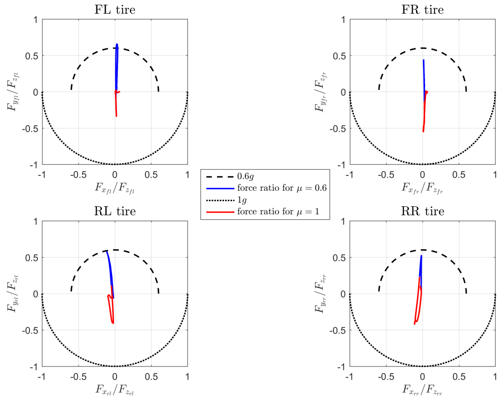

(l) Kamm Circle

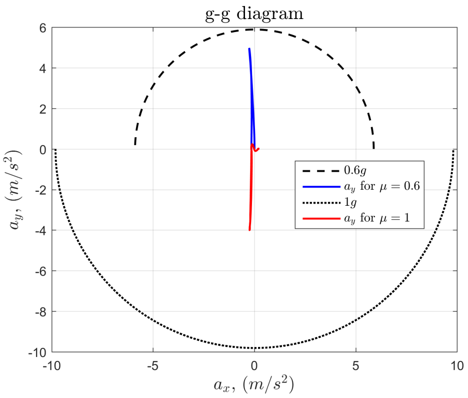

(m) g-g diagram

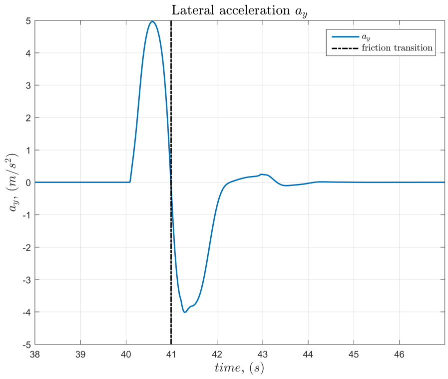

(n) Lateral acc. a_y

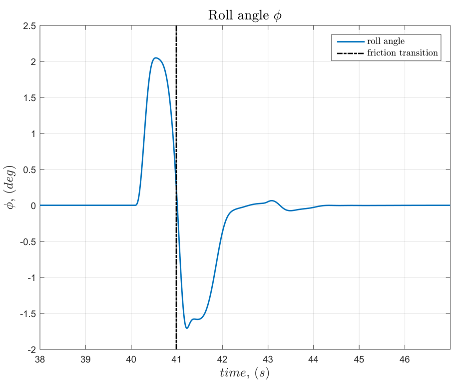

(o) Roll angle ϕ

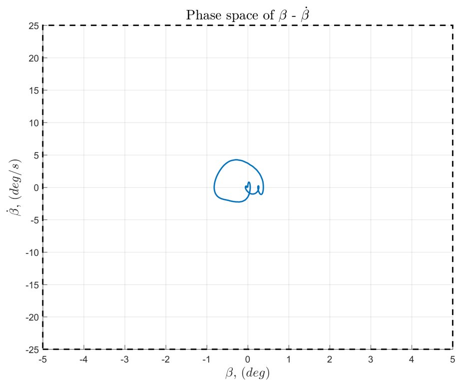

(p) β - $\dot{\beta}$ phase space

Figure C.13: Simulation result for Low to High μ jump: $v_x = 80 km/hr$

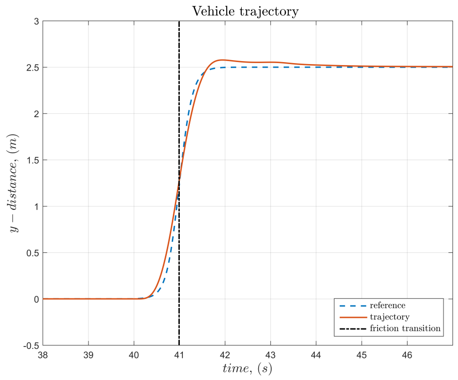

(a) Lateral position y_p

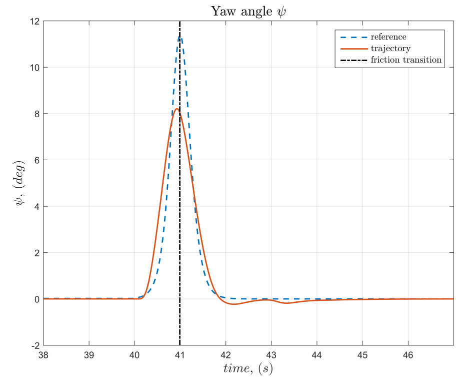

(b) Yaw angle ψ

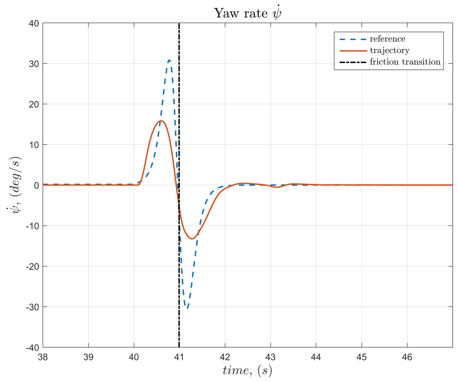

(c) Yaw rate $\dot{\psi}$

S No.	M_p	T_s	T_r	y_{RMS}	ψ_{RMS}	$\dot{\psi}_{\mathrm{RMS}}$	DTC	$a_{y_{\max}}$
-	[%]	[s]	[s]	[%]	[%]	[%]	[m]	[m/s^2]
1	7.82	5.21	0.52	5.61	69.04	414.41	0.60	5.64

(d) KPI table

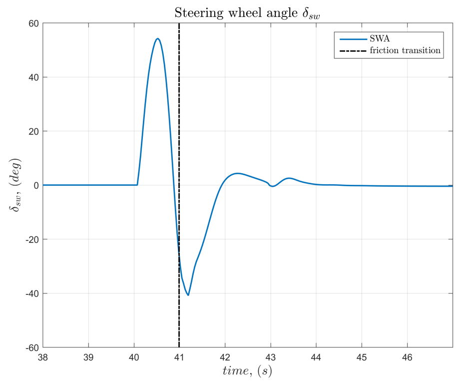

(e) SWA δ_{sw}

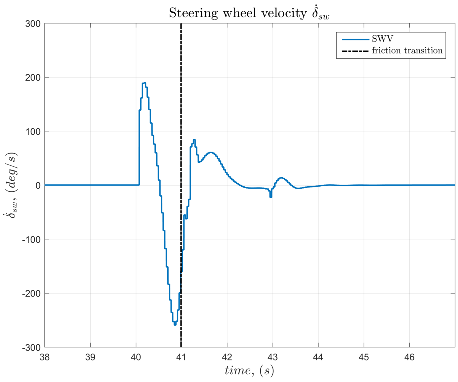

(f) SWV $\dot{\delta}_{\mathrm{sw}}$

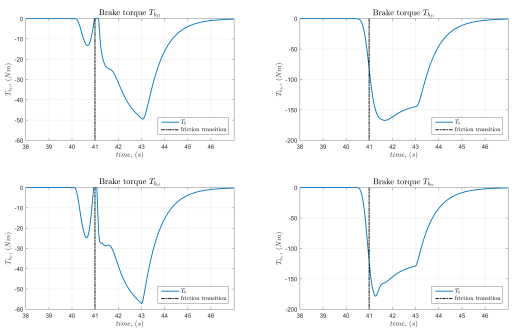

(g) Brake Torques T_b

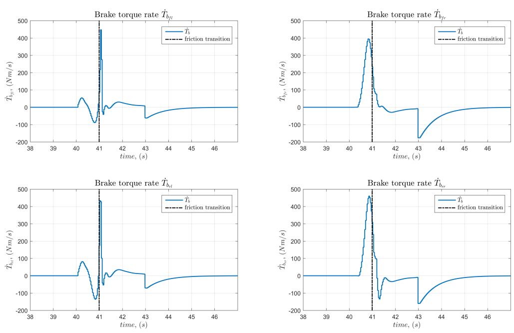

(h) Brake torque rates $\dot{T}_b$

Simulation result for High to Low μ jump: $v_x = 80 km/hr$

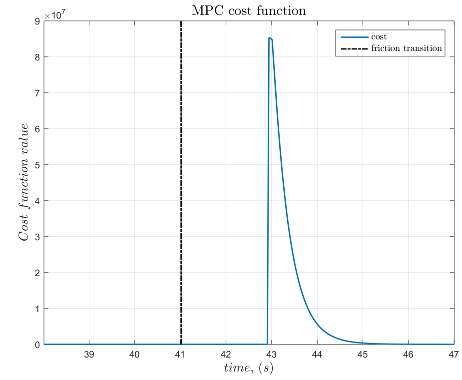

(i) Cost function value

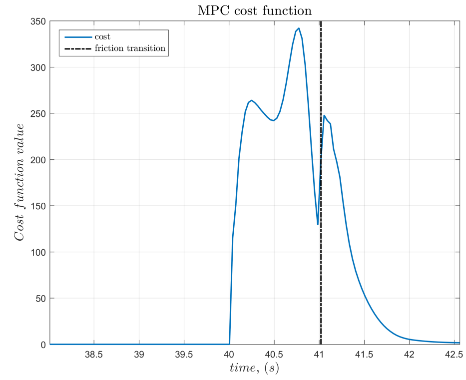

(j) Cost function value

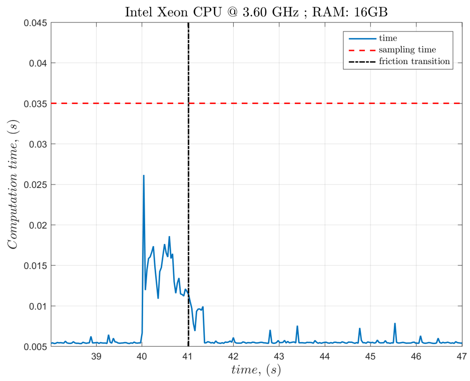

(k) Computation time

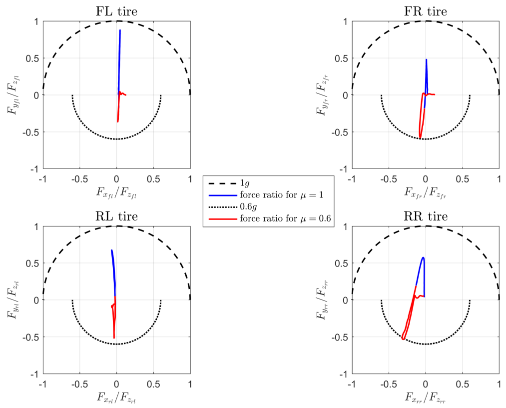

(l) Kamm Circle

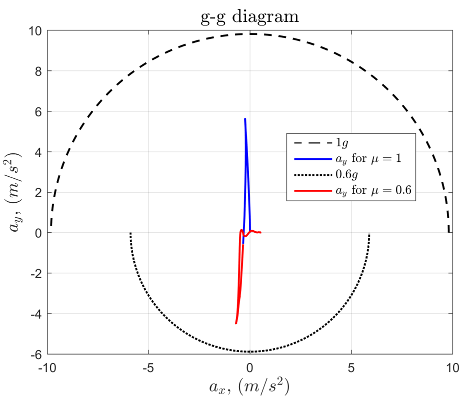

(m) g-g diagram

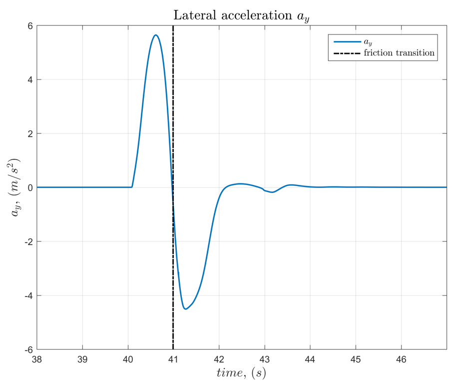

(n) Lateral acc. a_y

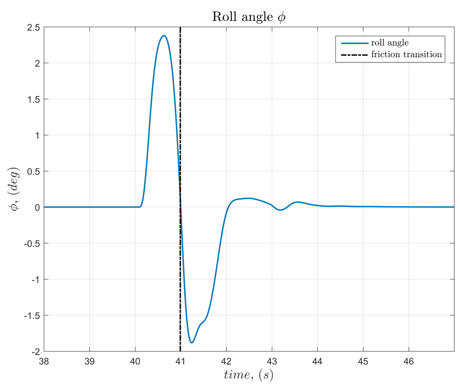

(o) Roll angle ϕ

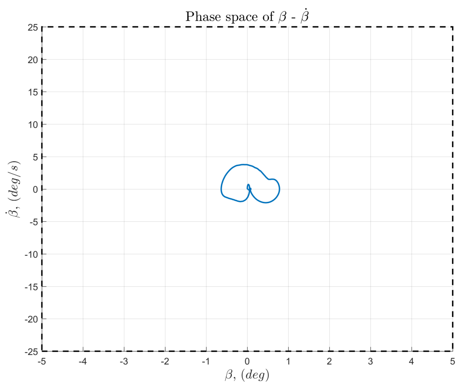

(p) β - $\dot{\beta}$ phase space

Figure C.14: Simulation result for High to Low μ jump: $v_x = 80 km/hr$

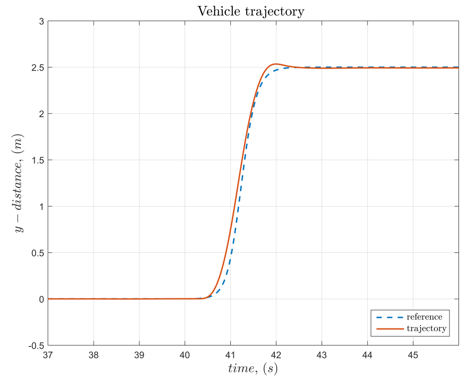

(a) Lateral position y_p

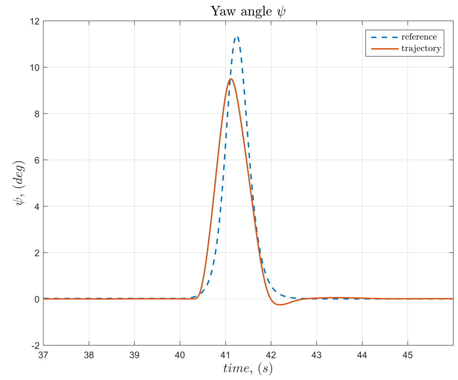

(b) Yaw angle ψ

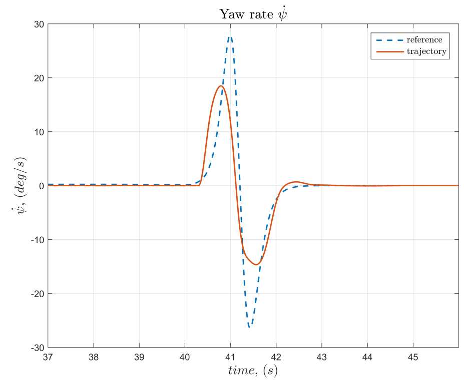

(c) Yaw rate $\dot{\psi}$

S No.	M_p	T_s	T_r	y_{RMS}	ψ_{RMS}	$\dot{\psi}_{RMS}$	DTC	$a_{y_{max}}$
-	[%]	[s]	[s]	[%]	[%]	[%]	[m]	[m/s^2]
1	3.39	3.24	0.51	6.86	77.89	371.93	0.80	5.75

(d) KPI table

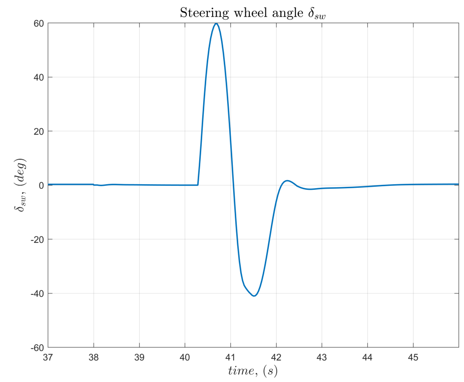

(e) SWA δ_{sw}

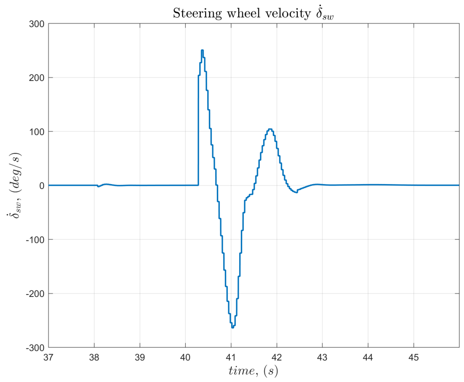

(f) SWV $\dot{\delta}_{\text{sw}}$

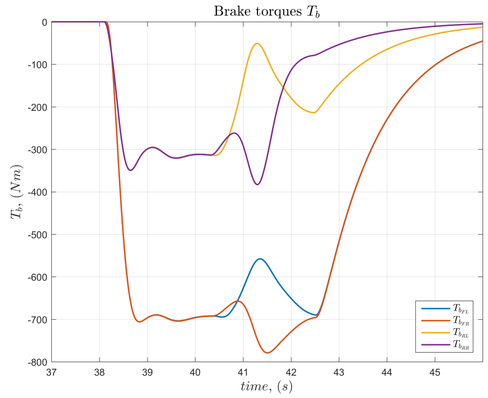

(g) Brake Torques T_b

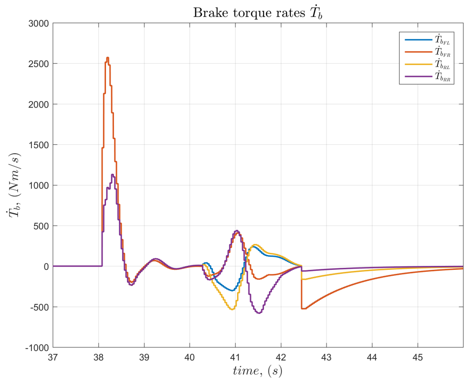

(h) Brake torque rates $\dot{T}_b$

Simulation result for Pre-Braking: $\mu = 0.9$, $v_x = 100 km/hr$

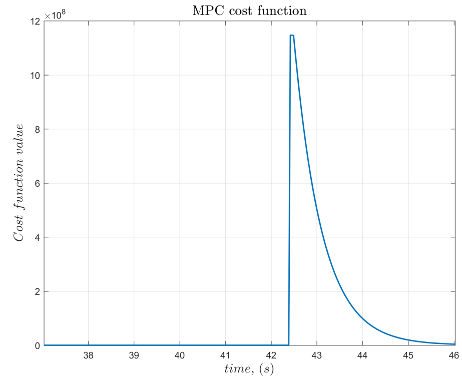

(i) Cost function value

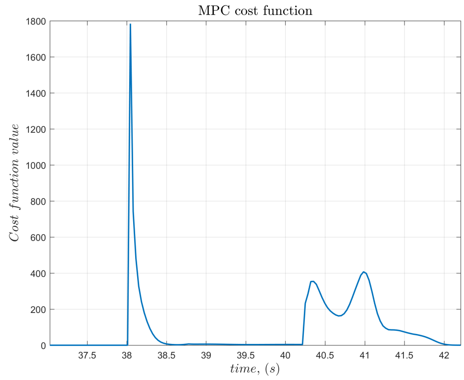

(j) Cost function value

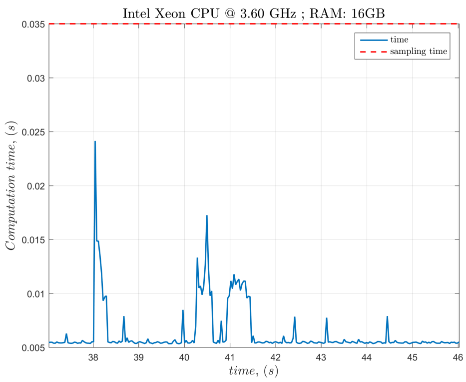

(k) Computation time

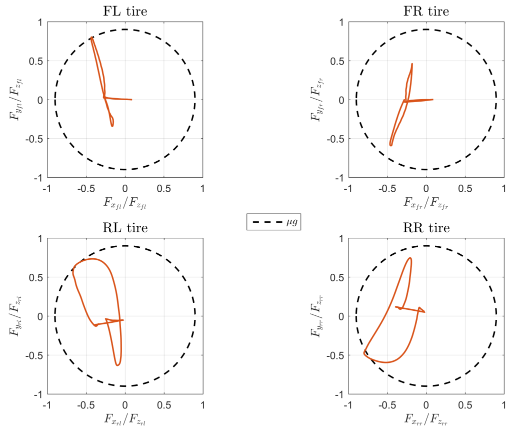

(l) Kamm Circle

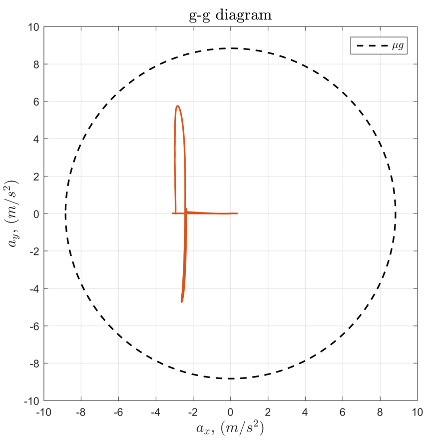

(m) g-g diagram

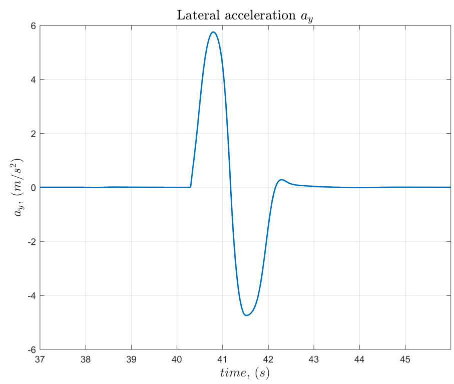

(n) Lateral acc. a_y

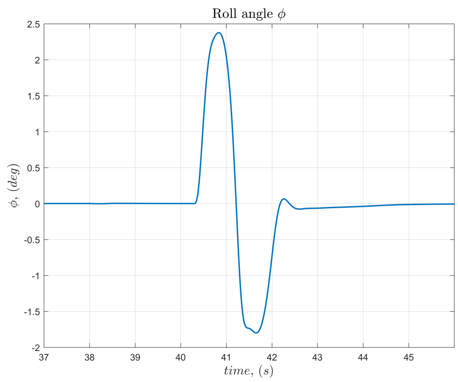

(o) Roll angle ϕ

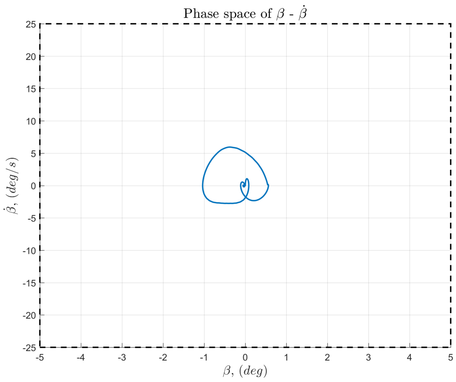

(p) β - $\dot{\beta}$ phase space

Figure C.15: Simulation result for Pre-Braking: $\mu = 0.9$, $v_x = 100km/hr$

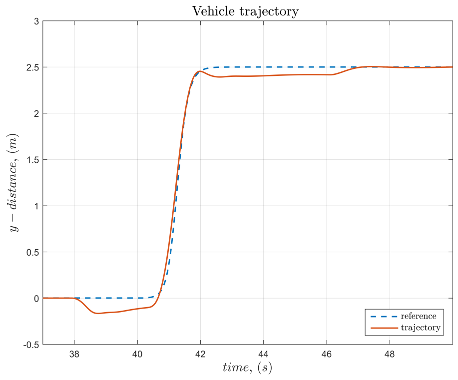

(a) Lateral position y_p

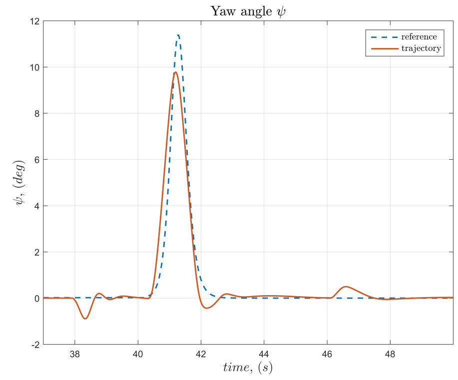

(b) Yaw angle ψ

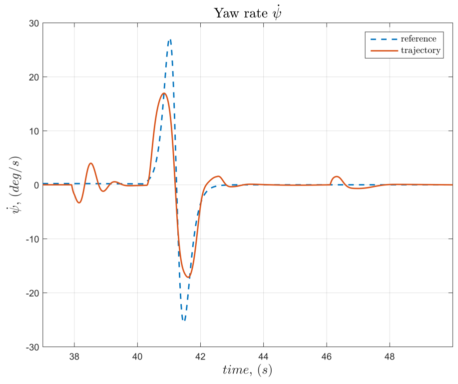

(c) Yaw rate $\dot{\psi}$

S No.	M_p	T_s	T_r	y_{RMS}	ψ_{RMS}	$\dot{\psi}_{RMS}$	DTC	$a_{y_{max}}$
-	[%]	[s]	[s]	[%]	[%]	[%]	[m]	[m/s^2]
1	0.47	6.74	0.54	8.51	60.82	264.45	0.75	5.25

(d) KPI table

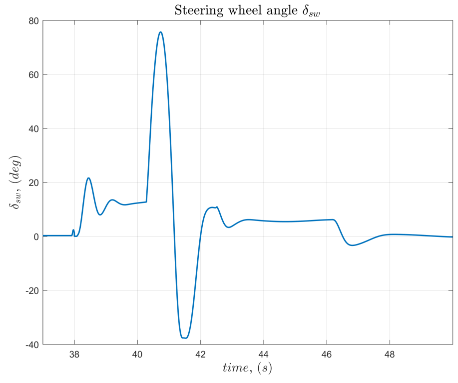

(e) SWA δ_{sw}

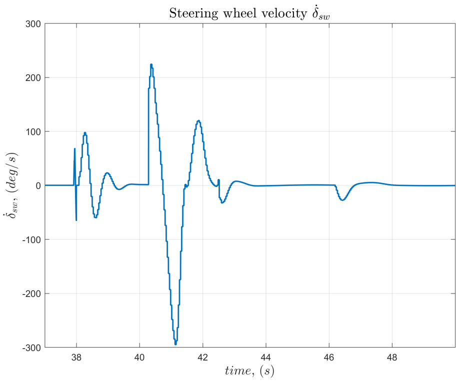

(f) SWV $\dot{\delta}_{sw}$

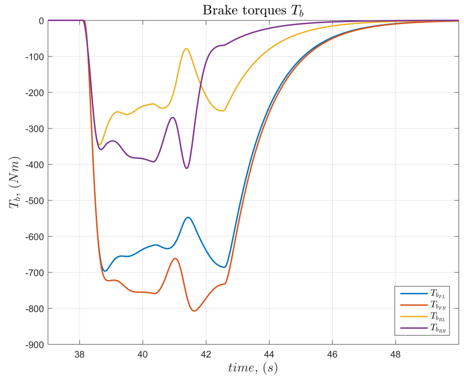

(g) Brake Torques T_b

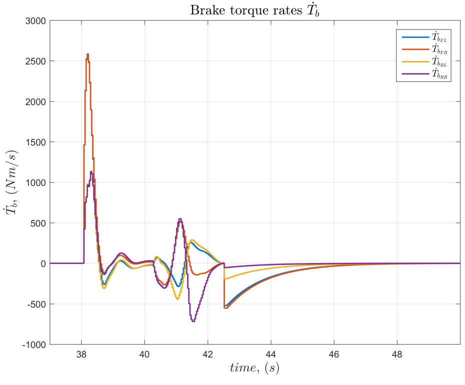

(h) Brake torque rates $\dot{T}_b$

Simulation result for Pre-Braking in wind: $\mu = 0.9$, $v_x = 100 km/hr$, $v_w = 50 km/hr$

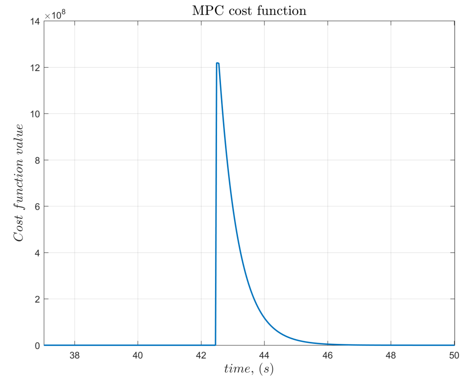

(i) Cost function value

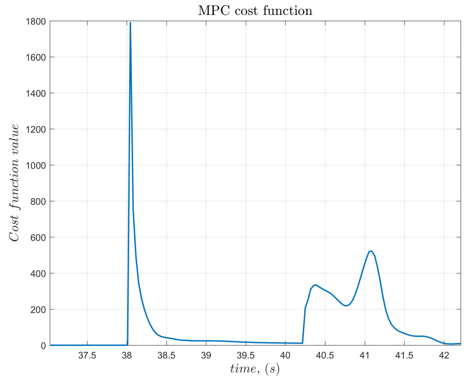

(j) Cost function value

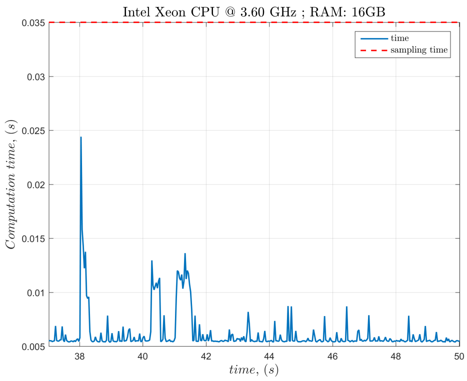

(k) Computation time

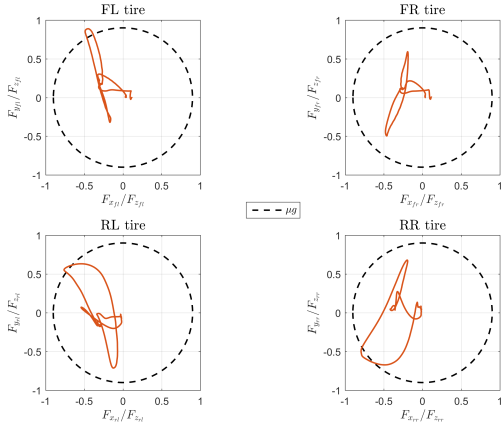

(l) Kamm Circle

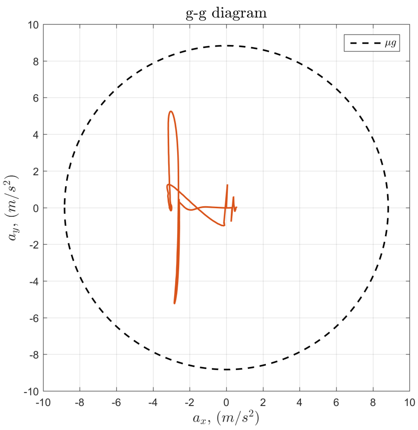

(m) g-g diagram

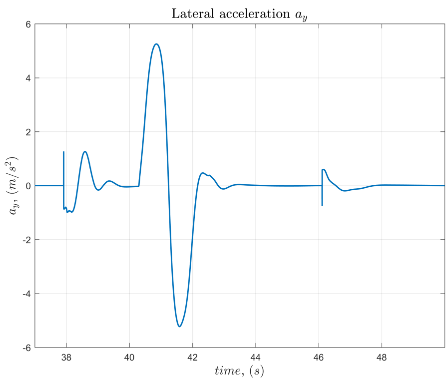

(n) Lateral acc. a_y

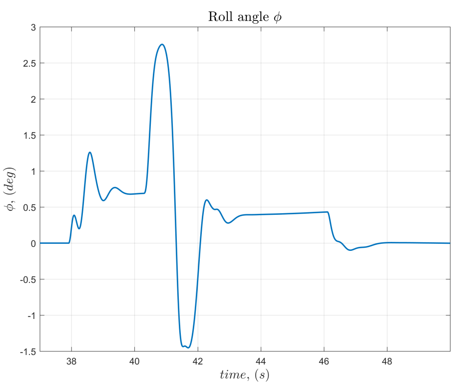

(o) Roll angle ϕ

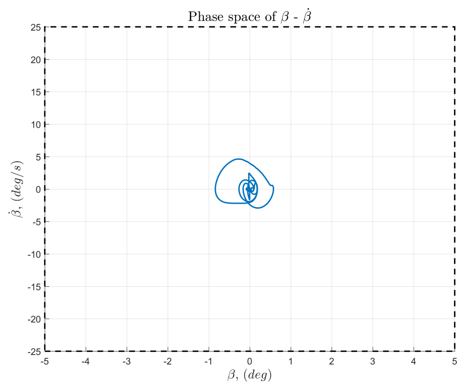

(p) β - $\dot{\beta}$ phase space

Figure C.16: Simulation result for Pre-Braking in wind: $\mu = 0.9$, $v_x = 100 km/hr$, $v_w = 50 km/hr$

D

Vehicle Modelling

D.1. Introduction

In order to ensure that the results from the simulations are as realistic as possible to the ones with real-life implementation of controls in an actual car, it is extremely important that the simulation vehicle used captures all the essential force and moment dynamics in all the three longitudinal, lateral and vertical directions. This was very well modeled and captured in the multi-body Toyota vehicle used for simulation designed in the IPG CarMaker software. This Appendix section gives an in-detailed description of all the equations used to model a vehicle in virtual environment (ranging from chassis to actuator modeling) with all the dynamics captured to high accuracy.

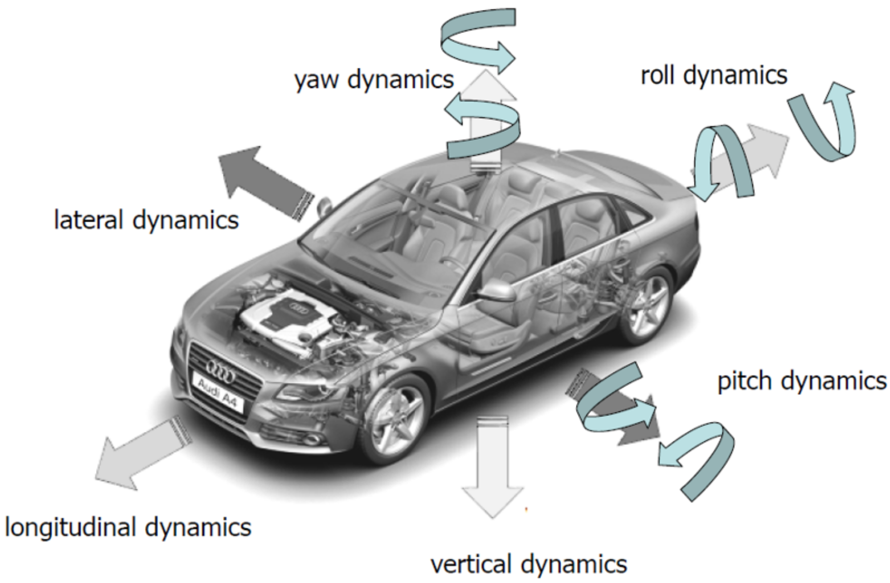

Figure D.1: Six major vehicle motions [16]

D.2. Chassis Dynamics

The full vehicle model consists of a sprung mass (assumed to be the vehicle body) and four tires represented as unsprung masses rigidly connected to the vehicle body. The sprung mass is allowed to roll, pitch and yaw and also allowed to be displaced in longitudinal, lateral and vertical directions giving 6 DoF. Each wheel is allowed to rotate about the y-axis giving another 4 DoF. The suspension modelling has not been reported here but was considered in the vehicle dynamics of IPG CarMaker. The same holds true for the aerodynamic modelling.

The vehicle model is a front wheel drive car with only the front two wheels allowed to steer. A few assumptions were made while modelling the vehicle. All the vehicle body mass comprising of engine, seats, dashboard etc. have been lumped into one single vehicle sprung mass. It is assumed that the vehicle remains grounded with all four tires, not losing contact with road while driving. Lastly, the vehicle is considered symmetric about the *xz*-plane. The values of all the vehicle parameters such as mass, inertia, wheelbase and all other components were set exactly as that of the real vehicle for realistic simulation results.

The following equations from Eq (D.1) - Eq (D.20) represent the 6 DoF of the vehicle model.

Longitudinal Motion:

$$m\left(\frac{dv_x}{dt} - r_{\text{ang}}v_y + q_{\text{ang}}v_z\right) - m_s g\sin\theta = \sum F_x \tag{D.1}$$

Lateral Motion:

$$m\left(\frac{dv_y}{dt} + r_{\text{ang}}v_x - p_{\text{ang}}v_z\right) + m_s g\cos\theta\sin\phi = \sum F_y \tag{D.2}$$

Vertical Motion:

$$m\left(\frac{dv_z}{dt} + p_{\text{ang}}v_y - q_{\text{ang}}v_x\right) + m_s g\cos\theta\cos\phi = \sum F_z \tag{D.3}$$

Roll Motion:

$$I_{xx}\frac{dp_{\text{ang}}}{dt} + \left(I_{zz} - I_{yy}\right)q_{\text{ang}}r_{\text{ang}} - I_{xz}\left(\frac{dr_{\text{ang}}}{dt} + p_{\text{ang}}q_{\text{ang}}\right) - m_s a_y h_r\cos\phi = \sum M_\phi \tag{D.4}$$

Pitch Motion:

$$I_{yy}\frac{dq_{\text{ang}}}{dt} + \left(I_{xx} - I_{zz}\right)p_{\text{ang}}r_{\text{ang}} + I_{xz}\left(p_{\text{ang}}^2 - r_{\text{ang}}^2\right) + m_s a_x h_p\cos\phi\cos\theta = \sum M_\theta \tag{D.5}$$

Yaw Motion:

$$I_{zz}\frac{dr_{\text{ang}}}{dt} + \left(I_{yy} - I_{xx}\right)p_{\text{ang}}q_{\text{ang}} - I_{xz}\left(\frac{dp_{\text{ang}}}{dt} - q_{\text{ang}}r_{\text{ang}}\right) = \sum M_\psi \tag{D.6}$$

The right hand side of the equations written above are described below.

$$\sum F_x = F_{x_{fl}} \cos\delta_{fl} + F_{x_{fr}} \cos\delta_{fr} + F_{x_{rl}} + F_{x_{rr}} - F_{y_{fl}} \sin\delta_{fl} - F_{y_{fr}} \sin\delta_{fr} - F_x^{\text{aero}} \tag{D.7}$$

$$\sum F_y = F_{y_{fl}} \cos\delta_{fl} + F_{y_{fr}} \cos\delta_{fr} + F_{y_{rl}} + F_{y_{rr}} + F_{x_{fl}} \sin\delta_{fl} + F_{x_{fr}} \sin\delta_{fr} - F_y^{\text{aero}} \tag{D.8}$$

$$\sum F_z = F_{s_{fl}} + F_{s_{fr}} + F_{s_{rl}} + F_{s_{rr}} - F_z^{\text{aero}} \tag{D.9}$$

$$\sum M_\phi = m_s g h_\text{r} \cos\theta \sin\phi + m_s a_x h_\text{r} \sin\theta \sin\phi + \frac{t_f}{2}\left(F_{s_{fl}} - F_{s_{fr}}\right) + \frac{t_r}{2}\left(F_{s_{rl}} - F_{s_{rr}}\right) \tag{D.10}$$

$$\sum M_\theta = m_s g h_\text{p} \sin\theta \cos\phi + \cos\phi\left(F_{s_{rl}} l_r + F_{s_{rr}} l_r - F_{s_{fl}} l_f - F_{s_{fr}} l_f\right) \tag{D.11}$$

$$\begin{aligned}\sum M_\psi = {} & -m_s a_x h_\text{r} \sin\phi - m_s a_y h_\text{r} \cos\phi \sin\theta + l_f\left(F_{x_{fl}} \sin\delta_{fl} + F_{x_{fr}} \sin\delta_{fr}\right) + \\ & l_f\left(F_{y_{fl}} \cos\delta_{fl} + F_{y_{fr}} \cos\delta_{fr}\right) - l_r\left(F_{y_{rl}} + F_{y_{rr}}\right) + \frac{t_f}{2}\left(F_{x_{fr}} \cos\delta_{fr} - F_{x_{fl}} \cos\delta_{fl}\right) \\ & + \frac{t_f}{2}\left(F_{y_{fl}} \sin\delta_{fl} - F_{x_{fr}} \sin\delta_{fr}\right) + \frac{t_r}{2}\left(F_{x_{rr}} - F_{x_{rl}}\right) + \sum_{ij=1}^{4} M_{z_{ij}}\end{aligned} \tag{D.12}$$

Here, the roll rate, pitch rate and yaw rate are defined by Eq (D.13) - Eq (D.15).

$$\dot{\phi} = p_\text{ang} + r_\text{ang} \cos\phi \tan\theta + q_\text{ang} \sin\phi \tan\theta \tag{D.13}$$

$$\dot{\theta} = q_\text{ang} \cos\phi - r_\text{ang} \sin\phi \tag{D.14}$$

$$\dot{\psi} = \frac{r_\text{ang} \cos\phi}{\cos\theta} + \frac{q_\text{ang} \sin\phi}{\cos\theta} \tag{D.15}$$

In the above equations, the vehicle mass, wheelbase and chassis acceleration terms have been defined as mentioned below.

$$m = m_s + m_\text{uf} + m_\text{ur} \tag{D.16}$$

$$L = l_f + l_r \tag{D.17}$$

$$a_x = \frac{dv_x}{dt} - r_\text{ang} v_y + q_\text{ang} v_z \tag{D.18}$$

$$a_y = \frac{dv_y}{dt} + r_\text{ang} v_x - p_\text{ang} v_z \tag{D.19}$$

$$a_z = \frac{dv_z}{dt} + p_\text{ang} v_y - q_\text{ang} v_x \tag{D.20}$$

D.2.1. Tire slip angle

By integrating a_x and a_y and with some approximations, one can get the chassis velocity v_x and v_y which can be used to calculate the tire slip angle for each tire based on the following equations from Eq (D.21) - Eq (D.24).

$$\alpha_{fl} = \delta_{fl} - \tan^{-1}\left(\frac{\left(v_y + l_f r\right)\cos\delta_{fl} - \left(v_x - \frac{t_f r}{2}\right)\sin\delta_{fl}}{\left(v_y + l_f r\right)\sin\delta_{fl} + \left(v_x - \frac{t_f r}{2}\right)\cos\delta_{fl}}\right) \tag{D.21}$$

$$\alpha_{fr} = \delta_{fr} - \tan^{-1}\left(\frac{\left(v_y + l_f r\right)\cos\delta_{fr} - \left(v_x + \frac{t_f r}{2}\right)\sin\delta_{fr}}{\left(v_y + l_f r\right)\sin\delta_{fr} + \left(v_x + \frac{t_f r}{2}\right)\cos\delta_{fr}}\right) \tag{D.22}$$

$$\alpha_{rl} = -\tan^{-1}\left(\frac{v_y - l_r r}{v_x - \frac{t_r r}{2}}\right) \tag{D.23}$$

$$\alpha_{rr} = -\tan^{-1}\left(\frac{v_y - l_r r}{v_x + \frac{t_r r}{2}}\right) \tag{D.24}$$

D.2.2. Tire normal load

Since the vehicle's sprung mass is connected to unsprung masses elastically via the use of suspensions, this elastic connection allows for rolling and pitching motion of the vehicle which leads to variations in normal loads about each corner (Fig D.2). This phenomenon is very important as more the normal load present at a corner, more is the tire's ability to generate cornering and driving/braking forces. The performed maneuver is a single lane change with both steering and braking, therefore it involves load transfer due to both rolling and pitching of vehicle significantly affecting each tire's force generation capabilities. This section describes the coupled normal load equations for each tire due to these longitudinal and lateral load transfer effects.

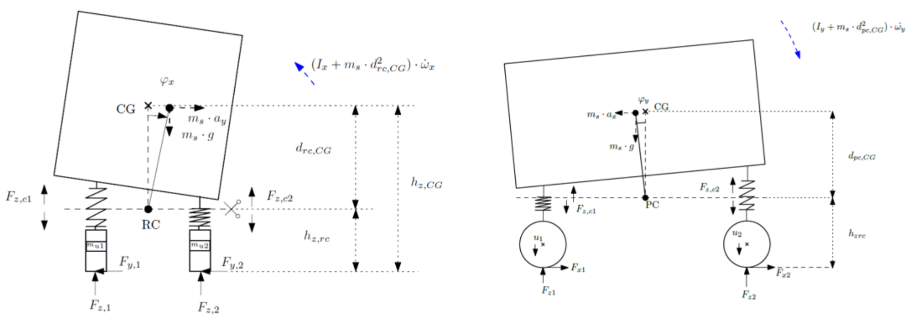

Figure D.2: Vehicle roll and pitch motion [17]

The first component that contributes to the normal load is the forces exerted due to gravity.

$$F_{z,g}^{\text{front}} = \frac{mgl_f}{2L} \tag{D.25}$$

$$F_{z,g}^{\text{rear}} = \frac{mgl_r}{2L} \tag{D.26}$$

The second part is the load transfer per wheel due to longitudinal acceleration.

$$F_z^{\text{long}} = \frac{m_s h_{\text{cg}} + m_{\text{uf}} h_{\text{uf}} + m_{\text{ur}} h_{\text{ur}}}{2L} a_x \tag{D.27}$$

Next part is the lateral load transfer effect due to lateral acceleration.

$$F_{z,\text{front}}^{\text{lat}} = \left(\frac{m_{\text{uf}} h_{\text{uf}}}{t_f} + \frac{m_s l_r h_{\text{rf}}}{t_f L} \right) a_y \tag{D.28}$$

$$F_{z,\text{rear}}^{\text{lat}} = \left(\frac{m_{\text{ur}} h_{\text{ur}}}{t_r} + \frac{m_s l_f h_{\text{rr}}}{t_r L} \right) a_y \tag{D.29}$$

The normal load component because of roll motion is described below.

$$F_{z,\text{front}}^{\text{roll}} = \frac{1}{t_f} \left(K_{\phi,f} \phi + C_{\phi,f} \frac{d\phi}{dt} \right) \tag{D.30}$$

$$F_{z,\text{rear}}^{\text{roll}} = \frac{1}{t_r} \left(K_{\phi,r} \phi + C_{\phi,r} \frac{d\phi}{dt} \right) \tag{D.31}$$

Lastly, the normal load component due to pitch motion of vehicle is mentioned below.

$$F_{z,\text{front}}^{\text{pitch}} = l_f \left(K_{\theta,f} \theta + C_{\theta,f} \frac{d\theta}{dt} \right) \tag{D.32}$$

$$F_{z,\text{rear}}^{\text{pitch}} = l_r \left(K_{\theta,r} \theta + C_{\theta,r} \frac{d\theta}{dt} \right) \tag{D.33}$$

The final normal load equation for each tire is a combination of Eq (D.25) - Eq (D.33) as written below.

$$F_{z_{t_{\text{fl}}}} = F_{z,g}^{\text{rear}} - F_z^{\text{long}} - F_{z,\text{front}}^{\text{lat}} - F_{z,\text{front}}^{\text{roll}} + F_{z,\text{front}}^{\text{pitch}} \tag{D.34}$$

$$F_{z_{t_{\text{fr}}}} = F_{z,g}^{\text{rear}} - F_z^{\text{long}} + F_{z,\text{front}}^{\text{lat}} + F_{z,\text{front}}^{\text{roll}} + F_{z,\text{front}}^{\text{pitch}} \tag{D.35}$$

$$F_{z_{t_{\text{rl}}}} = F_{z,g}^{\text{front}} + F_z^{\text{long}} - F_{z,\text{rear}}^{\text{lat}} - F_{z,\text{rear}}^{\text{roll}} - F_{z,\text{rear}}^{\text{pitch}} \tag{D.36}$$

$$F_{z_{t_{\text{rr}}}} = F_{z,g}^{\text{front}} + F_z^{\text{long}} + F_{z,\text{rear}}^{\text{lat}} + F_{z,\text{rear}}^{\text{roll}} - F_{z,\text{rear}}^{\text{pitch}} \tag{D.37}$$

D.3. Tire Dynamics

One of the most important component of a car are the tires. The whole motion of the vehicle happens only due to the force generation capabilities of the tire and therefore accurate prediction of the lateral and longitudinal forces of tire is extremely important.

Over the years, a lot of tire models has been developed for accurate predictions of tire forces. The two main modelling approaches for tire forces are physical methods and empirical approach. Physical methods involve the designing of physical mechanisms that generates tire forces. Mechanical representation is used for this, ranging from simple physics to finite element methods and heavy computer simulations. The contact of the tire with road is modelled through spring-mass-damper mechanical systems which deform as the tire comes in contact with ground and begins to roll. Various models such as LuGre model, Dugoff tire model and Brush tire model have been developed which gives good accuracy in linear regime of motion but are limited in reproducing the tire forces in nonlinear regime.

Empirical methods involve curve fitting or interpolation in which a set of variables are defined to formulate a curve that fits well to the tire characteristics. This method requires heavy usage of tire data for accurate fitting. The most successful and famous empirical, transient tire model is the Magic Formula (MF) developed by Hans B. Pacejka [68]. The formula was derived based on fitting of the tire measurement data to a model involving many coefficient for accurate fitting. The basic formulas for pure longitudinal and lateral forces using MF have been reported in Eq (D.38) - Eq (D.39). The reader is advised to refer [68] for further in-depth understanding.

The pure longitudinal and lateral force equations are given below.

$$F_{x0} = D_x \sin\left(C_x \arctan(B_x\kappa_x - E_x\left(B_x\kappa_x - \arctan(B_x\kappa_x)\right))\right) + S_{V_x} \tag{D.38}$$

$$F_{y0} = D_y \sin\left(C_y \arctan\left(B_y\alpha_y - E_y\left(B_y\alpha_y - \arctan\left(B_y\alpha_y\right)\right)\right)\right) + S_{V_y} \tag{D.39}$$

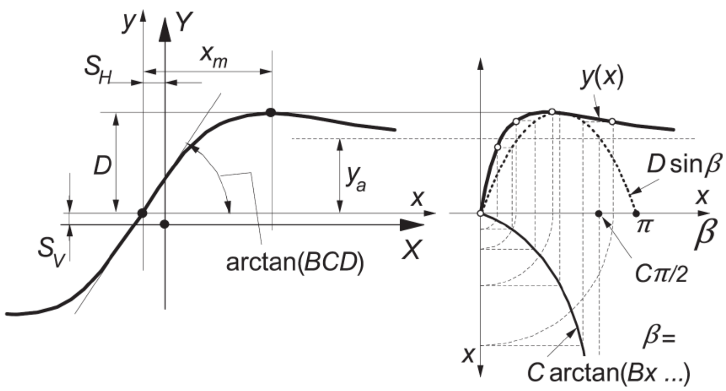

Figure D.3: Curve produced by Eq (D.38) with fitting parameters [7]

Here, the parameters have the following physical meaning.

- κ_x - longitudinal slip ($\kappa_x = \kappa + S_{H_x}$)

- α_y - lateral slip angle ($\alpha_x = \alpha + S_{H_y}$)
- D_x, D_y - Peak Factor i.e. indicates the peak value of the friction function
- C_x, C_y - Shape Factor
- B_x, B_y - Stiffness Factor
- E_x, E_y - Curvature Factor
- C_x, C_y - Shape Factor
- S_{H_x}, S_{H_y} - Horizontal shift
- S_{V_x}, S_{V_y} - Vertical shift

All these parameters further depend on many other curve fitting and scaling parameters which have been well documented in [68] in detail. In this research, all the simulations performed have used MF model for systematic, detailed and realistic tire force calculations.

D.4. Single Corner Dynamics

The 6 DoF of the vehicle body was defined in Section D.2 and the remaining 4 DoF will be defined in this section to complete the 10 DoF vehicle model formulation. The rotation of the vehicle about the y-axis contains significant dynamic information about the brake torques and tire longitudinal forces among its total 6 DoF. Therefore other DoF of the tire will not be discussed here. A single corner model captures the tire rotational DoF about y-axis very well.

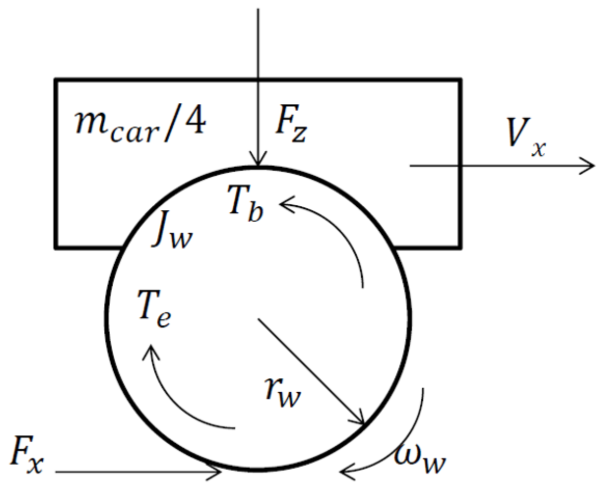

Figure D.4: Single Corner Model [16]

Based on the single corner model geometry shown in Fig D.4, the equation describing the wheel dynamics in y-axis is written below in which the rolling resistance moment has been neglected.

$$J_{yy_{ij}}\dot{\omega}_{ij} = T_{e_{ij}} - T_{b_{ij_{act}}} - F_{x_{ij}} r_{eff_{ij}} \quad , \quad ij = (fl, fr, rl, rr) \tag{D.40}$$

Another definition apart from wheel speeds and slip angles (Section D.2.1) is the wheel longitudinal slip κ which is defined in Eq (D.41).

$$\kappa_{\text{ij}} = \frac{|\omega_{\text{ij}} r_{\text{eff}_{\text{ij}}} - v_{x_{\text{ij}}}|}{\max\{v_{x_{\text{ij}}}, r_{\text{eff}_{\text{ij}}} \omega_{\text{ij}}\}} \tag{D.41}$$

With $\kappa \in [0,1]$, the wheel slip defines the state of the motion of the wheel, representing the relative motion between tire elements in contact with the road surface and tire body. This relative motion causes the tire slippage with road. By definition, $\kappa = 0$ defines the pure rolling of the wheel and $\kappa = 1$ represents a locked wheel.

D.5. Actuator Dynamics

A major part of the equations written above cover the motion of vehicle accurately. But, actuator dynamics is another aspect which affects the dynamics of the overall vehicle. One part is calculating the SWA and brake torques, but these calculated inputs are not directly applied on the wheels. There are other subsystems in the vehicle which are combination of many other mechanical components such as gears, bushings, shafts, motor, springs etc. which brings into account various other performance losses due to coupled mechanical components, compliance, inertia, vibrations etc. Hence it is extremely important to model these actuator systems carefully and consider its dynamics in the simulation to get meaningful and realistic results. Since the research done considers steering and braking as its control action, therefore the dynamics of both these lateral and longitudinal dynamics respectively have been presented here and powertrain modelling is not reported.

D.5.1. Steering Dynamics

The steering system considered in the simulation is a high fidelity 3 DoF steering model with column-assist EPS logic which has been validated with full vehicle testing extensively and is implemented in the Toyota's high-end driving simulator [69]. Fig D.5 shows the components of steering system comprising of a steering wheel, torsion bar, steering column, assist electric motor, pinion and rack, tie rod to finally the wheels of the car.

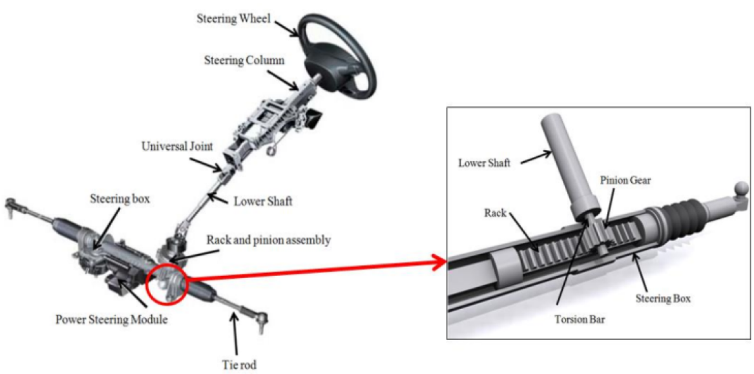

Figure D.5: Steering system component [17]

The schematic layout of the steering system is shown in Fig D.6 which highlights the inclusion of various compliance and system inertia terms in modelling the steering system.

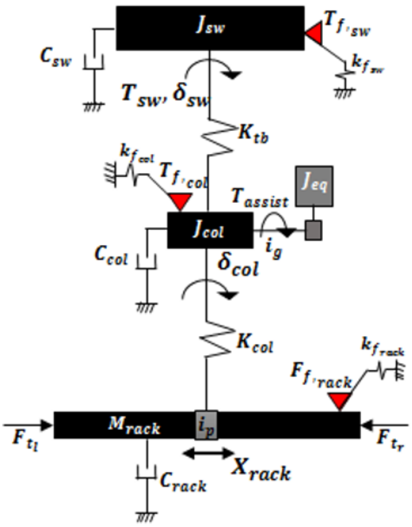

Figure D.6: Steering model layout

Following are the equations used to model the 3 DoF steering model.

The steering wheel dynamics is modelled as:

$$J_{\text{sw}}\ddot{\delta}_{\text{sw}} + C_{\text{sw}}\dot{\delta}_{\text{sw}} + T_{f,\text{sw}} = T_{\text{sw}} - K_{\text{tb}}\left(\delta_{\text{sw}} - \delta_{\text{col}}\right) \tag{D.42}$$

The column dynamics for the case of column-assist EPS is formulated as:

$$\left(J_{\text{col}} + J_{\text{eq}} i_g^2\right)\ddot{\delta}_{\text{col}} + C_{\text{col}}\dot{\delta}_{\text{col}} + T_{f,\text{col}} = K_{\text{tb}}\left(\delta_{\text{sw}} - \delta_{\text{col}}\right) - K_{\text{col}}\left(\delta_{\text{col}} - \frac{x_{\text{rack}}}{i_p}\right) + T_{\text{assist}}\, i_g \tag{D.43}$$

The rack dynamics comprises the third and final DoF and is modelled as:

$$\left(m_{\text{rack}} + m_{\text{susp}}\right)\ddot{x}_{\text{rack}} + C_{\text{rack}}\dot{x}_{\text{rack}} + F_{f,\text{rack}} = \frac{K_{\text{col}}}{i_p}\left(\delta_{\text{col}} - \frac{x_{\text{rack}}}{i_p}\right) - F_{\text{rack}} \tag{D.44}$$

The model with the EPS assist On/Off showed good correlation with experimental data with Pearson correlation coefficient above 0.98.

D.5.2. Brake Actuator Dynamics

The brakes considered in this research are floating point disc brakes with conventional HAB system which uses hydraulic, pneumatic and mechanical components to generate the necessary brake pressure. Since hydraulic brakes are considered here, a first order transfer function is sufficient to capture the dynamics of the pressure buildup, nonlinearities and the delays associated with it.

As the designed controller is active system rather than an assistance system, the brake pedal dynamics, vacuum booster and master cylinder dynamics have not been modelled. The brake ECU shall directly regulate the pressure at each tires through the solenoid valve movement and therefore only modelling of the brake calipers is sufficient.

The brake actuator dynamics modelling was taken from [70]. An extensive research and comparison with real-life nonlinear vehicle data was used by [70] to derive the transfer function described in Eq (D.45). Also, due to mechanical capabilities, the total pressure as well as the pressure rate also needs to be bounded which also has been take care of.

$$\frac{P_{\text{act}}}{P_{\text{cal}}} = \frac{e^{-T_d s}}{T_l s + 1} \quad , \quad \dot{P}_{\text{act}} \leq \text{RateLim} \tag{D.45}$$

The parameters for the front axle are $T_d = 0.06s$, $T_l = 0.12s$ and RateLim = $230 bar/s$. For the real axle, the parameters are $T_d = 0.02s$, $T_l = 0.05s$ and RateLim = $550 bar/s$. The maximum pressure P_{max} that the brakes can achieve is taken as $160 bar$. The parameters taken here capture the reality very well. In a conventional HAB system, the pressure build-up in the rears is faster than the front which has been considered here with small T_d and T_l parameter values and higher RateLim value for rear brakes as compared to the front. Also, the front calipers are larger in size as compared to rear calipers due to which the maximum pressure rate in the rears will be higher than the front which again is considered here.

To convert the brake pressure to brake torque, Eq (D.46) from [71] was used for individual front and rear brake respectively.

$$T_{b_{\text{ij}_{\text{act}}}} = P_{\text{act}_{\text{ij}}} A_{\text{wc}_{\text{ij}}} \eta_{c_{\text{ij}}} 2 \mu_{L_{\text{ij}}} r_{\text{ij}} \quad , \quad \text{ij} = (\text{fl}, \text{fr}, \text{rl}, \text{rr}) \tag{D.46}$$

The brake material is cast iron and neglecting the seal retraction force and the hysteresis from the clearance, the parameters for the above formula were taken from TME of a real brake system. This gave the conversion value from brake pressure to brake torques for front and rear to be $30.53m^3$ and $10.08m^3$ respectively. Again the front brakes have more area than the rear brakes for more pressure build up therefore the front conversion value is greater than the rear ones. Thus all the parameters along with the transfer function and delay are sufficient to model a realistic brake actuator dynamics with rear brake dynamics faster than the front ones also modelled correctly.

D.6. Summary

The aim of this Appendix was to provide reader with the EoM that are used to model the real vehicle with high precision. Equations to define a 10 DoF vehicle model was explained in detail to cover the force and moment equations of the vehicle in all the three directions as well as the tire rotation dynamics using the single corner model. Equations for tire slip angle, tire longitudinal slip and normal load transfer was explained and then MF was reported to complete the whole tire modelling. Finally, equations used to model the steering and brake actuator dynamics were documented to complete the whole vehicle modelling from vehicle motion to tires to actuator modelling, barring the suspension and aerodynamic modelling which was not reported here but has been considered and modelled well in the simulation vehicle.

E
Reference Tracking Issue

In all the reference lateral position y_p plots shown in Section 6.3, especially with the case of nonlinear bicycle based MPC control performance in Set 1 - Case 1 (Fig 6.3) and the pre-braking scenario in Fig 6.24, it was observed that for most of the maneuver, the vehicle was seen to perform the maneuver even before the reference trajectory was calculated. Fig E.1 highlights the same issue.

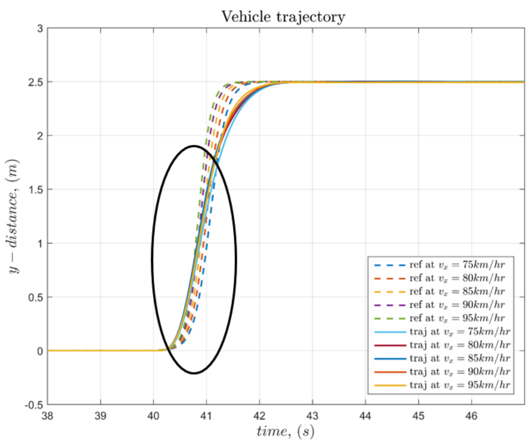

(a) Nonlinear bicycle model MPC in Set 1 - Case 1 scenario

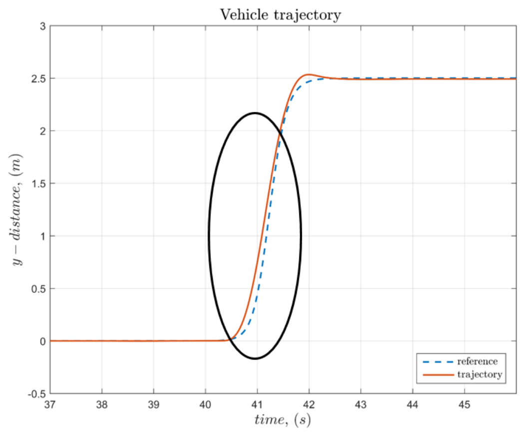

(b) Planar car model MPC in pre-braking scenario

Figure E.1: Pre-tracking issue

It was seen that instant of an active control action, a pre-active control action was given by the controller as a result the reference trajectory was followed even before it was calculated. This was odd and such pre-reference scheme are not ideal. The difference in trajectory tracking though remains to be very small as seen in all the y_{RMS} values, but still, it was confusing to see such behaviour shown by the controller.

On investigating, it was found that the issue was not with the MPC controller's design formulation but instead was to do with the reference generation points along the prediction horizon calculated by the reference generator. In this research, a constant point is not given as a reference value along the horizon. This degrades the future prediction due to limited reference values and impedes the controller's performance. Since a mathematical method was used to get the reference points, it was possible to easily calculate the future reference points along the horizon.

The Sigmoid curve is a function of vehicle's longitudinal position as seen in Eq (4.10). To calculate the future reference points, the future reference longitudinal position were therefore required. An assumption was made that the vehicle along the horizon travels with same speed $v_{x_{\text{current}}}$. By doing so and using Newton's Law of Motion, Eq (E.1) was used to calculate the future reference longitudinal position x_{ref}.

$$x_{\text{ref}(i)} = x_{\text{current}} + i\, t_s\, v_{x_{\text{current}}} \quad \text{where} \quad i = 1, 2, 3, ..., N_p \tag{E.1}$$

It was seen that the calculation of these reference points made a significant difference in the definition of the cost function and overall desired position tracking of the controller. Reported by [51] and quoted below.

"In order to obtain the reference trajectories in the prediction horizon, the assumption on the constant travel velocity is invalid especially in extreme handling situations, which can affect the performance and stability of the closed-loop system."

To verify this effect, the number of reference points that were passed to the controller along the horizon were varied from 1 point to all the points with increments and the controller's tracking performance was noticed. Fig E.2 - Fig E.6 shows the various tracking performance by the nonlinear bicycle model based MPC for the case $\mu = 0.9$ and $v_x = 75 km/hr$.

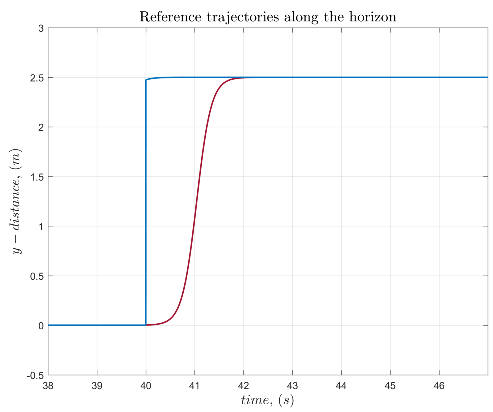

(a) Reference trajectories

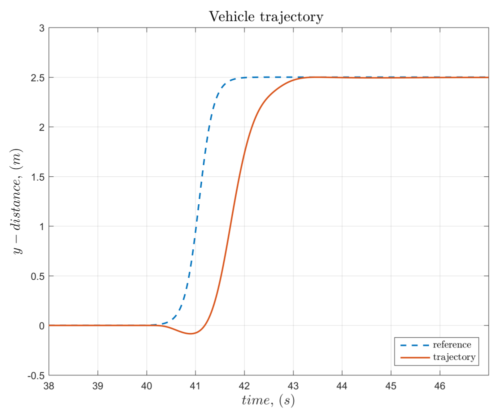

(b) Vehicle tracking trajectory

Figure E.2: MPC - Nonlinear bicycle model performance with 1 reference point

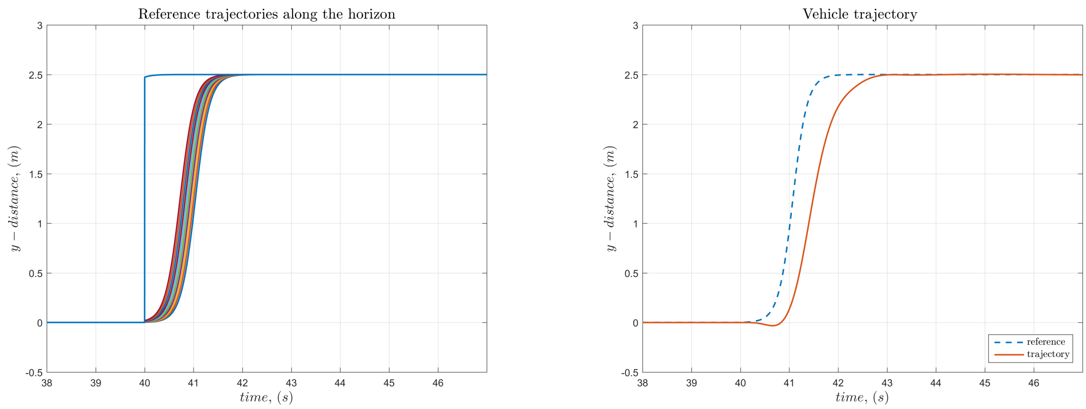

(a) Reference trajectories

(b) Vehicle tracking trajectory

Figure E.3: MPC - Nonlinear bicycle model performance with 10 reference points

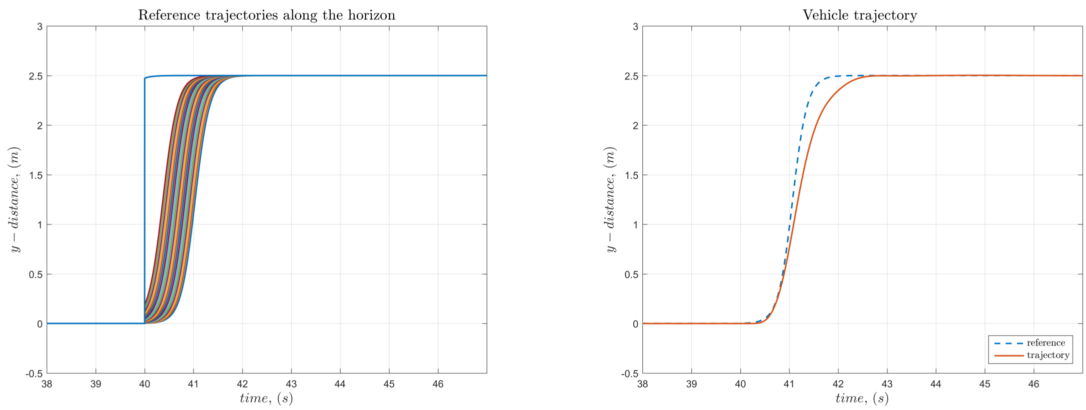

(a) Reference trajectories

(b) Vehicle tracking trajectory

Figure E.4: MPC - Nonlinear bicycle model performance with 20 reference points

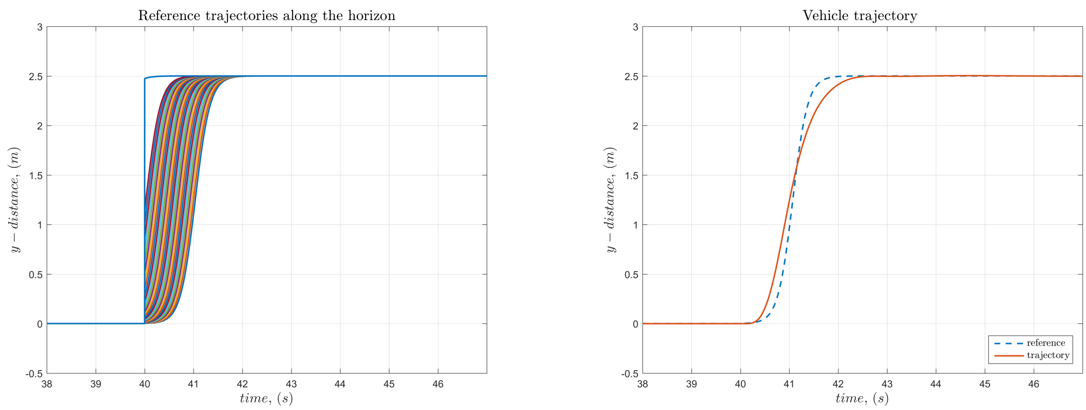

(a) Reference trajectories

(b) Vehicle tracking trajectory

Figure E.5: MPC - Nonlinear bicycle model performance with 30 reference points

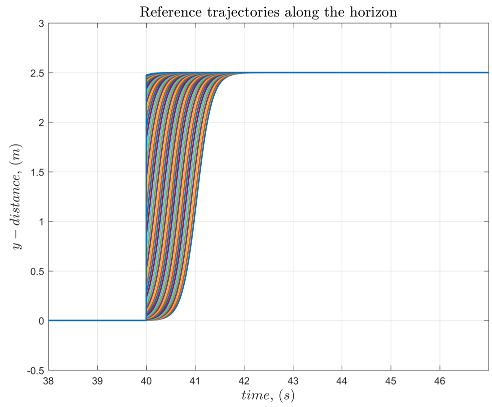

(a) Reference trajectories

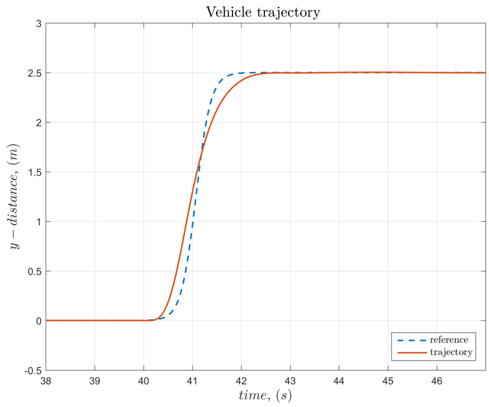

(b) Vehicle tracking trajectory

Figure E.6: MPC - Nonlinear bicycle model performance with 50 reference points

In all the reference values, the terminal reference is also given for the terminal part of the cost function calculated at the last prediction horizon i.e. $N_p = 50$. It is seen that the way the points are calculated makes a huge difference in how the tracking is performed. MPC control is a predictive control and is sensitive to future predictions. If the future information is given incorrectly then this will be reflected in the controller's performance which was noticed in the plots.

The controller's performance is directly linked to the reference trajectory. As a path planner, one needs to correctly calculate the future predictions to ensure that the subsequent control action is not hampered. This issue has nothing to do with too much future predictions. The thumb rule of more the predictions, better the performance is still valid as was shown to be true in Section 5.2. The issue is with the incorrect information that is being calculated along the horizon and passed to the controller.

The second reason for this phenomenon is the use of kinematic reference generator in this research. It was seen that the unrealistic reference yaw rate values were passed to the controller. All the reference values were not precisely derived and did not respect the vehicle dynamics. If this is improved, the author believes that the performance of the controller will further improve and better KPI values will be achieved.

Since this research is based on a comparative analysis on the control scheme and not on trajectory generation techniques, the same reference trajectory generation method was used for all the three controllers. To not limit the performance in any way, the prediction points along the entire horizon was given to all the three controllers. And subjective comparison was performed for these controllers to analyze how the controller behaves to improper reference points and how well can they dynamically control the car with kinematic reference trajectories. Hence the comparisons made and the conclusions reported still holds true. The performance though can further be improved with better formulated Reference Generator.

F

Dugoff tire model fitting

Dugoff tire model fitting on the magic formula for the case of $F_{z_t} = 5000N$ for all the μ values.

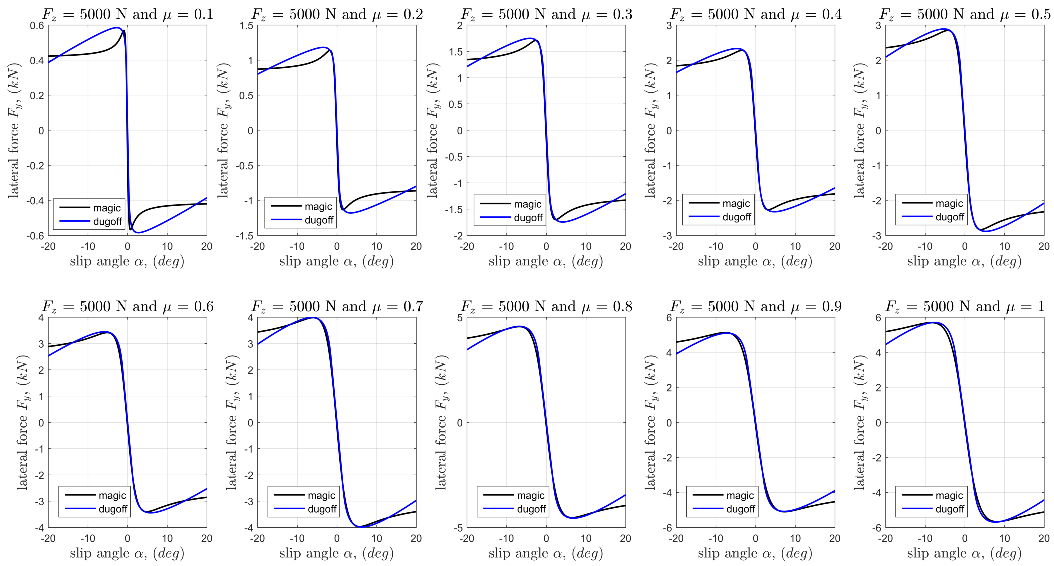

Figure F.1: Dugoff tire model fitting

G
Glossary

G.1. List of Acronyms

ABS	Anti-lock Brake System
ACADO	Automatic Control and Dynamic Optimization
ACEA	European Automobile Manufacturers Association
ADAS	Advance Driver Assistance System
AFS	Active Front Steering
ASM	Active Set Method
DB	Differential Braking
DoF	Degrees of Freedom
DTC	Distance To Collision
EBD	Electronic Brake Distribution
ECU	Electronic Control Unit
EDS	Emergency Driving System
Euro NCAP	The European New Car Assessment Programme
EoM	Equations of Motion
EPS	Electric Power Assist
HAB	Hydraulically Applied Brakes
IP	Interior Point
IPC	Inter-Process-Communication
ISO	International Organization for Standardization
KPI	Key Performance Index
LHS	Left Hand Side
LMPC	Linear Model Predictive Control
LQR	Linear Quadratic Regulator
LTV	Linear Time Varying
LV	Lead Vehicle
MF	Magic Formula
MIMO	Multi-Input Multi-Output
MPC	Model Predictive Control
NHTSA	National Highway Traffic Safety Administration
NMPC	Non-linear Model Predictive Control

NLP	Non Linear Problem
OEM	Original Equipment Manufacturer
OCP	Optimal Control Problem
PID	Proportional-Integral-Derivative Controller
PRT	Perception Response Time
QP	Quadratic Programming
RHP	Receding Horizon Principle
RHS	Right Hand Side
RMS	Root Mean Square
RTI	Real Time Iteration
SQP	Sequential Quadratic Programming
SV	Subject Vehicle
SWA	Steering Wheel Angle
SWV	Steering Wheel Velocity
SWAcc	Steering Wheel Acceleration
TME	Toyota Motor Europe
TTC	Time To Collision
TTS	Time To Steer
TTB	Time To Brake
VSC	Vehicle Stability Control

G.2. List of Symbols

α_{ij}	Tire slip angle, $[rad]$
β	Vehicle bodyslip angle, $[rad]$
$\dot{\beta}$	Vehicle bodyslip angle rate change, $[rad/s]$
$\eta_{c_{\text{ij}}}$	Wheel cylinder efficiency for caliper ij, [-]
κ	Wheel longitudinal slip, [-]
$\mu_{L_{\text{ij}}}$	Brake lining coefficient of friction for caliper disc ij, [-]
μ_o	Peak friction coefficient, [-]
μ_{ij}	Friction coefficient of tire ij, [-]
ϕ	Chassis roll angle, $[rad]$
θ	Chassis pitch angle, $[rad]$
ψ	Chassis yaw angle, $[rad]$
ψ_{ref}	Reference heading angle, $[rad]$
δ_{col}	Steering column angle, $[rad]$
$\dot{\delta}_{\text{col}}$	Steering column velocity, $[rad/s]$
$\ddot{\delta}_{\text{col}}$	Steering column acceleration, $[rad/s^2]$
δ_{sw}	Steering wheel angle, $[rad]$
$\dot{\delta}_{\text{sw}}$	Steering wheel velocity, $[rad/s]$
$\ddot{\delta}_{\text{sw}}$	Steering wheel acceleration, $[rad/s^2]$
δ_{ij}	Wheel steer angle, $[rad]$
κ_{ij}	wheel longitudinal slip, [-]
ω_{ij}	Wheel angular speed, $[rad/s]$
$\dot{\omega}_{\text{ij}}$	Wheel angular acceleration, $[rad/s^2]$
a_x	Chassis longitudinal acceleration, $[m/s^2]$
a_y	Chassis lateral acceleration, $[m/s^2]$
$A_{\text{wc}_{\text{ij}}}$	Wheel cylinder area for caliper ij, $[m^2]$
$C_{\alpha_{\text{ij}}}$	Individual wheel lateral cornering stiffness, $[N/rad]$
C_{α_f}	Front cornering stiffness, $[N/rad]$
C_{α_r}	Rear cornering stiffness, $[N/rad]$
$C_{\kappa_{\text{ij}}}$	Individual wheel longitudinal slip stiffness, $[N]$
$C_{\phi,f}$	Front suspension roll damping coefficient, $[Nms/rad]$
$C_{\phi,r}$	Rear suspension roll damping coefficient, $[Nms/rad]$
$C_{\theta,f}$	Front suspension spring damping coefficient, $[Nms/rad]$
$C_{\theta,r}$	Rear suspension spring damping coefficient, $[Nms/rad]$
C_{col}	Steering column damping constant, $[Nms/rad]$
C_{rack}	Rack damping constant, $[Nms/rad]$
C_{sw}	Steering wheel damping constant, $[Nms/rad]$
d_{δ}	Control action wheel angle velocity, $[rad/s]$
$d_{T_{b_{\text{ij}}}}$	Control action brake torque rate for wheel ij, $[Nm/s]$
d_{ref}	Target lateral displacement by SV, $[m]$
e_r	Friction reduction coefficient, [-]
$F_{f,\text{rack}}$	Rack friction force, $[N]$
F_{rack}	Rack force (sum of left and right tie rod forces), $[N]$
$F_{s_{\text{ij}}}$	Suspension force (active + passive components both), $[N]$
$F_{x_{\text{ij}}}$	Tire longitudinal force, $[N]$

F_{x_f}	Front axle tire's total longitudinal force, $[N]$
F_{x_r}	Rear axle tire's total longitudinal force, $[N]$
$F_{y_{t_{\mathrm{ij}}}}$	Tire lateral force, $[N]$
$F_{z_{t_{\mathrm{ij}}}}$	Tire normal load, $[N]$
F_x^{aero}	Aerodynamic force in longitudinal direction, $[N]$
F_y^{aero}	Aerodynamic force in lateral direction, $[N]$
F_z^{aero}	Aerodynamic force in vertical direction, $[N]$
g	Acceleration due to gravity, $[m/s^2]$
h_p	Height of pitch centre from ground, $[m]$
h_{pf}	Height of front pitch centre from ground, $[m]$
h_{pr}	Height of rear pitch centre from ground, $[m]$
h_r	Height of roll centre from ground, $[m]$
h_{rf}	Height of front roll centre from ground,, $[m]$
h_{rr}	Height of rear roll centre from ground,, $[m]$
h_{cg}	Height of CoG, $[m]$
h_{uf}	Height of front unsprung mass CoG above origin, $[m]$
h_{ur}	Height of rear unsprung mass CoG above origin, $[m]$
i_g	EPS motor gear ratio, [-]
i_p	Steering gear ratio, [-]
I_{xx}	Moment of Inertia of sprung mass about x-axis, $[kgm^2]$
I_{yy}	Moment of Inertia of sprung mass about y-axis, $[kgm^2]$
I_{zz}	Moment of Inertia of sprung mass about z-axis, $[kgm^2]$
I_{xz}	Cross moment of Inertia of sprung mass about x-z-axis, $[kgm^2]$
J_{col}	Steering column moment of inertia, $[kgm^2]$
J_{eq}	EPS motor moment of inertia, $[kgm^2]$
J_{sw}	Steering wheel moment of inertia, $[kgm^2]$
$J_{\mathrm{yy_{ij}}}$	Wheel moment of inertia, $[kgm^2]$
$K_{\phi,f}$	Front suspension roll stiffness, $[Nm/rad]$
$K_{\phi,r}$	Rear suspension roll stiffness, $[Nm/rad]$
$K_{\theta,f}$	Front suspension spring stiffness, $[Nm/rad]$
$K_{\theta,r}$	Rear suspension spring stiffness, $[Nm/rad]$
K_{col}	Steering column stiffness coefficient, $[Nm/rad]$
K_{tb}	Torsion bar stiffness coefficient, $[Nm/rad]$
l_f	Vehicle front wheelbase, $[m]$
l_r	Vehicle rear wheelbase, $[m]$
L	Vehicle wheelbase, $[m]$
L_{ref}	Distance to LV, $[m]$
m	Total mass of the vehicle, $[kg]$
m_{rack}	Rack mass, $[kg]$
m_s	Vehicle Sprung mass, $[kg]$
m_{susp}	Suspension inertia translated to tie rods, $[kg]$
m_{uf}	Vehicle front unsprung mass, $[kg]$
m_{ur}	Vehicle rear unsprung mass, $[kg]$
$M_{y_{\mathrm{ij}}}$	Rolling Resistance Moment, $[Nm]$
$M_{z_{\mathrm{ij}}}$	Self Aligning Moment, $[Nm]$
N_c	Control Horizon, [-]

N_p	Prediction Horizon, [-]
p_{ang}	Chassis angular velocity about x-axis, $[rad/s]$
P_{act}	Actual Brake pressure post caliper dynamics applied at wheel, $[bar]$
$\dot{P}_{\text{act}}$	Actual Brake pressure rate, $[bar/s]$
P_{cal}	Calculated Brake pressure before caliper dynamics, $[bar]$
q_{ang}	Chassis angular velocity about y-axis, $[rad/s]$
r	yaw rate, $[rad/s]$
r_{ang}	Chassis angular velocity about z-axis, $[rad/s]$
r_{eff}	Wheel effective rolling radius, $[m]$
r_{ij}	Effective disc radius for rotor ij, $[m]$
r_{ref}	Reference yaw rate, $[rad/s]$
s_{st}	Steering ratio, [-]
T_{assist}	Assist torque, $[Nm]$
$T_{f,\text{col}}$	Steering column friction torque, $[Nm]$
$T_{f,\text{sw}}$	Steering wheel friction torque, $[Nm]$
T_{sw}	Steering wheel torque, $[Nm]$
$T_{e_{\text{ij}}}$	Applied engine torque, $[Nm]$
$T_{b_{\text{ij}_{\text{act}}}}$	Applied brake torque to wheel ij, $[Nm]$
$T_{b_{\text{ij}_{\text{cal}}}}$	Calculated brake torque before actuator dynamics, $[Nm]$
t_f	Vehicle front track width, $[m]$
t_r	Vehicle rear track width, $[m]$
t_s	MPC controller sampling time, $[s]$
$v_{x_{\text{ij}}}$	Wheel longitudinal speed, $[m/s]$
$V_{x_{\text{ij}}}$	Individual wheel longitudinal velocity, $[m/s]$
v_x	Chassis longitudinal velocity, $[m/s]$
v_y	Chassis lateral velocity, $[m/s]$
v_z	Chassis vertical velocity, $[m/s]$
x_p	Vehicle global position in longitudinal direction, $[m]$
x_{rack}	Rack longitudinal displacement, $[m]$
$\dot{x}_{\text{rack}}$	Rack longitudinal velocity, $[m/s]$
$\ddot{x}_{\text{rack}}$	Rack longitudinal acceleration, $[m/s^2]$
y_p	Vehicle global position in lateral direction, $[m]$
y_{ref}	Reference lateral position, $[m]$